THE MEMBRANE-MEDIATED CONFORMATION OF DYNORPHIN A-(1-13)

Dedicated to

Thomas,

my parents,

and Bettina

THE MEMBRANE-MEDIATED CONFORMATION

OF

DYNORPHIN A-(1-13)-PEPTIDE

AS STUDIED BY

NUCLEAR MAGNETIC RESONANCE SPECTROSCOPY,

CIRCULAR DICHROISM SPECTROPOLARIMETRY,

AND

MOLECULAR DYNAMICS

By

CHARLES ROY DESMOND LANCASTER

A Thesis

Submitted to the School of Graduate Studies

in Partial Fulfillment of the Requirements

for the Degree

Master of Science

McMaster University

MASTER OF SCIENCE (1990) McMASTER UNIVERSITY

(Biochemistry) Hamilton, Ontario

TITLE: The Membrane-Mediated Conformation of Dynorphin A-(1-13)-Peptide as Studied by Nuclear Magnetic Resonance Spectroscopy, Circular Dichroism Spectropolarimetry, and Molecular Dynamics.

AUTHOR: Charles Roy Desmond Lancaster

SUPERVISOR: Professor R. M. Epand

NUMBER OF PAGES: xxviii, 300

ABSTRACT

The structural requirements for the binding of dynorphin to the kappa opioid receptor are of profound clinical interest in the search for a powerful non-addictive analgesic. These requirements are thought to be met by the membrane-mediated conformation of the opioid peptide dynorphin A-(1-13), Tyr^{1}-Gly^{2}-Gly^{3}-Phe^{4}-Leu^{5}-Arg^{6}-Arg^{7}-Ile^{8}-Arg^{9}-Pro^{10}-Lys^{11}-Leu^{12}-Lys^{13}. Schwyzer [*Biochemistry* **25**: 4281-4286 (1986)] has proposed an essentially α-helical membrane-mediated conformation of the tridecapeptide. In the present study, the hydrophobic moment, the helix probability and a four-state secondary structure prediction were computed. They signified, in agreement with circular dichroism (CD) studies on phospholipid-bound dynorphin A-(1-13)-tridecapeptide, negligible helical content of the peptide. CD studies demonstrated that the aqueous-membraneous interphase can be mimicked by methanol. The 500 and 620 MHz ^{1}H nuclear magnetic resonance (NMR) spectra of dynorphin A-(1-13) in methanolic solution were sequence-specifically assigned with the aid of correlated spectroscopy (COSY), double-quantum filtered phase-sensitive COSY, relayed COSY (RELAY) and nuclear Overhauser enhancement spectroscopy (NOESY). 2-D CAMELSPIN/ROESY experiments indicated that at least the part of the molecule from Arg^{7} to Arg^{9} was in an extended or β-strand conformation, which was in

line with deuterium exchange and temperature dependence studies of the amide protons. $^{13}C_{\alpha}$ spin-lattice relaxation rate constants indicated a non-rigid backbone conformation. Transferred nuclear Overhauser effect studies on aqueous systems containing dynorphin A-(1-13) in the presence of dimyristoyl-phosphatidylcholine bilayers indicated a folded conformation from Tyr^1 to Leu^5. The findings were incorporated into a tentative molecular model, which also indicated a non-helical, non-extended conformation for the rest of the molecule in the presence of corresponding distance-restrained negative charges.

ACKNOWLEDGEMENTS

I am very grateful to the Tübingen-McMaster exchange programme for the financial and administrative support in making my stay at McMaster possible in the first place. I would also like to thank Mr. B. G. Sayer and Mr. J. I. A. Thompson from the McMaster NMR Facility and especially Dr. D. W. Hughes for his invaluable contribution (not only) at the beginning of the project, for training me to operate the 500 MHz spectrometer, and for continued helpful technical advice in the more advanced stages.

Dr. S. A. St.Pierre kindly supplied us with ever increasing amounts of dynorphin A-(1-13), Prof. Dr. A. D. Bain contributed helpful discussions and a T_1 calculation program, and Prof. Dr. M. A. Brook introduced me to the world of main-frame computing and the operation of molecular mechanics software packages.

I am indebted to Dr. P. K. Mishra for the operation of the 620 MHz spectrometer at the NMR Facility for Biomedical Studies, Carnegie-Mellon University, Pittsburgh, U.S.A, and wish to thank him and Prof. Dr. A. A. Bothner-By for beneficial discussions.

Professors Dr. R. A. Bell, Dr. B. E. McCarry, and Dr. E. Nieboer contributed promising suggestions during supervision of the project, and Dr. R.

F. Epand, Mr. A. R. Stafford, Mr. J. J. Cheetham, Mr. R. Bottega, Ms. B. Sweet, and Ms. L. Kush helped in so many minor matters, that these are too numerous to mention. I would also like to thank Dr. Leon van Gorkom for useful discussions in the terminal stages of the project.

Above all, I am very much indebted to Prof. Dr. R. M. Epand for continued enthusiastic support and constant positive motivation during the process of this project.

TABLE OF CONTENTS

LIST OF TABLES

LIST OF FIGURES

SYMBOLS and ABBREVIATIONS

SYMBOLS

In order to remain in agreement with conventional usage, some symbols have multiple meanings. The appropriate meaning should be obvious from the respective circumstances.

[]	reference
A	Absorbance
A_L	Absorbance for left circularly polarized light
A_R	Absorbance for right circularly polarized light
b	sample path length (expressed in cm)
B_i	effective field at a nucleus i
B_0	applied external static magnetic induction field or flux density
B_1	radio frequency oscillating magnetic induction field or flux density perpendicular to B_0
c	concentration (expressed in mol/L)
C	natural isotopic abundance (in %)
C	number of cycles (in NMR pulse sequence)
CD_3OD	perdeuterated (d_4-) methanol
CD_3OH	partially deuterated (d_3-) methanol
c_{lip}	lipid concentration
c_{pep}	peptide concentration
D	^2H
DC_H	decision constant for an α-helical conformation
DC_S	decision constant for a ß-strand conformation
$d_{N\alpha}(i,i)$	internuclear distance between the backbone amide proton and the alpha proton of the same amino acid residue
D_2O	^2H_2O
$d_{\alpha N}(i,i+1)$	internuclear distance between the alpha proton of the amino acid residue i and backbone amide proton of the following residue (i+1)
E	energy
f_a	relative population of rotamer state a (for χ_1 = -60°)
f_b	relative population of rotamer state b (for χ_1 = 180°)
f_c	relative population of rotamer state c (for χ_1 = 60°)
f_r	fraction of random coil content
f_t	fraction of ß-turn content
f_α	fraction of α-helical content
$f_ß$	fraction of ß-strand content
F_1	frequency domain obtained through FT of t_1

F_2	frequency domain obtained through FT of t_2
I	spin quantum number
I	intensity of an NMR resonance line
I	nuclear spin operator (components $\mathbf{I}_x$, $\mathbf{I}_y$, $\mathbf{I}_z$)
I_S	intensity of signal of I on saturation of S
I_0	initial intensity of signal of I
I_2	nucleus flip change in units of $\pi/2$'s (T_1 estimation)
I_3	normalised intensity of the largest point (T_1 estimation)
^nJ	nuclear spin-spin coupling constant through n bonds
$^3J_{HN\alpha}$	vicinal coupling constant between NH and adjacent αH
k	rate of exchange
k'	apparent first-order exchange rate (= k·c(solvent))
nK	n·1024 data points
m	mass (expressed in g)
M_r	molar mass (expressed in g/mol)
m_i	magnetic component quantum number (eigenvalue of $\mathbf{I}_z$)
m_T	total magnetic quantum number for a spin system
N	number of directly bonded protons attached to each carbon
n	amount of substance (expressed in mol)
n_i	amount of the substance i
P	nuclear angular momentum = spin
P_z	z-component of P
$r_{intr.}$	intraresidue distance $d_{N\alpha}(i,i)$, used only in equations
$r_{seq.}$	sequential distance $d_{\alpha N}(i,i+1)$, used only in equations
R_i	rotational strength (of a CD band)
R_1	spin-lattice (longitudinal) relaxation rate constant = T_1^{-1}
R_2	spin-spin (transverse) relaxation rate constant = T_2^{-1}
S_0	initial intensity of signal of S (NOE)
T_C	gel to liquid crystalline phase transition temperature
t_1	(incremented) evolution time
T_1	spin-lattice (longitudinal) relaxation time constant
t_2	acquisition time
T_2	spin-spin (transverse) relaxation time constant
T_{2*}'	field inhomogeneity contribution to T_2^*
T_2^*	total dephasing time constant for the x and y components of the bulk magnetization
V	volume (expressed in L)
x	axis perpendicular to the direction of B_0
x	mole fraction
x_i	mole fraction of the substance i = $n_i / \Sigma n$
x_{meth}	mole fraction of methanol

y	axis perpendicular to the direction of B_0
z	direction of the applied external magnetic field, B_0
α'	upfield α proton resonance (downfield resonance not explicitly symbolized)
β'	upfield β proton resonance (downfield resonance not explicitly symbolized)
γ	magnetogyric ratio
γ'	upfield proton resonance (downfield resonance not explicitly symbolized)
δ	angle separating consecutive residues along the peptide backbone (=360°/(# residues/turn), e.g. 100° for an α-helix)
δ	chemical shift (in ppm)
δ'	upfield δ proton resonance (downfield resonance not explicitly symbolized)
ΔA	differential absorbance (= A_L-A_R)
ΔE	energy difference
Δ_i	half-band width at $[\theta_i]/e$
Δm	change in magnetic quantum number
Δm_T	change in total magnetic quantum number of the spin system
$\Delta\nu$	chemical shift difference (expressed in Hz)
$\Delta\nu_{\frac{1}{2}}$	full width (in Hz) of a resonance line at half hight
ϵ	molar absorptivity (expressed in $dm^3 \cdot mol^{-1} \cdot cm^{-1}$)
ϵ_L	molar absorptivity for left circularly polarized light
ϵ_R	molar absorptivity for right circularly polarized light
θ	ellipticity (expressed in deg, measured in mdeg)
θ	dihedral angle
θ_{corr}	baseline corrected ellipticity
$\theta_{HN\alpha CH}$	$\lvert\phi$-60°$\rvert$ for torsional angle ϕ of L-amino acids
$[\theta]$	mean residue ellipticity (expressed in deg $\cdot$ cm^2 / dmol)
$[\theta]_\alpha$	mean residue ellipticity of the α-helix reference
$[\theta]_\beta$	mean residue ellipticity of the β-strand reference
$[\theta]_t$	mean residue ellipticity of the β-turn reference
$[\theta]_r$	mean residue ellipticity of the random coil reference
$[\theta]_{222}$	mean residue ellipticity at 222 nm
$[\theta']$	molar ellipticity (expressed in deg $\cdot$ cm^2 / dmol)
$[\theta_i]$	mean residue ellipticity at the CD band maximum
λ_i	wavelength of the CD band maximum
λ_{max}	wavelength of maximal absorbance
μ	hydrophobic moment
μ	nuclear magnetic moment
ν	frequency of radiation

ν_c	carrier frequency of the radiation
ν_i	Larmor precession frequency of the nucleus i
ν_0	spectrometer operating frequency
ν_1	frequency axis obtained through FT of t_1
ν_2	frequency axis obtained through FT of t_2
σ	shielding constant (in ppm)
τ	fixed delay (in NMR pulse sequences)
τ_c	correlation time
τ_m	mixing time (in NOESY pulse sequence)
ϕ	torsional angle $HNC_\alpha H$ [IUPAC-IUB, 1970]
ϕ	(as a subscript) phase of pulse in NMR phase cycling
$\propto$	proportional to

ABBREVIATIONS

aa	amino acid
BB	broadband ^{1}H decoupling gated on (NMR pulse sequences)
Boc	tert.-Butyloxycarbonyl- (amino acids)
BDNR	block diagonal Newton-Raphson (minimization algorithm)
BPTI	basic pancreatic trypsin inhibitor
CAR's	conformation-activity relationships
CAMELSPIN	cross-relaxation approriate for minimolecules emulated by locked spins
COSY	correlated spectroscopy
CD	circular dichroism
CP	composite pulse
CPD	composite pulse decoupling
CPU	central processing unit
CW	continuous wave (NMR spectroscopy)
CYCLOPS	cyclic ordered phase scheme
Da	Dalton (unit of mass equal to 1.0000 on the atomic mass scale)
DMPC	dimyristoyl-L-3-phosphatidylcholine
DMPG	dimyristoyl-L-3-phosphatidylglycerol
DMSO	dimethyl sulfoxide
DO	broadband ^{1}H decoupling gated off (NMR pulse sequences)
DQF	double quantum-filtered
Dyn.A-(1-13)	Dynorphin A-(1-13)
Dynorphin A-(1-13)	Dynorphin A-(1-13)-peptide (IUPAC-IUB, 1984)
FT	Fourier transform (NMR or IR spectroscopy)
GOR	Garnier-Osguthorpe-Robson algorithm
GPI	guinea pig ileum (assay)
IC_{50}	concentration for 50% inhibition
INEPT	Insensitive Nuclei Enhanced by Polarisation Transfer (NMR pulse sequence)
IR	Infrared (spectroscopy)
IR-ATR	Infrared Attenuated Total Reflection (spectroscopy)
M	as a unit = mol/L
mdeg	millidegrees
MLV's	multilamellar vesicles
mrc	mean residue concentration (= # residues · c)
MVD	mouse vas deferens (assay)
NOE	Nuclear Overhauser Effect
NOESY	Nuclear Overhauser and Exchange Spectroscopy

NMR	Nuclear Magnetic Resonance
POPC	1-palmitoyl-2-oleoyl-L-3-phosphatidylcholine
PRCG	Polak-Ribiere conjugate gradient (minimization algorithm)
ppb	parts per billion (1 ppb = 10^{-3} ppm)
ppm	parts per million (e.g. Hz/MHz)
RD	relaxation delay
RELAY	$^1H,^1H$ relayed COSY
RMS	root mean square
ROE	rotating frame nuclear Overhauser effect
$ROE_{intr.}$	intraresidue ROE
$ROE_{seq.}$	sequential ROE
ROESY	rotating frame Overhauser enhancement spectroscopy (= 2-D CAMELSPIN)
SAR's	structure-activity relationships
SD	steepest descent (energy minimization algorithm)
SDS	sodium dodecyl sulfate
SEFT	spin-echo fourier transform (NMR spectroscopy)
SUV's	small unilamellar vesicles
TFE	2,2,2-trifluoroethanol
TMS	tetramethylsilane
1-D	one-dimensional
2-D	two-dimensional
3-D	three-dimensional

PREFACE

DIVINUM EST OPUS SEDARE DOLOREM

The history of humanity's continuous struggle to alleviate pain extends at least 4000 years back to the Sumerians, where the earliest evidence for the cultivation of the poppy for extracting its powerful sap was found [Benedetti and Premuda, 1990, p. 3f.]. In a latinization of the Greek word *opos*, meaning juice, the Romans referred to this substance as "opium" [ibid, p. 2]. Hippocrates, Dioscorides, Galen, and other early physicians cherished opium's power to "*lull all pain and anger and bring relief to every sorrow*" [Gates, 1966].

By the first century A.D. at the latest, however, it was well known that the use of this drug had side effects: "Ye seed of the black poppy is given to drink with wine for ye flux of ye belly & ye womanish flux...but the liquor itself...is a pain easer & a sleep causer, & a digester, helping coughes...But being drank too much, it hurts, making men lethargic & it kills" [Dioscorides, translated by Goodyer, 1655, quoted by Tainter, 1948]. In the eighteenth century, the so-called Lancaster or Quaker's "black-drop", a liquid preparation of opium was a celebrated household remedy [Tainter, 1948, p. 7]. The recognition of the addiction potential is well documented by Thomas DeQuincey's "*Confessions of*

an English Opium Eater" written in 1821 [Benedetti and Premuda, 1990, p. 23]. Morphine dependency became known as the "soldiers disease", because it was prescribed freely to treat the pain suffered by wounded soldiers during the Franco-Prussian and American civil wars [ibid, p. 26f.].

A major advance in the understanding of the principles of analgesia was accomplished by Sertürner [1806] in 1803, who isolated the active constituent of opium and named the substance "morphine" after Morpheus, the Greek god of dreams [Tainter, 1948, p.8]. This stimulated attempts to find a substitute drug that would not be "burdened by this undesirable property" [Archer, 1986].

The discovery of endogenous opioid peptides caused the search for a powerful non-addictive analgesic to focus also on this class of substances. One very potent opioid peptide is dynorphin A-(1-13).

FOREWORD(S)

"The search for truth is in one way hard and in another easy, for it is evident that no one of us can ever master it fully nor miss it wholly. Each of us adds a little to our knowledge of nature and from all the facts assembeled arises a certain grandeur."

Aristoteles [350 B.C.]

"...conformational-biological activity relationships are not only an important approach to understanding the physical-chemical basis of life, but an essential requirement for determining the underlying principles that govern living processes."

V. J. Hruby [1985b, p. 2]

"...the study of *'the real thing'*, i.e. the natural flexible peptide, is at least as useful as the study of its rigid analogues."

P.A. Temussi et al. [1989, p. 96]

"Unfortunately, determining relationships between structure and activity in small peptides is an elusive goal"

G.D. Rose et al. [1985, p. 36]

"Laß die Moleküle rasen,
was sie auch zusammenknobeln!
Laß das Tüfteln, laß das Hobeln,
heilig halte die Ekstasen!"

Christian Morgenstern [1972, p. 15]

1. INTRODUCTION

The objective of this thesis project is to contribute to our knowledge on the membrane-mediated conformation of the opioid peptide dynorphin A-(1-13). Initially, some general considerations pertinent to the bioactive conformation of peptides are discussed. After focusing on general aspects of opioid peptides and receptors (section 1.1), a more detailed description of the opioid peptide dynorphin A-(1-13), its extraordinary biological and pharmacological effects (1.2), its structure-activity relationships (1.3), and the present knowledge and models of the molecular mechanism of its action (1.4 to 1.6) are presented.

In the highly complex multicellular systems that human beings represent, specific and complex inter- and intracellular communication is essential for the ability of these systems both to respond rapidly to changes in their environment and to have a long term influence in the differentiation and development of cells and organs [Hruby, 1985b]. The most numerous and important messengers of intercellular communication are proteins and peptides, both in the nervous system (neuropeptides [Alberts et al., 1989, p. 1093f.]), where they act as neuromodulators, and in the endocrine system, where they act as hormones [Alberts et al., 1989, p. 682f.].

As peptides are generally too hydrophilic to pass directly through the lipid bilayer of a target-cell membrane, they elicit a cellular response by binding to specific membrane proteins termed receptors. Most peptide hormones and neurotransmitters appear to interact with a variety of receptors on different cell types [Hruby et al., 1983, p. 518]. To date, it is still unclear whether these multiple receptor types or subtypes are derived from different genes and therefore have completely unrelated amino acid sequences or whether the different ligand specificity is due to post-transcriptional modification of closely related proteins [Hruby, 1990]. The multiplicity of "the opioid receptor" has been a major focus of research in the last 25 years. The findings relevant to the framework of this project are summarized in section 1.1.

In order to understand at a molecular level the mechanism of a peptide hormone's biological action before, during and after binding to the receptor, the conformation, flexibility, and dynamics of the peptide have to be analyzed. The interaction of a peptide agonist with its receptor must involve complementarity in terms of charge distribution, hydrophobicity and hydrogen bonding capacity of the two molecular surfaces [Blundell and Wood, 1982]. Conformational flexibility may be a biological necessity as conformational changes may be required upon binding to the receptor in order to activate the biological response [ibid]. Also flexibility may be important for the clearance of the peptide from circulation or deactivation by proteolysis [ibid]. So although it is tempting to reduce the conformational flexibility of the peptide through the design of more rigid (cyclic) analogues [Hruby, 1983], this approach is inherently a reductionist one, as only

one specific set of conformational requirements can be probed (e.g. receptor binding). This means that only through the study of "the real thing", i.e. the natural flexible peptide [Temussi et al., 1989], will we be able to analyze the full range of conformational flexibility and dynamics.

To this end, experimental and theoretical approaches are employed (vide infra). The most outstanding techniques are nuclear magnetic resonance (NMR) spectroscopy (Chapters 4 to 6) and molecular dynamics (in conjunction with energy minimization, Chapter 7), respectively.

1.1. Opioid Receptors and Opioid Peptides

1.1.1. Opioid Receptors

In the case of "the opioid[1] receptor", the existence of multiple opioid receptors was first suggested by Porthoghese [1965] and substantiated by the observation of pharmacological differences between morphine and synthetic analogues (ketocyclazocine [Michne and Albertson, 1972] and SKF-10,047) in chronic spinal dog preparations, which indicated the existence of three types of opioid receptors, named μ, κ and σ, respectively [Martin et al., 1976].

---

[1] "opiates" are plant alkaloids derived from the opium poppy [Hughes and Kosterlitz, 1983], an "opioid" is any compound that is opiate-like in its action [Goldstein, 1984], the respective receptors are termed "opioid receptors" rather than "opiate receptors".

In 1975, Hughes, Kosterlitz and collaborators discovered two endogenous pentapeptides in the porcine brain with potent opioid activity [Hughes et al., 1975]: [Met]enkephalin and [Leu]enkephalin. This was the first evidence that the brain produces its own opioids. Profiles in two bioassay systems, which disagreed with the assumption of a single opioid receptor, led to another distinction of opioid receptor subtypes [Lord et al., 1977; Chang and Cuatrecasas, 1979; Childers et al., 1979]. Opiates were more potent than enkephalins in inhibiting electrically induced contractions of the longitudinal muscle of the guinea pig ileum (GPI assay) while the opposite applied to the mouse vas deferens (MVD) assay. It was concluded that two different receptor subtypes, μ (for **m**orphine, in the GPI) and δ (for **d**eferens, in the MVD) predominate in the two tissues. To date, there is a consensus in assuming the existence of at least three distinct opioid receptor types in the CNS with μ, δ and κ sites [Mansour, 1988; Rees and Hunter, 1990]. The σ-site has been shown not to be an opioid receptor [Zukin and Zukin, 1981].

A precise relationship between the transmembrane signal transduction mechanisms and the functional effects of opioids has not yet been clearly established [Rees and Hunter, 1990]. All three major opioid receptor types are coupled to adenylate cyclase in at least some tissues. However there is no evidence that adenylate cyclase mediates opioid analgesia [Loh and Smith, 1990]. Opioid mediated inhibition of transmitter release involves either a reduction in the influx of Ca^{2+} through activation of κ receptors or an increased outward

K^+ conductance through Ca^{2+}-activated K^+ channels following activation of either μ or δ receptors [Rees and Hunter, 1990].

Many full or partial purifications of opioid receptors have been reported [Maneckjee et al., 1985; McLawhon et al., 1983; Simonds et al., 1985; Zipser et al., 1988] but there are considerable discrepancies regarding the characterization of the preparations (e.g. molecular weights; see a recent review by Loh and Smith [1990] for a detailed discussion).

1.1.2. Opioid Peptides

Since the discovery of the enkephalins, many more peptides from brain and pituitary have been isolated (e.g. the endorphins [Bradbury et al, 1976; Li and Chung, 1976; Lin et al., 1976] leading to the proposal of an ϵ-receptor for β-endorphin [Li et al. 1980; Barnard and Demoliou-Mason, 1983; James, 1986]) and synthetic peptides with opioid properties have been prepared [Fukushima et al., 1980; Gottschlich, 1990; Hruby, 1990; Kaiser, 1989a,b; Kaiser and Kézdy, 1984; Kimura et al., 1990; König, 1980; Morley, 1983; Schiller, 1988; Schwyzer, 1988; Taylor, 1990; Taylor and Kaiser, 1986, 1989; Vaughn and Taylor, 1989]. One of the main hopes driving a great number of these activities was that of finding a powerful analgesic with no addiction liability [Millan, 1986, 1990]. This

was based on the hope that the "the human body would not synthesize compounds which would be addictive" [Archer, 1986][2].

1.2. Dynorphin and Dynorphin A-(1-13)

The opioid peptide dynorphin was first isolated from the porcine pituitary by Goldstein and associates in 1979 [Goldstein et al., 1979]. Since then it has been purified from the rat pituitary [Goldstein et al., 1981] and the porcine duodenum [Tachibana et al., 1982] and has been identified in the mammalian spinal chord and dorsal root ganglia [Botticelli et al., 1981], in the bovine adrenal medulla [Lemaire et al., 1982], and in the placenta [Lemaire et al., 1983]. Its extraordinary potency was demonstrated in the GPI assay: dynorphin (with an IC_{50} of 630 pM!) is 730 times more potent than [Leu]enkephalin, its N-terminal pentapeptide [Goldstein et al., 1979].

A considerable specificity for the κ opioid receptor in the GPI assay [Chavkin and Goldstein, 1981] and in binding assays with membranes from the guinea pig brain [Chavkin et al., 1982] was reported for dynorphin and its N-terminal tridecapeptide fragment dynorphin-(1-13). The different specificities of the enkephalins (δ), β-endorphin (ϵ) and dynorphin (κ) for the different receptor subtypes is particularly striking, because they all possess the same N-terminal tetrapeptide sequence (Figure 1.1).

---

[2] This hypothesis has been refuted by recent evidence on the biosynthesis of morphine by mammalian liver [Weitz et al., 1987; Kosterlitz, 1987].

[Met]enkephalin	**Tyr-Gly-Gly-Phe**-Met
β-Endorphin	**Tyr-Gly-Gly-Phe**-Met-Thr-Ser-Glu-Lys-Ser-Gln-Thr-Pro-Leu-Val-Thr-Leu-Phe-Lys-Asn-Ala-Ile-Ile-Lys-Asn-Ala-Tyr-Lys-Lys-Gly-Glu
[Leu]enkephalin	**Tyr-Gly-Gly-Phe**-Leu
Dynorphin	**Tyr-Gly-Gly-Phe**-Leu-Arg-Arg-Ile-Arg-Pro-Lys-Leu-Lys-Trp-Asp-Asn-Gln

Figure 1.1. Structures of opioid peptides. Adapted from: [Morley, 1983].

These opioid peptides are derived from three biosynthetic precursors [Numa, 1984] of approximately 260 amino acids each including a signal peptide. The corticotropin-β-lipotropin precursor (ACTH-β-LPH precursor or alternatively prepro-opiomelanocortin [Nakanishi et al., 1979]) contains the sequences of β-endorphin (the 31 carboxy-terminal residues of β-lipotropin) and the non-opioid peptide hormones ACTH, α-MSH, β-MSH, and γ-MSH [Civelli et al., 1984]. [Met]Enkephalin and [Leu]enkephalin sequences [Noda et al., 1982] are found on preproenkephalin [Udenfriend and Kilpatrick, 1984] and preprodynorphin [Kakidani et al., 1982] contains the sequences of neoendorphin, dynorphin (or dynorphin A), and leumorphin (whose 13 amino-terminal residues represent rimorphin (or dynorphin B).

On all three precursors these peptide units are bounded by basic amino acid residues, mainly Lys-Arg, which are thought to represent preferred sites of proteolytic cleavage [Numa et al., 1984].

The validity of the conclusions drawn by Goldstein's group concerning the κ specificity of dynorphin has been questioned (Smith and Lee, 1988). Recent evidence obtained by comparison of the pharmacological profile of dynorphin

with that of the diaminocyclohexane derivative U-50,488H (a highly specific κ agonist developed by Upjohn, cf. [James, 1986]) in the spinal chord [Jhamandas et al., 1986] suggests that the dynorphin receptor is different from the κ receptor [Stevens and Yaksh, 1986].

The vast spectrum of pharmacological effects of dynorphin has recently been reviewed [Smith and Lee, 1988]. Apart from analgesic properties, pronounced effects on the mammalian motor system, cardiovascular effects, effects on respiration, temperature control, feeding behaviour, hormones, stress and trauma, and in tumour formation have been reported [Smith and Lee, 1988]. As is the case for its effects on temperature control and respiration, dynorphin's properties regarding the modulation of analgesia are dependent on whether the animal is morphine-naive or morphine-tolerant. Although dynorphin itself is not analgesic in the brain, it can substitute for morphine in morphine-dependent animals as was shown in studies with rats [Khazan et al., 1983], monkeys [Aceto et al., 1982], and human heroin addicts [Wen and Ho, 1984]. Termination of dynorphin administration resulted in no withdrawal signs in rats [Khazan et al., 1983]. This finding has fuelled speculation that a detailed knowledge of the mechanism of action of dynorphin could lead to the development of a non-addicting powerful analgesic irrespective of whether the dynorphin receptor is actually identical to the κ-receptor or not. Dynorphin has been reported to be involved in the endogenous analgesia of pregnancy [Sander et al., 1989].

Recently, a non-opioid inhibition of a growth-hormone releasing peptide has been demonstrated for dynorphin [Codd et al., 1990][3].

The N-terminal fragment dynorphin A-(1-13) has approximately the same high potency as the natural heptadecapeptide [Goldstein et al., 1979; Tachibana et al., 1982], so that most of the attention has focused on the tridecapeptide (Tyr^1-Gly^2-Gly^3-Phe^4-Leu^5-Arg^6-Arg^7-Ile^8-Arg^9-Pro^{10}-Lys^{11}-Leu^{12}-Lys^{13}).

1.3. Structure-Activity Relationships for Dynorphin A-(1-13)

Chavkin and Goldstein [1981b] have demonstrated the following structure-activity relationships for dynorphin A-(1-13):

- removal of Tyr^1 abolishes the biological activity

- substitution of Gly^2 by $D\text{-}Ala^2$ reduces potency. This is the opposite effect compared to the corresponding enhancement of potency in the case of [Leu]enkephalin indicating a different tetrapeptide "message"[4] pocket for the dynorphin receptor.

---

[3] Evidence for the non-opioid characteristics are the similar potency of the non-opioid peptide des-[Tyr]-dynorphin (cf. opioid "structure-activity relationships") and the weak inhibition by the κ-selective ligand U50,488 [Codd et al., 1990].

[4] The concept of "message" and "address" sequences was introduced by Schwyzer [1977]. The "message" sequence is comprised of those amino acid residues that are responsible for triggering a given response. The "address" segment represents those residues that add to the specificity of binding to the receptor without being able to trigger the response.

- successive removal of the carboxy-terminal amino acids from dynorphin A-(1-13) demonstrates important contributions of Lys^{13}, Lys^{11}, Arg^{7} to the potency (in order of increasing importance).

- both the introduction of a Gly between Leu^{5} and Arg^{6} and the deletion of Arg^{6} result in a decrease in potency by 90%, demonstrating the importance of the precise location of the critical Lys^{13}, Lys^{11}, and Arg^{7} groups.

1.4. Molecular Mechanism of Dynorphin's Action

The basis of dynorphin's unusual ability to bind with high affinity to multiple opioid receptors is not known, but it may involve interaction with lipids. Sargent and Schwyzer [1986] have emphasized the importance of the membrane lipid phase as a catalyst for peptide-receptor interactions. The flexible peptide agonist is assumed to have little, if any, order in the intercellular fluid. This assumption is compatible with experimental evidence concerning peptide hormones in general [Blundell and Wood, 1982] and the following experimental observations: CD [Maroun and Mattice, 1981; Kojro et al., 1987], ^{1}H-NMR [Zhou and Gibbons, 1986; Renugopalakrishnan et al., 1988], IR/ATR [Erne et al., 1985] , FT-IR [Surewicz and Mantsch, 1989] and laser Raman [Rapaka et al., 1987] studies have suggested that dynorphin (1-13) exhibits random structure in aqueous solution. Fluorescence energy transfer studies [Schiller, 1983] of [Trp^{4}]-

dynorphin (1-13) and the heptadecapeptide indicate an extended conformation in buffered solution.

The peptide is electrostatically accumulated at the surface of the membrane bilayer. The first contact upon approaching the cell membrane is much more likely to be with the lipid phase than directly with the receptor. In the membrane-water interphase, the peptide assumes a preferred conformation (and orientation) on the basis of its amphiphilicity, a property which is quantified by its hydrophobic moment [Eisenberg et al., 1982]. The membrane-bound conformation and orientation of the peptide agonist would thus be the one meeting the receptor requirements rather than the random structures in solution. In addition to encouraging a conformational change, the membrane catalyst would reduce the three-dimensional search for the receptor into a two dimensional process [Schwyzer, 1986b].

This model could also, for instance, explain the heterogeneity of the opioid receptor subtypes as the membrane-mediated conformation would depend on the exact nature of the lipid environment [Sargent and Schwyzer, 1986].

1.5. Peptide Structures Associated with Peptide-Lipid Interactions

One mechanism for the interaction of peptides with lipids is the formation of amphipathic structures on the part of the peptide [Epand, 1983; Kaiser and Kézdy, 1983]. In addition to polar amino acid side chains, the amide bonds linking amino acids residues are also polar and are hydrogen-bonded to water

when the peptide is in aqueous solution. These hydrogen bonds have to be replaced by intramolecular hydrogen bonds in the lipid bound form, although some non-hydrogen bonded amides could exist in the membrane if the loss of energy is compensated by other favourable interactions [Epand and Epand, 1991].

1.5.1. The Amphiphilic β-Strand

One possible structure is an amphiphilic β-strand, as has been shown for the interaction of an atrial natiuretic peptide with lipid [Surewicz et al., 1987].

1.5.2. The Amphipathic Helix

The most familiar amphipathic structure of peptides is the amphipathic helix. Originally identified as an important structural feature in the folding of globular proteins [Perutz et al, 1965], the relevance to protein-lipid interactions was first proposed for serum apolipoproteins [Segrest et al., 1974]. The potential importance of the amphipathic helix for the binding of peptide hormones to membranes was first established for glucagon-lipid interactions [Epand et al., 1977] and has since been demonstrated for β-endorphin [Kaiser et al., 1984], salmon calcitonin and synthetic calcitonin derivatives [Epand et al., 1986]. These non-homologous polypeptide hormones share common properties [Epand, 1983]. They are linear sequences of approximately 30 amino acids and their hydro-

phobic residues are regularly spaced at every third or fourth amino acid residue. The amphipathic helix has also been associated with mitochondrial signal sequences, ion channels, cytotoxic peptides and pulmonary surfactant proteins [Epand and Epand, 1991; Kaiser and Kézdy, 1987].

1.6. The Membrane-Mediated Conformation of Dynorphin A-(1-13)

Schwyzer has proposed a mechanism of the interaction of dynorphin A-(1-13) with a model membrane [Schwyzer, 1986a]. The conformation of the peptide upon binding to the membrane is assumed to be mainly α-helical with the first nine residues forming a helix followed by a random coil segment consisting of Pro^{10} to Lys^{13}. Although there has been some experimental evidence in support of dynorphin (1-13) adopting a helical conformation after binding to the lipid membrane [Maroun and Mattice, 1981; Erne et al., 1985; Bean et al., 1988; Rapaka et al., 1987b], pharmacological studies indicate that the replacement of the helix-breaking Pro^{10} residue by helix-forming residues results in less potency [Turcotte et al., 1984] or decreased selectivity for the κ opioid receptor [Nakajima et al., 1988]. Conversely, a D-Pro^{10} containing analogue of dynorphin A-(1-11) has been reported [Gairin et al., 1984, 1986] to be more potent and just as selective as U-50,488H, the most κ-selective ligand. These results indicate that an α-helical conformation does not seem to be a requirement for the κ opioid receptor.

The hydrophobic moment profile [Eisenberg et al., 1984] and preliminary experiments suggested to us that the lipid-induced conformation is not α-helical. The tridecapeptide has a distinctly shorter chain length than the aforementioned polypeptide hormones: the presence of the helix breaking Pro^{10} limits the occurrence of a helical structure to the first nine residues. The occurrence of positive charges at Arg^6, Arg^7, and Arg^9 decreases the amphiphilicity of the postulated nonapeptide helix, so that its formation in a membrane environment intuitively seems unlikely. Indeed, regular alternation of hydrophilic and nonpolar side chains in the amino acid sequence from Arg^7 to Lys^{13} indicates the possibility of the formation of an amphiphilic β-strand (vide infra).

1.7. Thesis Objectives

The objective of this project was to further clarify the nature of the membrane-mediated conformation of dynorphin A-(1-13) with the help of circular dichroism (CD) spectropolarimetry (cf. Chapter 3) and various homo- and heteronuclear one- and two-dimensional nuclear magnetic resonance (NMR) techniques (cf. Chapters 4 - 6). Prior to this, predictive algorithms were employed to investigate conformational characteristics of dynorphin A-(1-13) and to create feasible reference models for the interpretation of the experimental data (cf. Chapter 2). The findings were incorporated into a model in Chapter 7. The thesis was summarized in Chapter 8.

2. INITIAL THEORETICAL CONSIDERATIONS AND PREDICTIVE ALGORITHMS

The interpretation of NMR data regarding conformational features is greatly facilitated by prior knowledge on conformational aspects of the molecule under investigation. Without access to a distance geometry[1] computer program (cf. [Lautz et al., 1989]), the best approach is to compare expected NMR parameters of specific conformational [Hagler, 1985] and dynamic [Jardetzky, 1979] models with experimental results. The methods described below have all been developed for proteins and are not necessarily applicable to short peptide fragments, so all results and interpretations should be viewed with caution.

The purpose of this chapter was to examine some conformational characteristics of the opioid peptide dynorphin A-(1-13) based on predictive algorithms, compare these characteristics to the model proposed by Schwyzer [1986a], and present possible models which could be tested for validity by comparison with the results of the NMR studies.

---

[1] Recently, it has been demonstrated [Metzler et al., 1989], that standard distance geometry calculations generally sample a very limited region of conformational space and preferentially generate extended structures.

As was already discussed in Chapter 1, peptides can interact with lipids through the formation of amphipathic structures. One method designed to quantify the amphiphilicity of a periodic secondary structure utilizes the concept of the hydrophobic moment (cf. section 2.1.1). This method does not, however, yield information on the probability of the amphiphilic structures.

In the case of the proposed helical conformation, statistical mechanical theory of helix-coil transitions allows the calculation of helix probabilities for the individual amino acid residues (i.e. the calculation of a helix probability profile, section 2.1.2). The advantage of this method is that it allows the evaluation of the effect of anionic lipids[2] , which cause most biological membranes to have a net negative fixed charge potential [Schwyzer, 1986b].

More general secondary structure prediction methods (for reviews cf. [Argos and MohanaRao, 1986; Fasman, 1989; Kabsch and Sander, 1983; Rooman and Wodak, 1988; Schulz, 1988]) have been used extensively to delineate regions of ordered structures in amino acid sequences of soluble proteins. In general, they distinguish between four states, i.e. regions of α-helical, β-strand, turn, and coil conformation. One of the most sophisticated methods is the method of Garnier, Osguthorpe, and Robson [Garnier et al., 1978], which will be referred to as the GOR method (section 2.1.3). In order to use structures predicted in such a way as models of reference for NMR studies, they have to optimized to a minimum of potential energy. This is especially important for the

[2] An analogous method based on the β-sheet to coil transition has been introduced [Mattice, 1989] but it does not allow the evaluation of the effect of anionic lipids.

discussion of the interresidue relationships in different conformations. Energy minimization is achieved through a molecular mechanics method (section 2.1.4).

2.1. Methods

2.1.1. Hydrophobic Moment Calculations

The selectivity for the kappa opiate receptor site is not only one for specific basic residues [Chavkin and Goldstein, 1981] but is also governed by the amphiphilicity of the agonist [Schwyzer, 1986b]. Dynorphin A-(1-13) displays significant amphiphilicity in its primary structure [Erne et al., 1985]. The N-terminal pentapeptide is hydrophobic, whereas five charged side chains in the C-terminal eight residues renders this end hydrophilic.

The amphiphilicity of the secondary structure of a peptide is quantified by its hydrophobic moment [Eisenberg et al., 1982a,b, 1989]. The hydrophobic moment of a peptide is computed as a function of the angle separating consecutive residues along the backbone, δ (= 360°/(# of residues per turn). For an α-helix δ is 100°, for a β strand it is 160° to 180°.

The hydrophobic moment, μ, can be calculated from the relationship [Eisenberg et al., 1984]:

$$\mu(\delta) = \{[\Sigma H_n \sin(\delta_n)]^2 + [\Sigma H_n \cos(\delta_n)]^2\}^{1/2},$$

where H_n is the numerical hydrophobicity of the n'th residue. As different experimental and computational methods have been applied in order to obtain hydrophobicity scales, the determined values tend to diverge. A consensus scale derived from the free energy of transfer of amino acid side chains from water to ethanol, from water to vapour, from the surface to the interior of a protein, and from aqueous to non-aqueous media has been obtained [Eisenberg et al., 1982b]. The values applied in the present case are listed in Table 2.1.

Table 2.1. Numerical hydrophobicities used for the calculation of the hydrophobic moment profiles.

Residue i	H_i	Residue i	H_i
Ile	0.73	Pro	-0.07
Phe	0.61	(Asn	-0.64)
Leu	0.53	(Gln	-0.69)
(Trp	0.37)	(Asp	-0.72)
Gly	0.16	Lys	-1.10
Tyr	0.02	Arg	-1.76

The hydrophobic moment of the dynorphin A fragments (1-8), (1-9), (1-13) and (1-17) were calculated for δ values from 80° to 180° in 10° increments.

2.1.2. Helix Probability Calculations

The helix-forming probability profiles for dynorphin A-(1-13) in water, anionic detergent, and in the presence of zwitterionic lipids were calculated as described by Epand et al. [1986] according to the Mattice theory [Mattice and Robinson, 1981a], a statistical mechanical theory of helix-coil transitions [Zimm and Bragg, 1959].

The probability for an amino acid residue to be in a helical state was calculated from the configuration partition function for the peptide, which consisted of statistical weight matrices for each amino acid residue. These in turn contained parameters denoting statistical weights for the propagation of a helical segment and for an amino acid residue i at either end of a helical segment and took into account nearest neighbour interactions (i-4 to i and i-3 to i+1). The statistical weights employed for amino acid residues in water were those listed by the Mattice group (cf. Table 2.2) from experimental data of model peptides.

For the calculation of the conformational properties of peptides in anionic detergent, the statistical weights (and therefore ultimately the probability of helix formation) were increased for cationic amino acid residues, leaving all other statistical weights unchanged [Mattice and Robinson, 1981a].

Table 2.2. Statistical weight parameters employed for calculations of the helix probability profiles for dynorphin A fragments in water and anionic detergent [Mattice and Robinson, 1981a].

	Aqueous Solution		Anionic Detergent	
	$\sigma \cdot 10^4$	s (at 30°C)	$\sigma \cdot 10^4$	s (at 30°C)
Tyr	66	0.96	66	0.96
Gly	0.1	0.615	0.1	0.615
Phe	18	1.069	18	1.069
Leu	33	1.14	33	1.14
Arg	0.01	1.017	500	1.7
Ile	55	1.11	55	1.11
Pro		0		0
Lys	1.0	0.947	500	1.7
Trp	70	1.06	70	1.06
Asp	50	0.63	50	0.63
Asn	0.1	0.806	0.1	0.806
Gln	6.0	0.97	6.0	0.97

a: Helical amino acid residues have a statistical weight of s_i, if they are in the interior of a segment.

b: Amino acid residues at either end of a helical segment have a statistical weight of $\sigma_i^{\frac{1}{2}} s_i$.

For calculations with peptides in the presence of zwitterionic lipids, an enhanced[3] probability of helix formation was taken into account, when side chains bearing charges of opposite signs were situated on the same side of the α-helix but are displaced from one another by one turn [Hamed et al., 1983]. In the case of dynorphin A-(1-13), this result was not expected to differ from that obtained for the peptide in water, as the peptide does not contain any negative charges at neutral pH (apart from the C-terminal carboxy group).

[3] = three- or four-fold; we assumed a threefold enhanced probability.

2.1.3. Four State Secondary Structure Prediction

Predictions based on statistical analyses of protein data bases are widely used in the prediction of protein secondary structure [Rooman and Wodak, 1988]. The overall accuracy of these methods does not exceed 56% [Kabsch and Sander, 1983]. The method of Garnier, Osguthorpe, and Robson [1978; Garnier and Robson, 1989] is mathematically more sophisticated and has a higher degree of accuracy than the most widely known Chou and Fasman [1978a,b] method [Kabsch and Sander, 1983]. The advantage of the GOR method is its ability to examine the interaction of side chains as far as eight residues away in either terminal direction and to weight the validity of the interaction according to statistical analysis of the available data [Garnier et al., 1978]. If the relative abundances of helical, extended chain, reverse turn, and random coil conformations have been determined by circular dichroism, the prediction can be optimized by adjusting the decision constants (parameters used in the decision between different conformational states [Garnier et al, 1978]).

Secondary structure predictions of the membrane-bound opioid peptide dynorphin A-(1-13) were computed on an IBM PS/2 using the Predict7 software package [Cármenes et al., 1989]. The predictions were performed, firstly, with the unbiased decision constants[4] ($DC_H = DC_S = 0$) and, secondly, with optimized

[4] DC_H = decision constant for an α-helical conformation
DC_S = decision constant for a ß-strand conformation

decision constants of DC_H = 158 and DC_S = -87.5 [Garnier et al., 1978]. These decision constants were selected according to the relative abundances of the secondary structural motifs as determined by circular dichroism studies on an aqueous solution of dynorphin A-(1-13) in the presence of DMPG vesicles (cf. Chapter 3).

2.1.4. Molecular Mechanics Energy Minimization

Molecular mechanics methods [Burkert and Allinger, 1982] are at present the only technique (as opposed to ab initio and semi-empirical quantum mechanics methods) capable of calculating and minimizing the potential energy of a tridecapeptide.

The potential energy "surface"[5] is expressed by an empirically derived set of functions, referred to as the "force field". The force field contains adjustable parameters derived from experimental data of model compounds (e.g. equilibrium bond lengths and angles from microwave and neutron diffraction studies, torsional angles from NMR studies) that have been optimized to obtain the best fit of calculated and experimental properties (e.g. geometries, conformational energies, heats of formation) of other compounds. The underlying assumption

[5] The potential energy "surface" is the multidimensional "surface" that describes the energy of the molecule in the ground electronic state as a function of nuclear positions [Burkert and Allinger, 1982].

in molecular mechanics is that corresponding parameters may be transferred from one molecule to another.

We employed the AMBER force field introduced by Kollman and collaborators [Weiner et al., 1984, 1986]. It includes bonding interactions (acting to restore equilibrium bond lengths, bond angles, and torsional angles), non-bonding interactions (steric (van der Waals), electrostatic, and improper[6] torsional interactions) and an additional term for hydrogen-bonded interactions. In order to make more efficient use of computer time, it is implemented as a "united atom" field. CH, CH_2, and CH_3 groups are represented as spheres, i.e. only hydrogens on heteroatoms are explicitly considered [Weiner et al., 1984]. This compromise can lead to less than optimum fits of the calculated data with the experimental data in some cases [Weiner et al., 1986], but should not affect our calculations at the present level of sophistication (see below).

We employed a combination of minimization algorithms. The starting structure was initially minimized by a conjugate gradient (PRCG) method [Fletcher and Reeves, 1964] modified by Polak and Ribiere [1969], a first-derivative technique [Burkert and Allinger, 1982]. In order to improve the convergence, the minimization was continued utilizing a second-derivative Newton-Raphson technique. The full matrix version could not be implemented because of the large size of the molecule. Instead, all off-diagonal 3x3 submatrices of the second-

---

[6] Improper torsional interactions are introduced for two reasons:
1. to ensure the planar tendency of sp^2 atoms
2. to present chiral centres (e.g. the C_α's of amino acids) from racemizing when the united-atom approximation is applied [Weiner et al., 1984]

derivative matrix were neglected by employing the block diagonal Newton Raphson (BDNR) technique, which had to be applied together with a linesearching (quadriatic interpolation) routine [Mackay et al., 1989, p. 322] to prevent up-gradient movements [Still, 1989] and stabilize the minimization procedure.

Energy minimizations were performed on a MicroVax II computer with the MacroModel software package (cf. section 9.2). All structures were minimized until the energy gradient RMS[7] was at least below 0.04 kJ/Å·mol (convergence criterion). The total minimization time was at least 100 000 CPU[8] seconds.

---

[7] RMS = root mean square

[8] CPU = central processing unit

2.2. Results and Discussion

The hydrophobic moment profiles of the dynorphin A fragments (1-8), (1-9), (1-13), and (1-17) are displayed in Figure 2.1. The profiles of dynorphin A-(1-8), (1-9), and (1-13) differ considerably from one another, whereas those of dynorphin A-(1-13) and the full heptadecapeptide do not. Whether this correlation of the amphiphilicity profiles with pharmacological[9] differences is of any biological significance or not, remains to be seen. At this point, it seems appropriate to stress that these amphiphilicity profiles are derived from regular periodic structures only. Any aperiodic secondary structure which displays a higher degree of amphiphilicity can not be detected by this method. Concentrating on the profile of dynorphin A-(1-13), there is a local maximum at δ = 100°, i.e. the value corresponding to an α-helix, the global maximum is at δ = 180°, i.e. the angle complying with an extended structure.

[9] As already pointed out in Chapter 1, dynorphin and dynorphin A-(1-13) display approximately the same high potency and pharmacological profile [Goldstein, 1985]. Dynorphin A-(1-8) and dynorphin A-(1-9), however, have distinctly different profiles from dynorphin A-(1-13) [Weber et al., 1982; Corbett et al., 1982].

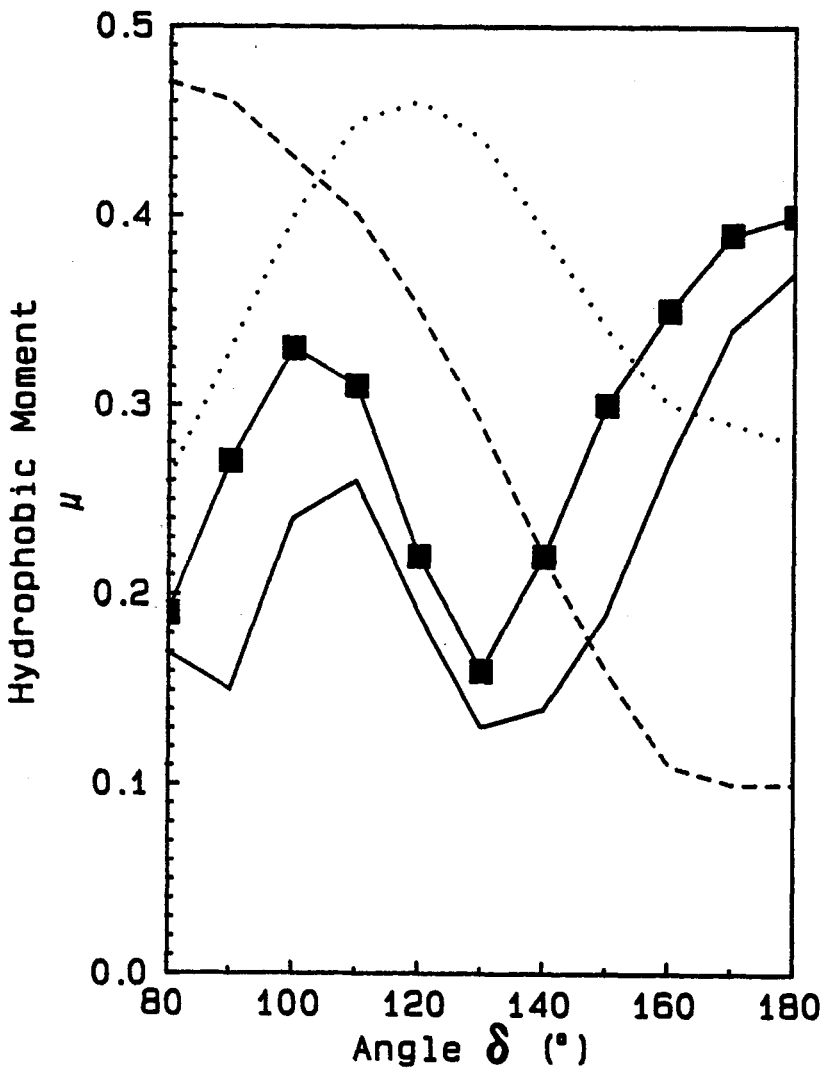

Figure 2.1. The hydrophobic moment profiles of the dynorphin A fragments (1-8) (--), (1-9) (••), (1-13) (–▪–), and (1-17) (—).

The hydrophobic moment profiles for model segments for an α-helical and β structure both show additional peaks at other angles [Eisenberg et al., 1984] due to the finite length of the segment. These subsidiary peaks are more intense relative to the main maximum for a β structure than for an α-helix and are located at approximately 100° in the case of a β structure and at approximately 130° to 140° for α-helices [Eisenberg et al., 1984]. This additional information reinforces the interpretation that, on the basis of the hydrophobic moment profile, dynorphin A-(1-13) will adopt an extended structure for maximum amphiphilicity.

The geometry underlying the calculation of the hydrophobic moment at δ = 100° is illustrated by the helical wheel representation [Schiffer and Edmundson, 1967] in Figure 2.2. However it is well established that the Pro residue is rarely found in α-helical conformations. This is partly due to the absence of an amide proton as a hydrogen bond donor, but mainly because of steric repulsions between the side chain of the preceding residue and the δ-methylene group of the pyrolidine ring [Schimmel and Flory, 1968]. This excludes the ψ angle of the preceding residue from adopting the value necessary for an α-helical conformation ($\psi \approx$ -60° [Richardson, 1981, p.185]). A proline incorporated into the helix will introduce a bend into the helix, but the pattern of hydrogen bonding need not be interrupted [Richardson, 1981, p.185].

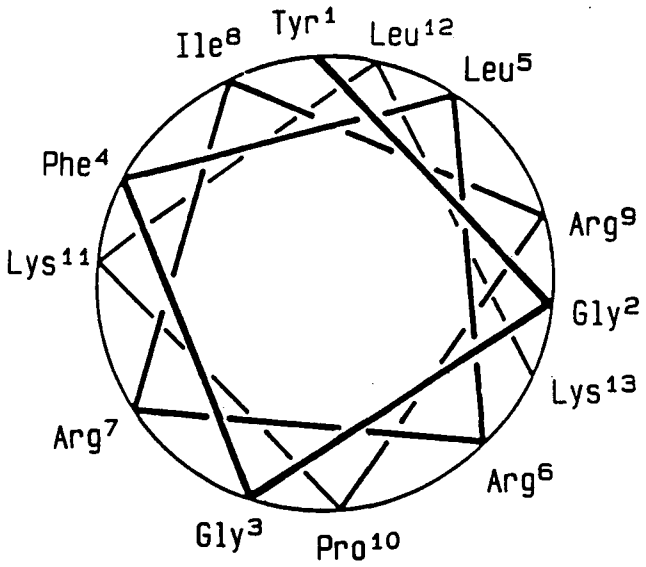

Figure 2.2. Dynorphin A-(1-13) at δ = 100°

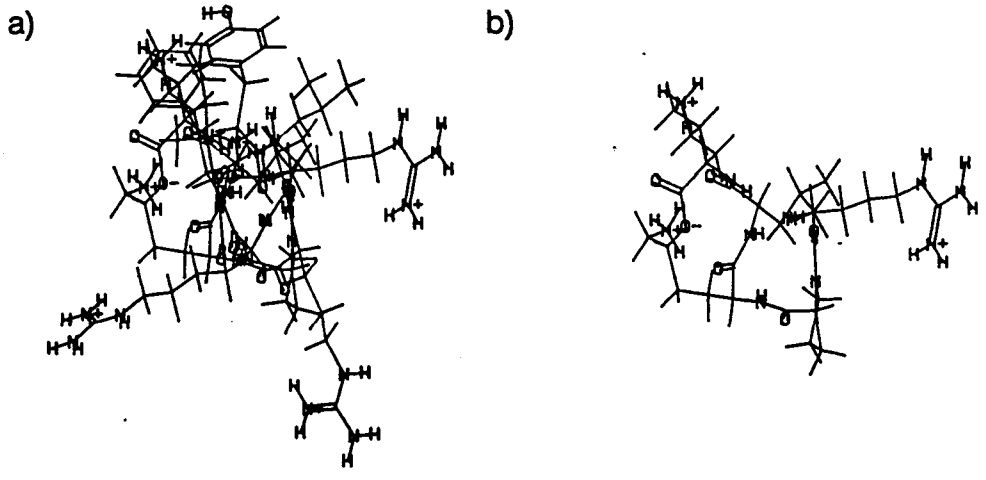

Figure 2.3. Dynorphin A-(1-13) in an α-helical conformation after being subjected to energy minimization for just over 100 000 CPU seconds (cf. text and section 2.1.4 for details). 21 Intramolecular hydrogen bonds were found. a) a view down the helix axis analogous to Figure 2.2. and b) the C-terminal residues of a). The position of the Lys^{13} is exactly to the opposite side of the axis as was indicated by Figure 2.2.

A different approach was attempted by the calculation of the helix-probability profiles of the dynorphin A fragments (1-8), (1-9), (1-13), and (1-17) in the presence of anionic detergent (Figure 2.4). As was expected, the probability of helix formation increases with the length of the peptide fragment and the presence of the Pro[10] residue seriously disrupts the profiles of the tridecapeptide and dynorphin[10]. Significant helix probability (>30%) for these two peptides is detected only for the four residues from Arg[6] to Arg[9], roughly equivalent to one turn.

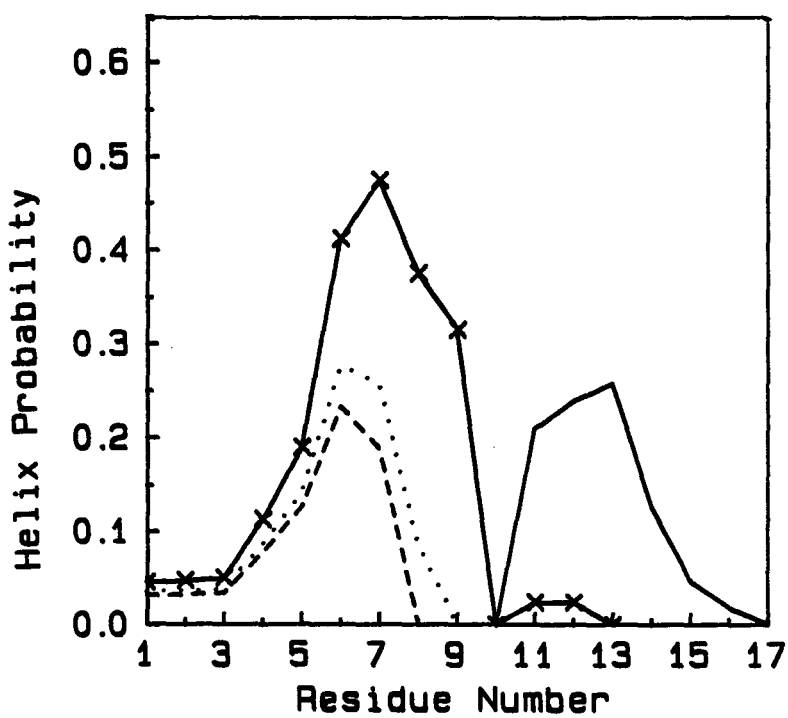

Figure 2.4. Helix probability profiles for the dynorphin A of the dynorphin A fragments (1-8) (--), (1-9) (••), (1-13) (-X-), and (1-17) (—) in the presence of anionic detergent.

[10] The statistical weight of the Pro residue is assigned the value of zero (cf. Table 2.2).

Table 2.3. Helix probability profiles for dynorphin A-(1-13) in water, anionic detergent, and the presence of zwitterionic lipids.

Individual Probabilities[a]	Aqueous Solution	Anionic Detergent	Zwitterionic Lipid
Tyr^{1}	0.007	0.045	0.007
Gly^{2}	0.007	0.047	0.007
Gly^{3}	0.007	0.050	0.007
Phe^{4}	0.015	0.113	0.012
Leu^{5}	0.019	0.190	0.016
Arg^{6}	0.013	0.412	0.014
Arg^{7}	0.014	0.475	0.014
Ile^{8}	0.014	0.375	0.013
Arg^{9}	0.000	0.315	0.000
Pro^{10}	0	0	0
Lys^{11}	0.001	0.024	0.000
Leu^{12}	0.001	0.024	0.000
Lys^{13}	0	0	0.000
Sum of All Probabilities	0.1	2.1	0.1
Overall Helical Content[b]	0.7%	15.9%	0.7%

a: probability for each amino acid to be in a helical conformation

b: overall helical content = sum of all probabilities / # of residues

In the case of dynorphin A-(1-13), the profiles were also calculated for the peptide in water and in the presence of zwitterionic lipids (Table 2.3). The results for the aqueous solution of the peptide (Table 2.3) indicate that the overall helical content of the tridecapeptide is negligible. This correlates well with the experimental evidence derived from CD studies (cf. Chapter 3).

As expected (cf. section 2.1.2), the results for the peptide in a zwitterionic environment do not differ significantly from those in aqueous solution. In both cases the overall helical content was negligible. The overall helical content was dramatically increased for dynorphin A-(1-13) in anionic detergent, but the calculated value of 16% was too low to account for a helix long enough to represent a stable secondary structure. Although this value was lower than one of 19% previously calculated by Maroun and Mattice [Maroun and Mattice, 1981], it was higher than the helical content experimentally derived from CD studies (cf. Chapter 3).

If, as the above results suggest, the membrane-mediated conformation is not α-helical, then it is of prime interest to define an alternative. An answer to this question was attempted by employing the GOR method for four-state secondary structure predictions. However, the effect of lipid environment could not be included in these calculations.

The secondary structure profiles with default decision constants (a) and optimized [Garnier et al., 1978] decision constants (b) are shown in Figure 2.5. The probability for an α-helical conformation is negligible for all residues, which is in line with the results discussed above. The Tyr^1, Gly^2, Pro^{10}, and Lys^{11} are predicted to be in a reverse-turn conformation in both profiles. This prediction seems reasonable, because pharmacological studies on dynorphin analogues indicate a decreased kappa-potency upon replacement of the Gly^2 residue by

several L-amino acids [Bergland et al., 1989] or the Pro^{10} residue by more helix-forming residues [Turcotte et al., 1984; Nakajima et al., 1988] or β-strand formers [Yang and Taylor, 1989].

Discrepancies between the two profiles are observed for Gly^3 (assigned to a reverse-turn conformation in the "default" profile), Arg^9, and Lys^{13} (both random coil) are all assigned to a β-strand conformation after optimization. In a similar approach, Snell [1984] has employed the statistical methods of Chou and Fasman to predict the conformation of dynorphin A-(1-17) resulting in a β-strand for the eight N-terminal residues Tyr^1 to Ile^8 and a β-bend for the four C-terminal residues Trp^{14} to Gln^{17}. Considering the experimentally demonstrated importance of the Gly^2 residue mentioned above and the higher degree of accuracy of the GOR method (cf. 2.1.3), our prediction seems more reliable than Snell's both on experimental and theoretical grounds. On the basis of the optimized profile, a model was constructed with two reverse turns located at the residues discussed above and an extended conformation elsewhere (cf. Figure 2.6). This structure was subjected to energy minimization (as described in section 2.1.4) and was referred to as the "GOR" model in the context of this study.

a)

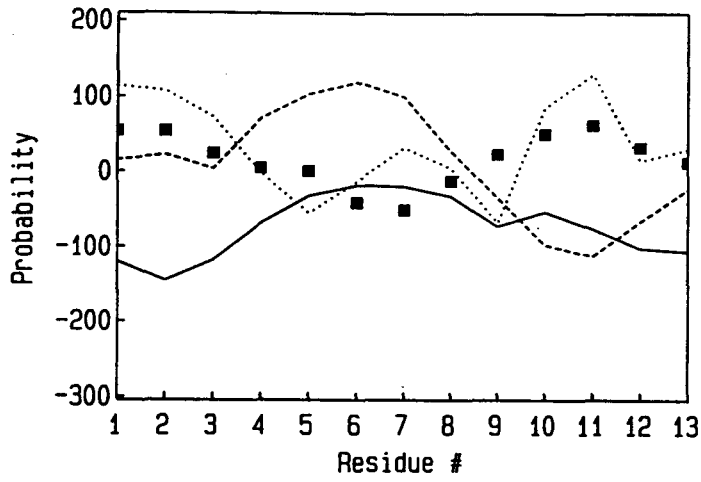

b)

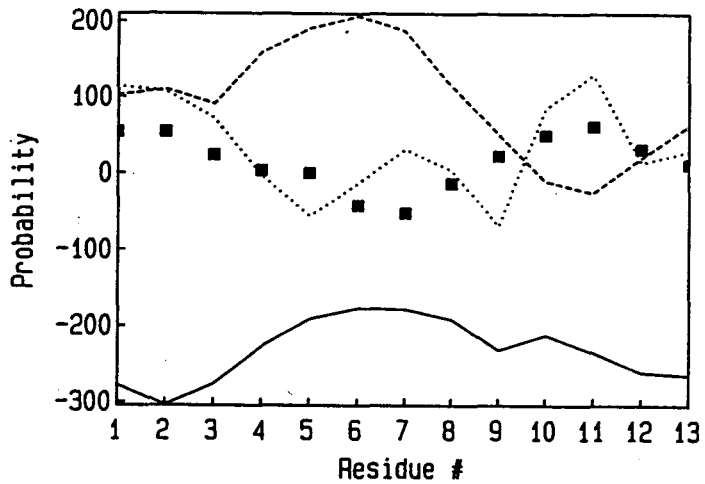

Figure 2.5. Secondary structure probability profiles of dynorphin A-(1-13) (α-helix (—), β-strand (--), reverse turn (••), random coil (■) calculated by the GOR method [Garnier et al., 1978]
a) with default decision constants $DC_H = 0$, $DC_S = 0$, and,
b) with default decision constants $DC_H = 158$ and $DC_S = -87.5$ on the basis of the CD results for the peptide in the presence of an aqueous dispersion of DMPG bilayers. The probability scaling is arbitrary.

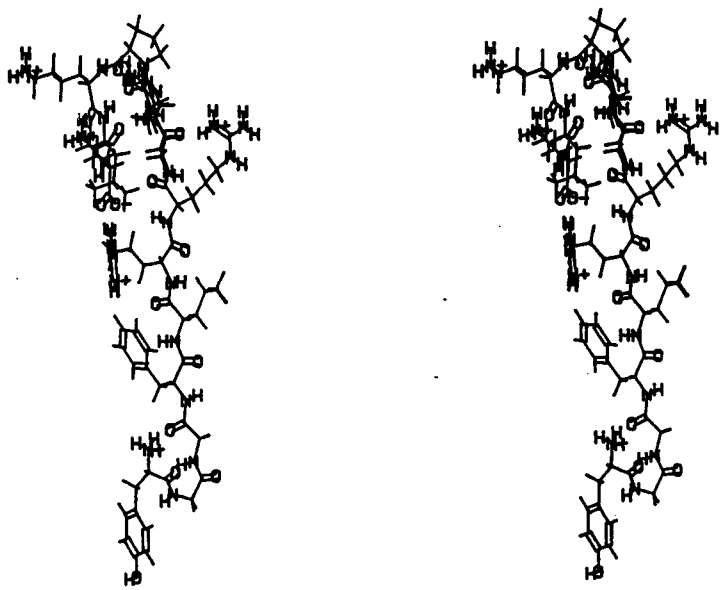

Figure 2.6. A stereo view of the "GOR" conformation of dynorphin A-(1-13) after energy minimization for over 200 000 CPU seconds. The final energy gradient RMS was 0.036 kJ/Å·mol. This conformation gave rise to 18 intramolecular hydrogen bonds

In summary, two working models were constructed under the crude assumption that the backbone conformation of the residues was limited to the four major classes of conformational states of polypeptide conformation[11]. One was associated with the α-helical conformation suggested by Schwyzer's group [Erne et al., 1985], the other was derived from the GOR four-state secondary structure prediction method [Garnier et al., 1978] for the backbone conformation of soluble proteins. It is stressed that these structures were pure working models in aid of the interpretation of NMR data and were not considered as anything else but working hypotheses pending further experimental evidence.

In the case of enkephalins, sophisticated molecular mechanics calculations have yielded seven distinct low energy conformers [Manavalan and Momany, 1981a,b] from a set of starting geometries selected from the respective dipeptide minima determined by Scheraga's group [Lewis et al., 1973]. Such an approach in the case of dynorphin A-(1-13) would be as arduous as it is interesting. The major problems are the lack of implementation of the full-matrix Newton-Raphson method for more than 200 atoms, and, more generally, the absence of a guarantee that the global minimum will be found [Burkert and Allinger, 1982, p. 275]. Nevertheless, an, admittedly large, set of minimum energy conformers would provide profoundly better reference models than we have to date.

[11] This limitation also applies to the analysis of the CD results (cf. Chapter 3).

3. CD STUDIES

Circular dichroism is a phenomenon observed when a sample displays differential absorbance for left and right circularly polarized light. Hence a molecule exhibiting circular dichroism must satisfy both of the following two requirements: it must contain a chromophore and the molecule must be dissymmetric, i.e. have a non-superimposable mirror image. Dissymmetry (chirality) includes asymmetry, as applies for a tetrahedrally substituted carbon whose all four substituents are different from one another. It also includes molecules with a resolved chirality, i.e. a left-handed (counterclockwise) or right-handed (clockwise) screw sense. An example of a structure possessing a right-handed screw sense is the α-helix, one of the most commonly observed protein secondary structures.

The peptide bond itself is a chromophore, with an absorption band near 220 nm and stronger additional absorption bands at lower wavelengths. The 220 nm band is assigned to the $n\text{-}\pi^*$ transition involving a transition from a non-bonding $2p_y$ orbital on the oxygen to an antibonding orbital primarily distributed about the plane of the bond but also delocalized over the 4-atom peptide moiety [Urry, 1985]. The transition gives rise to a change in the electron distribution.

This results in a circular motion of charge, giving rise to a magnetic moment along the C-O bond, the magnetic transition dipole moment. While the electric transition dipole moment is small, and therefore the associated absorption band is weak, the dot product of the electric and the magnetic dipole moment is large. This gives rise to a strong CD band with high rotational strength[1]. The bands at lower wavelengths result from the corresponding $\pi \rightarrow \pi^*$ transition.

Plane polarized light, which can be considered as the combination of left and right circularly polarized light of equal intensity and phase, is passed through a sample meeting these two requirements (i.e. chroma and dissymmetry). One circularly polarized component of the emergent beam will have incurred a greater loss in intensity than the other. The resulting emergent beam will therefore be elliptically polarized.

CD instruments create alternating left and right circularly polarized light, which is passed through the sample, and register the alternating voltage which is created in the dynode by the emergent beam. The property of measurement is the differential absorbance $A_L - A_R$, amounting to approximately 0.03% -0.3% of the total absorbance.

The differential absorbance can be converted into the ellipticity, θ (in degrees), with the following equation:

---

[1] The rotational strength of a CD band, R_i, is defined in analogy to the dipole strength of an absorption band: $R_i = 1.23 \cdot 10^{-42} \cdot ([\theta_i] \cdot \Delta_i)/\lambda_i$, where λ_i is the wavelength of the band maximum, $[\theta_i]$ the molar ellipticity at the band maximum, and Δ_i is the half-band width at $[\theta_i]/e$ [Urry, 1985, p.293].

$$\theta = \frac{1}{\log e} \cdot \frac{180}{4 \cdot \pi} \cdot (A_L - A_R) = 32.98 \cdot A \qquad (3.1.-1.)$$

The ellipticity in degrees per unit length, θ, is defined as the angle whose tangent is the ratio of the minor to major axis of the ellipse described by the electric vector of the emergent beam:

$$\theta = \arctan \frac{|E_R| - |E_L|}{|E_R| + |E_L|} \qquad (3.1.-2.)$$

where E_R and E_L are the magnitudes of the electric vectors describing the electric moments of left and right circularly polarized light, respectively.

Circular dichroism spectra are expressed in terms of molar ellipticity, $[\theta']$, which at a given wavelength is defined as:

$$[\theta'] = \frac{100 \cdot \theta}{(c \cdot b)} = 3298\ (\epsilon_L - \epsilon_R) = 3298 \cdot \frac{(A_L - A_R)}{(c \cdot b)} \qquad (3.1\text{-}3.)$$

where ϵ_L and ϵ_R are the molar absorptivities and A_L and A_R are the absorbances for left and right circularly polarized light, respectively, c is the concentration in moles per litre and b is the path length in cm.

In protein circular dichroism, the molar ellipticity, $[\theta']$, is divided by the number of amino acid residues in order to obtain the mean residue ellipticity, $[\theta]$, as the concentration dependence of the ellipticity θ is actually a dependence on the concentration of the peptide chromophore:

$$[\theta] = [\theta']/\#\ \text{aa residues} \qquad (3.1.-4.)$$

The expression of CD spectra in terms of mean residue ellipticity not only enables us to visually compare the spectra of peptides of different chain lengths, but also provides a standardized input format for numerical data analysis (cf. 3.1.5.4.).

A problem with CD experiments on peptide-lipid systems is that transparent sample solutions are required in order to avoid artifacts due to differential light scattering [Urry et al., 1971]. This can be achieved by perceptive choice of the lipid-to-peptide ratio, the application of sonication to disperse the lipid into small vesicles, the use of anionic lipids with short acyl chains, and arranging the photomultiplier as near to the sample as possible.

A second artifact is created by absorption flattening [Urry et al., 1971; Wallace and Teeters, 1987] due to nonrandom distribution of chromophores in solution, an effect also referred to as the Duysens effect [Duysens, 1956]. The Duysens effect can be reduced by creating smaller particles (through sonication as already mentioned above) and by using more concentrated samples in cells of shorter pathlengths.

3.1. Materials and Methods

Choice of Solvent Systems

SDS micelles have been reported to mimic the membrane environment quite well [Wu and Yang, 1981; Wu et al., 1982]. There is strong evidence supporting the idea that methanol [Yang et al., 1977, Tappin et al., 1988] and trifluoroethanol [Urry et al., 1971; Gráf et al., 1977; Clore et al., 1986b; Mammi et al., 1988] mimic influences of membranes on peptide conformation [Wu and Yang, 1981]. Therefore CD spectropolarimetry was employed to obtain a global indication of the aqueous and membrane mediated secondary structure of the tridecapeptide. In addition to this, the ability of SDS micelles and organic solvents to mimic the phospholipid environment was compared in order to derive conditions more amenable to a detailed approach employing NMR spectroscopic methods. Popular organic solvents in use for NMR studies are deuterated chloroform ($CDCl_3$) and perdeuterated dimethyl sulfoxide (d_6-DMSO) [Stern et al., 1968; Roques et al., 1976; Jones et al., 1976]. These could, however not be employed in the present study because their UV cutoffs at 245 nm and 268 nm [Przybytek, 1982, p. 142] do not permit CD studies in the range between 190 nm and 250 nm.

3.1.1. Materials

Dynorphin A-(1-8) (M = 981.2 g/mol) was obtained from CRB (Cambridge Research Biochemicals, Harston, Cambridgeshire, England).

Dynorphin A-(1-13) (M = 1604.19 g/mol was kindly provided by Serge A. St-Pierre, Department of Physiology and Pharmacology, Faculty of Medicine, University Hospital Centre, Sherbrooke, Québec J1H 5N4 (present address: INRS-Sante, Pavillon Gamelin, 7401 Hochelaga, Montréal, Québec H1N 3M5). The preparation [Turcotte et al., 1984] was achieved by the use of preformed symmetrical anhydrides of Boc-amino acids [Lemaire et al., 1978] and Merrifield's solid phase method [Merrifield, 1963]. The peptide was purified by reverse phase HPLC [Turcotte et al., 1984].

Dimyristoyl-L-3-phosphatidylglycerol (= DMPG, M = 666.89 g/mol) and dimyristoyl-L-3-phosphatidylcholine (DMPC, M = 677.95 g/mol) were purchased from Avanti Polar Lipids Inc., Birmingham, AL, U.S.A.

Sodium dodecyl sulfate (SDS, M = 288.38 g/mol) was purchased from BioRad (Canada), Mississauga, Ont., methanol (hplc-grade), acetonitrile (hplc-grade), and chloroform were purchased from Caledon Laboratories, Georgetown, Ont., and trifluoroethanol (TFE) from Pierce, Rockford, IL, USA.

Acetic acid (M = 60.05 g/mol, density = 1.0492 g/mL) and sodium dihydrogenphosphate ($NaH_2PO_4 \cdot H_2O$, M = 137.99 g/mol) were purchased from Fisher Scientific, NJ, USA.

3.1.2. Preparation of Lipid Suspensions

The lipid suspensions were completely prepared before adding the peptide to the sample. Addition of the peptide, particularly to the small unilamellar vesicles created by sonication, can induce aggregation and fusion of the vesicles [Stegmann et al., 1989]. With this in mind, the samples originally containing small unilamellar vesicles are referred to simply as "sonicated lipid bilayers" with no reference to the probable size of the vesicles.

3.1.2.1. Multi-Lamellar Suspensions

The lipid was dissolved in a mixture of chloroform and methanol (2:1, v/v). The solvent was evaporated with a stream of dry nitrogen leaving the lipid as film on the walls of a glass test tube. Last traces of solvent were removed into a liquid nitrogen trap by placing the sample under high vacuum for at least 90 min. The lipid film was resuspended in the appropriate solvent (buffer or water) by warming the tube to about 45°C and vortexing vigorously for about 30 s.

3.1.2.2. Sonication

The multi-lamellar suspension (3.1.2.1.) was sonicated [Chapman et al., 1968] for 60 minutes to visual clarity in a 60 W sonicating bath.

3.1.3. UV Absorption Spectrometry

In those cases where a molar absorptivity ϵ at the wavelength of the maximal absorbance of the tyrosine residue in the respective solvent was known, the peptide concentrations were checked by measuring the UV absorbance at the appropriate wavelength. The spectrometer employed was a Perkin-Elmer "Lambda 4B UV/VIS Spectrophotometer". Quartz sample cells were used (Markson Science Inc., Del Mar, CA, USA).

3.1.4. Data Acquisition

CD spectra were obtained with an Aviv model 60 DS circular dichroism spectropolarimeter described by Epand et al. [1986]. The general principle of the instrument has been outlined by Horwitz [1976]. The instrument had been calibrated with a sample of d-camphor-10-sulfonate in water ($n\text{-}\pi^*$ transition at 290 nm) [Cassim and Yang, 1969; Chen and Yang, 1977; Yang et al., 1986]. A 1 mm sample cell was used and the sample temperature was 25°C unless stated otherwise. The cell was maintained at constant temperature with a thermostated cell holder. The region from 250 to 190 nm was scanned every 0.5 nm with a bandwidth of 1.5 nm. Four or five scans were averaged. The improvement resulting from the averaging of four scans in comparison to the acquisition of single scans is illustrated in Figure 3.1 and 3.2. Figure 3.1 demonstrates the

presence of considerable noise at wavelengths lower than 199 nm for single scans. This is due to considerable absorption on the part of the solvent. Averaging of four scans reduces the noise considerably down to about 194 nm (Figure 3.2). Another effect observed was that the spectra of three samples prepared from three different lots of the peptide and recorded on different days were not identical. The consequence of this finding for the results of the secondary structure predictions is discussed in section 3.1.5.4.

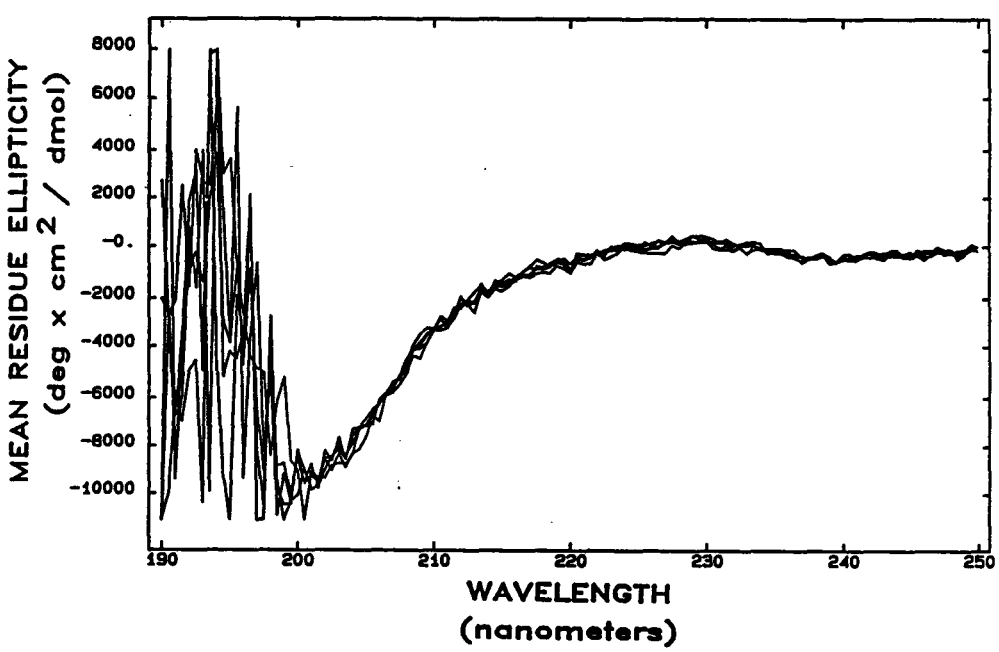

Figure 3.1. Circular dichroism spectra of a methanolic solution of 0.24 mM dynorphin A-(1-13) at 25°C. Five single scans of one sample were overlayed.

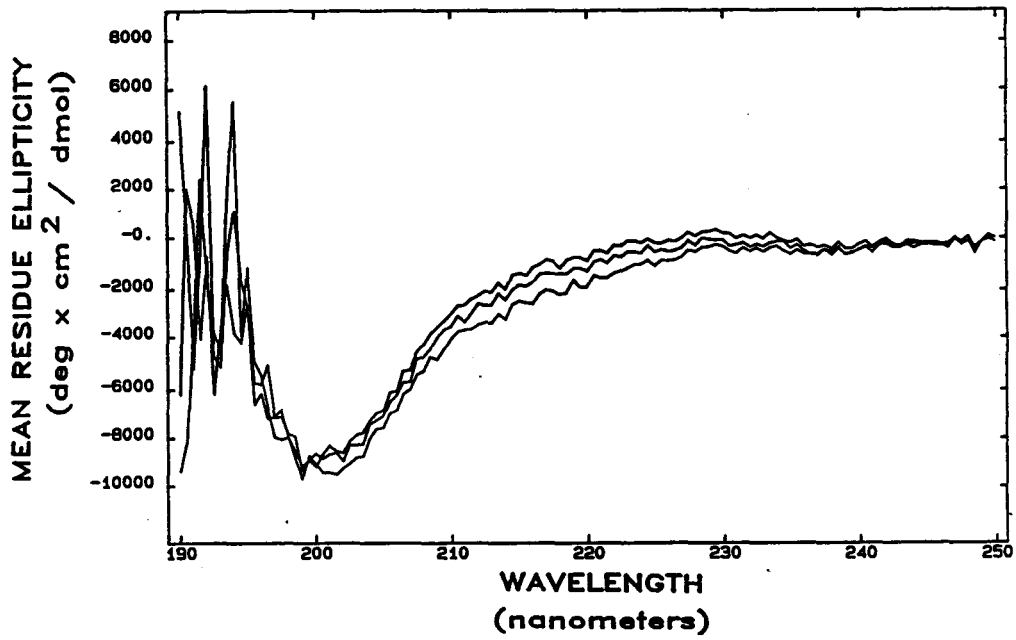

Figure 3.2. Circular dichroism spectra of methanolic solutions three different lots of dynorphin A-(1-13) recorded at 25°C on different days. Each of them is an average of four scans. Sample concentrations were between 0.16 and 0.24 mM.

3.1.5. Data Processing

3.1.5.1. Determination of the Peptide Molar Concentrations

The concentration of dynorphin A-(1-13) was checked by UV absorption spectrometry (3.1.3.) when literature data was available (3.1.6.1.). In all over

cases, the concentration was calculated from the amount of peptide weighed out and the amount of solvent used.

3.1.5.2. Baseline Correction

The CD spectra of the pure solvents were recorded under the same conditions and subtracted from the sample spectra. The corrected ellipticity is denoted θ_{corr}.

3.1.5.3. Calculation of the Multiplication Factors for Display of the Spectra in Terms of Mean Residue Ellipticity $[\theta]$

The corrected data set was multiplied by a constant to obtain the mean residue ellipticity, $[\theta]$:

$$[\theta] = \frac{100 \cdot \theta_{corr}}{mrc \cdot b} \left[\frac{deg \cdot cm^2}{dmol}\right]$$

The instrument records θ in millidegrees:

$$\frac{[\theta]}{\theta} = \frac{1}{mrc \cdot b} \left[\frac{L}{mol \cdot mm}\right]$$

The multiplication factors are calculated by taking the reciprocal of the product of the mean residue concentration (mrc, in mol/L) and the sample cell path length (in this case in mm). The mrc is the product of the number of amino acid residues and the peptide molar concentration.

3.1.5.4. Estimation of the Secondary Structure Fractions

The principal assumption made when deducing average secondary structure information from measured CD spectra is that the far UV CD spectrum (between 190 nm and 240 nm) is dominated by the optical activity of the peptide backbone. This is the case as long as the fraction of aromatic amino acids is not too high because aliphatic side chains do not have a marked effect on the CD spectrum in this region[2].

The computer program used for secondary structure analysis is based on a program described by J.T. Yang [Chang et al., 1978]. The circular dichroism of the secondary structural elements in a peptide molecule is assumed to be additive. Consequently, the mean residue ellipticity, $[\theta]$, of a peptide in solution at any wavelength of the spectrum can be expressed as a linear combination of the linearly independent functions of the mean residue ellipticities of reference structural elements at this specific wavelength:

---

[2] The inherently asymmetric nonplanar disulfide (R-S-S-R) is an important chromophore in near UV spectra (240-300 nm) as are the aromatic rings of tyrosine and tryptophan. Phenylalanine and histidine show only minor contributions to the spectrum [Kahn, 1979].

$$[\theta] = f_\alpha \cdot [\theta]_\alpha + f_\beta \cdot [\theta]_\beta + f_t \cdot [\theta]_t + f_r \cdot [\theta]_r ,$$

where f_α, f_β, f_t, and f_r refer to the fractions of α-helical, β-sheet, β-turn and random structural content, respectively, and the $[\theta]_i$'s refer to the mean residue ellipticities of the respective reference structures.

Reference spectra of an α-helix, a β-sheet, a β-turn and a random structure have been computed by J.T. Yang and coworkers from experimental data of 15 globular proteins of known three-dimensional structure and are shown in Figure 3.3. The reference spectrum for the α-helix reveals three bands: a positive[3] π-π^* band near 193 nm (polarized perpendicularly to the helix axis), a negative π-π^* band near 210 nm (polarized parallel to the helix axis), and a negative n-π^* band near 223 nm. These bands are distinctly different from those reported for model polypeptides (e.g. poly-L-alanine in TFE with a positive π-π^* band near 190 nm, a negative π-π^* band near 204 nm, and a negative n-π^* band near 220 nm [Holzwarth and Doty, 1965]). This is predominantly due to

[3] Splitting of the π-π^* band in a helix is due to exciton resonance interactions [Kasha, 1963]. Absorption of light by a chromophore results in a change in the electric dipole moment of the absorbing unit. The difference in the electric dipole moment in the ground and excited states is referred to as the electric transition dipole moment. Intramolecular dipole-dipole interaction of the transition dipole moments causes electrostatic perturbation of the excited states and gives rise to allowed and forbidden exciton states. Components of the peptide chromophore transition dipole moment parallel to the helix axis interact to give rise to a lower energy exciton band. Components perpendicular to the helix axis interact to form two degenerate exciton states, giving rise to two bands of the same energy with perpendicular polarization vectors oriented perpendicular to the helix axis.

the chain length dependence of the rotational strength of each transition for the helix.

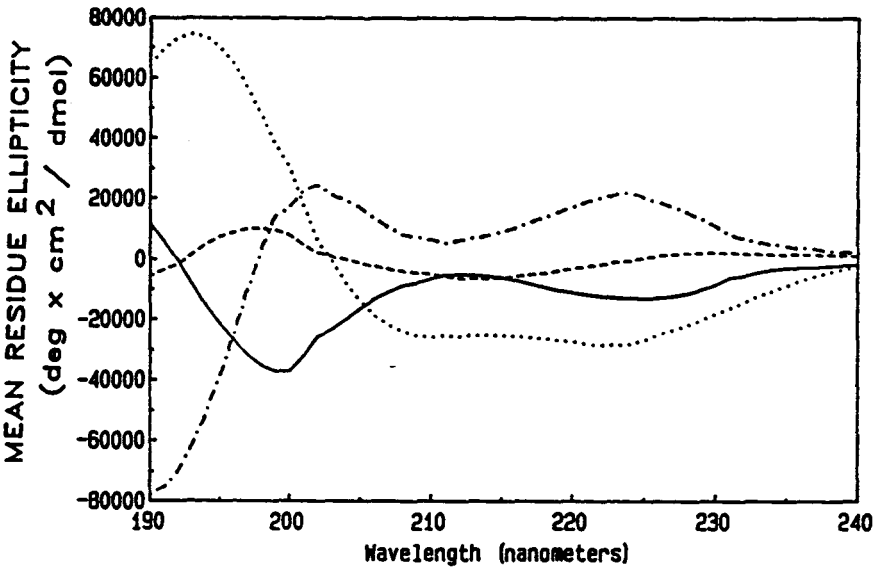

Figure 3.3. Circular dichroism reference spectra of a ten-amino-acid-residue α-helix (·····), the β-strand (- - -), the β-turn (-·-·-), and the aperiodic random coil form (———) calculated by J.T. Yang and coworkers [Chang et al.,1978].

The chain-length dependence of the CD spectrum of an α-helix has been established by J.T. Yang and coworkers from myoglobin data [Chen et al., 1974]. Neglect of this can lower the determined fraction of α-helical content by as much as 30% [Chang et al., 1978]. The number of residues per helical segment used for the computation of the reference data displayed in Figure 3.3 is 10, which is very close to the membrane mediated nine-residue helical segment postulated for dynorphin A-(1-13) [Schwyzer, 1986a]. In contrast to this, the classical model polypeptides are homopolymers of over 500 residues

[Holzwarth and Doty, 1965]). Consequently, the reference data of Yang's group is better suited for the recognition of shorter helical segments than that derived from model peptides.

An example for a model system of a β-pleated sheet is poly-L-serine with a degree of polymerisation of 20 in 80% TFE / 20% water (antiparallel β-pleated sheet [Quadrofoglio and Urry, 1968]). A negative $n\text{-}\pi^*$ band near 220 nm and a positive band near 197 nm (which is thought to be the higher wavelength band resulting from the exciton resonance splitting of the $\pi\text{-}\pi^*$ absorption band at 190 nm. The CD spectrum of a type II β-turn (e.g. the polytetrapeptide of elastin (poly-(L-Val-L-Pro-Gly-Gly)) [Urry et al., 1974]) can be assigned in the same manner. Again the negative band at 220 nm results from the $n\text{-}\pi^*$ transition of the chromophore and the other bands (positive at 203 nm, negative at 190 nm) originate from the $\pi\text{-}\pi^*$ absorption band. Many variants of both the β-form and the β-turn (and obviously of the unordered form too) occur in protein molecules. The reference data of Yang's group takes this better into account than the aforementioned model peptide systems.

In summary, although the reference data employed was originally deduced from studies on globular proteins, it constitutes a better standard than model peptide systems, especially with respect to the determination of helical content.

The fractions of these secondary structural elements can be calculated if the mean residue ellipticity is known at at least four different wavelengths. In order to obtain reliable values, the above equation must be approximated for a large number of wavelengths and the solution estimated by a nonlinear, least

squares curve-fitting program as introduced by J.T. Yang's group [Chang et al., 1978]. The authors evaluate their procedure in the following way: "...The computed helical content is usually good to excellent...Inclusion of the β-turn in the analysis improves the correlation for the estimates of the β-form, but the computed β_t values are not significantly correlated with the X-ray results..." [Chang et al., 1978, p.13].

Figure 3.3 illustrates the importance of including the lower wavelength region between 190 and 200 nm into the estimation, as this is the region where the reference spectra exhibit the greatest differences. Comparison of Table 3.1 with Figure 3.1 suggests that the error in the estimation of peptide secondary structure is only in the order of ±0.03 (if the calculated content for β-strand and β-turn are combined and viewed together) although there is considerable noise in the lower wavelength region.

Table 3.1. Estimation of the secondary structure fractions of dynorphin A-(1-13) in methanolic solution from the circular dichroism spectra shown in Figure 3.1.

Run #	********** Fractions of total **********			
	α-helix	β-sheet	β-turn	random
1	0.00	0.60	0.07	0.33
2	0.00	0.65	0.06	0.30
3	0.00	0.51	0.12	0.36
4	0.00	0.66	0.03	0.32
5	0.00	0.62	0.05	0.33

Averaging of scans reduces this error as is indicated in Figure 3.2 and Table 3.2. Although these spectra were recorded on three samples prepared from different lots of dynorphin A-(1-13) on three separate days and they appear slightly offset from one another, the relative error in secondary structure estimation is minimal. The results displayed in Table 3.2 indicate that the precision of the secondary structure analysis on the basis of independently recorded CD spectra is ±0.02.

Table 3.2. Estimation of the secondary structure fractions of dynorphin A-(1-13) in methanolic solution from the circular dichroism spectra shown in Figure 3.2.

Run	c_{pep} (mM)	********** Fractions of total **********			
		α-helix	β-sheet	β-turn	random
A	0.17	0.00	0.58	0.06	0.36
B	0.24	0.00	0.61	0.04	0.35
C	0.16	0.00	0.60	0.05	0.35

3.1.6. Solvent Dependence of the CD Spectra of Dynorphin A-(1-13)

The CD spectra of dynorphin A-(1-13) in various solvents and solvent environments were recorded and processed as indicated above. The objective of this set of experiments was to obtain an indication of the difference in conformation between the lipid-bound peptide (sample H) and the free peptide

in aqueous solution (sample A). In addition to this, the peptide conformations in other solvent environments (samples B - G, I) were compared to the lipid-induced one in view of obtaining a simpler system more accessible to an experimental approach employing NMR techniques.

As already indicated in the introduction of section 3.1, the samples containing SDS micelles, trifluoroethanol and methanol were examined because it was feasible to assume that they might mimic the membrane environment adequately. DMPC was included in this set of experiments because DMPC SUV's provided a powerful NMR sample. The contents of the respective samples are listed in Table 3.3.

The concentration of dynorphin A-(1-13) was checked by UV absorption spectrometry (3.1.3.) where literature data was available, and by calculations on the basis of weight-to-volume ratios in all other cases (cf. section 3.2.1).

Table 3.3. Overview of CD samples.

	m_{pep} (mg)	V (mL)	Solvent (mM)	c_{pep}	c_{lip}/c_{pep}
A	1.20	3.0	water	0.24[a]	-
B	1.10	3.0	methanol	0.24[a]	-
C	-	3.0	"50% methanol"	0.24[b]	-
D	1.00	3.0	"9.8 mM SDS"[c]	0.21	47
E	1.00	3.0	"9.8 mM SDS pH 2.8"[d]	0.21	47
F	0.93	3.0	trifluoroethanol	0.19	-
G	1.25	3.0	"30% TFE"[e]	0.26	-
H	0.50	2.0	"1.8 mM DMPG"[f]	0.16	11
I	0.60	2.0	"2.0 mM DMPC"[g]	0.16	11

a = peptide molar concentrations determined by UV absorption spectrometry (see below)

b = 1.5 ml sample A were added to 1.5 ml sample B and the peptide concentration calculated by averaging the concentrations of the two original samples: c = 0.24 mM

c = 8.5 mg SDS in 3.0 ml water

d = sample D + 8.5 μl acetic acid (final concentration 50 mM)

e = TFE/water (3:7, v/v)

f = 2.33 mg DMPG in 10 mM NaH_2PO_4 pH 7.46, unsonicated (MLV's)

g = 2.67 mg DMPC in water, sonicated (SUV's)

c_{lip} = concentration of lipid or detergent, respectively

3.1.7. Temperature Dependence of the CD Spectra in Methanolic Solution

0.8 mg Dynorphin A-(1-13) were dissolved in 3 mL of methanol. Spectra were recorded at temperatures of 20°C, 25°C, 30°C, 35°C, 40°C, and 45°C. All other conditions were the same as described above (cf. 3.1.4.).

3.1.8. Concentration Dependence of the CD spectra in Methanolic Solution

The sample prepared in section 3.1.7. was also used for this experiment. The peptide concentration of the first sample was checked by UV absorption spectrometry (3.1.3.). After recording the CD spectrum at 25°C, the sample was mixed with an identical volume of pure solvent. Consequently, the concentration of the sample was iteratively halved after each set of scans. spectra of dynorphin A-(1-13) in methanol were recorded at five sample concentrations, 0.16, 0.08, 0.04, 0.02, and 0.01 mM. The cell path length was 1 mm in the first, 2 mm in the second and 10 mm in the last three experiments. All other conditions were the same as described above (cf. 3.1.4.).

3.1.9. CD spectrum of Dynorphin A-(1-8) in Methanolic Solution

1.0 mg of dynorphin A-(1-8) was dissolved in 3 mL of methanol and the CD spectrum was acquired as described in section 3.1.4.

3.2. Results and Discussion

3.2.1. Solvent Dependence of the CD Spectra of Dynorphin A-(1-13)

CD spectra of dynorphin A-(1-13) in aqueous and organic solution, in SDS micelles, and in phospholipid vesicles were recorded. The contents of the samples are listed in section 3.1.6. The peptide concentration was checked by UV absorption spectrometry (3.1.3.) where literature data was available (cf. Table 3.4).

Table 3.4. Determination of the peptide molar concentrations by UV absorption spectrometry.

Experimental Data

sample (cf. Tab 3.3)	A	B
solvent	water	methanol
path length b [cm]	1	1
λ_{max} [nm]	275.4	277.7
A_{max}	0.3473	0.4215

Literature data [Sober, 1970, B-74]
for the N-acetyl-methyl ester of tyrosine

solvent	water	ethanol
A_{max} [nm]	274.6	278.4
ϵ_{max} [$M^{-1}cm^{-1}$]	1420	1790
$c_{pep} = A_{max}/(\epsilon_{max} b)$ [mM]	0.24	0.24

Calculation of the concentrations by weight-to-volume ratios yield comparable concentrations of 0.25 mM for dynorphin A-(1-13) in water and 0.23 mM for dynorphin A-(1-13) in methanol. Therefore no severe error is anticipated by calculating the concentrations of the other samples from the weight-to-volume ratios (cf. below).

Disregarding any volume effects of mixing, the peptide molar concentration of the sample with 50% methanol was calculated by averaging the concentrations of the two original samples (cf. caption of Table 3.3). In all other cases, concentrations were calculated by weight-to-volume ratios:

$$c = n / V$$
$$= m / (M_r \cdot V)$$

The peptide concentrations and the detergent-to-peptide and lipid-to-peptide ratios are listed in Table 3.3. Listed in Table 3.5 are the multiplication factors $[\theta]/\theta$ for the display of the spectra in terms of mean residue ellipticity $[\theta]$, which were calculated as described in section 3.1.5.3 and the results of the secondary structure analysis described in section 3.1.5.5. The difference in the CD spectra of dynorphin A-(1-13) in aqueous solution and in DMPG bilayers is illustrated in Figure 3.4, as is the similarity of the spectra recorded in methanol and in SDS micelles to that in a DMPG environment.

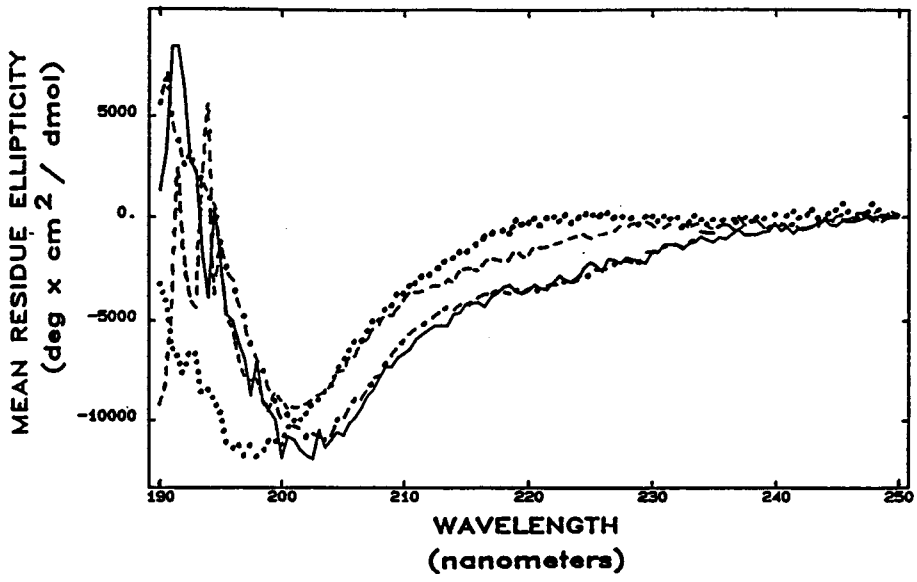

Figure 3.4. Circular dichroism spectra of dynorphin A-(1-13) solutions in water (•••••), methanol (- - -), aqueous SDS micelles (•-•-•), and aqueous DMPG bilayers [4](———). The temperature was 25°C.

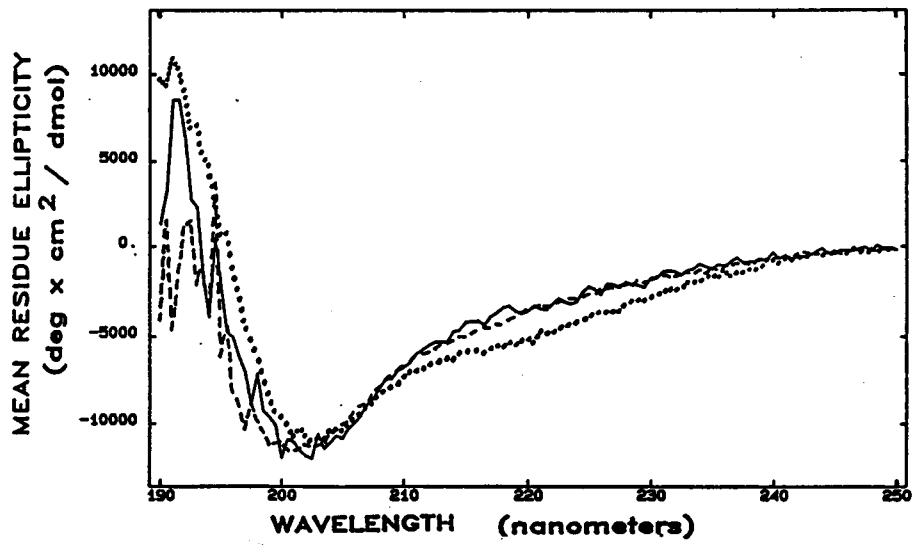

Figure 3.5. Circular dichroism spectra of dynorphin A-(1-13) solutions in TFE (•••••), 30% TFE/water (- - -), and aqueous bilayers of DMPG (——). The temperature was 25° C.

[4] previously recorded by Dr. R. F. Epand.

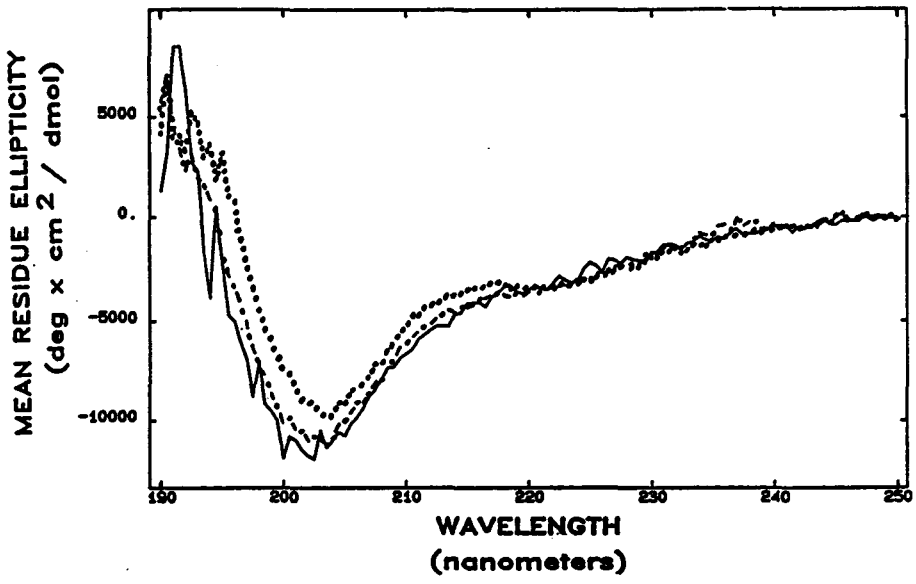

Figure 3.6. Circular dichroism spectra of dynorphin A-(1-13) solutions in aqueous SDS micelles (·····), in aqueous SDS micelles pH 2.8 (·····), and aqueous DMPG bilayers (———). The temperature was 25° C.

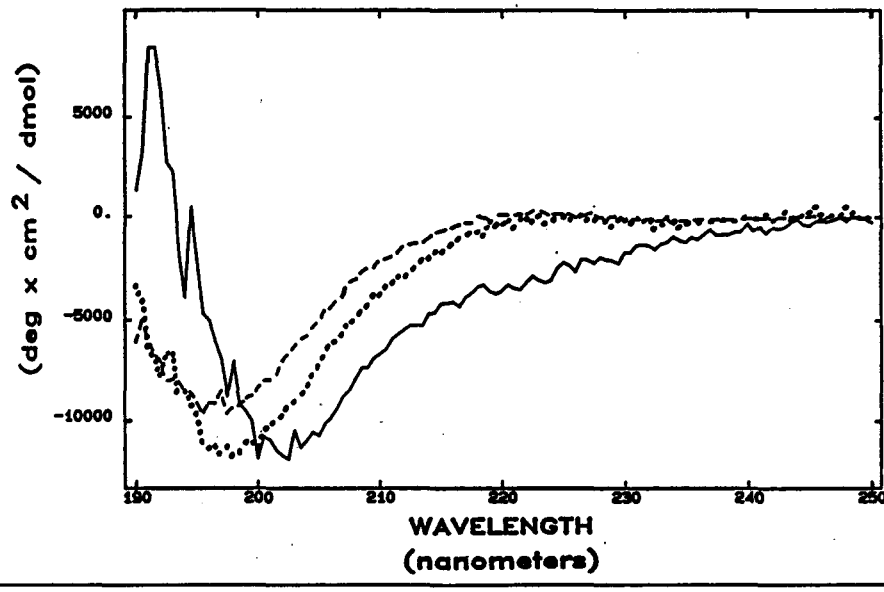

Figure 3.7. Circular dichroism spectra of dynorphin A-(1-13) solutions in aqueous solution (·····), DMPG bilayers (———), and sonicated DMPC bilayers (- - -). The temperature was 25° C.

Table 3.5. Estimation of the secondary structure fractions of dynorphin A-(1-13) in different solvent environments from circular dichroism

Sample (cf. 3.1.6)	$[\theta]/\theta$ ($M^{-1}\cdot mm^{-1}$)	******** Fractions of total *******			
		α-helix	β-sheet	β-turn	random
A "Water"	314.6	0.0	0.44	0.13	0.44
B "Methanol"	326.8	0.0	0.60	0.05	0.35
C "50% Methanol"	320.5	0.0	0.55	0.04	0.41
D "SDS"	370.2	0.02	0.59	0.0	0.39
E "SDS/pH 2.8"	370.2	0.04	0.63	0.0	0.33
F "TFE"	398.1	0.08	0.51	0.0	0.41
G "30% TFE"	296.2	0.0	0.53	0.04	0.43
H "DMPG"	493.6	0.02	0.57	0.0	0.41
I "DMPC"	411.3	0.0	0.49	0.13	0.37

Visual comparison of the spectra (Figure 3.5) of dynorphin A-(1-13) in aqueous solution to those of the peptide in methanolic solution and in the presence of SDS micelles and DMPG bilayers revealed a substantial difference in aqueous solution compared to the other samples. This is semi-quantitatively manifested in the estimated secondary structure fractions listed in Table 3.5[5]. The correspondence of the results for "SDS" (D) and "DMPG" (H) is within the estimated error margin. In the case of "methanol" (B) and "DMPG" (H), the correlation is not as good, but the differences in the values are only slightly greater than the error margin. This is not the case for the CD spectrum of dynorphin A-(1-13) in aqueous solution.

[5] The error in secondary structure determination was estimated at ±0.02 (cf. Table 3.2).

Correspondence of the spectra of the peptide solution in methanol or in SDS detergent micelles with that in DMPG bilayers supports the idea that the membrane-mediated conformation of the peptide can be mimicked in these systems, which led to the design of two corresponding classes of samples for NMR studies (cf. Chapter 4). The above finding also applied to the mixed solvent systems of 50% methanol (Table 3.5) and 30% TFE (Figure 3.5). Nevertheless, these solvent schemes were not employed for NMR investigations, as they would have entailed suppressing two different strong and broadened solvent signals.

30% TFE mimics the membrane environment better than 100% TFE does (Figure 3.5). The probable reason for this is that TFE alone is too apolar to resemble the hydrophobic-hydrophilic interphase of a membrane surface.

Adjustment of the pH to a value of 2.8 only mildly altered the CD spectrum of dynorphin A-(1-13) in SDS micelles (Figure 3.6). The spectrum still correlates well with that in DMPG bilayers. This finding is important for choosing an appropriate NMR sample, as the important backbone NH resonances are observed in aqueous solution only at approximately pH 3.

The CD spectrum of dynorphin A-(1-13) with sonicated DMPC bilayers in water is distinctly different from the one with anionic DMPG bilayers. A possible reason for this is that the majority of the cationic peptide remained unbound to the zwitterionic lipid. The spectrum may be dominated by the unbound conformation since it is more similar to that of the peptide in aqueous solution than to the others. Although this finding was originally discouraging, the analogous NMR sample turned out to be quite useful because of this property (cf. Chapter 6).

A possible criticism of the experiment with DMPG is that the lipid was not sonicated. Although DMPG is soluble in water, and the sample did not show any visible effect of light scattering, absorption line flattening due to the Duysens effect (cf. Chapter 1) is a possible consequence of not sonicating the lipid. As, however, the positively charged peptide probably induces aggregation and fusion of the lipid vesicles, sonication of the lipid before addition of the peptide will not assist in solving the problem. The magnitude of this effect is, however, considered to be minute as the sample concentration was comparatively high and the cell path length relatively short.

A finding of prime importance is that the calculated α-helical content is negligible in all cases ($\leq$ 4 %), except for the system with pure TFE (Table 3.4). Similar results were obtained by Kojro et al. [1987] for CD spectra in water and TFE respectively. As the detection of α-helical content is generally regarded as the prime feature of protein secondary structure analysis by CD spectropolarimetry, this is taken as a strong indication for the absence of α-helical features in the case of the membrane-mediated conformation of dynorphin A-(1-13).

These results are in stark contrast to those obtained by Maroun and Mattice [1981], who reported a helical content of 5% for dynorphin A-(1-13) in water and 17% in SDS micelles on the basis of the measured ellipticity at 222 nm. The lipid-to-peptide ratio was not explicitly reported, but can be inferred to be between 400 and 1200 as opposed to 47 in the present case. Nevertheless, the main source of deviation of the results cannot lie in the differing lipid-to-

peptide ratios because the reported helical content for the peptide in water is also overemphasized in comparison to our results. A possible source of divergence could lie in the fact that the Mattice group worked at lower peptide concentrations (3-12 μM), but this factor has been ruled out at least for the sample in methanol (cf. 3.1.3.), so it would seem unlikely to be significant. The most probable origin of the disagreement of the results appears to be the difference in secondary structure analysis. Indeed, application of the method employed by Maroun and Mattice[6] for the estimation of α-helical content to our data yields considerably higher values in all cases (Table 3.6).

Table 3.6. Estimation of the α-helical content of dynorphin A-(1-13) in different solvent environments from circular dichroism by the methods of (A) Maroun and Mattice [1981] and (B) Chang et al. [1978, cf. section 3.1.5.4].

Sample	θ_{222}	(A)	(B) [from Table 3.3]
"Water" (A)	43	0.04	0.0
"Methanol" (B)	-1374	0.07	0.0
"50% Methanol" (C)	-1646	0.08	0.0
"SDS" (D)	-3381	0.13	0.02
"SDS/pH 3" (E)	-3253	0.12	0.04
"TFE" (F)	-4780	0.17	0.08
"30% TFE" (G)	-3266	0.12	0.0
"DMPG" (H)	-3177	0.12	0.02
"DMPC" (I)	252	0.03	0.0

$[\theta]_{222}$ = mean residue ellipticity at 222 nm (in deg · cm^2 / dmol)
(A) $f_\alpha = (1400 - [\theta]_{222}) / 37400$

[6] originally described by Beychok [1967, p. 233].

Although the initial assumption that the Tyr^1 chromophore does not significantly contribute to the spectrum may apply when considering the whole far UV region, it does not hold true for the analysis at the single wavelength of 222 nm. The ^1L_a [7] transition of tyrosine gives rise to a positive Cotton effect at approximately 223 nm [Hooker and Schellmann, 1970]. Slight differences in orientation can lead to a reversal of the sign of the Cotton effect [Hooker and Schellmann, 1970; Snow and Hooker, 1975]. A negative Cotton effect at this wavelength would lead to an overestimation of the helical content by the method of Maroun and Mattice [1981]. Although the method of Yang's group [Chang et al., 1978] has been shown to be unsatisfactory in the prediction of β-forms [Yang et al., 1986], its CD estimates of helical content are within ± 0.10 of available X ray results [Yang et al., 1986]. In summary, all available evidence suggests that our interpretation of the data employing Yang's curve-fitting approach gives a better approximation of the actual helical content of the peptide.

Confirmation of Schwyzer's model would require a helical content of 69% (= 9/13), any value under 28% (= 3.6/13; one turn) does not indicate a physically significant level of helical content. Consequently, neither the findings of Maroun and Mattice nor our present study can confirm the validity of Schwyzer's model. On the contrary, they indicate that the proposed conformation is improbable.

---

[7] The notation used was proposed by Platt [1949]. The transition moment orientations in phenolic systems have been described in detail by Hooker and Schellmann [1970].

3.2.2. Temperature Dependence of the CD Spectra of Dynorphin A-(1-13) in Methanolic Solution

Sample preparation and experimental conditions were described in section 3.1.7. The peptide concentration was calculated as: c = 0.8 / (1604.19 • 3) = $1.662 \cdot 10^{-4}$ M ≈ 0.17 mM. The calculation of the multiplication factor $[\theta]/\theta$ was performed as described in section 3.1.5.3: $[\theta]/\theta$ = 462.8 ($M^{-1} \cdot mm^{-1}$). The spectra are shown in Figure 3.8. No significant temperature dependence of the CD spectrum of dynorphin A-(1-13) in methanolic solution could be observed in the temperature range studied.

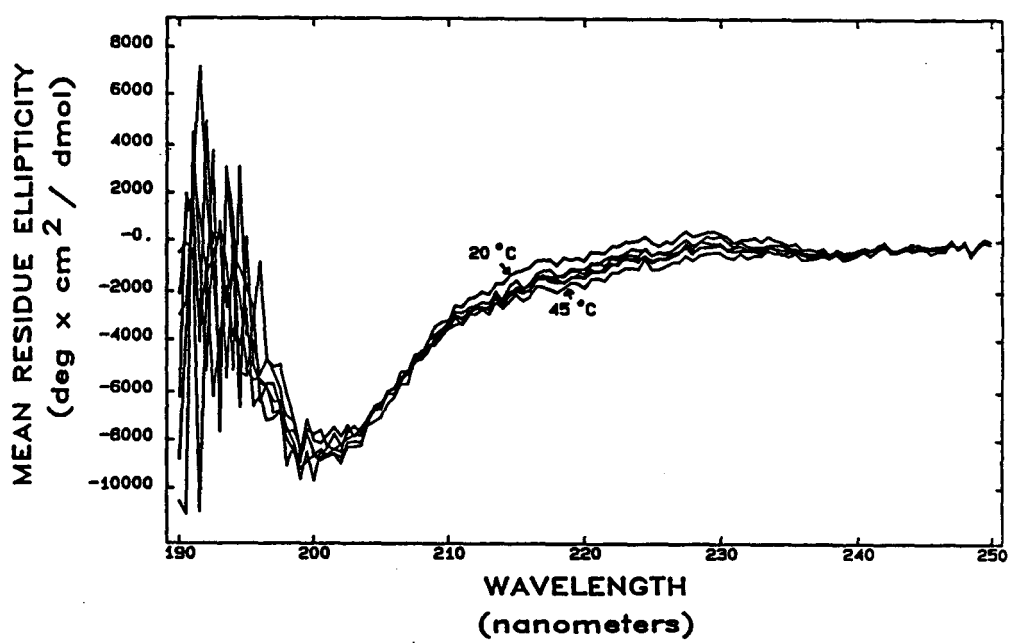

Figure 3.8. Circular dichroism spectra of a 0.17 mM dynorphin A-(1-13) solution in methanol at 20°C, 25°C, 30°C, 35°C, 40°C, and 45°C.

Table 3.7. Estimation of the secondary structure fractions of dynorphin A-(1-13) in methanolic solution from circular dichroism at different temperatures.

(°C)	α-helix	β-sheet	β-turn	random
20	0.00	0.59	0.06	0.35
25	0.00	0.58	0.06	0.36
30	0.00	0.61	0.06	0.34
35	0.00	0.60	0.05	0.35
40	0.00	0.64	0.03	0.33
45	0.00	0.62	0.03	0.34

3.2.3. Concentration Dependence of the CD Spectra of Dynorphin A-(1-13) in Methanolic Solution

Sample preparation and experimental conditions were described in section 3.1.8. The peptide concentration of the first sample was checked by UV absorption spectrometry (cf. Table 3.8).

The peptide concentrations, the multiplication factors $[\theta]/\theta$ for the display of the spectra in terms of mean residue ellipticity $[\theta]$, and the results of the secondary structure analysis (described in sections 3.1.5.3 and 3.1.5.4, respectively) are listed in Table 3.9. The spectra are shown in Figure 3.9.

Table 3.8. Determination of the peptide molar concentration by UV absorption spectrometry.

Experimental Data

solvent	methanol
path length b [cm]	1
λ_{max} [nm]	278.0
A_{max}	0.2940

Literature data [Sober, 1970, B-74]
for the N-acetyl-methyl ester of tyrosine

solvent	ethanol
A_{max} [nm]	278.4
ϵ_{max} [$M^{-1}cm^{-1}$]	1790
$c_{pep} = A_{max}/(\epsilon_{max} b)$ [mM]	0.16

Table 3.9. Estimation of the secondary structure fractions from circular dichroism of dynorphin A-(1-13) in methanol at different peptide concentrations. Sample cell path lengths and multiplication factors $[\theta]/\theta$ are also listed.

c_{pep}	cell path length b	$[\theta]/\theta$	****** Fractions of total ******			
(mM)	(mm)	(M^{-1}·mm^{-1})	α-helix	β-sheet	β-turn	random
0.16	1	468.5	0.00	0.60	0.05	0.35
0.08	2	468.5	0.00	0.64	0.00	0.36
0.04	10	187.6	0.06	0.68	0.07	0.19
0.02	10	375.2	0.00	0.67	0.02	0.31
0.01	10	769.2	0.00	0.47	0.09	0.43

c_{pep} = peptide concentration

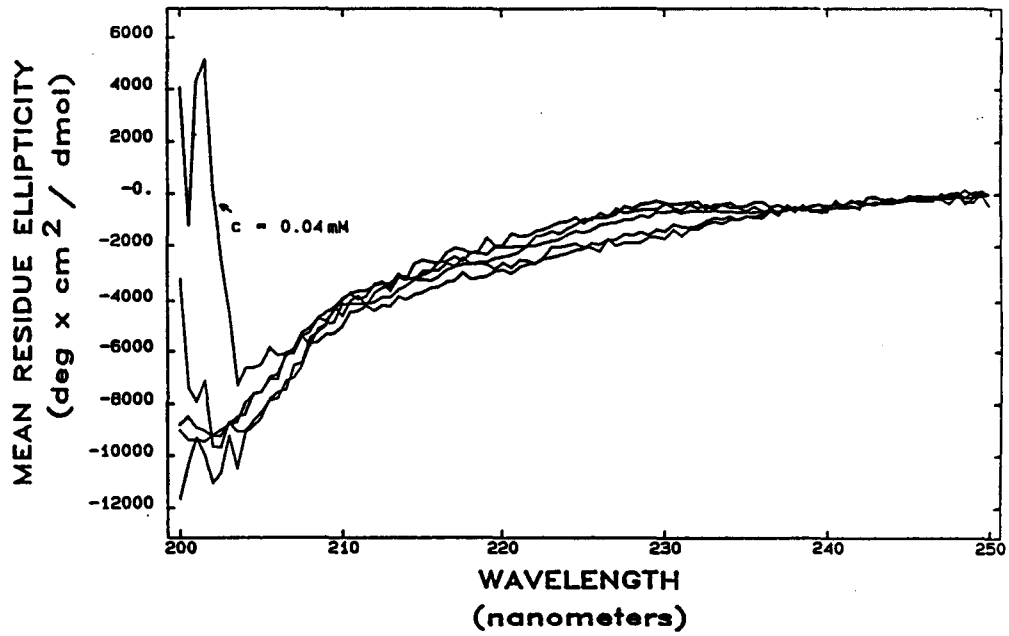

Figure 3.9. Circular dichroism spectra of dynorphin A-(1-13) solutions in methanol at 25°C. The peptide concentrations were 0.16 mM, 0.08 mM, 0.04 mM, 0.02 mM, and 0.01 mM.

No significant concentration dependence of the CD spectrum of dynorphin A-(1-13) in methanolic solution could be observed. The slight aberration of the estimated secondary structure fractions in the case of 0.04 mM peptide is taken to result from apparently deviant readings at these lower concentrations.

The results of the temperature (3.2.2.) and concentration (3.2.3.) dependent studies support the idea that the CD spectra of dynorphin A-(1-13) in methanolic solution are not influenced by self-aggregation phenomena. This is an important finding because amphiphilic β-strands have the tendency to self-associate to amphiphilic β-sheets [Osterman and Kaiser, 1985] and the results of the secondary structure estimation do not rule out the possibility of a β-

structure. Self-association is, however, not very probable in the present case due to the net positive charge of the peptide. No indication in this direction can be derived from the above sets of experiments.

Another indication from the lack of any significant temperature or concentration dependence is that the CD spectra do not constitute the equilibrated average of several distinctly different conformations of significant abundance. If this were so, an effect on the CD spectrum should be observed with the alteration of temperature and concentration.

3.2.4. Comparison of the CD spectra of Dynorphin A-(1-13) and of Dynorphin A-(1-8) in Methanolic Solution

Sample preparation and experimental conditions were described in section 3.1.9.

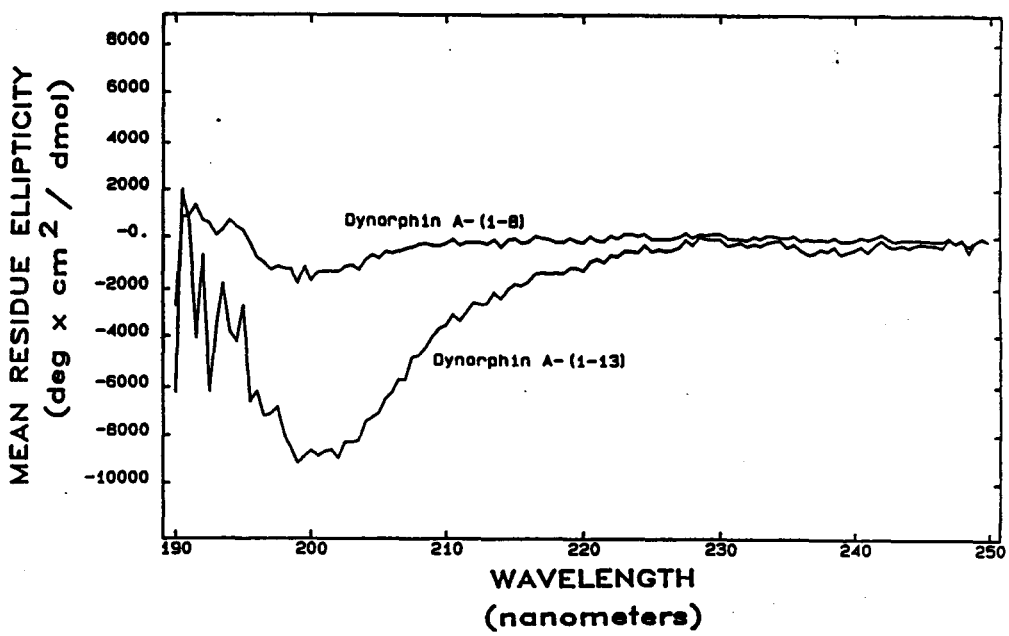

Figure 3.10. Circular dichroism spectra of a 0.24 mM dynorphin A-(1-13) and a 0.34 mM dynorphin A-(1-8) solution in methanol at 25°C.

Table 3.10. Estimation of the secondary structure fractions of dynorphin A-(1-13) and dynorphin A-(1-8) in methanolic solution from circular dichroism

Sample	$[\theta]/\theta$	c_{pep}	****** Fractions of total ******			
	(M^{-1}·mm^{-1})	(mM)	α-helix	β-sheet	β-turn	random
Dynorphin A-(1-13)	326.8	0.16	0.00	0.60	0.05	0.35
Dynorphin A-(1-8)	367.6	0.34	0.00	0.76	0.05	0.19

c_{pep} = peptide concentration

The spectra are completely different. The fundamental importance of the C-terminal residues for the overall conformation of the tridecapeptide is illustrated by these results. Another conclusion that can be drawn is that although no helix breaking Pro^{10} is present, the octadecapeptide shows no affinity for adopting an α-helical conformation in methanol. This stands in marked contrast to the hydrophobic moment profile of dynorphin A-(1-8) (cf. Chapter 2), which indicates a fourfold increased hydrophobic moment in the case of an α-helical conformation as compared to an extended secondary structure. The chain length is probably too short to stabilize a helical structure in the case of dynorphin A-(1-8), as well as for the postulation of a nonapeptide helix in the case of the tridecapeptide.

4. NMR STUDIES

4.1. Conformational Analysis by NMR Spectroscopy

A more detailed description of the conformational properties of dynorphin A-(1-13) than by CD spectropolarimetry can be achieved by nuclear magnetic resonance (NMR) spectroscopy [Abragam, 1961; Derome, 1987; Freeman, 1988; Harris, 1986; Jardetzky and Roberts, 1981; Sanders and Hunter, 1987; Wüthrich, 1976, 1986]. With the advent of high-field [Bothner-By and Dadok, 1979] Fourier transform [Ernst and Anderson, 1966], two- [Aue et al., 1976a], three- [Oschkinat et al., 1988] and four-dimensional techniques [Kay et al., 1990], NMR spectroscopy has become an increasingly more powerful tool for the conformational analysis of peptides and proteins [Wüthrich, 1989b]. A generally accepted strategy [Bax, 1989; Clore and Gronenborn, 1989; Kessler et al., 1985c; Kessler and Bermel, 1986; Wagner, 1990; Wüthrich, 1986] for NMR studies of peptides and proteins consists of the establishment of individual resonance assignments before conformational features are discussed, because the unambiguous assignment of all the resonance lines in the ^{1}H (and ^{13}C, where applicable) NMR spectrum is a prerequisite for the extraction of information on the spatial arrangement of the molecule.

4.1.1. Sequence Specific Assignments

The first step is the recognition of individual amino acid spin systems by their different through-bond correlation patterns with the aid of two-dimensional (2-D) $^1H,^1H$ COSY(-90), $^1H,^1H$ COSY-45, phase sensitive COSY with a double quantum filter (DQF phase-sensitive COSY), long-range $^1H,^1H$ COSY, and relayed $^1H,^1H$ COSY (RELAY) experiments. This task is by no means trivial, especially if the molecule contains a number of residues with several side chain methylene protons. Sequence specific resonance assignments (in addition to conformational information, see below) are obtained by through-space connectivities, which are most conveniently measured by the NOESY experiment.

4.1.2. Conformational Analysis

Conformational analysis is obtained through the extraction of various parameters in different experimental schemes.

4.1.2.1. The Nuclear Overhauser Effect

Proximity relationships can be derived from the observations of the Nuclear Overhauser Effect (NOE) [Noggle and Schirmer, 1971; Neuhaus and Williamson, 1989] in a transient NOE experiment [Soloman, 1955] or its two-dimensional version with cross-relaxation in the laboratory frame, NOESY [Macura and Ernst,

1980; Jeener et al., 1979], or in the rotating frame, 2-D CAMELSPIN/ROESY [Bothner-By et al, 1984; Bax and Davis, 1985].

4.1.2.2. Spin-Spin Coupling Constants

An indication of torsional angles can be derived from the appropriate spin-spin coupling constants [Karplus, 1959; Bystrov, 1976], primarily the torsional angle ϕ [IUPAC-IUB, 1970] from the vicinal coupling constant $^3J_{HN\alpha}$ [Bystrov, 1976; Pardi et al., 1984].

4.1.2.3. Chemical Shifts

A third set of parameters yielding information on conformational properties are the chemical shifts. Chemical shifts are primarily determined by the covalent structure of the peptide and the magnetic susceptibility of the solvent environment, but there are conformational aspects. Ring current shifts of up to 2 ppm upfield can occur, especially for methyl groups, when this methyl group is in close proximity to the aromatic ring plane of an aromatic amino acid side chain [Sternlicht and Wilson, 1967; McDonald and Phillips, 1967]. Strongly shifted NH protons are often assumed to be hydrogen-bonded [Emsley et al., 1965], but results from this method are not unambiguous for peptides because too many other conformational effects influence the NH resonances.

4.1.2.4. Temperature Dependence of the Amide Proton Chemical Shifts

Amide protons involved in intramolecular hydrogen bonds or otherwise shielded from the solvent will not only have different chemical shifts from the solvent-exposed amide protons, but also show a distinct difference in the temperature dependence of the chemical shifts.

4.1.2.5. Solvent Exchange

The application of the study of ^{1}H-^{2}H exchange rates of backbone amide protons as an indication of peptide secondary structure has a long tradition in biophysical chemistry [Berger and Linderstrøm-Lang, 1957] and was first reported in NMR studies by Craig and coworkers [Stern et al., 1968]. A slow exchange is indicative of intramolecular hydrogen-bonding, while rapid exchange suggests ready accessibility to the solvent. Measurement of deuterium-proton exchange between solvent molecules and backbone amide groups can be accomplished by two different approaches. Saturation transfer experiments [Hoffman and Forsén, 1966] for faster exchange rates (>1 sec^{-1}) and by dissolving the protonated compound in a perdeuterated protic solvent and recording the spectrum at variable times after sample preparation for slower exchange rates. Although there are primary structure effects on the rate of up to about tenfold, the effect of neighbouring peptide groups on the exchange rate of a central peptide has been quantitatively established [Molday et al., 1972], and decreases

in the exchange rate due to solvent inaccessibility and hydrogen bonding are often substantially larger than this.

4.1.3. ^{13}C NMR Studies

^{13}C NMR studies are a valuable complement to ^{1}H NMR studies. The advantages of ^{13}C NMR include [Wüthrich, 1976] better spectral resolution, as the carbon resonances are separated over ca. 200 ppm (as opposed to ca. 10 ppm in the case of ^{1}H), a more direct observation of the molecular backbone, and the possibility of observing carbonyl carbons. A fundamental disadvantage is the low sensitivity[1], $|\gamma^3 \cdot C|$, of the carbon nucleus, which is approximately 1/6000 compared to ^{1}H. The parameters of greatest practical interest in broadband decoupled[2] ^{13}C NMR studies are the chemical shift values [Howarth and Lilley, 1978] and the longitudinal relaxation times [Deslauriers and Smith, 1976].

---

[1] γ is the gyromagnetic ratio and C the natural abundance of the nucleus.

[2] In non-decoupled spectra, i.e. by performing heteronuclear J,δ spectroscopy [Bodenhausen et al., 1976a,b, 1977], spin-spin coupling constants can provide a great deal of useful information for assignment purposes, structure elucidation, stereochemical studies, rotamer population studies, substituent effect studies, and demonstration of the existence of hydrogen bonds [Hansen, 1981].

4.1.4. Conformational Heterogeneity of Linear Peptides in Solution

Conformational analysis of linear oligopeptides must take into account that often many energetically nearly equivalent conformations are simultaneously present in a rapid equilibrium situation [Wüthrich, 1976, p.92]. If the timescale of the associated exchange process is fast with respect to the parameters of interest, the observed NMR parameters correspond to a weighted average taken over numerous rotational states [cf. Jardetzky and Roberts, 1981, pp. 115-142]. Distances or torsional angles calculated from such averaged NMR parameters are physically meaningless[3] [Jardetzky, 1980; Kessler, 1982]. Evidence for the dominance of one conformation in the equilibrium is given by several criteria [Kessler et al., 1985c].

1. Considerable differences in the spectral parameters (^1H and ^{13}C chemical shifts and coupling constants) of equal amino acids in the sequence.

2. Considerable differences in the amide proton chemical shift values and their temperature dependence of the different amino acid residues in the molecule.

3. Vicinal coupling constants $^3J_{HN\alpha}$ that differ greatly from a mean value of about 7.5 Hz.

---

[3] This would only then not be the case, if the NMR parameters were linearly dependent on distances or angles (which applies neither to coupling constants nor NOE's) and if the process of averaging were symmetric about a single energy minimum [Jardetzky and Roberts, 1981, p.129].

4. Strong splittings of the diastereotopic $C_\alpha H$ protons of glycine.

5. Side chain fixation, which can be detected through observation of considerable differences in the chemical shifts and coupling constants of β protons in aromatic side chains.

6. Linearity of the NH chemical shift variation with temperature, indicating apparent temperature independence of conformations.

Nevertheless, a number of linear peptides have been shown to exhibit a preference for a specific conformation in organic solution (e.g. methionine-enkephalin [Jones et al., 1976; Roques et al., 1976; Higashijima et al., 1979; Miyazawa and Higashijima, 1981], leucine-enkephalin [Jones et al., 1976; Stimson et al., 1979], and receptor selective opioid peptides [Doi et al., 1988] in DMSO, δ-hemolysin in methanol [Tappin et al., 1988], and des-Trp^1,Nle^{12}-minigastrin [Mammi et al., 1988] and human growth hormone releasing factor analogues [Clore et al., 1986] in TFE-water mixtures) and even in aqueous solution (e.g. the tridecapeptide α-conotoxin G1 [Pardi et al., 1989] and immunogenic peptide fragments [Dyson et al., 1985, 1988a]).

4.2. Materials and Methods

On the basis of the CD results (cf. Chapter 3), four different classes of NMR samples were studied: dynorphin-A-(1-13) in methanolic solution, in aqueous solution, in the presence of SDS detergent micelles, and in the presence of lipid SUV's.

4.2.1. Materials

Dynorphin A-(1-13) was kindly provided by Serge A. St-Pierre (cf. Chapter 3).

Deuterium oxide (^2H_2O), [$^2H_4$]-methanol ($C^2H_3O^2H$), partially deuterated methanol (C^2H_3OH), perdeuterated sodium dodecyl sulfate (d_{25}-SDS, M_r = 313.53 g/mol), and perdeuterated acetic acid ($C_2{}^2H_5COO^2H$, M_r = 66.09 g/mol, Density = 1.05 g/mL) were purchased from Merck Sharpe and Dome (MSD Isotopes), Montreal.

[$^2H_{54}$]-Dimyristoyl-L-3-phosphatidylcholine (= d_{54}-DMPC, M_r = 732.24 g/mol) was purchased from Serdary Research Laboratories, London, Ontario, for the 500 MHz studies, and from Avanti Polar Lipids Inc., Birmingham, AL, U.S.A. for the 620 MHz studies. Dimyristoyl-L-3-phosphatidylglycerol (DMPG, M_r = 666.89 g/mol) was also purchased from Avanti Polar Lipids.

4.2.2. Samples

4.2.2.1. Dynorphin-A-(1-13) in Methanolic Solution

Studies on the non-labile protons were performed in CD_3OD, the labile protons were included in studies in CD_3OH. The amounts of peptide, the sample volumes, and the resulting concentrations are listed in Table 4.1.

4.2.2.2. Dynorphin A-(1-13) in Aqueous Solution

Studies on the non-labile protons were performed in D_2O, the labile protons were observed in mixtures of H_2O and D_2O with d_6-acetic acid (CD_3COOD) added. The small amount of D_2O was necessary for the operation of the deuterium lock, which is essential for compensation of long term instabilities of the static magnetic field. The acidic environment was required to retard backbone amide proton exchange, so that the backbone amide proton resonances were NMR-observable [Wüthrich, 1986, p. 24]. The amounts of peptide, the sample volumes, and the resulting concentrations are listed in Table 4.1.

4.2.2.3. Dynorphin A-(1-13) in the Presence of Lipids

For the sample studies in anionic detergent, see Table 4.1. The phospholipid samples were prepared in analogy to the CD samples (section 3.1.2). The phospholipid was dissolved in a mixture of chloroform and methanol (2:1, v/v). The solvent was evaporated with a stream of dry nitrogen leaving the lipid as film on the walls of a glass test tube. Last traces of solvent were removed into a liquid nitrogen trap by placing the sample under high vacuum overnight. The phospholipid film was resuspended in D_2O (or in CD_3COOD in H_2O/D_2O, cf. section 4.2.2.2 and Table 4.1) by warming the tube to about 45°C and vortexing vigorously for about 30 s. When the removal of HDO was desired, the multilamellar suspension was lyophilized overnight and the deposit was resuspended in D_2O. The multilamellar suspensions were sonicated to visual clarity in a sonicating bath at 60 W. In unsuccessful cases, the samples were subjected to five freeze-thaw and 10 extrusion cycles [Hope et al., 1985; Mayer et al., 1986] in a Lipex Biomembranes extruder with a 100 nm filter before sonication was continued.

The opalescent samples became slightly turbid after addition of the peptide. This was attributed to peptide-induced aggregation and fusion (cf. section 3.1.2) of the lipid vesicles. This phenomenon, however, did not cause severe problems, as it did not detrimentally affect the NMR spectrum.

Table 4.1. Overview of NMR samples (titration experiments not included).

m_{pep} (mg)	V (mL)	Solvent	c_{pep} (mM)	c_{lip}/c_{pep}
5.0	0.5	CD_3OD	6	-
6.2	0.7	CD_3OH	5.5	-
21.7	0.7	CD_3OH	20	-
21.7	0.35	CD_3OD	40	-
21.7	0.35	CD_3OH	40	-
20.3	0.5	CD_3OD	25	-
5.0	0.5	D_2O	6	-
10.0	0.5	D_2O	12.5	-
5.0	0.5	"H_2O"[a]	6	-
10.0	0.45	"H_2O"[b]	14	-
7.2	0.8	"400 mM d_{25}-SDS/H_2O"[c]	5.5	71
0	0.7	"32 mM d_{54}-DMPC/D_2O"[d]	0	-
9.0	0.7	"32 mM d_{54}-DMPC/D_2O"[d]	8	4
9.0	0.7	"32 mM d_{54}-DMPC/H_2O"[e]	8	4
0	0.7	"32 mM DMPG/D_2O"[f]	0	-
9.0	0.7	"32 mM DMPG/D_2O"[f]	8	4
0	0.5	"50 mM d_{54}-DMPC/D_2O"[g]	0	-
10.0	0.5	"50 mM d_{54}-DMPC/D_2O"[g]	12.5	4
10.0	0.45	"56 mM d_{54}-DMPC/H_2O"[h]	14	4

a: "H_2O" = CD_3COOD in H_2O/D_2O (4:1, v/v), pH 2.8
b: "H_2O" = CD_3COOD in H_2O/D_2O (9:1, v/v), pH 2.95
c: "400 mM d_{25}-SDS/H_2O" = 100 mg d_{25}-SDS in H_2O/D_2O (7:1, v/v), pH 2.8
d: "32 mM d_{54}-DMPC/D_2O" = 16.4 mg d_{54}-DMPC (Serdary) in 0.7 mL D_2O
e: "32 mM d_{54}-DMPC/H_2O" = 16.4 mg d_{54}-DMPC (Serdary) in 0.7 mL "H_2O"
(= CD_3COOD in H_2O/D_2O (6:1, v/v), pH 2.8)
f: "32 mM d_{54}-DMPG/D_2O" = 15.3 mg DMPG in 0.7 mL D_2O
g: "50 mM d_{54}-DMPC/D_2O" = 18.3 mg d_{54}-DMPC (Avanti) in 0.5 mL D_2O
h: "56 mM d_{54}-DMPC/H_2O" = 18.3 mg d_{54}-DMPC (Avanti) in 0.45 mL "H_2O"
(= CD_3COOD in H_2O/D_2O (9:1, v/v), pH 2.95)

4.2.3. One-Dimensional 500 MHz NMR Studies

500 MHz NMR spectra were recorded on a Bruker AM-500 spectrometer equipped with an Aspect 3000 computer at the NMR facility of the Department of Chemistry, McMaster University. Quadrature detection was used for all experiments allowing the carrier frequency to be placed at the centre of the spectrum.

One-dimensional ^{1}H and ^{13}C spectra were recorded at a magnetic field of 11.74 Tesla, with protons resonating at 500 MHz, carbons at 125 MHz.

4.2.3.1. Routine ^{1}H NMR Spectra

Proton spectra were acquired at 500.138 MHz using a 5 mm dual frequency $^{1}H/^{13}C$ probe over a spectral width of 4200 - 5000 Hz in 16K data points (1.950 - 1.638 s acquisition time). Sample temperature was maintained at 30(±1)°C by a Bruker B-VT 1000 variable temperature unit. The solvent resonance was suppressed by presaturation during a 1.0 s delay prior to acquisition.

The free induction decays were processed using Gaussian multiplication for resolution enhancement [Ernst, 1966, pp. 50-64] and were zero-filled to 32K before Fourier transformation [Bracewell, 1990; Press et al., 1986, pp. 381-453].

The digital resolution was between 0.26 and 0.31 Hz/point (depending on the spectral width employed). Chemical shifts are reported in ppm relative to TMS using the residual solvent signals at 3.30 ppm (methanol) and 4.80 ppm (water) as internal references.

These conditions apply to all other ^{1}H NMR experiments unless stated otherwise.

Temperature Dependent Studies

Temperature dependent studies are usually performed by increasing the probe temperature (e.g. 5 to 65°C [Zhou and Gibbons, 1986], 25 to 85°C [Schwyzer et al., 1972]). As, however, it is not advisable to heat the methanolic solution significantly higher without incurring the danger of considerable evaporation of the solvent, the probe temperature was reduced. Routine proton spectra were recorded as described above over a spectral width of 4545.455 Hz (1.802 s acquisition time). 56 Scans were accumulated at temperatures of 30°C, 11°C, -31°C, -20°C, and -10°C.

Saturation Transfer Experiments

Routine proton spectra were recorded as described above over a spectral width of 5000 Hz (1.6384 s acquisition time).

Variation of the Decoupler Power Level

The decoupler power level was increased from 2 μW (50dB) to 6.3 mW (15 dB) in increments of 5dB. Eight scans were accumulated for each spectrum. The presaturation time was kept constant at 1.0 s.

Variation of the Presaturation Time

The presaturation time was increased from 0.1 to 3.0 s in increments of 0.1 up to 1.0 s and of 0.5 thereafter. Eight scans were accumulated for each spectrum. The decoupler power level was kept constant at 0.2 mW (30dB).

Comparison of Selective Excitation and Selective Saturation

256 scans were accumulated both in a selective excitation experiment and under totally analogous conditions in a presaturation experiment with a presaturation time of 1.0 sec and a decoupler power level of 2 mW (20dB).

The selective excitation experiment was performed employing the 1-1 hard pulse technique [Clore et al., 1983]. The pulse sequence applied was:

$$RD - (\pi/4)_{\phi} - \tau - (\pi/4)_{\phi} - FID$$

The carrier frequency is set near the region of interest. ν is the difference in frequencies between the carrier and the solvent resonance. The delay time τ is selected at $1/2\ \nu$, so that the carrier frequency is $1/2\tau$ away from the solvent resonance. The solvent magnetization is returned entirely to the z axis and not detected in the xy plane. At all other resonance frequencies, some magnetization is flipped into the xy plane, although the line intensities near the solvent resonance are reduced. A high degree of accuracy is required for both the pulse length and the delay τ.

Methanol Titration Experiments

Perdeuterated methanol (CD_3OD) was added in four 0.1 mL increments to the sample containing 6.2 mM dynorphin A-(1-13) in H_2O/pH 2.8. Proton spectra were acquired over a spectral width of 4200 Hz in 16K data points (1.950 s acquisition time). The H_2O solvent resonance was suppressed by presaturation during a 1.0 s delay prior to acquisition. The free induction decays were processed using Gaussian multiplication for resolution enhancement and were

zero-filled to 32K before Fourier transformation. The digital resolution was 0.26 Hz/point.

140 mM d_6-acetic acid (CD_3COOD) in H_2O (pH 2.8) was added in four 0.1 mL increments to the sample containing 25 mM dynorphin A-(1-13) in CD_3OD. Proton spectra were acquired over a spectral width of 5000 Hz in 16K data points (1.638 s acquisition time). The methanolic OH solvent resonance was suppressed by presaturation during a 1.0 s delay prior to acquisition. The free induction decays were processed using Gaussian multiplication for resolution enhancement and were zero-filled to 32K before Fourier transformation. The digital resolution was 0.31 Hz/point.

4.2.3.2. Routine ^{13}C NMR spectra

Carbon-13 spectra were recorded at 125.76 MHz using the 5 mm dual frequency $^{1}H/^{13}C$ probe over a spectral width of 29412 Hz in 16K data points (0.279 s acquisition time). Protons were decoupled by applying composite pulse decoupling [Levitt and Freeman, 1981; Levitt, 1986]. The ^{13}C $\pi/2$ pulse was 7.3 μs. A relaxation delay of 0.5 s was used. Exponential multiplication for sensitivity enhancement was applied to the FID's before Fourier transformation. The digital resolution was 3.6 Hz/point. Chemical shifts for ^{13}C spectra are reported in ppm relative to TMS using the methanol signal at 49.0 ppm as an internal reference.

These conditions apply to all other ^{13}C NMR experiments unless stated otherwise.

Spectral editing was achieved by employing the standard J-modulated spin-sort pulse sequence.

4.2.3.3. Spin-Echo Experiments

The spin-echo sequence, RD - $\pi/2$ - τ - π - τ - FID [Hahn, 1950], is not only employed to determine spin-spin relaxation time constants (see below), but can also be utilized for spectral simplification in ^{1}H NMR [Campbell et al., 1975] and ^{13}C NMR [Rabenstein and Nakashima, 1979].

<u>^{1}H Homonuclear Modulation</u>

Methods for the simplification of ^{1}H NMR spectra for weakly coupled spins (ν_A-ν_X >> J_{AX}) have been introduced by Campbell and coworkers [1975]. As the transverse magnetization generated by the $\pi/2$ pulse is modulated by spin coupling effects, it is possible to select resonances on the basis of their multiplicity. During the total time ($=2\tau$) between the application of the $\pi/2$ pulse and the start of the acquisition of the FID, the transverse magnetization of singlet resonances will decay exponentially according to their time constant, T_2. The

transverse magnetization of a doublet of coupling constant J, however, will not only decay but also change phase with $\cos(2\pi J\tau)$, so that at $\tau = 1/2J$ the signal is 180° out of phase with respect to the singlet. The central component of a triplet resonance behaves in the same way as a singlet, but the two outer components are modulated at twice the frequency of the doublet resonances, i.e. with $\cos(4\pi J\tau)$. At $\tau = 1/2J$, they will be back in phase with the singlet.

In spectral regions where the resonances possess similar J values (±1 Hz), e.g. in methyl protons regions, resonances can therefore be selected on the basis of their multiplicity. Doublets can be separated from triplets if a delay time $\tau = 1/2J$ is selected.

The Ile$^{8}\delta CH_3$ resonance is the only triplet in the methyl region of dynorphin A-(1-13) and should therefore be easily separated from the other methyl resonances in the region (Ile$^{8}\gamma CH_3$, Leu$^{5,12}\delta,\delta'CH_3$'s) by application of the Hahn-spin-echo experiment. This experiment was performed on 5.5 mM dynorphin A-(1-13) in CD_3OH. As the vicinal coupling constants of interest ranged from 6.5 to 7.5 Hz (cf. section 4.2), τ was selected to be 0.069 s, corresponding to an optimal J value of approximately 7.2 Hz. The solvent resonance was suppressed by presaturation during a 3.0 s delay prior to application of the $\pi/2$ pulse. The spectrum was acquired in 256 scans using a spectral width of 4545 Hz in 16K data points (1.802 s acquisition time), resulting in a digital resolution of 0.28 Hz/point after zero filling to 32K.

^{13}C Spin-Sort Experiment

The transverse magnetization can also be modulated by *heteronuclear* spin-spin coupling. This is the case in the ^{13}C NMR spin-echo experiment [Rabenstein and Nakashima, 1979]. The ^{13}C transverse magnetization is modulated by its various ^{1}H-^{13}C couplings, but the modulation is dominated by the ^{1}J couplings to directly bonded protons. Therefore this experiment can be used to determine the number of protons attached to the carbon of the respective resonance line.

The ^{13}C NMR spectra obtained from the spin-echo experiment with broadband ^{1}H decoupling will not offer the desired results, because broadband ^{1}H decoupling eliminates any modulation from ^{1}H coupling. If the decoupler is gated off during evolution and on during acquisition, the ^{13}C precession vectors will fan out before the π pulse, but refocus during the second τ delay. The acquired spectrum will still not contain the desired information. Phase modulation of the resonances will, however, occur if the decoupler is on during just one of the two evolution periods, because the different vectors will not be refocused. As the precession frequencies differ during only one of the two delay periods, the frequency of phase modulation is only half of that of homonuclear coupling. Therefore, the CH_2 signals (and the quarternary carbons) will be 180° out of phase with respect to the CH and CH_3 signals if τ is selected to be 1/J.

The following pulse sequence was used:

^{13}C: RD - $\pi/2$ - τ - π - τ - FID

^{1}H: BB - DO ------ BB --------

i.e. the broadband decoupling was gated off only during the first evolution. This experiment was performed on 20 mM dynorphin A-(1-13) in CD_3OH). With J ≈ 125 Hz, τ was selected to be 0.008 s. The spectrum was acquired in 3500 scans using a spectral width of 29412 Hz in 16K data points (0.279 s acquisition time), resulting in a digital resolution of 3.6 Hz/point.

T_2 Measurements with the CPMG Sequence

Hahn's [1950] spin-echo experiment can also be employed for the measurement of the spin-spin relaxation time constant, T_2. In liquids, however, the Brownian motion of the dipole moments carried by neighbouring molecules undergoing molecular diffusion severely affects the relaxation processes. Carr and Purcell [1954] therefore modified the spin-echo sequence by repeating the π pulse after a delay of 2τ:

RD - $\pi/2$ - (τ - π - τ) • C - FID

Instead of incrementing τ, the number of cycles, C, is varied, thus circumventing the effect of diffusion. Meiboom and Gill [1958] further improved the method by shifting the phase of the π pulse by 90° relative to the $\pi/2$ pulse and by making successive π pulses coherent (180° phase shift). This modification

was regarded as successful in causing the cancellation of imperfections in the π pulses, although Vold and coworkers [1973] have shown that the Meiboom-Gill phase shift is only partially effective in preventing cumulative errors from imperfect π pulses. Nevertheless, they claim that measurements of T_2 with an accuracy of ± 1-2% are feasible if certain criteria are met [Vold et al., 1973].

Other problems are caused by J-modulation. Of course, all couplings are removed in ^{13}C spectra by broadband decoupling. However, decoupling might not be sufficient to remove J-modulation completely [Lilley and Howarth, 1977], and cross-relaxation between carbon and proton spins can lead to false T_2 values [Freeman and Hill, 1975, p.160].

^{13}C spin-spin relaxation time constants were measured on a sample containing 25 mM dynorphin A-(1-13) by applying the CPMG sequence:

$$RD - \pi/2 - (\tau - \pi - \tau) \cdot C - FID$$

The sample had been degassed by gently passing argon through it for at least 20 minutes. The ^{13}C $\pi/2$ pulse was 6.4 μs. A relaxation delay of 4 s was employed. The delay time τ was set to 2.5 ms and spectra were recorded for C values of 2 (corresponding to a total delay time $C \cdot 2\tau$ of 10 ms), 4, 8, 16, and 32[4]. 1280 scans were accumulated over a spectral width of 29400 Hz in 16K data points (0.279 s acquisition time). In a second experiment, only four C values (corresponding to total delay times of 10, 20, 40, and 80 ms) were employed,

[4] C had to be an even number to provide for the cancellation of π pulse errors (Meiboom-Gill incrementation).

but 2600 scans were accumulated per FID. Protons were decoupled by composite pulse decoupling. The FID's were subjected to zero-filling to 64K and exponential multiplication for sensitivity enhancement (10.0 Hz line broadening) before Fourier transformation. The digital resolution was 0.90 Hz/point.

T_2 values were determined by linear regression of $\ln(I) = \ln(I_0) - (1/T_2)\cdot(C\cdot 2\tau)$, with I being the scaled intensity at the total delay time $C\cdot 2\tau$. As the initial intensities I_0 were not known, the intensities were plotted on an arbitrary (but consistent) scale. Consequently, the regression lines did not pass through the origin (i.e. I_0 was not equal to 1 on this scale). This uncertainty, however, only affects the offset from the x-axis, but not the slope. Therefore it does not interfere with the determination of T_2.

4.2.3.4. Inversion Recovery Experiments

^{13}C spin-lattice relaxation time constants were measured on a degassed sample containing 25 mM Dynorphin A-(1-13) by applying the inversion recovery sequence [Vold et al., 1968]:

RD - π - τ - $\pi/2$ - FID

with 11 different delay times, τ (6, 20, 50, 90, 120, 200, 300, 400, 500, 800, and 4000 ms). 1136 scans were accumulated per FID. A second experiment was performed with only seven delay times, τ, (6, 50, 90, 120, 200, 650, 2000 ms)

with 3500 scans per FID. Protons were decoupled by composite pulse decoupling. Each spectrum was acquired over a reduced spectral width of 20000 Hz in 16K data points (0.279 s acquisition time). The relaxation delay was 4 s. The ^{13}C $\pi/2$ pulse was 6.4 μs. The FID's were subjected to exponential multiplication for sensitivity enhancement (10.0 Hz line broadening) before Fourier transformation. The digital resolution was 2.4 Hz/point.

Spin-lattice relaxation time constants, T_1, were determined by a non-linear least squares fitting computer program kindly provided by Dr. A.D. Bain [cf. section 9.2]. For each resonance line the intensities I were expressed as a function of the delay times τ:

$$I = A_3 - A_2 \cdot e^{(-\tau/T_1)}$$

where A_2 is the nucleus flip change in units of $\pi/2$'s (i.e. for a π-pulse as the first pulse, $A_2 = 2$), and A_3 is the normalized intensity of the largest point. The calculations were performed on an IBM PS/2 computer equipped with an 80287 math coprocessor. The actual calculations were completed instantaneously, but the error estimation took 10-15 minutes for good data sets. Error estimations which were not completed after 20 min were aborted and the determined parameters were not used.

4.2.3.5. 1-D NOE Spectroscopy

The mutual effect of two spins on each other's relaxation, represented by a zero-quantum transition process W_0 (corresponding to a mutual spin flip) and a double quantum transition process W_2 (corresponding to a simultaneous relaxation of both spins) is referred to as *cross-relaxation*. The processes W_2 and W_0 do not satisfy the quantum mechanical selection rule for the observation of NMR transitions ($\Delta m = \pm 1$) and lead to non-observable NMR lines, but they nevertheless affect relaxation.

Of the principal relaxation mechanisms (cf. [Abragam, 1961, Chapter VIII; Noggle and Schirmer, 1971, Chapter 2; Jardetzky and Roberts, 1981, 52-68; Wüthrich, 1976, 140-150]) the most important for ^1H and ^{13}C is *dipolar relaxation*, which is a *through-space* effect. The magnetic moment of a nucleus S (or of unpaired electrons contained in contaminants, e.g., O_2, Cr(III), Fe) will give rise to a local magnetic field, which, at the location of another nucleus, will be inversely proportional to the third power of the internuclear distance. The fluctuations in the magnetic moment result from changes in the angle between the external magnetic field and the line connecting the two nuclei and in the internuclear distance. These can arise from the Brownian motion of the molecules, rotations in the molecule, or chemical exchange. A characteristic measure of such a motion is the correlation time τ_c, i.e. the reciprocal of the rate of tumbling in solution of the relevant piece of the molecule.

The Nuclear Overhauser Effect

If the nucleus S is irradiated to saturation in a double irradiation experiment, then the dipolarly coupled nucleus I will experience a rapidly fluctuating magnetic field and will be relaxed more efficiently (cross-relaxation). This will cause the intensity of the resonance line of I to be enhanced. Such a fractional change in the intensity of one NMR line when another resonance is irradiated is known as the *Nuclear Overhauser Effect*[5], NOE:

$$NOE = (I_S - I_0)/I_0$$

where I_0 is the signal without irradiation and I_S the signal in the double irradiation experiment. The efficiency of the cross-relaxation depends on the (inverse sixth power of the) internuclear distance, the nature of the relaxing nuclei (i.e. the squared product of their magnetogyric ratios, ^1H-^1H-NOEs are by far the strongest) and on the effective correlation time of the vector joining these two nuclei.

In pioneering work, Bell and Saunders [1970] demonstrated a linear relationship between the intramolecular nuclear Overhauser effect and the sixth power of the reciprocal of the internuclear distance for protons in rigid small organic molecules. Apart from the $^3J_{HN\alpha}$ coupling constants, most of the structural

[5] This effect was originally predicted for the enhancement of nuclear polarization in metals as the result of paramagnetic relaxation processes that occur when the electron-spin resonance is saturated [Overhauser, 1953]. Bloch [1954] extended this concept to the dipole-dipole interaction of nuclei.

information on peptides in NMR spectroscopy is obtained from transient NOE [Soloman, 1955] experiments or its two-dimensional equivalent, the NOESY experiment.

Transferred Homonuclear $^1H,^1H$ NOE's

One-dimensional NOE experiments were performed on the samples containing dynorphin A-(1-13) in an aqueous dispersion of DMPC bilayers. In these systems, transferred nuclear Overhauser effects [Clore and Gronenborn, 1982] can be observed [cf. Chapter 6].

NOE difference spectra were obtained by subtraction of the off-resonance control from the on-resonance FID. The signal of interest was selectively saturated for 0.35 to 1.0 s and the decoupler was gated off during acquisition. A 1.5 s relaxation delay was employed before irradiation. Eight scans were accumulated over a spectral width of 5000 Hz in 16 K data points for each irradiation and the cycle of irradiations repeated 32 or 96 (for 0.35 s irradiation) times. Exponential multiplication was applied to the FID's (4.0 Hz line broadening) before Fourier transformation. The digital resolution was 0.61 Hz/point.

Heteronuclear $^{1}H,^{13}C$ NOE's

One method of obtaining measurements of heteronuclear NOE's is by comparing the peak intensities [Gerken et al., 1989] or the integrals (as was the case in the present study) of normal broadband-decoupled (full NOE) and NOE-suppressed spectra obtained by inverse-gated heteronuclear decoupling. More sophisticated schemes have been reviewed by Kövér and Batta [1987].

Normal broadband-decoupled (full NOE) spectra were acquired in the standard manner (cf. "Routine ^{13}C NMR Spectra") with an extended relaxation delay of 5 s. The $\pi/2$ pulse was 6.4 μs. 1280 scans were accumulated for the FID, which was zero-filled to 64K and subjected and subjected to exponential multiplication with a line broadening of 10 Hz for sensitivity enhancement. The digital resolution was 0.9 Hz/point. NOE suppressed spectra were acquired with identical parameters with composite pulse decoupling gated on only during the acquisition.

4.2.4. Two-Dimensional 500 MHz NMR Studies

4.2.4.1. Homonuclear Correlated Spectroscopy

The traditional method for determining which protons share coupling to a given proton is the use of the homonuclear spin decoupling experiment. To fully examine all of the spins in a complex molecule the series of experiments can be very tedious, because each proton must be irradiated and a spectrum recorded. Incrementing the decoupling frequency across the region of interest would ultimately result in a 2-D CW-FT experiment. In addition to the usual disadvantages of a CW experiment (e.g. slow extraction of information, most of the experimental time is spent recording noise), resonances which are close in frequency to the frequency of irradiation can experience partial decoupling and displacement from their usual chemical shift value (Bloch Siegert shifts).

A 2-D NMR [Ernst et al., 1987; Kessler et al., 1988a] experiment providing the same (homonuclear coupling) information with none of the difficulties described above is the COSY (Correlated Spectroscopy) experiment [Aue et al., 1976a], based on an experiment proposed by Jeener [1971]. The basic pulse sequence is: RD - $\pi/2$ - t_1 - $\pi/2$ - t_2.

The first $\pi/2$ pulse develops magnetization in the xy-plane (transverse magnetization). The spin vectors precess in the xy-plane at rates determined, firstly, by their Larmor precession frequencies ν_i relative to ν_c (the rotation frequency of the rotating frame of reference) , i.e. by the chemical shift δ of the

nucleus, and, secondly, by their spin-spin coupling constants, ^{n}J. Hence the transverse magnetisation created by the first $\pi/2$ pulse evolves under the influence of chemical shift and spin-spin coupling during the evolution time t_1. The populations of all connected transitions will change at a frequency ν_i during t_1. For nuclei with no scalar couplings, the t_1 dependent modulation of the magnetisation is determined only by $|\nu_i-\nu_c|$.

The second $\pi/2$ pulse mediates coherence transfer amongst all the transitions of a spin system, i.e. it converts portions of the magnetisation arising from one transition into magnetisations of all connected transitions of the coupled system. "This is a little tricky to conceive, as everything is being mixed with everything else at the same time.."[Derome, 1987, p.189][6]. This leads to differences in the modulation frequencies of the magnetisation during t_1 and t_2, resulting in off-diagonal peaks in the two-dimensional (ν_2 vs. ν_1) spectrum. These off-diagonal peaks lie at the δ coordinates of the coupled nuclei.

The portion of magnetisation that is not transferred during the second pulse has the same frequency $|\nu_i-\nu_c|$ both during t_1 and t_2. This gives rise to peaks along the diagonal of the two-dimensional spectrum containing no information not already displayed by the one-dimensional spectrum.

Proton COSY 2-D NMR spectra were acquired in the absolute value and in the phase-sensitive mode.

---

[6] A clearer picture can be obtained in the superspin formulism [Bain, 1988] or by operator-development graphs [Eggenberger and Bodenhausen, 1990].

Phase correction cannot be applied to the 2-D data set in an analogous manner to 1-D phase correction because of insufficient arithmetic capacity of the NMR data processing system. In standard COSY, peaks are displayed in the "absolute value" or magnitude mode. The absolute value is the square root of the sum of the squares of the real and imaginary parts of the spectrum. This display mode avoids the calculation of phases. The resulting absolute value lineshape, however, is broadened in comparison to the pure absorption mode lineshape because of dispersion components contributing to the signal. Strong resolution enhancement functions, "window functions" must be applied to achieve an acceptable resolution. All the window functions operate by reducing the decay in the first part of the FID, and relatively amplifying the later, noisier parts of the FID. This leads to a general reduction in sensitivity, but can also result in the loss of cross-peaks due to differential loss in sensitivity for resonances with different linewidths.

The advantage of running phase-insensitive experiments is that they require substantially less time both in acquisition and processing than phase-sensitive experiments and no adjustment of phase.

Phase-sensitive experiments do not require magnitude calculation and strong resolution enhancement functions. Therefore resolution and sensitivity are considerably superior to that of the absolute value spectra. Hence phase-sensitive $^{1}H,^{1}H$ COSY is used as an approach when complicated spin systems with much overlap have to be investigated [Kessler et al., 1987]. Phase relations

between peaks are helpful in assigning the spectrum and coupling constants can be measured quite exactly from cross-sections parallel with ν_2.

One disadvantage is that components of multiplets will give rise to off-diagonal antiphase pairs with the possibility of overlapping positive and negative peaks cancelling. Another is that the phases of diagonal and cross-peaks differ by 90°. The cross-peaks are adjusted to pure absorption, leaving the diagonal in a dispersive mode, leaving important spectral regions near the diagonal precluded from spectral analysis. This problem can be solved by the application of a *double-quantum filter* [Piantini et al., 1982].

An extra $\pi/2$ pulse is added immediately after the end of the COSY sequence:

$$RD - (\pi/2)_\phi - t_1 - (\pi/2)_\phi - (\pi/2)_x - FID_\phi$$

This third pulse allows for multiple quantum coherences[7] that happen to exist before the third pulse to be converted back to observable magnetisation. The phase of signals resulting from transfer back to single quantum from p-quantum

---

[7] The coherence across one transition (e.g. phase coherence between the α and β spin states created by $\pi/2$ pulse) is termed single quantum coherence ($\Delta m_T = 1$). This transition fulfils the quantum-mechanical selection rule ($\Delta m = \pm 1$) and gives rise to observable magnetisation.

The coherence across two transitions is referred to as double quantum coherence ($\Delta m_T = 2$). For instance this is the case when phase coherence is established between the $\alpha\alpha$ and $\beta\beta$ states of an AX spin system. This is created by a selective $\pi/2$ pulse across transition A_1 [Derome, 1987, p. 189], installing single quantum coherence between the $\alpha\alpha$ and $\alpha\beta$ states followed by a selective π pulse across transition X_1 completely transferring phase information present in $\alpha\beta$ to $\beta\beta$ [ibid, p. 216; Freeman, 1987, p. 129].

coherence is p times as sensitive to phase shifts in the pulses which excited it than is the phase of directly excited single quantum coherence. Suitable phase cycles of pulses and receiver can therefore select between various coherence pathways through which the system has been sent on its way towards the measured precessing transverse magnetisation.

If the phase of all the pulses applied before the coherence is created is shifted by 90°, the phase of the signal arising via double quantum coherence is inverted. Inverting the receiver phase (i.e. subtracting the 90° from the 0° experiment) selects the component which passed through the double quantum coherence.

The substantial advantage of the application of a double-quantum filter is the simplification of spectra. As multiple quantum coherences can only be generated in coupled systems, double-quantum coherence can only arise between at least two coupled spins-½. Singlets, for instance the solvent line, which causes the worst t_1 noise[8], are eliminated in the double quantum experiment.

A second advantage lies in the improvement of the phase sensitive COSY experiment. Both diagonal and cross-peaks can be adjusted into pure absorption phase. Therefore phase sensitive COSY experiments run with a double-quantum

---

[8] t_1 noise [Mehlkopf et al., 1984] arises from instabilities in the field frequency ratio or from imperfect pulses. These instabilities cause false frequency modulation of signals during t_1 and give rise to noise along sections in the ν_1 dimension which intersect signals. The solvent and methyl signals are worst hit.

filter (phase sensitive DQF $^1H,^1H$ COSY) are the method of choice for the assignment of coupling networks.

$^1H,^1H$ COSY

The absolute value spectra were generated by the pulse sequence:

RD - $(\pi/2)_{\phi 1}$ - t_1 - $(\pi/2)_{\phi 2}$ - FID_{ϕ}

where $\phi 1$, $\phi 2$, and ϕ are the respective phases for phase cycling of the pulse sequence. The sixteen step phase cycle consisted of a standard combination of the ν_1 quadrature detection scheme by echo detection[9], axial peak suppression[10] and the CYCLOPS (cyclic ordered phase scheme) procedure for the reduction of quadrature images[11] [Hoult and Richards, 1975]. The $\pi/2$ pulse width was 19 μs.

---

[9] a.k.a. N-type peak selection

[10] axial peaks are artifacts arising from longitudinal relaxation during t_1 and can be suppressed by alternating the second $\pi/2$ pulse by 180° and adding the pair of scans [Nagayama et al., 1980].

[11] arising from imbalances between the two receiver channels during quadrature detection

DQF Phase-sensitive $^1H,^1H$ COSY

Phase-sensitive COSY experiments were performed with a double-quantum filter [Piantini et al., 1982; Rance et al., 1983]. Time proportional phase incrementation (TPPI) [Drobny et al., 1979; Marion and Wüthrich, 1983] was employed for the implementation of quadrature detection in ν_1. The phase of the first pulse is incremented by 90° for successive t_1 values while the phase of the second pulse is kept constant. This incrementation of the phase shifts causes the frequency to be increased by F/2, where F is the spectral width [Derome, 1987, p.83]. Relative to the reference frequency, the frequency range will no longer be from -F/2 to +F/2, but from 0 to F. The input to Fourier transformation no longer consists of complex pairs, but of real numbers and thus requires different 2-D transform and display routines.

The pulse sequence employed was:

$$RD - (\pi/2)_{\phi 1} - t_1 - (\pi/2)_{\phi 2} - \tau - (\pi/2)_{\phi 3} - FID_{\phi}$$

where $\phi 1$, $\phi 2$, $\phi 3$, and ϕ are the respective phases for phase cycling of the pulse sequence. The interval τ was set to 3 μs to allow for phase switching between the second and the third pulse. A 16 step phase cycle was utilized.

$^1H,^1H$ COSY-45

A simplification of the appearance of the COSY spectrum around the diagonal is achieved by replacing the second pulse in the basic COSY sequence by a $\pi/4$ pulse. This reduces the proportion of coherence transfer between indirectly connected transitions in complex spin systems in favour of transfer between directly connected transitions [Bax and Freeman, 1981]. There is a reduction in the cross-peaks within multiplets which leads to a simplification of the spectrum. Relative to the basic COSY experiment, COSY-45 is less sensitive and cannot be performed in the phase-sensitive mode because the signals are not experiencing pure amplitude modulation [Bax and Freeman, 1981].

The spectra were generated by the pulse sequence:

$$RD - (\pi/2)_{\phi 1} - t_1 - (\pi/4)_{\phi 2} - FID_{\phi}$$

Long Range $^1H,^1H$ COSY

In order to detect small couplings (^4J or ^5J), which are roughly in the range of 0.1 to 0.5 Hz, and therefore unresolvable in the 1-D experiment, we need acquisition times in both dimensions around $2 \cdot T_2$. This is achieved by introducing fixed delays into the t_1 and t_2 intervals [Bax and Freeman, 1981]:

$$RD - \pi/2 - \Delta - t_1 - \pi/2 - \Delta - FID$$

The requirement for the acquisition times is now reduced to:

$$A_{t1,t2} \approx 2 \cdot T_2 - 2 \cdot \Delta$$

Transverse relaxation during will reduce all intensities. It is possible for correlations due to large couplings to be further reduced in intensity if $J \cdot (T_2 -)$ is close to an integral value (e.g. for $J \approx 7$ Hz for typical proton T_2's of 0.2 s to 0.6 s). A standard $^1H,^1H$ COSY spectrum should consequently also be acquired.

The precise pulse sequence applied was:

RD - $(\pi/2)_{\phi 1}$ - Δ - t_1 - $(\pi/2)_{\phi 2}$ - Δ - FID_{ϕ}

64 Scans were accumulated for each of the 256 FID's containing 2048 data points in F2 over a 4545.455 Hz spectral width. The fixed delay employed was Δ = 0.15 s. All other parameters were exactly the same as for the standard $^1H,^1H$ COSY spectra.

4.2.4.2. Relayed homonuclear correlated spectroscopy (=RELAY)

A problem with the identification of individual spin systems with the regular COSY experiment is its application to more complex systems. Ambiguities concerning cross-peaks arise when members of different spin systems have degenerate chemical shifts [Wagner, 1983]. If the α-proton resonances are not well resolved, establishing connectivities between amide NH resonances and the rest of the amino acid spin system on the basis of a regular COSY spectrum is not unambiguous.

Relayed coherence transfer spectroscopy [Eich et al., 1982] attempts to solve this problem by propagating the magnetisation transferred from one spin to another in the normal COSY experiment on through further couplings experienced by this second nucleus [Derome, 1987, p. 232]. Thus coherence is generated between two nuclei not directly J coupled but each coupled to a common spin. This is accomplished through application of a third $\pi/2$ pulse to cause another redistribution of coherence. In order to make the result independent of the chemical shift differences a π pulse is inserted in the middle of the delay period between second and third $\pi/2$ pulse:

RD - $(\pi/2)$ - t_1 - $(\pi/2)$ - τ - (π) - τ - $(\pi/2)$ - FID

The effectiveness of relayed coherence transfer for different spin systems has been discussed in detail [Bax and Drobny, 1985]. The choice of τ is selected for maximum relay of magnetization and is dependent on the kind of spin system and the size of the coupling constants involved. Consequently, no single optimum value for the mixing time in RELAY experiments exists.

A problem in interpreting RELAY spectra is that direct connectivities no distinction can be made between original COSY and extra RELAY peaks. This difficulty can be solved by running a corresponding COSY experiment.

A relayed coherence transfer spectrum was recorded on 5.5 mM dynorphin A-(1-13) in CD_3OH. The pulse sequence employed was:

RD - $(\pi/2)_{\phi 1}$ - t_1 - $(\pi/2)_{\phi 2}$ - τ - $(\pi)_{\phi 3}$ - τ - $(\pi/2)_{\phi 3}$ - FID_{ϕ}

where $\phi 1$, $\phi 2$, $\phi 3$ and ϕ are the respective phases for phase cycling of the pulse

sequence. Phase cycling was performed in order to eliminate undesired signals, e.g. axial peaks and nuclear Overhauser effects [Wagner, 1983]. The phase cycling scheme reported by Hughes and collaborators [Hughes et al., 1985] was employed. The delay time τ was set to 0.013 s according to the spin system analysis of Bax and Drobny [Bax and Drobny, 1985], resulting in a total mixing time of 0.026 s. 96 scans were accumulated for each of the 256 FID's. All other acquisition parameters were the same as for the respective COSY experiment.

4.2.4.3. Heteronuclear $^{1}H,^{13}C$ Correlated Spectroscopy

The fundamental principle of the heteronuclear H,X correlation experiment is that the amplitude of the X (^{13}C) signal detected during t_2 is modulated as a function of t_1 by the frequencies of the ^{1}H spins. In comparison to the homonuclear COSY experiment, the coherence transfer process of the second pulse is extended to another nucleus by providing a simultaneous pulse at another frequency.

The experiment can also be considered as a variation of the INEPT (Insensitive Nuclei Enhanced by Polarisation Transfer) experiment [Morris and Freeman, 1979]. INEPT uses non-selective pulses to set up the polarisation of all ^{1}H transitions and a spin-echo sequence to exclude the effects of the chemical shifts of the ^{1}H spins. The pulse sequence is as follows:

^{13}C: ---------- π_x - τ - $(\pi/2)_x$ - FID

^{1}H: $(\pi/2)_x$ - τ - π_x - τ - $(\pi/2)_y$

By omitting the spin-echo and incrementing the delay, t_1, between $(\pi/2)_x$ and $(\pi/2)_y$, the amplitude of the ^{13}C signal is modulated as a function of t_1 by the frequencies of the ^{1}H spins. In comparison to the homonuclear COSY experiment, the coherence transfer process of the second pulse is extended to another nucleus by providing a simultaneous pulse at another frequency:

^{13}C: ---------- $(\pi/2)$ - FID

^{1}H: $(\pi/2)$ - t_1 - $(\pi/2)$

This is the basic heteronuclear shift correlation sequence.

The presence of ^{1}H,^{13}C couplings in both dimensions is deleterious for sensitivity and simplicity of interpretation of the spectrum. Coupling in ν_2 is eliminated by introducing a delay, Δ_2, between polarization transfer and acquisition of the FID. This causes the multiplet components to refocus, so that broadband proton decoupling can be turned on during t_2. Coupling in ν_1 can be eradicated by inserting a delay Δ_1 between evolution time and polarization transfer: this allows for decoupling during t_1, but still ensures the generation of antiphase lines ready for polarisation transfer during Δ_1 (when decoupling is off!):

^{13}C: RD - Decoupling - DO - $(\pi/2)$ - Δ_2 - FID

^{1}H: DO - $(\pi/2)$ - t_1 - Δ_1 - $(\pi/2)$ - BB

This is the experimental scheme for the heteronuclear decoupled shift correlation experiment [Maudsley et al., 1977].

The presence of $^1H,^1H$ couplings in ν_1 broadens the correlations considerably which dramatically reduces sensitivity. $^1H,^1H$ decoupling is effected by introduction of the 'bilinear rotation operator' [Garbow et al., 1982] half-way through t_1. This so-called BIRD sequence consists of:

^{13}C: π

^1H: $(\pi/2)_x - 1/(2{\cdot}^1J_{CH}) - \pi_x - 1/(2{\cdot}^1J_{CH}) - (\pi/2)_{-x}$

This sequence is effectively a π pulse for protons not directly coupled to a ^{13}C nucleus (e.g. proton M, coupled to ^{12}C), while those attached to ^{13}C (e.g. proton A) essentially remain unchanged [Bax, 1983]. If M is, e.g., in the m = +½ state before the application of the BIRD sequence, it will then be inverted to the -½ state. So A will be coupled to M in the +½ state for ½t_1 and to M in the -½ state for another ½t_1. Overall, therefore, A will precess in the xy-plane only depending on the chemical shift δ_A, A and M are essentially decoupled. Only geminal $^1H,^1H$ couplings remain since both geminal protons are correlated to the same ^{13}C nucleus.

Artifacts due to errors in the $1/(2{\cdot}^1J_{CH})$, or Δ, delay are reduced by phase cycling in 90° steps of all of the ^1H pulses of the BIRD sequence while keeping the receiver phase constant [Wilde and Bolton, 1984]. Another problem is the rate of transverse relaxation [Derome, 1987, p.253] of the protons. If T_2 is too small, the extra 1/J interval of the BIRD sequence will cause a considerable loss in signal intensity.

The ^{13}C-^{1}H 2-D chemical shift correlation spectrum was recorded using the standard pulse sequence incorporating the BIRD (Bilinear Rotation Decoupling) pulse during the evolution period for ^{1}H-^{1}H decoupling in F1:

^{13}C: RD - Decoupling - π^{12}(CP) - DO - $(\pi/2)$ - Δ_2- FID

^{1}H: DO - $(\pi/2)$ - ½t_1 - $(\pi/2)_x$ - Δ - π_x - Δ - $(\pi/2)_{-x}$ - ½ t_1 - Δ_1- $(\pi/2)$ - BB

The spectra in F2 were acquired over the aliphatic carbon spectral range of 7575 Hz in 4K data points. The 128 FID's in the F1 dimension were obtained over a spectral width of 1157 Hz. The fixed delays in the pulse sequence were a relaxation delay of 0.5 s, BIRD pulse, Δ, and polarization transfer, Δ_1, delays, $1/(2^{1}J_{CH})$, of 0.00333 s, and a refocussing, Δ_2, delay, $1/(4^{1}J_{CH})$, of 0.00167 s.

4.2.5. 620 MHz NMR studies

620 MHz NMR spectra were recorded on the spectrometer at the NMR Facility for Biomedical Studies, Mellon Institute, Carnegie-Mellon University, Pittsburgh, PA. The spectrometer was equipped with a Varian XL400 console using Varian software 6.1 revision B.

[12] composite π pulse: $(\pi/2)_x$ - $(4\pi/3)_y$ - $(\pi/2)_x$

4.2.5.1. One-Dimensional Spectroscopy

Proton spectra were acquired at 620.166 MHz over a spectral width of 5200.2 Hz in 30016 data points (2.886 s acquisition time). The sample temperature was 23°C. The solvent resonance was suppressed by presaturation during a 1.5 s delay prior to acquisition.

The free induction decays were processed using Gaussian multiplication for resolution enhancement and were zero-filled to 65536 data points before Fourier transformation. The digital resolution was 0.16 Hz/point. Chemical shifts are reported in ppm relative to TMS using the residual solvent signals at 3.30 ppm (methanol) and 4.80 ppm (water) as internal references.

4.2.5.2. Two-Dimensional NMR Spectroscopy

^{1}H,^{1}H COSY (Correlated Spectroscopy)

Absolute value spectra were generated by the pulse sequence:

RD - $(\pi/2)_{\phi 1}$ - t_1 - $(\pi/2)_{\phi 2}$ - FID_{ϕ}

where $\phi 1$, $\phi 2$, and ϕ are the respective phases for CYCLOPS phase cycling [Hoult and Richards, 1975] of the pulse sequence. The $\pi/2$ pulse width was 12.6 μs.

Nuclear Overhauser and exchange spectroscopy (NOESY)

In the COSY sequence, part of the transverse magnetization modulated by t_1 is returned to the z axis by the second pulse. After this second pulse, a nucleus whose z magnetisation was modulated by one chemical shift during t_1 can migrate to another site (chemical exchange). If a third $\pi/2$ pulse is applied after a mixing time τ_m, i.e. the pulse sequence:

RD - $(\pi/2)$ - t_1 - $(\pi/2)$ - τ_m - $(\pi/2)$ - FID

is employed, the z-magnetisation is returned to the xy-plane and the magnetisation will be modulated by a different chemical shift during t_2. Apart from chemical exchange, the nuclear Overhauser effect allows changes in the z magnetisation (i.e. any disturbance from equilibrium) to lead into variations in the z magnetisation of another nucleus.

Both effects give rise to cross-peaks in the resulting 2-D spectrum, referred to as NOESY (Nuclear Overhauser and Exchange Spectroscopy). Three main problems are associated with NOESY [Wüthrich, 1986, pp. 105-110; Derome, 1987, pp. 240-242].

First of all, chemical or physical exchange processes and NOE interactions are not distinguishable, but this is also the case in the equivalents 1-D transient NOE experiment (cf. 4.2.3.5).

A second, more serious problem is choosing τ_m, which should be selected so that the maximum NOE builds up before the z magnetisation is sampled by

the final pulse. The build up of the NOE is limited by the rate of longitudinal relaxation. NOE's between more distant nuclei have slower build up rates, so longer τ_m's are required. However, the intensity of the cross-peaks in these cases will be weak because of longitudinal relaxation.

The third, perhaps the most serious problem, is the potential presence of interfering cross-peaks due to J-coupling, which has been studied theoretically and experimentally by Ernst and coworkers [Macura et al., 1981]. The NOESY sequence is very similar to that used for DQF phase-sensitive COSY. Consequently, various coherence transfer signals may be present. As the phase of the signals arising from the transfer of z magnetisation into the xy-plane through the third pulse is dependent only on the phase of this pulse (and, of course, the receiver phase), undesired signals can be eliminated by appropriate phase cycling. This is successful for all COSY signals except for those which have passed through zero quantum coherence.

Suppression of zero-quantum components is attempted by random variation between scans in the mixing time τ_m [Macura et al., 1981]. The intensity of NOE cross-peaks varies only slowly with changes in τ_m, whereas the coherence transfer peaks are modulated with the zero-quantum frequencies, i.e. the chemical shift differences between the coupled nuclei. However, zero-quantum coherence transfer is only a problem at short mixing times [Wüthrich, 1986, p. 107].

Rotating-Frame Overhauser enhancement spectroscopy (ROESY)

In the case of oligopeptides in solution, positive and negative NOE's can be observed simultaneously due to internal (segmental) motion. It is well possible that certain intramolecular motions will cause the respective correlation times governing the cross-relaxation between two proximate protons to approach the reciprocal of the Larmor frequency of the protons at 620 MHz (i.e. $3.9 \cdot 10^9$ $rad \cdot s^{-1}$). In such cases, the intensities of the related NOE's will be close to zero.

Observation of transient NOE's in the rotating frame (ROE's) under spin-locked conditions with the CAMELSPIN experiment[13] has been reported to overcome these difficulties [Bothner-By et al., 1984]. In this experiment [Neuhaus and Williamson, 1989, pp. 312-327], enhancements evolve not between elements of longitudinal magnetization as in conventional NOE experiments, but instead between elements of transverse magnetization during a period of spin-locking.

Spin locking is achieved by preparing the spin system with a $\pi/2$-pulse (e.g. a $(\pi/2)_x$-pulse), and then immediately applying a strong, continuous radio-frequency field (the spin-locking field) along a transverse (e.g. y- or -y-) axis perpendicular to that of the pulse. In other words, the spin-locking field is applied parallel to the axis along which the macroscopic magnetization vector **M** lies. The role of the spin-lock is to suppress the relative precession of the various

---

[13] CAMELSPIN = cross-relaxation appropriate for minimolecules emulated by locked spins.

magnetizations that constitute the NMR spectrum once they are in the transverse plane. The relative precession of different signals is abolished. A constant phase relationship is imposed between them, which allows enhancements to build up consistently in one direction.

The great advantage of the CAMELSPIN experiment over the conventional NOE experiment is that the rotating-frame NOE (ROE) has a markedly different dependence on molecular tumbling from that shown by the conventional NOE [Neuhaus and Williamson, 1989, p. 312]. This is demonstrated in Table 4.2.

Table 4.2. Maximum transient NOE enhancements in the laboratory frame (NOE) and in the rotating frame (ROE) attainable for a homonuclear two-spin system as a function of $\omega_0\tau_c$.

$\omega_0\tau_c$ [a]	NOE [b]	ROE [c]
0.1	38%	38%
1	0%	50%
10	-100%	65%

a: ω_0 = Larmor precession frequency due to B_0 [rad s^{-1}]
τ_c = correlation time [s]

b: from Neuhaus and Williamson [1989, p. 132]

c: from Neuhaus and Williamson [1989, p. 318], assuming $\omega_1\tau_c$ [d] << 1

d: ω_1 = Larmor precession frequency due to B_1 [rad s^{-1}]

In CAMELSPIN, the maximum achievable enhancement becomes more strongly positive for slowly tumbling molecules than it is at the extreme narrowing

limit $\omega_0\tau_c$ « 1. All ROE's are positive and there is no "difficult region" of $\omega_0\tau_c$ for which the enhancements are necessarily small or zero. Cross-peaks due to saturation transfer or chemical exchange are negative and can easily be distinguished from direct enhancements [Neuhaus and Williamson, p. 313].

The 2-D CAMELSPIN[14] has basically the same experimental scheme as a phase sensitive COSY, the difference being that the $\pi/2$ mixing pulse applied immediately before the detection of the FID is replaced by the application of a spin-locking field along the y axis during a relaxation period t_{max}. Spin-locking experiments could not be performed at McMaster at the time of this study, so the experiments were realized at the NMR Facility for Biomedical Studies, the Mellon Institute, Carnegie-Mellon University, Pittsburgh, PA. The 2-D CAMELSPIN /ROESY experiment was performed on 20 mM dynorphin A-(1-13) in CD_3OH. The pulse sequence used was:

$$RD - (\pi/2)_{\phi 1} - t_1 - \text{SPIN-LOCK} - FID_{\phi}$$

The relaxation delay was 4 s. The $\pi/2$ pulse was 77.5 μs. The spin-lock was applied for 500 ms. 32 scans were accumulated for each of the 256 FID's containing 1024 data points in F2 over a 5200 Hz spectral width (0.098 s acquisition time). The data were zero-filled in both dimensions to 2048 data points. Gaussian window functions were applied to both dimensions before Fourier transformation. The digital resolution was 5.1 Hz/point in both dimensions.

---

[14] The 2-D CAMELSPIN experiment is also referred to as ROESY (rotating frame nuclear Overhauser enhancement spectroscopy [Bax and Davis, 1985]).

At a later date and with updated software, an analogous experiment with a mixing time of 200 ms was performed. 38 scans were accumulated for each of the FIDs, and the data were zero-filled only in the F1 dimension to 1024 data points. All other parameters were the same as above, resulting in a digital resolution of 10.2 Hz/point in both dimensions.

4.2.6. Negative NOE's and Positive Contour Levels

In order to stay in line with the conventional usage in one-dimensional difference spectroscopy, the following nomenclature is employed. Positive cross-peaks in NOESY spectra, which are observed as negative NOE's in a one-dimensional experiment are referred to as negative NOE's, negative NOESY cross-peaks as positive NOE's. Similarly, 1-D CAMELSPIN effects, which are invariably positive, appear as negative cross-peaks in the 2-D experiment, but are nevertheless referred to as positive ROE's.

4.3. General Remarks On Data Acquisition and Processing

The data acquisition and processing parameters are given in the respective figure captions in chapters 5 and 6. Unless stated otherwise, all spectra were subjected to symmetrization [Baumann et al., 1981] after Fourier transformation, if the size in the F1 and F2 dimension was identical.

5. NMR STUDIES OF DYNORPHIN A-(1-13) IN METHANOLIC SOLUTION

5.1. The One-Dimensional ^{1}H NMR Spectrum

The 620 MHz ^{1}H NMR spectrum of dynorphin A-(1-13) in CD_3OH is displayed over the full spectral width of 5200 Hz in Figure 5.1. On the basis of standard reference data [Bundi et al., 1979; Wüthrich, 1986, p.18], the spectrum was subdivided into regions containing different groups of hydrogen nuclei with similar chemical shifts. The backbone amide proton resonances are located in the region from 9.0 to 7.7 ppm (Figure 5.2). Not all of the signals are completely resolved. Further upfield (7.7 to 6.6 ppm), the Arg side chain guanidino and the aromatic ring proton signals can be found (Figure 5.3). The broad hump underneath these resonances is considered to be caused by the rapidly exchanging Lys ϵNH_3^+ protons and the n protons of the Arg guanidino groups [Wüthrich, 1986, p.17].

Upfield from the broad CD_3OH solvent resonance ($\approx$ 4.85 ppm), in the region from 4.65 to 3.55 ppm, the α proton and the Pro δ proton resonances can be detected (Figure 5.4). In the case of the perdeuteriated solvent, the α proton region is a little less cluttered (Figure 5.5), because the backbone amide

resonances and their vicinal NH-α couplings are not observable. Nevertheless, not all α proton resonances are individually resolved.

The Arg δ, Phe β, Tyr β, and Lys ϵ methylene proton resonances (Figure 5.6) are expected upfield (3.25 to 2.9 ppm) from the CHD_2 solvent signal ($\equiv$ 3.30 ppm). The Arg δ resonances partially extend over the $Phe^4\beta$ resonances, which in turn partially coincide with the $Tyr^1\beta$ proton signals. The $Tyr^1\beta'$ signal is just detected next to the $Lys\epsilon$ methylene proton resonances.

Another area with a large number of partially overlapping and therefore poorly resolved signals is from 2.35 to 1.1 ppm, where most of the aliphatic methylene and methine proton resonances are localized (Figure 5.7).

The methyl proton resonances are observed at highest field (1.00 to 0.8 ppm, Figure 5.8).

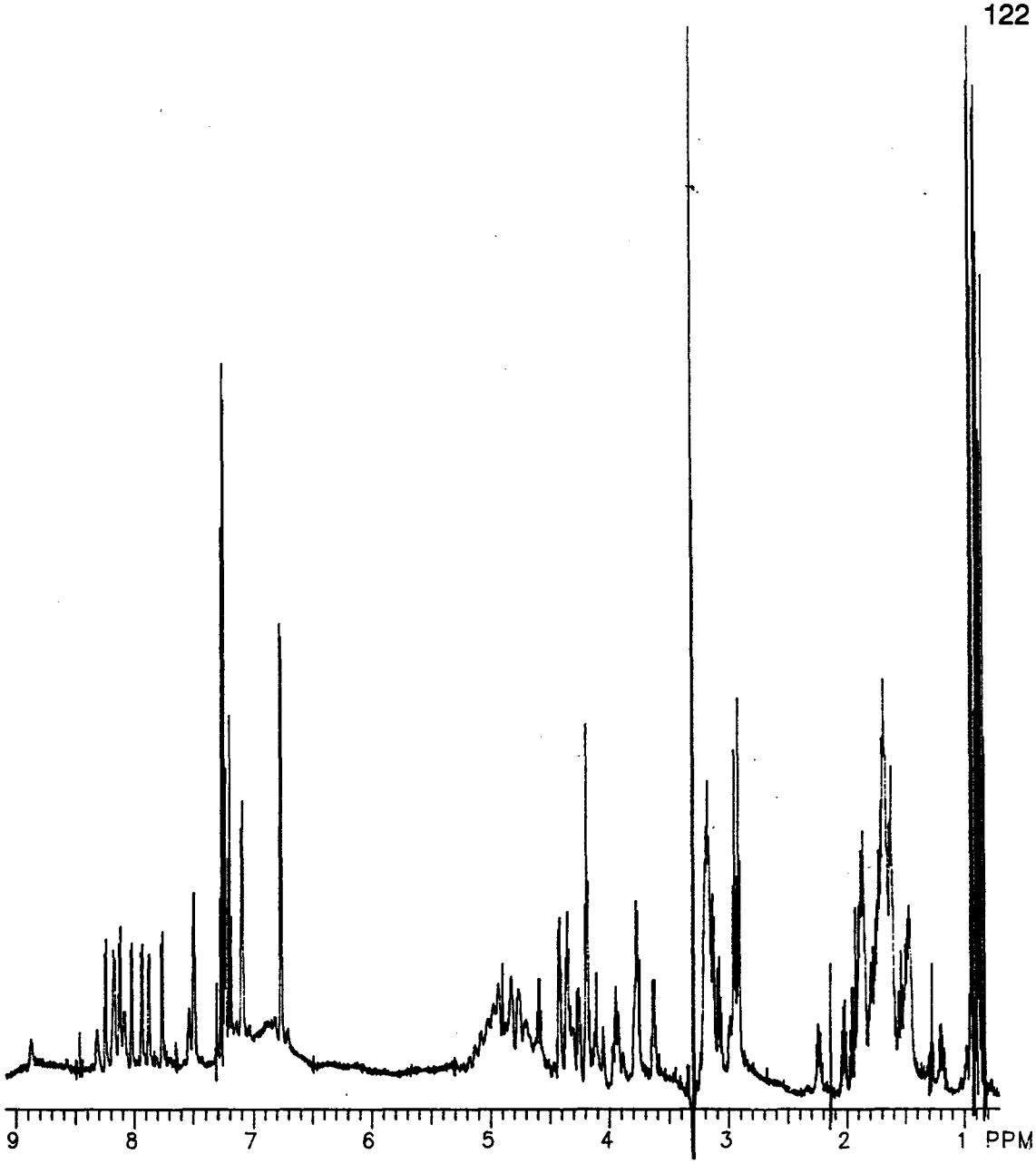

Figure 5.1. The 620 MHz one-dimensional spectrum of 20 mM dynorphin A-(1-13) in CD_3OH. 480 scans were accumulated over a spectral width of 5200 Hz in 30016 data points (2.886 s acquisition time). The solvent resonance was suppressed by presaturation during a 1 s delay prior to acquisition. The free induction decay was processed using Lorentz-Gauss transformation with **G** = $e^{t/0.09}e^{-t^2/0.270}$ for resolution enhancement and was zero-filled to 64K before Fourier transformation. The digital resolution is 0.16 Hz/point.

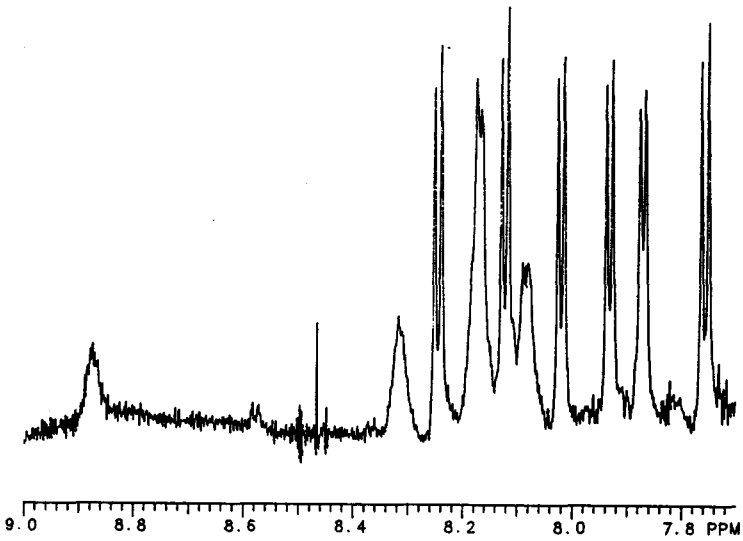

Figure 5.2. An expansion of Figure 5.1. The backbone amide proton region. Six signals were resolved well enough, that their $^{3}J_{HN\alpha}$ values could be extracted from the 1-D spectrum. All signals were sequence specifically assigned.

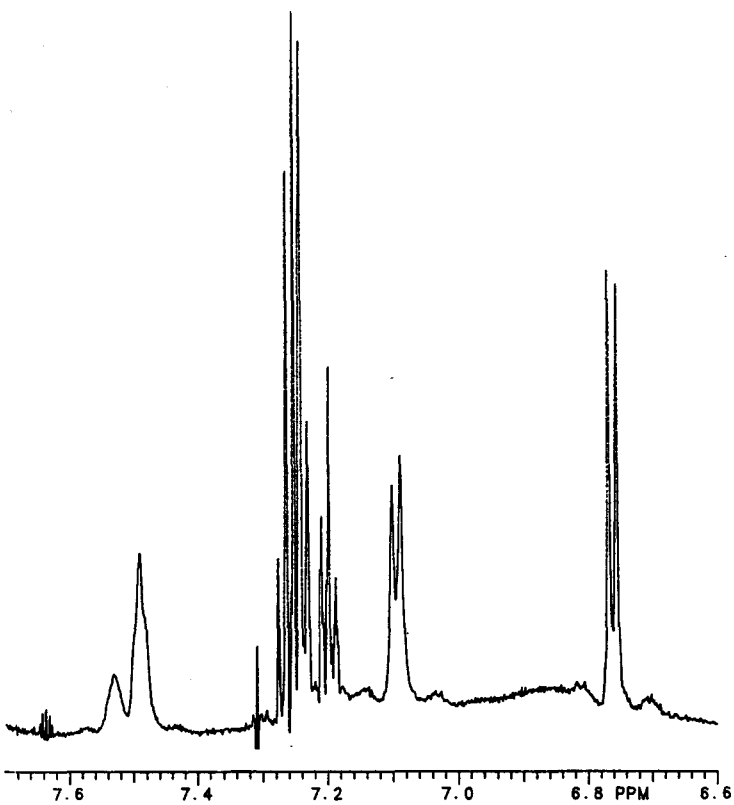

Figure 5.3. An expansion of Figure 5.1. The region containing the three Arg side chain guanidino NH protons (7.48 to 7.43 ppm), the Phe^{4} aromatic spin system (7.3 to 7.2 ppm), and the Tyr^{1} aromatic ring proton signals (7.11 and 6.77 ppm). Two of the broadened Arg ϵNH signals overlap, the third is located slightly downfield from the others.

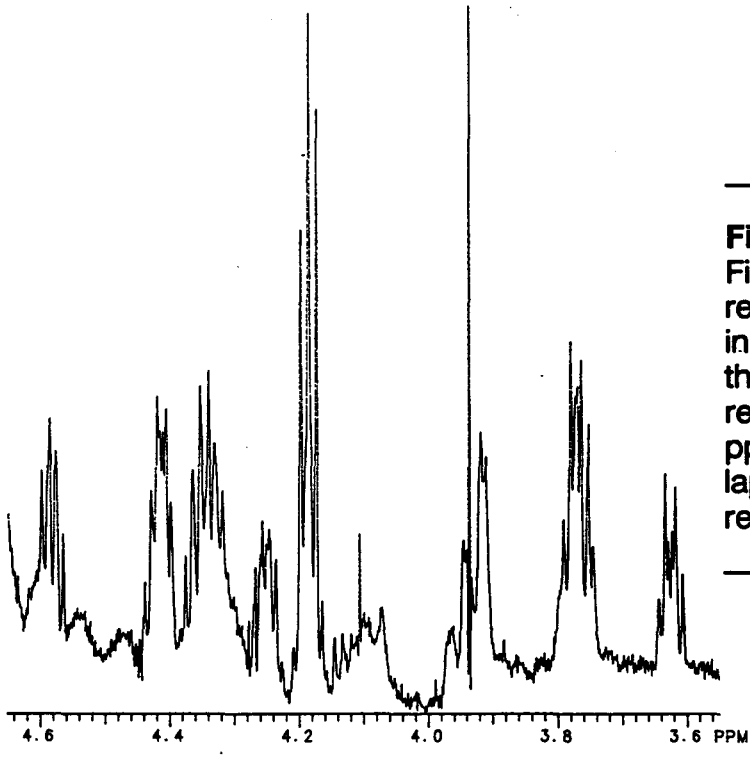

Figure 5.4. An expansion of Figure 5.1. The α proton region of dynorphin A-(1-13) in CD_3OH. Also contained are the Pro δ and δ' proton resonances (3.77 and 3.61 ppm). The former is overlapped by the Gly α' resonances.

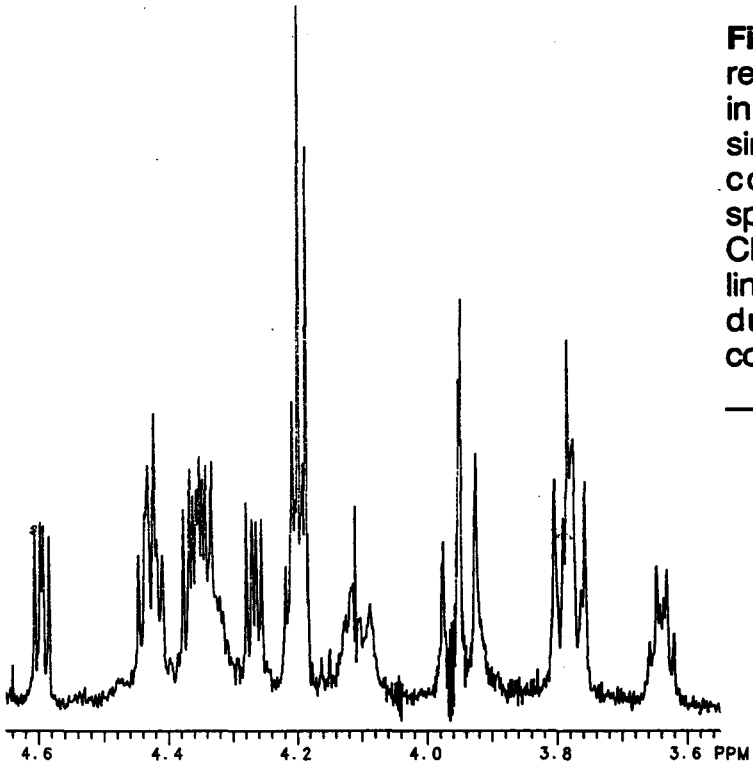

Figure 5.5. The α proton region of dynorphin A-(1-13) in CD_3OD. This region is simplified considerably in comparison with the spectrum of the peptide in CD_3OH (Figure 5.8) as no line splittings are incurred due to vicinal NH-α couplings.

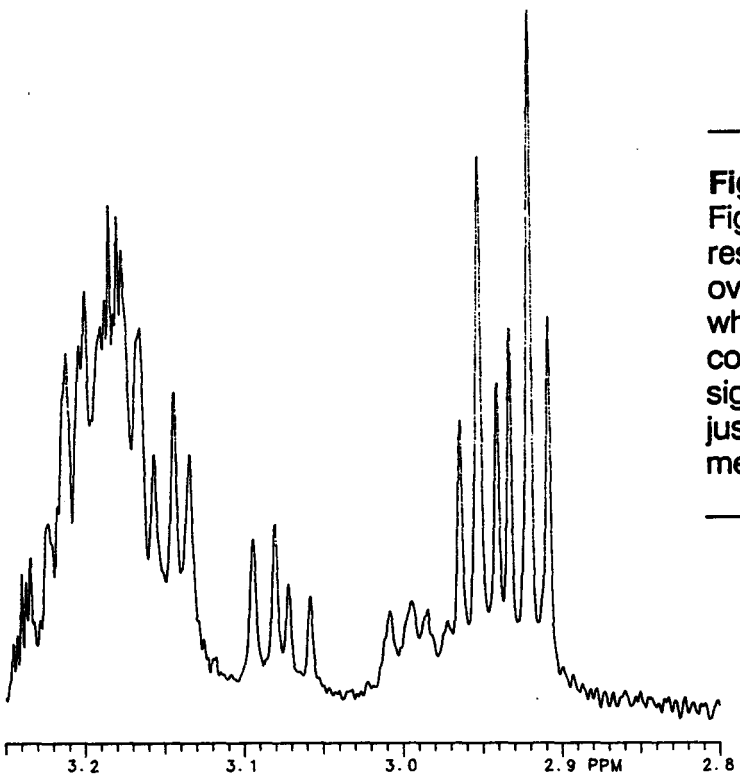

Figure 5.6. An expansion of Figure 5.1. The Arg δ resonances partially extend over the Phe$^{4}\beta$ resonances, which in turn partially coincide with the Tyr$^{1}\beta$ proton signals. The Tyr$^{1}\beta$' signal is just detected next to the Lysϵ methylene proton.

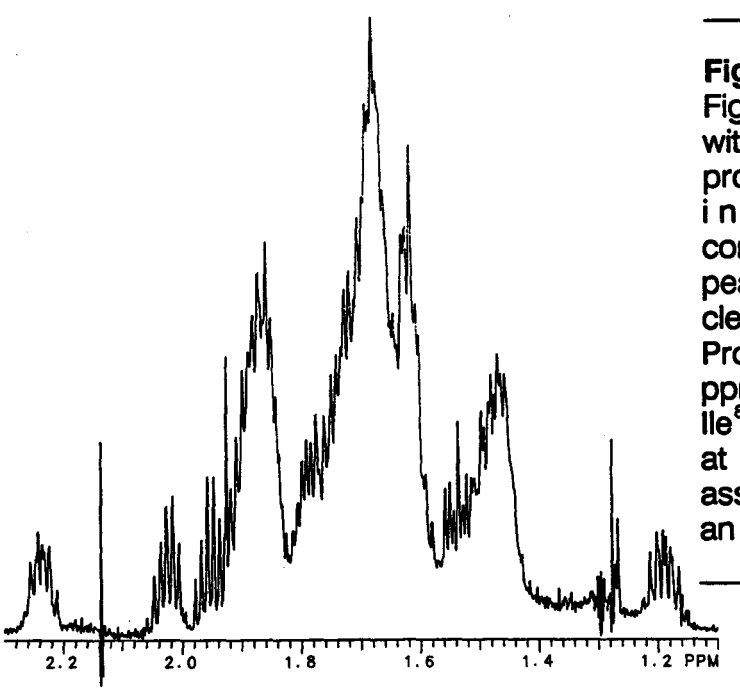

Figure 5.7. An expansion of Figure 5.1. This is the region with most of the aliphatic proton resonances, which inevitably causes considerable overlap of the peaks. The only signals clearly resolved are those of Pro$^{10}\beta$ (2.23 ppm), γ(2.03 ppm), γ'(1.96 ppm), and Ile$^{8}\gamma$'(1.19 ppm). The signal at 1.23 ppm could not be assigned and was considered an artifact.

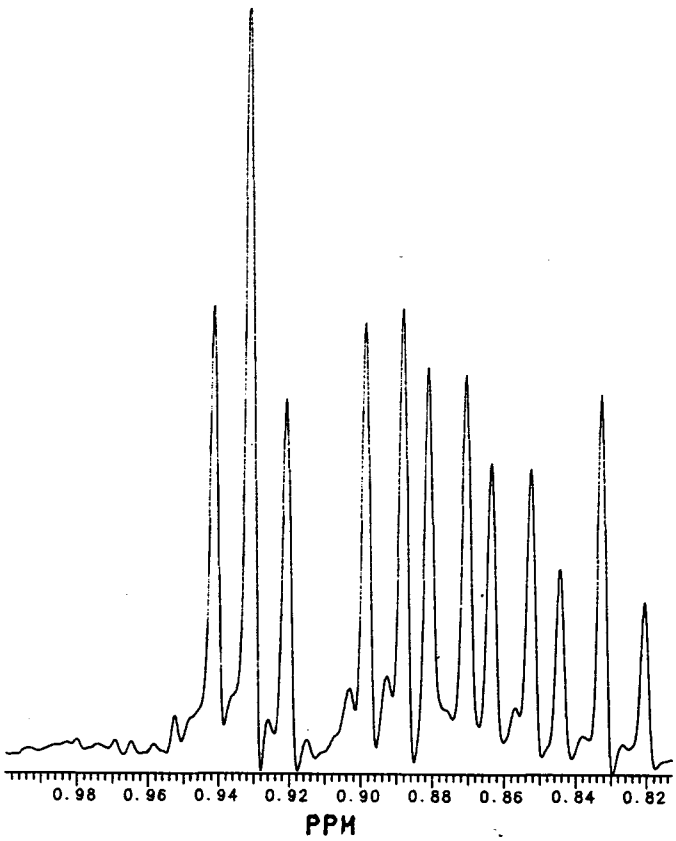

Figure 5.8. An expansion of Figure 5.1. The methyl proton region.

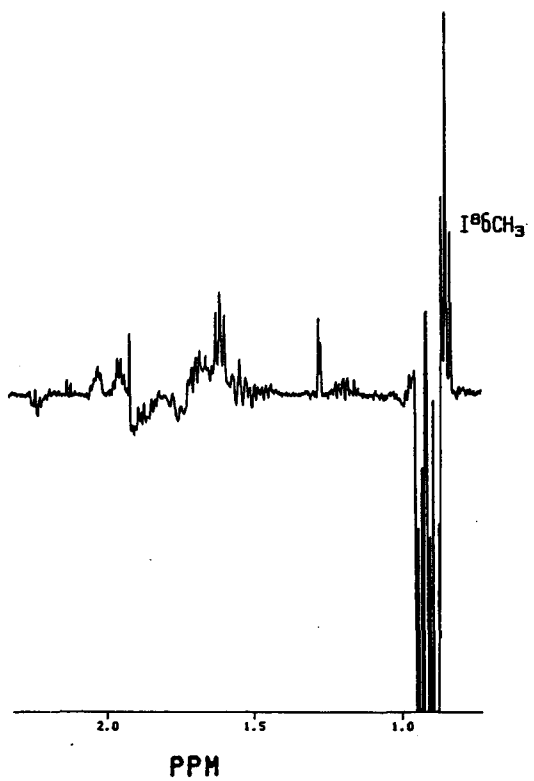

Figure 5.9. The Hahn spin-echo experiment as described in section 5.1. The Ile^{8}-δCH$_3$ resonance is the only positive signal in the region and can be readily identified as the resonance at highest field.

5.2. Recognition of the Amino Acid Spin Systems

Although the ^1H NMR spectrum of dynorphin A-(1-13) in aqueous solution has been assigned [Zhou and Gibbons, 1986], the assignment of the spectrum recorded of the peptide in methanolic solution is by no means trivial. In general, protons will experience deshielding to a lesser extent in a less polar solvent, so the chemical shift values should normally decrease. If, however, a conformational change occurs, the chemical shifts will be affected individually. This applies especially, but not exclusively, to the amide proton chemical shifts (cf. methanol titration experiments). In some cases, our assignments differ considerably from those of Zhou and Gibbons.

The non-labile protons were assigned on the basis of a variety of one- and two-dimensional experiments. The assignments are outlined mainly on spectra obtained from a double quantum filtered phase sensitive COSY experiment (Figures 5.10 -5.12). The labile protons were assigned on the basis of 500 MHz COSY and RELAY spectra (Figures 5.15 and 5.16), which also resolved ambiguities among the non-labile protons (Figures 5.13 and 5.14).

Dynorphin A-(1-13)-peptide (Tyr^1-Gly^2-Gly^3-Phe^4-Leu^5-Arg^6-Arg^7-Ile^8-Arg^9-Pro^{10}-Lys^{11}-Leu^{12}-Lys^{13}) consists of 15 spin systems. The residues Gly, Leu, Ile, and Lys have unique non-labile proton spin systems, and the aromatic spin systems of Tyr and Phe are also characteristic. Upon inclusion of labile protons through employing CD_3OH as a solvent, the spin systems of Arg and Pro differ from one another, as do the backbone spin systems of Phe^4 and Tyr^1.

A major problem is the multiple existence of a number of residues in the peptide. Gly, Leu, and Lys occur twice and Arg is encountered three times. Nevertheless, it was possible to unambiguously assign all but very few of the resonances sequence specifically. These sequence specific resonance assignments were achieved in the manner recommended by Wüthrich [1986, Chapter 8]. After identification of the individual spin systems, sequential interresidue NOE connectivities were derived from NOESY spectra in conjunction with COSY spectra (Figures 5.21 and 5.22).

Coupling constants were determined by analysis of the line splitting in the one-dimensional spectrum (where possible) and from the examination of DQF phase-sensitive COSY cross-sections (cf. Figures 5.17, 5.18, 5.22 and 5.25) which had individually been subjected to zero-filling in order to achieve adequate digital resolution. As Wüthrich [1986, p. 83] has pointed out, the apparent separation of antiphase lines is larger than the true separation due to the effects of finite linewidth and limited digital resolution. Therefore the reliability of the exact values determined has to be viewed with caution. The accuracy of the determined coupling constants is estimated at under ± 0.3 Hz (corresponding to two data points). More complicated multiplets and doublets in regions of considerable overlap were not analyzed at all because of the apparent cancellation of antiphase components. An improvement in the analysis in these cases is possible by the application of the DISCO (differences and sums of traces within COSY spectra) technique [Oschkinat and Freeman, 1984; Kessler and Oschkinat, 1985; Kessler et al., 1985b].

The alphabetical notation for spin systems within molecules introduced by Pople, Schneider, and Bernstein [Pople et al., 1959, p.98] was used to describe the spin systems. Only non-labile protons were considered for the nomenclature, i.e. in all cases except for Tyr^1 and Pro^{10}, a further spin, the backbone amide proton, must be included for the experiments in CD_3OH. Under these circumstances, the Arg spin systems also include the ϵ guanidino NH, so that two additional spins have to be considered. The individual spin systems are discussed below.

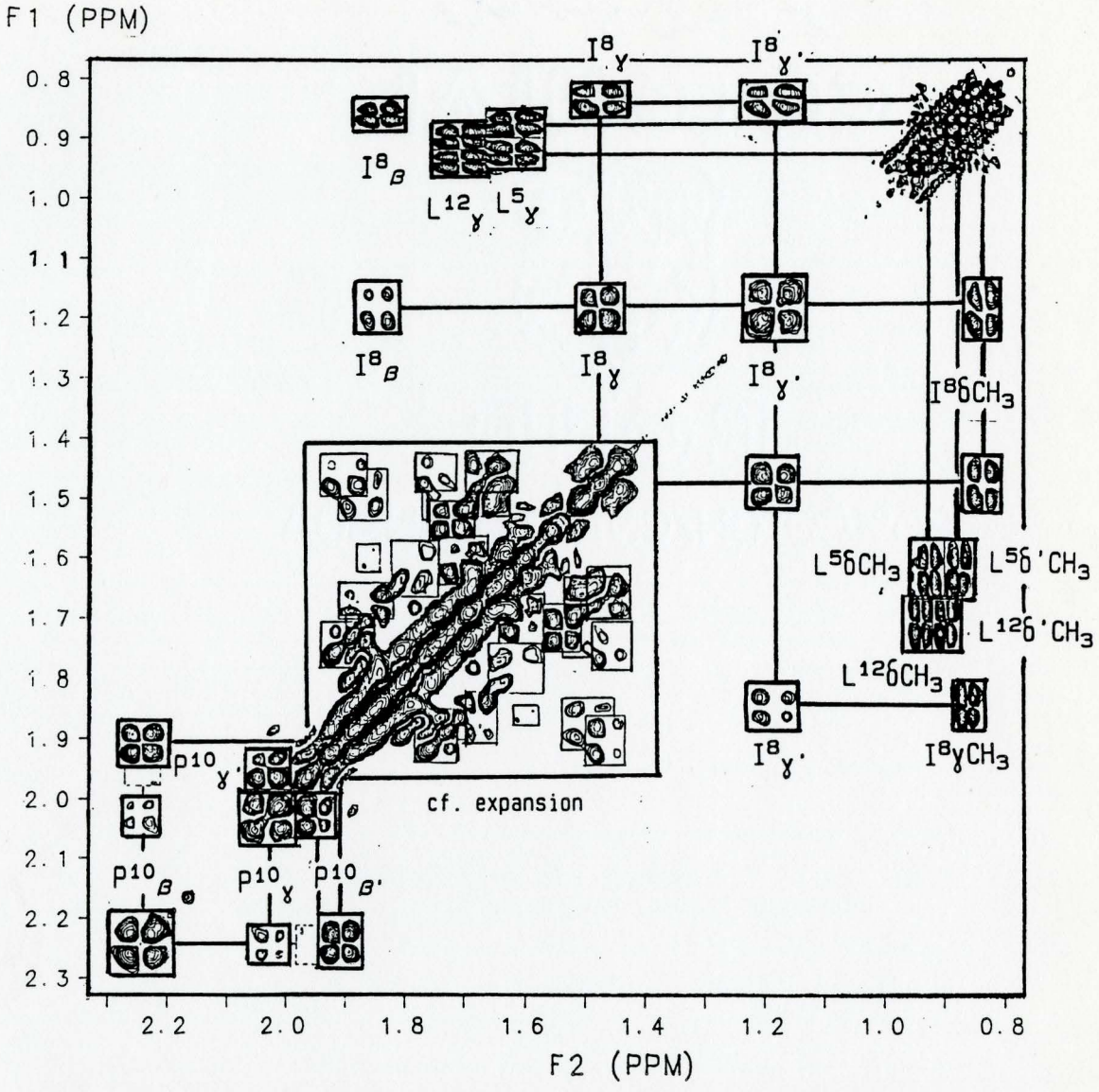

Figure 5.10. An upfield expansion of the 620 MHz double-quantum filtered phase sensitive COSY spectrum of 40 mM dynorphin A-(1-13) in CD_3OD. The relaxation delay (which was also the period for presaturation of the solvent) was 2 s. 36 scans were accumulated for each of the 256 FID's containing 1024 data points in F2 over a reduced spectral width of 4200 Hz. Zero-filling was applied in both dimensions to 2048 data points. Strong window functions ($f(t) = e^{-t/3.183} \cdot e^{-t^2/0.072^2}$) were applied to both dimensions before Fourier transformation. The digital resolution was 4.1 Hz/point in both dimensions.

The Pro^{10}, Ile^8, Leu^{12}, and Leu^5 connectivities are indicated. The central region was too crowded to be labelled and was expanded further in Figure 5.11.

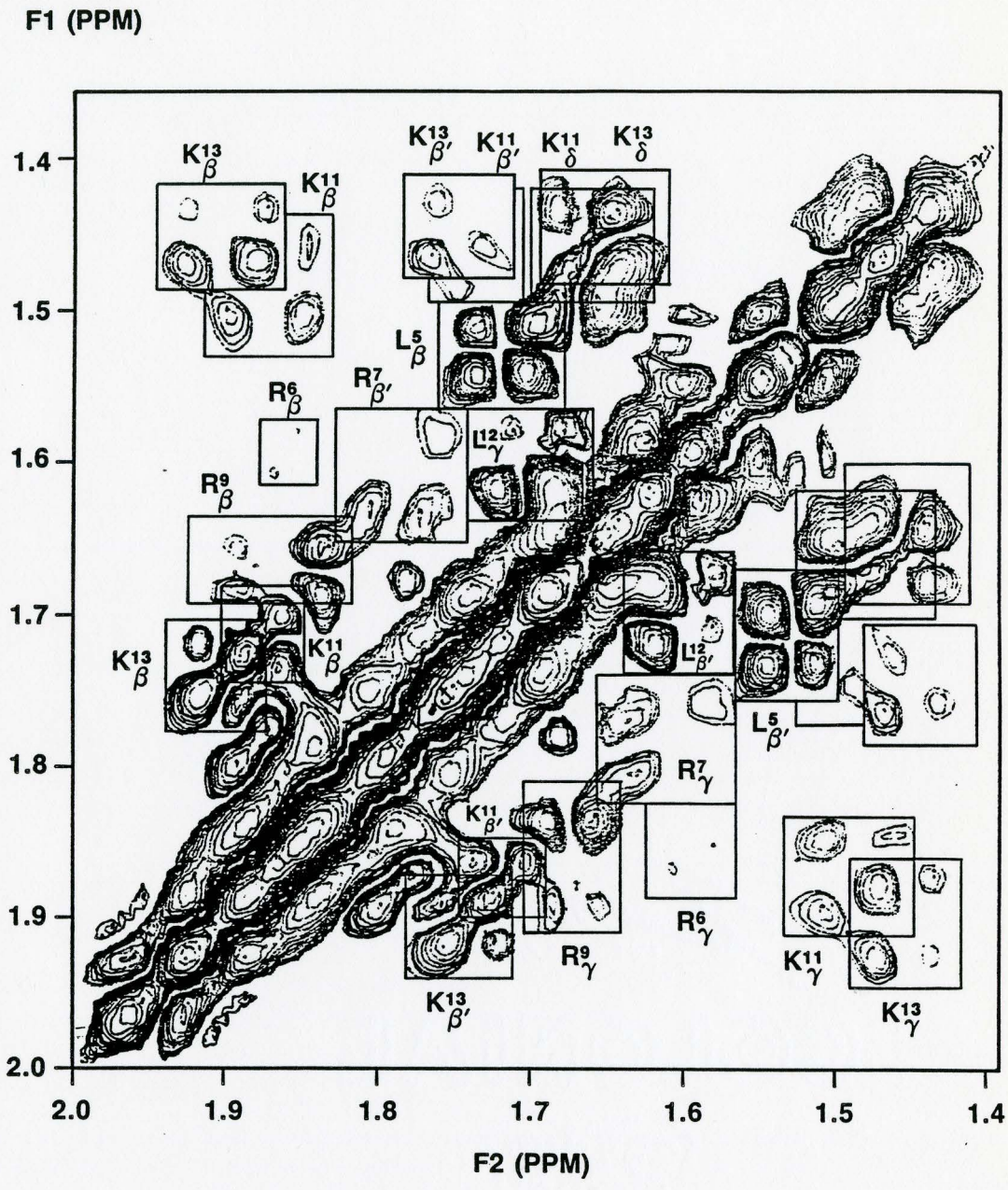

Figure 5.11. An expansion of the central region of Figure 5.10.

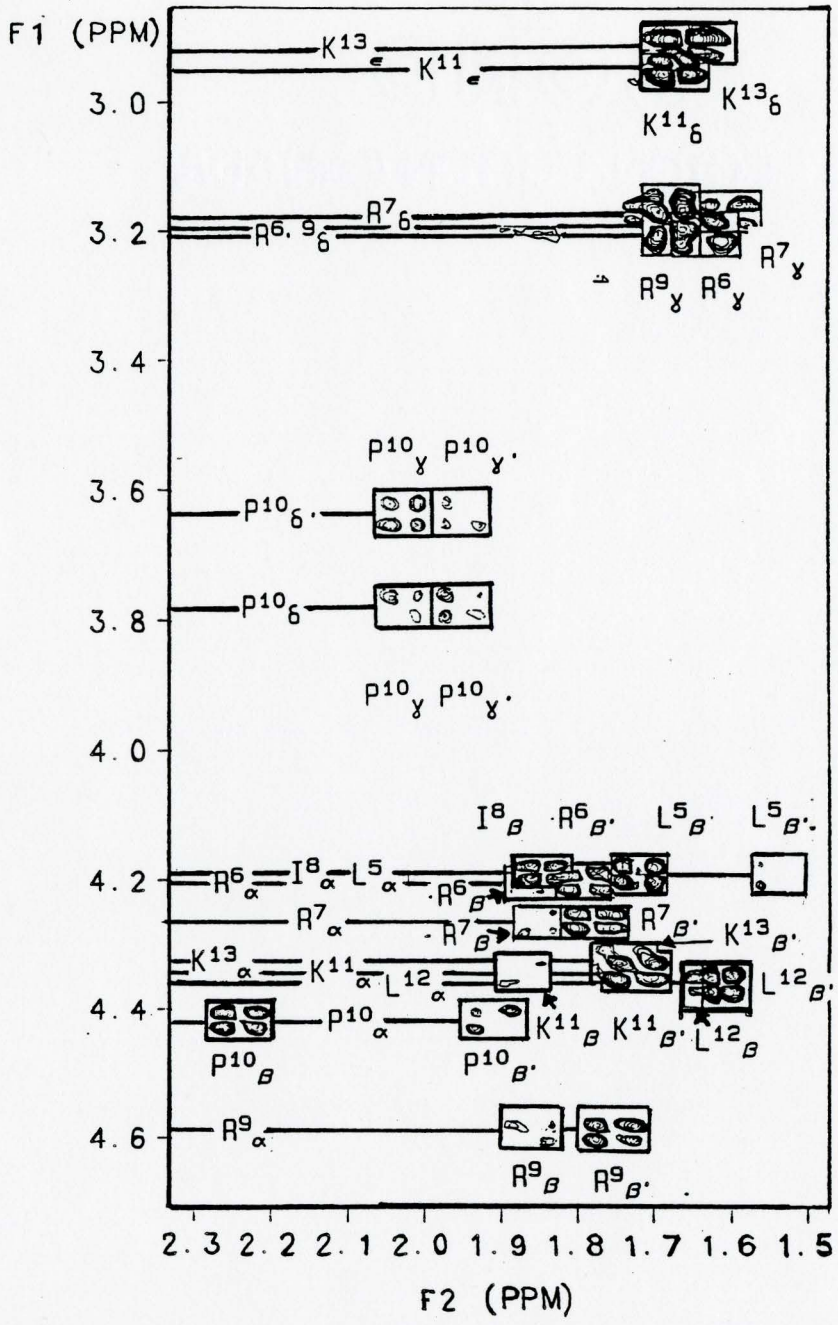

Figure 5.12. The α-β connectivity region of the 620 MHz double-quantum filtered phase sensitive COSY spectrum of 40 mM dynorphin A-(1-13) in CD_3OD. Details of the experiment are described in the caption of Figure 5.10. The Pro^{10} δ-γ, Arg δ-γ, and Lys ϵ-δ connectivities are indicated.

5.2.1. Ile^8

The A_3B_3MPTX spin system of the Ile^8 resonance was one of the most straightforward to assign. The $Ile^8\delta CH_3$ resonance is the only triplet in the methyl region (1.0 to 0.8 ppm, cf. Figure 5.8) and was therefore easily separated from the other methyl resonances in the region ($Ile^8\gamma CH_3$, $Leu^{5,12}\delta,\delta'CH_3$'s) by application of a Hahn spin-echo experiment (Figure 5.9). All the other methyl signals are doublets and appear 180° out of phase with respect to the triplet. The $Ile^8\delta CH_3$ resonance is the only positive signal in the region and can therefore be readily identified as the resonance at highest field (δ = 0.85 ppm).

The $Ile^8\gamma'$, γ, β, and γCH_3 resonances were assigned from the DQF COSY spectrum in Figure 5.10. The $Ile^8\alpha$ proton resonance could not be assigned on the basis of the COSY spectrum alone, as there were many β-α cross-peaks in the region of interest. It was, however unambiguously identified by the RELAY experiment described in the caption of Figure 5.13. This was highlighted by a cross-section taken at the position of the well isolated $Ile\gamma'$ resonance (Figure 5.14b). The Ile^8-NH resonance was also assigned on the basis of this RELAY experiment (Figures 5.15 and 5.16).

The chemical shifts for the Ile^8 residue are summarized in Table 5.1. Only the amide resonance shows a significant deviation from the standard reference values for random coil peptides [Bundi and Wüthrich, 1979; Wüthrich, 1986, p.17] and the values assigned to dynorphin A-(1-13) in aqueous solution [Zhou and Gibbons, 1986].

Table 5.1. The Ile[8] spin system.

	NH	α	β	γ	γ'	γCH_3	δCH_3
Chemical shift δ (ppm)	7.76	4.19	1.85	1.48	1.19	0.87	0.85
	$^3J_{HN\alpha}$	$^3J_{\alpha\beta}$	$^3J_{\beta\gamma'}$	$^3J_{\beta\gamma CH3}$	$^3J_{\gamma\delta CH3}$	$^3J_{\gamma\delta' CH3}$	
Coupling constants ^nJ (Hz)	8.1	7.5	9.0	6.8	7.8	7.5	

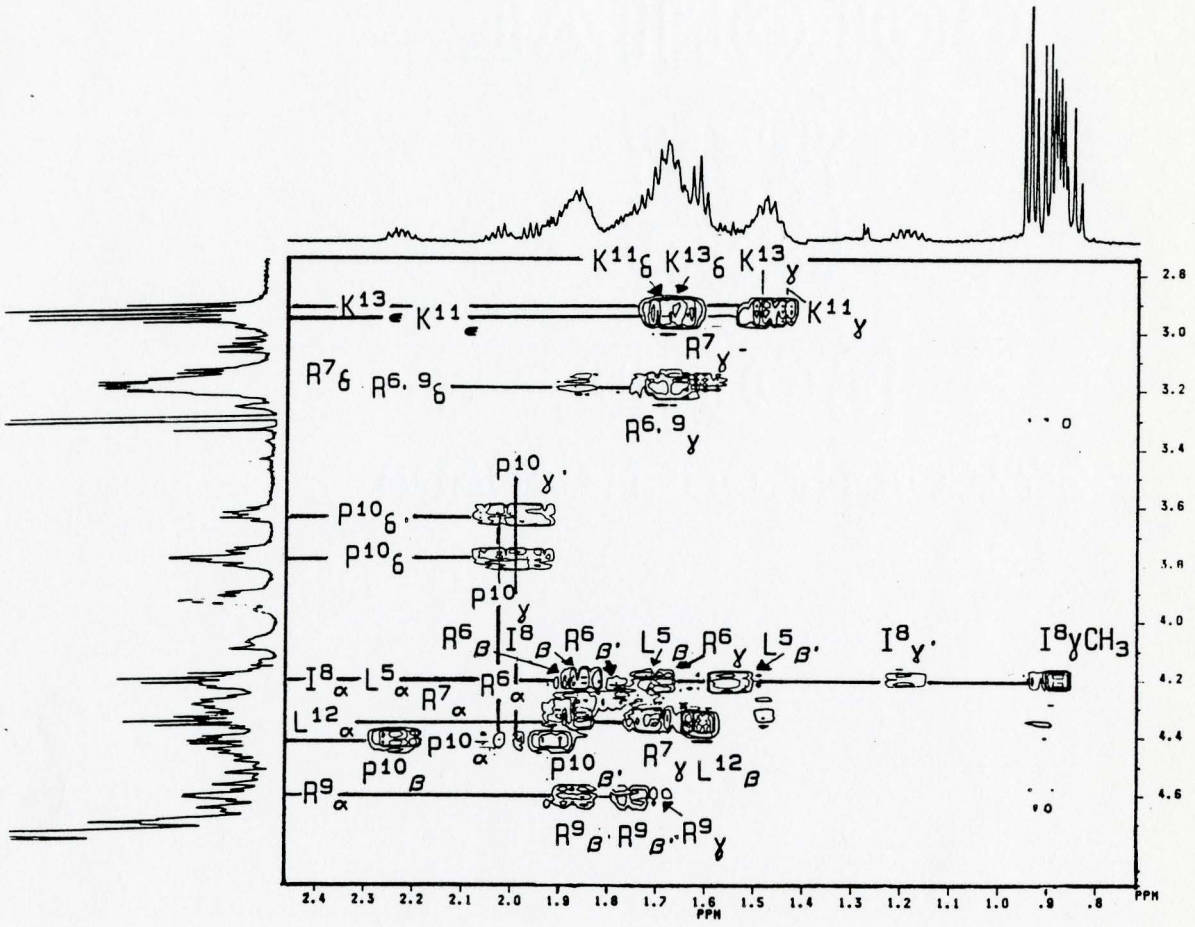

Figure 5.13. An upfield expansion of the 500 MHz $^1H,^1H$ RELAY experiment on 5.5 mM dynorphin A-(1-13) in CD_3OH. The delay time τ was 0.013 s, resulting in a total mixing time of 0.026 s. 96 scans were accumulated for each of the 256 FID's containing 2048 data points in F2 over a 4545.455 Hz spectral width. A relaxation delay of 2.0 s was employed. The data were zero-filled in the t_1 dimension to 1024 data points. Squared sine-bell window functions were applied to both dimensions before Fourier transformation. The digital resolution was 4.4 Hz/point in both dimensions.
The α-β-γ, Arg δ-γ-β and Lys ϵ-δ-γ connectivities are indicated.

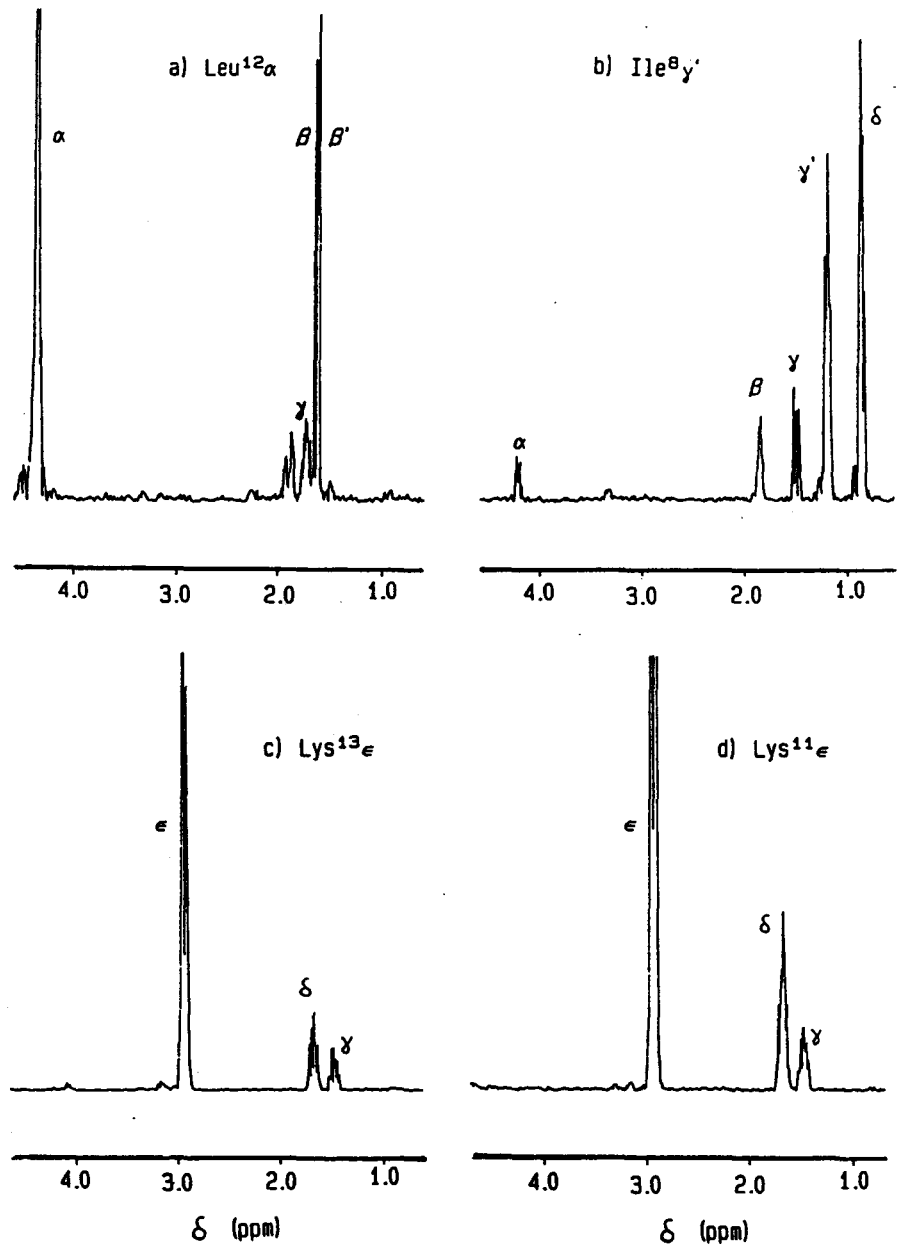

Figure 5.14. Cross-sections along F_2 of the $^1H,^1H$ relayed COSY spectrum of 5.5 mM dynorphin A-(1-13) in CD_3OH described in the caption of Figure 5.13. The cross-sections were taken at the F_1 resonance position of **a)** Leu^{12}_{α} (5.36 ppm), **b)** $Ile^{8}\gamma'$ (1.18 ppm), **c)** Lys^{13}_{ϵ} (2.95 ppm), and **d)** Lys^{11}_{ϵ} (2.92 ppm). The identified resonances are indicated.

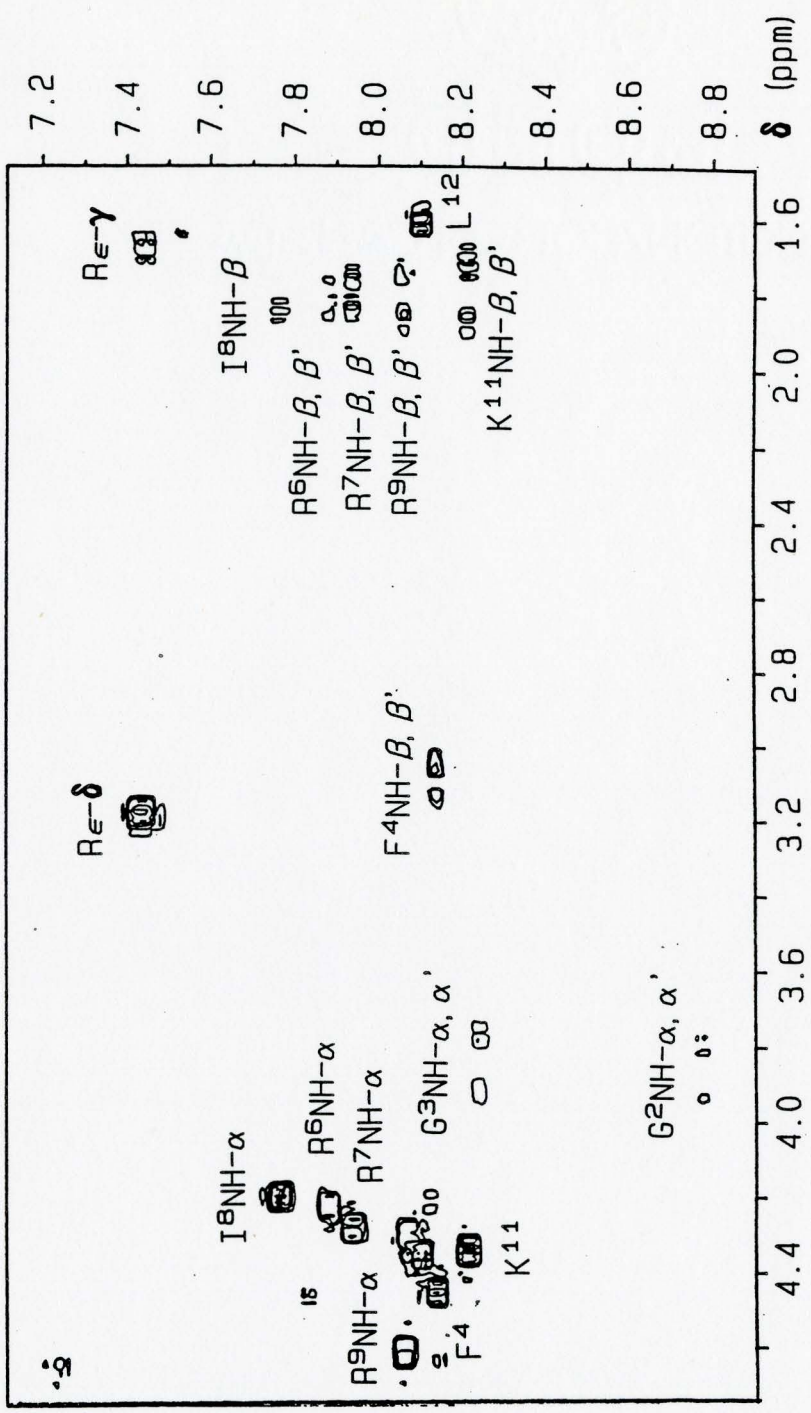

Figure 5.15. NH-α-β connectivities in the relayed COSY experiment on 5.5 mM dynorphin A-(1-13) in CD_3OH described in the caption of Figure 5.13.

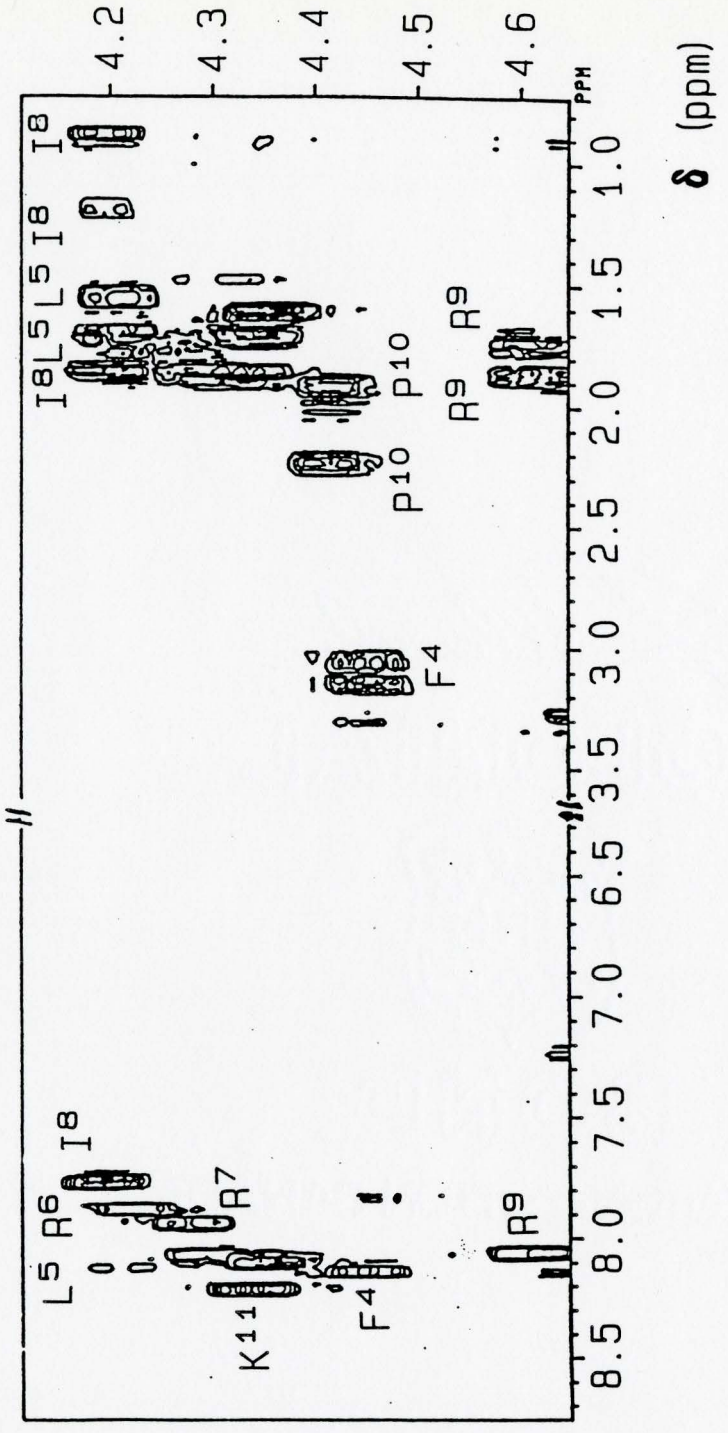

Figure 5.16. All of the connectivities in the relayed COSY experiment on 5.5 mM dynorphin A-(1-13) in CD_3OH described in the caption of Figure 5.13 in which α protons are involved (with the exception of the Tyr^1, Gly^2, and Gly^3 spin systems) are shown.

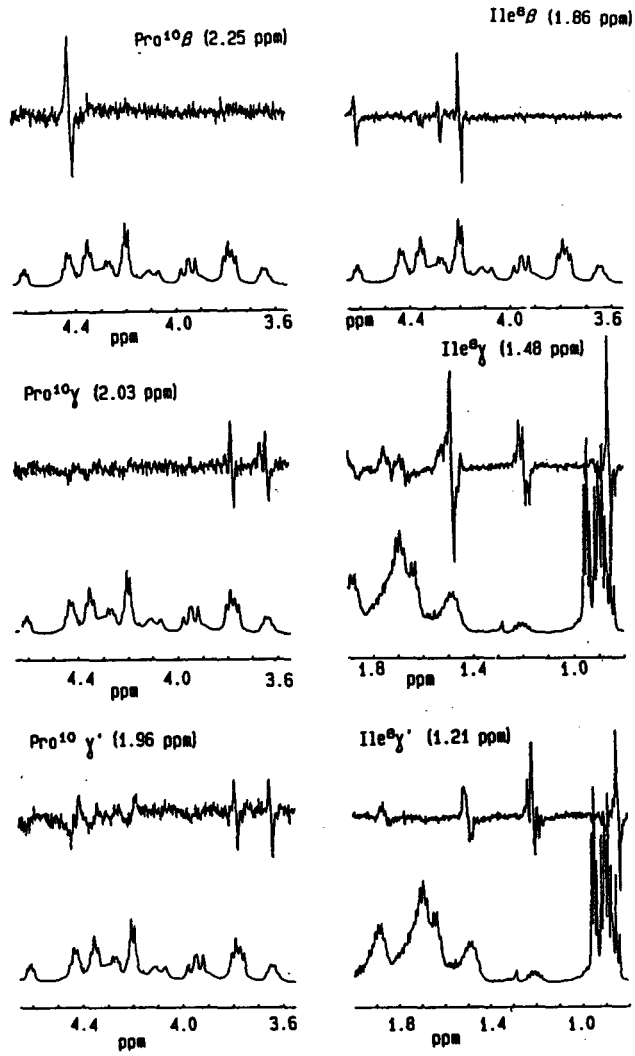

Figure 5.17. Cross-sections from the 500 MHz DQF phase-sensitive COSY spectrum recorded on 25 mM dynorphin A-(1-13) in CD_3OD. The relaxation delay (which was also the period for presaturation of the solvent) was 1 s. 56 scans were accumulated for each of the 512 FID's containing 4096 data points in F2 over a reduced spectral width of 2400 Hz (covering the region from 5.13 to 0.33 ppm). Zero-filling was applied only in the t_1 dimension to 2048 data points. Sine-bell window functions were applied to both dimensions before Fourier transformation. The digital resolution was 1.2 Hz/point in the F2 and 2.3 Hz/point in the F1 dimension.

The cross-sections were taken along F2 at the F1 positions indicated and subjected to inverse Fourier transformation, zero-filling to 32K data points, and renewed Fourier transformation. The improved digital resolution was 0.15 Hz/point.

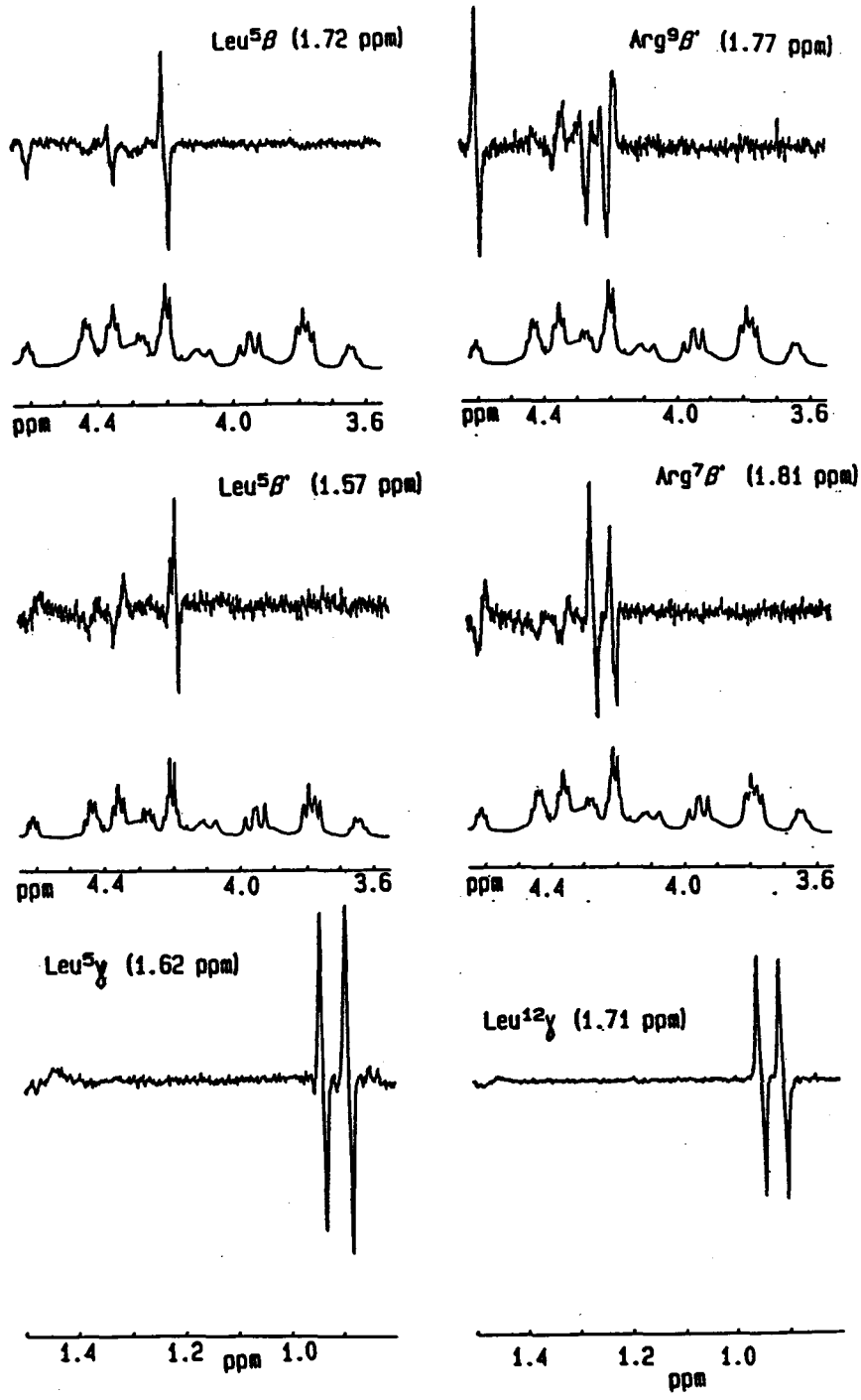

Figure 5.18. Further cross-sections from the 500 MHz DQF phase-sensitive COSY spectrum recorded on 25 mM dynorphin A-(1-13) in CD_3OD. For further details, see the caption for Figure 5.17.

5.2.2. Pro^{10}

The Pro^{10} AB(MP)EFX system was also readily assigned. The Pro δ', Pro β, and Pro γ multiplet structures are well separated from other resonances, so that the assignment of the entire spin system is possible on the basis of the DQF COSY spectrum alone (Figures 5.10 and 5.12). Noteworthy is the fact that the γ and γ' proton resonances could be distinguished (cf.Table 5.2).

Table 5.2. The Pro^{10} spin system.

	α	β	β'	γ	γ'	δ	δ'
Chemical shift δ (ppm)	4.42	2.24	1.91	2.03	1.96	3.78	3.64
	$^3J_{\alpha\beta}$	$^3J_{\alpha\beta'}$	$^3J_{\gamma\delta}$	$^3J_{\gamma\delta'}$	$^3J_{\gamma'\delta}$	$^3J_{\gamma'\delta'}$	$^2J_{\delta\delta'}$
Coupling constants ^nJ (Hz)	8.5	5.6	6.8	6.3	6.5	6.5	-10.2

Deber and coworkers [Deber et al., 1971] have derived a Karplus [1959] equation for the dihedral angles between the Pro ring protons which can be expressed as:

$$^3J_{HH} = 9.5 \cos^2\theta - 1.0 \cos\theta + 1.4$$

(Fig 5.17). More contour levels were identified for the Pro^{10} α-β than for the Pro^{10} α-β' connectivity, indicating that $\chi_{\alpha\beta}$ was smaller in magnitude than $\chi_{\alpha\beta'}$ (assuming that $\chi_{\alpha C}$ is the largest of the three torsional angles χ_1.

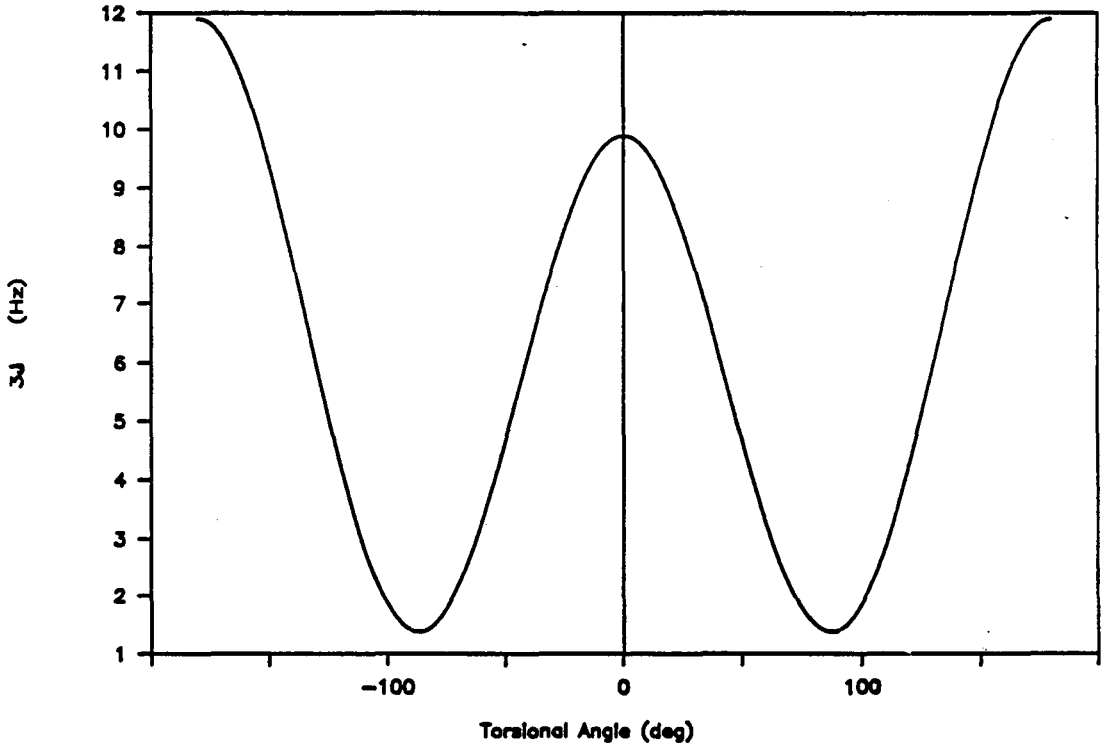

Figure 5.19. Dependence of the $^3J_{HH}$ spin-spin coupling constants on the torsional angles χ, with parameters proposed by Deber et al. [1971].

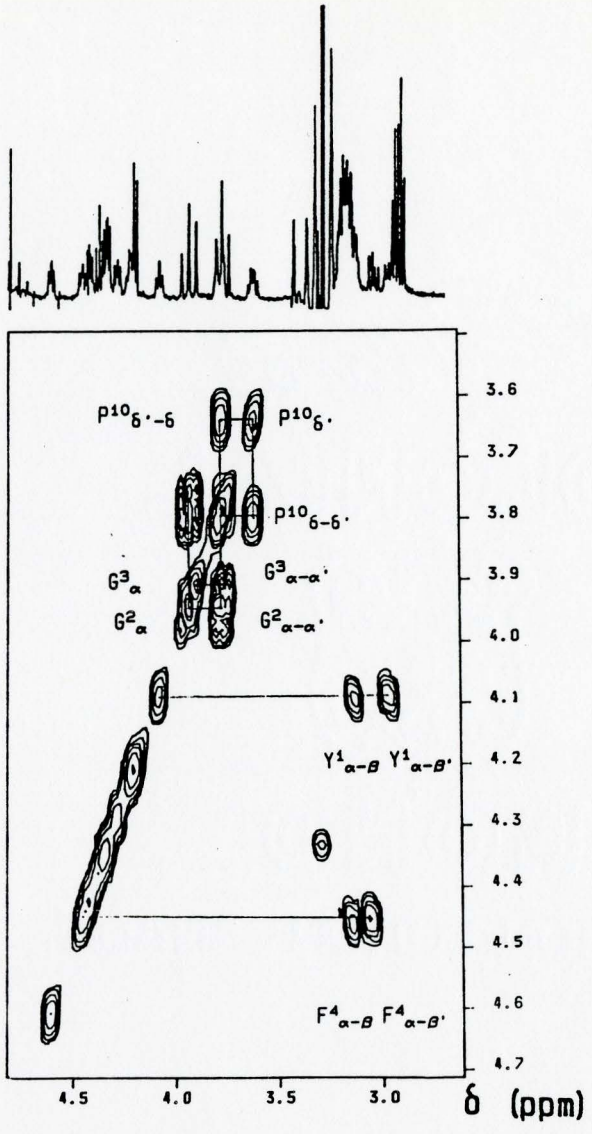

Figure 5.20. An expansion of a COSY-45 spectrum of 6.2 mM dynorphin A-(1-13) in CD_3OD. The $\pi/2$ pulse width was 21.2 μs, the $\pi/4$ pulse 10.6 μs. 160 scans were accumulated for each of the 256 FID's containing 1024 data points in F2 over a 3906.250 Hz spectral width (0.131 s acquisition time). A relaxation delay of 1.0 s was employed. The data were zero-filled in the t_1 dimension to 512 data points. As in the basic COSY experiment, squared sine-bell window functions were applied to both dimensions before Fourier transformation. All other details were as described for basic $^1H,^1H$ COSY. The digital resolution was 7.6 Hz/point in both dimensions.

The Pro^{10} δ'-δ, δ'-γ,δ'-γ',δ-γ, α-β, and α-β' connectivities are marked. Also indicated are the Gly α-$\alpha'$and the Tyr^1 and Phe^4 α,β and α-β' connectivities.

5.2.3. Gly^2 and Gly^3

The α proton resonances of the Gly AX systems were located in the COSY-45 spectrum (Figure 5.20) and were unambiguously assigned on the basis of their NH-α connectivities (Figure 5.21). The spin system containing the downfield amide proton was tentatively assigned to Gly^2 in accordance with the findings in aqueous solution [Zhou and Gibbons, 1986]. This was confirmed by the sequence specific resonance assignments. In contrast to the spectrum of the peptide in H_2O (cf. methanol titration experiments), the amide proton signals were broadened, so that individual multiplet components could not be observed. Nevertheless, it was possible to determine the $^3J_{HN\alpha}$ coupling constants from the appropriate cross-sections of the DQF phase-sensitive COSY experiment (Figure 5.22).

The chemical shifts of the amide proton resonances displayed a high degree of fluctuation with time. As these studies were conducted over a period of almost two years, long term changes in the resonance positions could be observed. The chemical shift of the Gly^2 NH resonance increased from 8.77 ppm via 8.82 ppm to 8.86 ppm, that of the Gly^3 resonance from 8.23 ppm via 8.28 ppm to 8.30 ppm. The change is considered not dramatic enough to be due to a chemical degradation of the sample. Methanol titration experiments (cf. 6.2) indicate that a conformational change results in a strong variation of the Gly NH chemical shifts. Perhaps a long term stabilization of the conformation of the molecule is taking place.

Table 5.3. The Gly^2 and Gly^3 spin systems.

Chemical shift δ (ppm)	NH	α	α'
Gly^2	8.77-8.86	3.94	3.77
Gly^3	8.23-8.30	3.91	3.76

Coupling constants ^nJ (Hz)	$^3J_{HN\alpha}$	$^3J_{HN\alpha'}$	$^2J_{\alpha\alpha'}$
Gly^2	7.5	6.9	-16.8
Gly^3	6.4	5.9	-16.7

An interesting feature derived from Table 5.3 is that the difference in the chemical shifts between the geminally coupled protons of the Gly residues is relatively large in our studies, resulting in the observation of AX systems as opposed to the strongly coupled AB systems obtained for the peptide in water [Zhou and Gibbons, 1986].

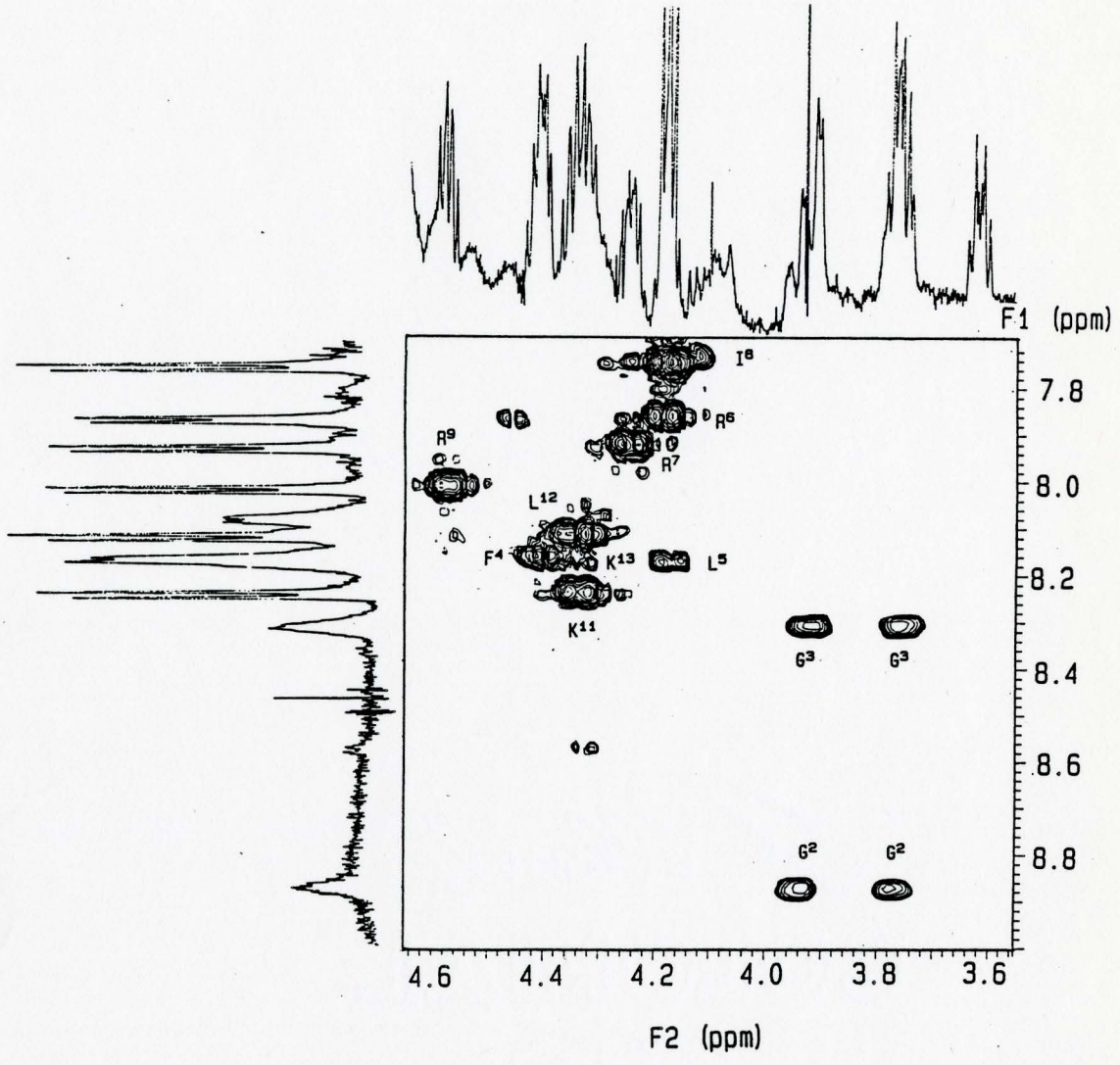

Figure 5.21. An expansion of a 620 MHz COSY spectrum on 40 mM dynorphin A-(1-13) in CD_3OH. 64 scans were accumulated in blocks of 16 scans for each of the 512 FID's containing 1024 data points in F2 over a 5200.2 Hz spectral width. A relaxation delay of 1.5 s was employed. The data were zero-filled in both dimension to 2048 data points. Resolution enhancement window functions were applied to both dimensions before Fourier transformation. The digital resolution was 5.1 Hz/point in both dimensions. The NH-α (and NH-α') connectivities are indicated.

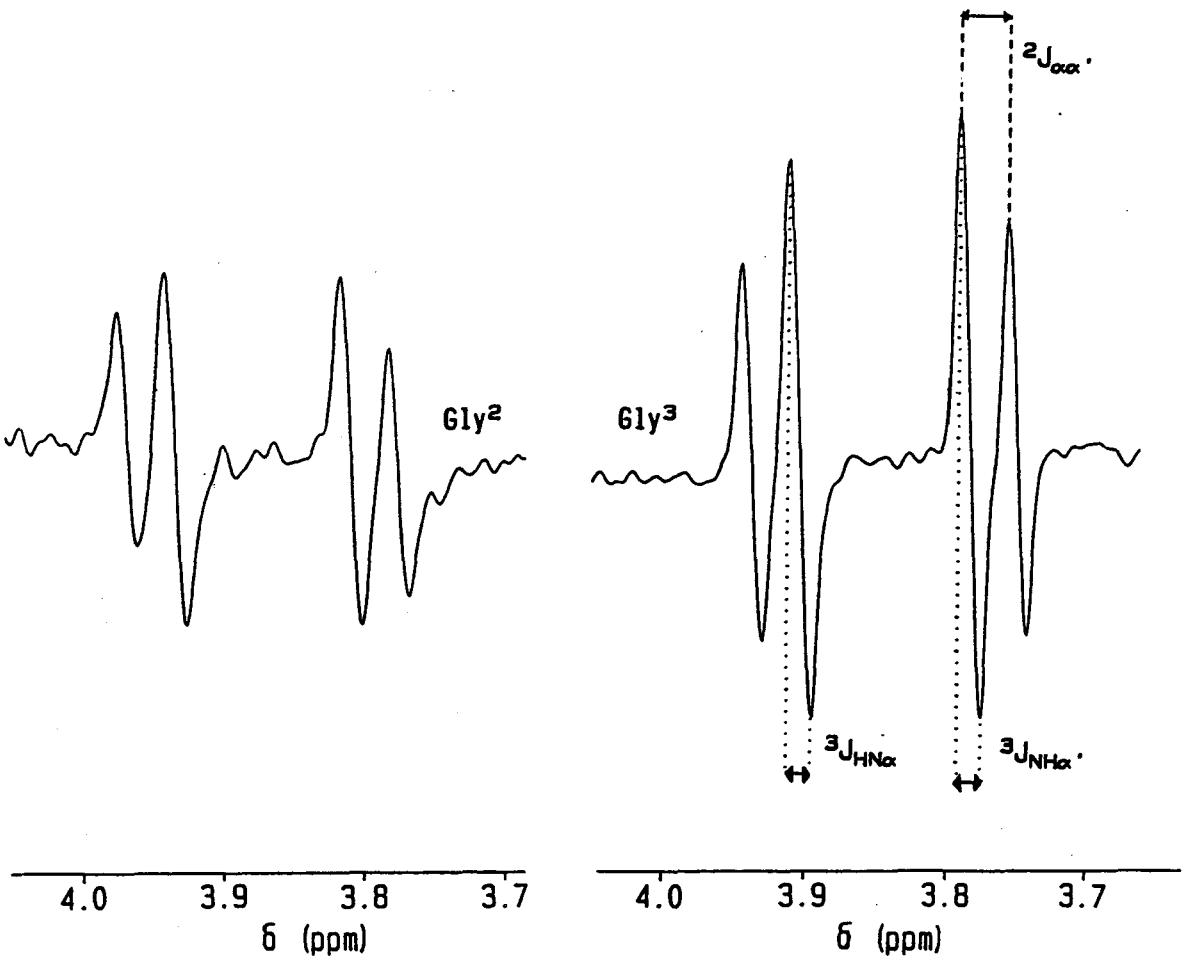

Figure 5.22. Cross-sections from the 500 MHz DQF phase-sensitive COSY spectrum recorded on 20 mM dynorphin A-(1-13) in CD_3OH. The relaxation and solvent presaturation delay was 2 s. 64 scans were accumulated for each of the 256 FID's containing 2048 data points in F2 over a spectral width of 4545 Hz. The data were zero-filled to 4096 data points in the t_2 dimension and to 2048 data points in the t_1 dimension. Sine-bell window functions were applied to both dimensions before Fourier transformation. The cross-sections were taken along F2 at the F1 positions of the Gly^2NH (8.77 ppm, left) and Gly^3NH (8.24 ppm, right), subjected to inverse Fourier transformation, zero-filling to 32K data points, and renewed Fourier transformation. The improved digital resolution was 0.28 Hz/point.

The extraction of coupling constants was performed as indicated on the right with the anti-phase components yielding the active coupling and the in-phase components displaying the passive coupling [Wüthrich, 1986, pp. 79-85].

5.2.4. Tyr[1] and Phe[4]

Each aromatic residue incorporates two separate spin systems: a backbone AMX spin system consisting of the α and β protons, and an aromatic spin system encompassing the non-labile protons of the aromatic ring [Wüthrich, 1986, p.16].

The Phe[4] AA'BB'C aromatic spin system was difficult to disseminate because of the strong coupling involved in the Phe ring, which resulted in a complicated appearance in the one- and two-dimensional spectra (Figure 5.23). The upfield triplet was assigned to the ζ proton as the line intensities indicated that this was the only signal arising from a single proton. The two ϵ protons were expected to give rise to a single triplet of double intensity due to proton exchange by interconversion through 180° ring flips [Jardetzky and Roberts, 1981, p.451]. This was located at 7.28 ppm. Based on the same argument, the ortho protons are expected to give rise to a doublet of double intensity. Such a doublet was identified at 7.26 ppm. The only two-dimensional experiment which yielded resolved cross-peaks at least partially amenable to connectivity analysis was the DQF COSY spectrum shown in Fig. 5.23. The connectivities detected agree with the above assignments. Additional signals in this region have yet to be explained. Perhaps this can be achieved by spectral simulation.

The Tyr[1] AA'XX' aromatic spin system was readily assigned (Figure 5.23 and Table 5.4). The broadened appearance of the Tyr δ doublet as compared to the Tyr ϵ doublet is attributed to the different time scales defined by the

chemical shift differences of the protons undergoing interconversion. In the rigid residue, the δ proton resonances are usually much further apart than the ϵ proton resonances and will thus define a much faster time scale [Wüthrich, 1986, pp. 7-10]. Thus, the same interconversion frequency for δ and ϵ protons resulted in an exchange regime which is slower on the time scale defined by the δ protons than on the ϵ proton time scale.

Table 5.4. The aromatic spin systems of Tyr^1 and Phe^4.

	Chemical shift δ (ppm)		
	δ	ϵ	ζ
Tyr^1	7.11	6.77	
Phe^4	7.26	7.28	7.21

With the exception of the Phe^4-δ protons, all resonances in Table 5.4 of the peptide in methanol were shifted slightly upfield compared to those of the peptide in aqueous solution (cf. Chapter 6). This was expected as the less polar solvent will cause a decrease in the extent of deshielding of the protons. The effect is strongest for the $Phe^4\zeta$ proton and the $Tyr^1\epsilon$ protons. This, too, was anticipated as these protons are more exposed to the solvent.

The β proton resonances of the aromatic residues are shifted downfield in comparison with other β proton resonances [Bundi and Wüthrich, 1979], which

facilitates recognition of the backbone spin systems. The cross-peaks connecting α and β protons are separated distinctly from all other connectivities (Figure 5.20). As the labile amino protons of Tyr^1 could not be observed due to fast exchange with the solvent, the Phe^4 backbone spin system was easily distinguished from the Tyr^1 system by the observation of NH-α connectivities in a $^1H,^1H$ COSY spectrum of dynorphin A-(1-13) in CD_3OH (Figure 5.24). The unambiguous assignment of the Phe^4 amide proton was achieved by observing the NH-α-β RELAY connectivities in the RELAY experiment described in Figure 5.15. The $Tyr^1\alpha$ resonance was not well resolved in both CD_3OH and CD_3OD and was shifted significantly upfield (Table 5.5) compared to the aqueous solution of the peptide (cf. Chapter 6).

The coupling constants listed in Table 5.5 were all determined from cross-sections of the DQF phase-sensitive COSY spectrum on 20 mM dynorphin A-(1-13) in CD_3OH as described in the caption of Figure 5.22. The α-β cross-sections are displayed in Figure 5.25.

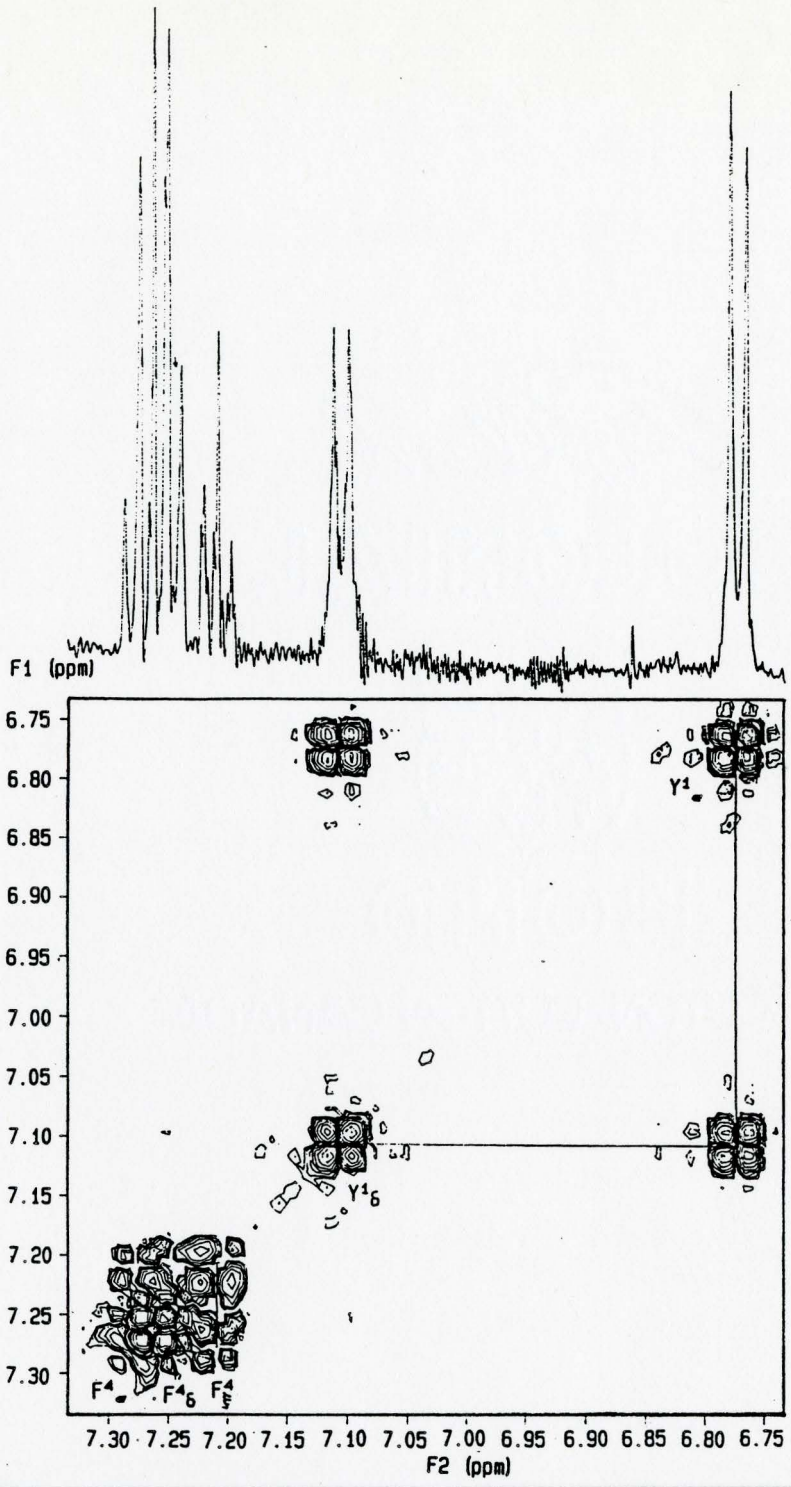

Figure 5.23. An expansion of the 620 MHz double-quantum filtered phase sensitive COSY spectrum of 40 mM dynorphin A-(1-13) in CD_3OD described in the caption of Figure 5.10. The connectivities of the aromatic ring protons are indicated.

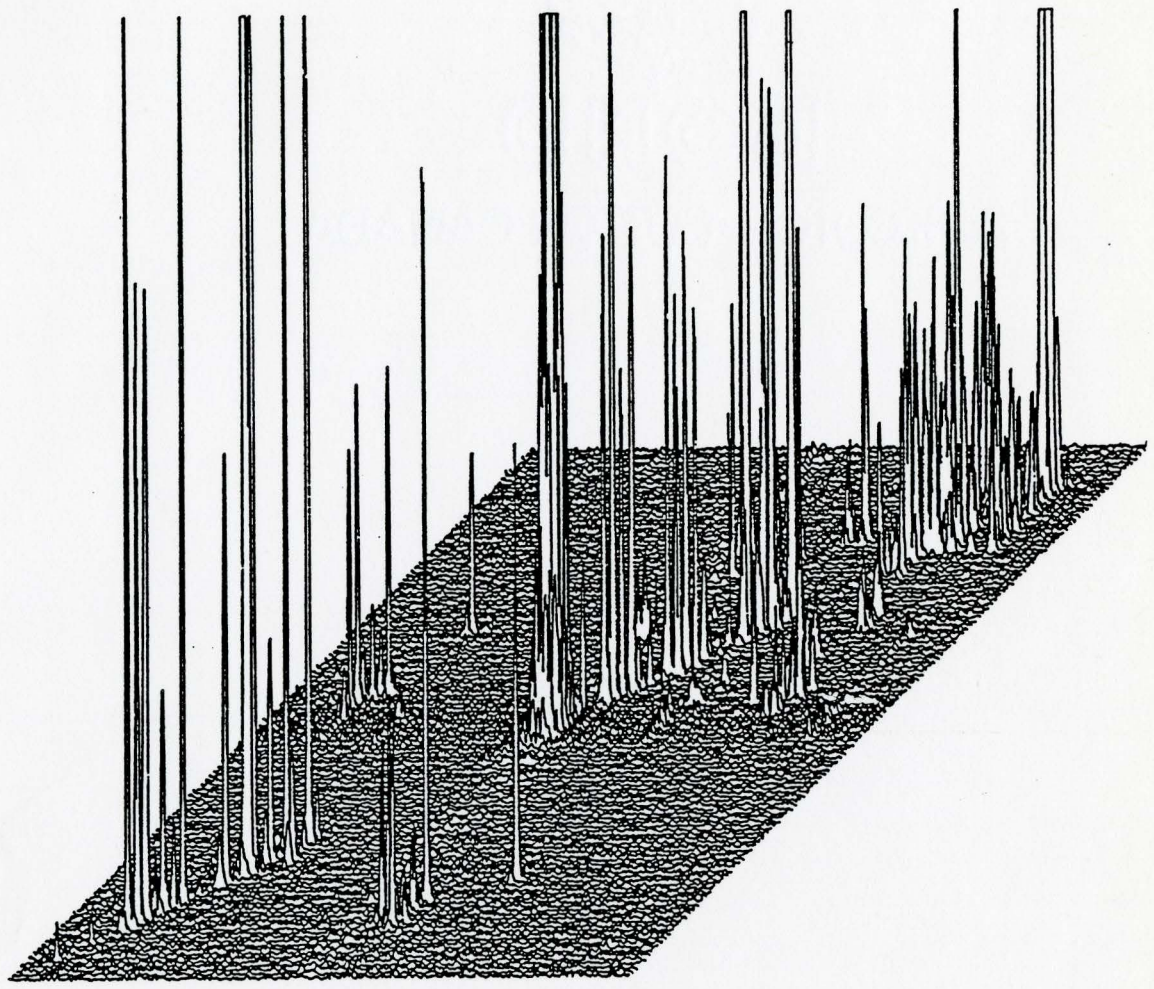

Figure 5.24. A stacked plot of the $^1H,^1H$ COSY spectrum of 5.5 mM dynorphin A-(1-13) in CD_3OH. Eighty scans were accumulated for each of the 256 FID's containing 2048 data points in F2 over a 4545.455 Hz spectral width. A relaxation delay of 2.0 s was employed. The data were zero-filled in the t_1 dimension to 1024 data points. Squared sine-bell window functions were applied to both dimensions before Fourier transformation. The digital resolution was 4.4 Hz/point in both dimensions.

High field in both dimensions ($\delta_1 = \delta_2 = 0$ ppm) is at the back on the right, low field in both dimensions ($\delta_1 = \delta_2 = 9$ ppm) is localized at the front on the left. The region containing the NH-α connectivities is located in at the front in the centre.

Table 5.5. The Tyr^1 and Phe^4 backbone spin systems.

Chemical shift δ (ppm)	NH	α	β	β'
Tyr^1		4.10	3.15	2.99
Phe^4	8.17-8.13	4.43	3.15	3.08

Coupling constants ^nJ (Hz)	$^3J_{HN\alpha}$	$^3J_{\alpha\beta}$	$^3J_{\alpha\beta'}$	$^2J_{\beta\beta'}$
Tyr^1	-	8.4	8.5	-14.9
Phe^4	7.1	6.2	8.6	-14.3

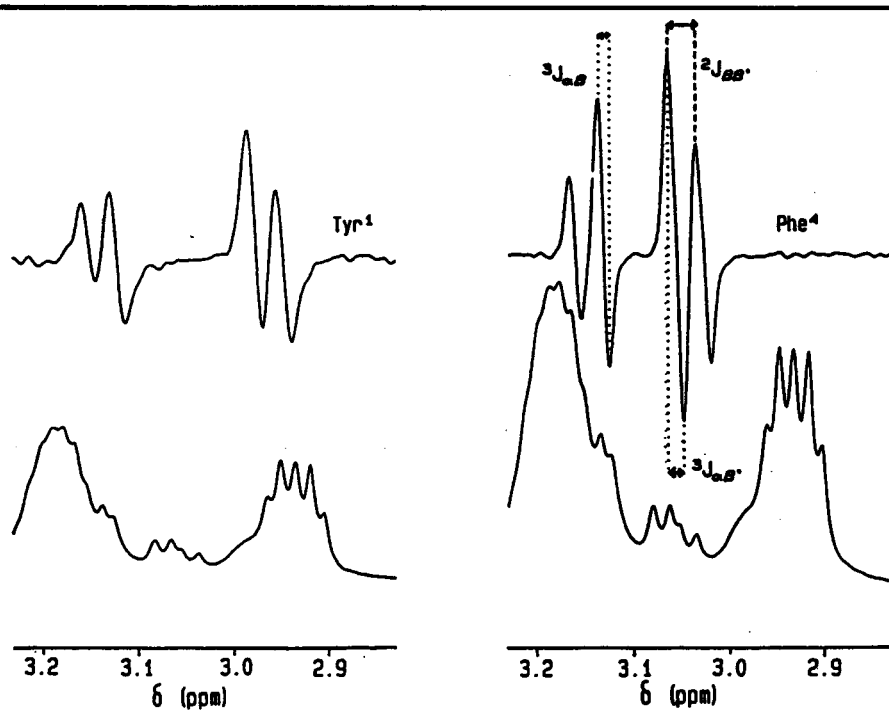

Figure 5.25. Cross-sections from the 500 MHz DQF phase-sensitive COSY spectrum described in the caption of Figure 3.22. These cross-sections were taken at the F1 positions of (left) the $Tyr^1{}_\alpha$ (4.07 ppm) and (right) the $Phe^4{}_\alpha$ (4.44 ppm) resonances.

5.2.5. Leu^5 and Leu^{12}

In both Leu A_3B_3MNOX spin systems, the γ-δ connectivities were easily recognizable (Figure 5.10). The δCH_3 resonances at 0.88 and 0.93 ppm displayed connectivities to a signal at 1.61 ppm, thus assigning the latter to a γCH resonance. The other δCH_3 resonances displayed connectivities to peaks further downfield (1.71 ppm), so that two separate γ,δ,δ' systems could be distinguished. The Leu α-β connectivities were initially assigned (Figure 5.12) on the basis of their upfield β-proton resonances [Wüthrich, 1986, p. 17]. The NH-α-β RELAY connectivities lead to the assignment of the amide protons (Figures 5.15 and 5.16). These assignments were later confirmed by sequence specific resonance assignments (cf. Figure 5.26). Assignment of the Leu^{12} spin system was supported by an appropriate 500 MHz RELAY cross-section (Fig. 5.14a), identifying a signal, albeit weak at 1.71 ppm. In the 500 MHz DQF COSY spectrum on 28 mM dynorphin in CD_3OD, a connectivity was detected between a resonance at 1.55 ppm (assigned to Leu^5-β') and two resonances at 1.73 (Leu^5-β) and 1.65 ppm (Leu^5-γ), respectively.

Table 5.6. The Leu[5] and Leu[12] spin systems.

Chemical shift δ (ppm)	NH	α	β	β'	γ	δCH_3	$\delta' CH_3$
Leu[5]	8.17-8.13	4.19	1.73	1.55	1.65	0.94	0.89
Leu[12]	8.10	4.37	1.63	1.60	1.71	0.95	0.91
Coupling constants ^nJ (Hz)	$^3J_{HN\alpha}$	$^3J_{\alpha\beta}$	$^3J_{\alpha\beta'}$	$^3J_{\gamma\delta}$	$^3J_{\gamma\delta'}$		
Leu[5]		10.1	4.9	6.6	6.5		
Leu[12]	7.5			6.5	6.5		

5.2.6. Lys[11] and Lys[13]

The Lys $A_2(K_2T_2)MPX$ spin systems were also problematic to assign. The most characteristic peaks were the ϵCH_2 signals at 2.95 and 2.92 ppm, respectively [Wüthrich, 1986, p.17]. Connectivities in the COSY (Figure 5.12.) and RELAY (Figures 5.13 and 5.14 c,d) experiments allowed the assignment of the δ and γ CH_2 proton signals. The β and β' resonances were assigned on the basis of the respective connectivities to the γ protons (Figure 5.11). One α proton, which was subsequently assigned to Lys[11] (cf. sequence specific

assignments), displayed easily detectable β- and β' connectivities (Figure 5.12). The other α proton resonance (Lys^{13}) could not be assigned in a straightforward manner. It was tentatively assigned to a position slightly upfield from $Lys^{11}{}_{\alpha}$ based on the integration of the one-dimensional spectrum and a slight indication of a cross-peak in the COSY spectrum. This was confirmed by the sequence specific assignments (Figure 5.26) and the corresponding NH-α COSY connectivity (Figure 5.21). The problem arose from the broadened nature of the $Lys^{13}{}_{\alpha}$ resonance and the consequent low intensity of the corresponding cross-peaks. No coupling constants could be determined for the Lys^{13} spin system.

The Lys^{13} amide proton resonance line exhibited a considerable susceptibility to changes in its chemical shift position as was observed through comparison of the COSY spectra in Figures 5.21 and 5.26.

Table 5.7. The Lys^{11} and Lys^{13} spin systems.

Chemical shift δ (ppm)	NH	α	β	β'	γ	δ	ϵ
Lys^{11}	8.25-8.21	4.35	1.84	1.73	1.50	1.68	2.95
Lys^{13}	8.17-8.07	4.33	1.91	1.76	1.47	1.67	2.92

Coupling constants ^{n}J (Hz)	$^{3}J_{HN\alpha}$	$^{3}J_{\alpha\beta}$	$^{3}J_{\alpha\beta'}$
Lys^{11}	7.6	5.4	8.9
Lys^{13}			

5.2.7. Arg^6, Arg^7, and Arg^9

The Arg^6, Arg^7, and Arg^9 $A_2(T_2)MPX$ spin systems possess characteristic ϵNH resonances which were found at approximately 7.48 ppm. Connectivities obtained from COSY (Figure 5.24 and 5.12) and RELAY (Figure 5.15) experiments yield the positions of the δ and γ methylene proton resonances, respectively. The β-γ connectivities were difficult to identify because all of the respective resonances were located in the extremely dense region between 1.9 and 1.6 ppm (cf. Figure 5.7). Nevertheless, connectivities were established between the γ protons and at least one of the β protons of each residue (Figure 5.10). The recognition of β-α (Figure 5.12) connectivities as well as NH-α-β RELAY connectivities (Figures 5.15 and 5.16) and sequence specific assignments (cf. 5.26) in all three cases led to complete assignments.

Table 5.8. The Arg[6], Arg[7], and Arg[9] spin systems.

Chemical shift δ (ppm)	NH	α	β	β'	γ	δ	δ'
Arg[6]	7.88	4.21	1.88	1.80	1.69	3.19	7.48[a]
Arg[7]	7.94	4.27	1.86	1.79	1.62	3.17	7.48[a]
Arg[9]	8.05	4.60	1.88	1.77	1.69	3.19	7.51[a]

Coupling constants ^nJ (Hz)	$^3J_{HN\alpha}$	$^3J_{\alpha\beta}$	$^3J_{\alpha\beta'}$
Arg[6]	6.6		
Arg[7]	7.0	5.3	9.1
Arg[9]	7.2	6.1	8.1

a = resonances which were not unambiguously assigned

5.3. Sequence Specific Assignments

Sequence specific assignments were obtained with the aid of NOESY and the respective COSY spectra (Figure 5.26). Non-bonding internuclear distances of up to 5 Å can manifest themselves in NOESY contour maps [Wüthrich et al., 1982]. This upper limit depends on the mixing time employed in the NOESY pulse sequence. At a mixing time of 100 ms, this upper limit is reduced to ≈3 Å between different protons of the polypeptide backbone [Wagner and Wüthrich, 1982]. The ^{1}H-^{1}H sequential distance $d_{\alpha N}(i,i+1)$ depends on the respective torsional angle ψ_i, but never exceeds ≈ 3.5 Å [Billeter et al., 1982]. In the same manner, the intraresidue ^{1}H-^{1}H distance $d_{N\alpha}(i,i)$ depends on the torsional angle ϕ_i, but does not exceed ≈ 2.8 Å [Wüthrich, 1986, p.120]. Consequently, both intraresidue and sequential through-space connectivities are established in the α-NH region of NOESY spectra. They can distinguished only by comparison of the NOESY spectra with COSY spectra acquired under the same conditions.

This is demonstrated in Figure 5.26. Some of the cross-peaks in the NOESY spectrum were intraresidue connectivities and were identified by comparison with the accompanying COSY spectrum. The $\alpha(i)$-NH$(i+1)$ connectivities are indicated and can be followed from the amino-terminus to the carboxy-terminus of the molecule. No connectivities could be detected between Tyr$^1\alpha$ and Gly^{2}NH. The one-dimensional spectrum (Figures 5.2 and 5.4) indicated that both peaks were broadened considerably, so that the respective NOESY cross-peak was not likely to be observed. The Gly$^2\alpha$-Gly^{3}NH connectivity was

also missing. No satisfying explanation for this has been found. These missing connectivities do not present a problem as the assignment of the Tyr^{1} backbone spin system was unambiguous and because the ensuing assignment of Gly^{3} spin system rendered the identification of the Gly^{2} spin system as equally obvious.

The $Gly^{3}\alpha$-$Phe^{4}NH$ connectivity is indicated. As the amide resonances of Phe^{4} and Leu^{5} overlapped (cf. COSY), no distinction could be made as to whether the NOESY cross-peak at the position of the $Phe^{4}\alpha$ resonance was an intraresidue ($Phe^{4}\alpha$-$Phe^{4}NH$) or sequential cross-peak ($Phe^{4}\alpha$-$Leu^{5}NH$) or both. From the $Leu^{5}\alpha$ proton resonance, the connectivity pattern could be followed through via $Arg^{6}NH$, $Arg^{6}\alpha$, $Arg^{7}NH$, $Arg^{7}\alpha$, $Ile^{8}NH$, $Ile^{8}\alpha$, and $Arg^{9}NH$ to the $Arg^{9}\alpha$ resonance, where the $\alpha(i)$-$NH(i+1)$ connectivity pattern was interrupted. This is due to the absence of an amide proton from the Pro^{10} residue.

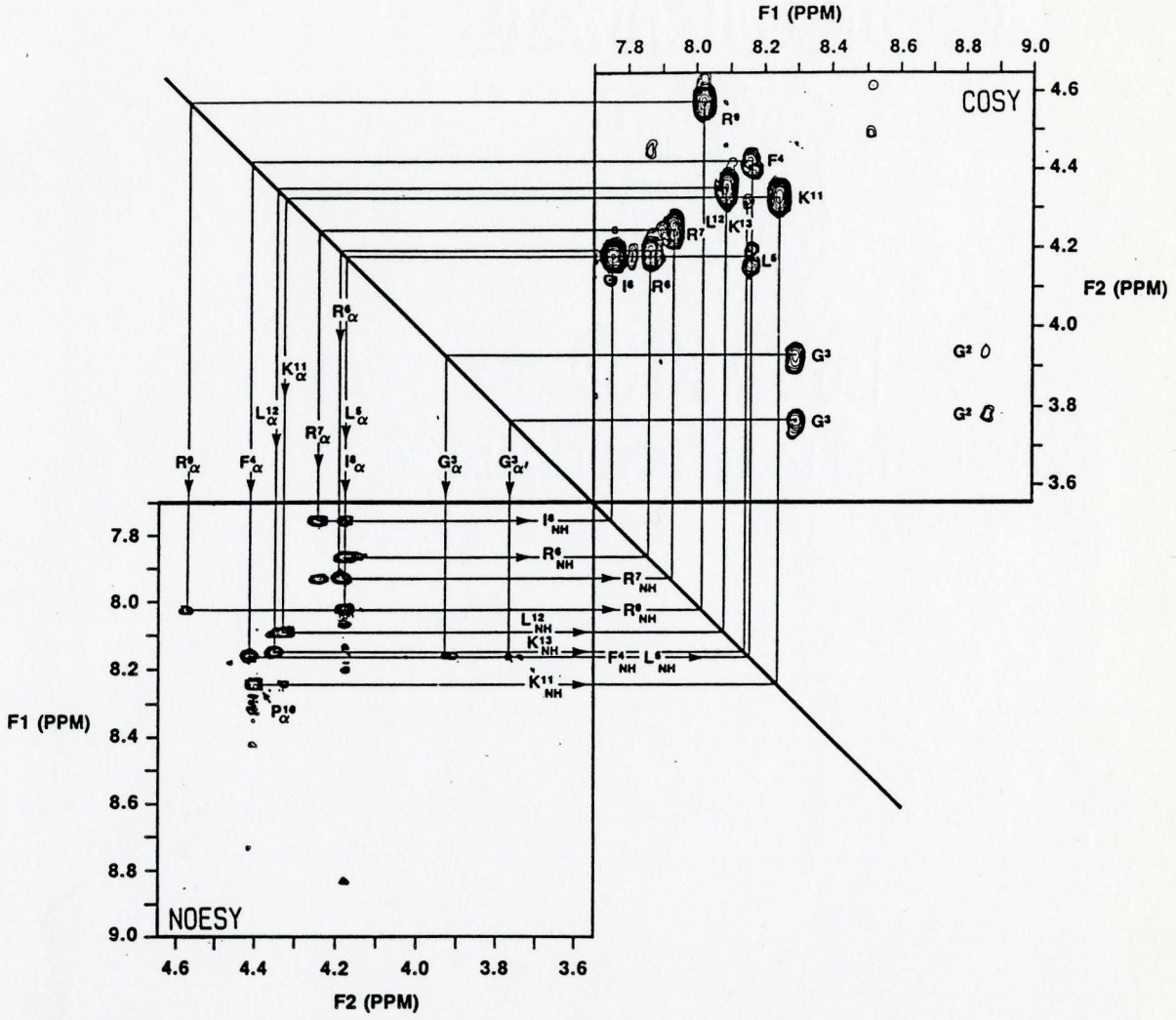

Figure 5.26. Combined COSY (top right) - NOESY (bottom left) connectivity diagram [Wagner et al., 1981] for sequential assignments via NOEs between α protons and the amide protons of the following residue, $_{\alpha}N(i,i+1)$ [Wüthrich, 1986]. The spectra were recorded on 20 mM dynorphin A-(1-13) in CD_3OH. For the COSY spectrum, eighty scans were accumulated for each of the 512 FID's containing 1024 data points in F2 over a spectral width of 5200 Hz. A relaxation delay of 1.5 s was employed. The data were zero-filled to 2048 data points in both dimensions. Pseudo sine-bell window functions were applied to both dimensions before Fourier transformation. The digital resolution was 5.1 Hz/point in both dimensions. Only positive contour levels (i.e. negative NOE's, cf. 4.2.6) are plotted in the case of the NOESY experiment which is described in the caption for Figure 5.27. The COSY expansion was plotted in exactly the same limits as the NOESY spectrum (as recommended by Wüthrich [1986]), and the COSY mirror image created photomechanically to fit into the diagram.

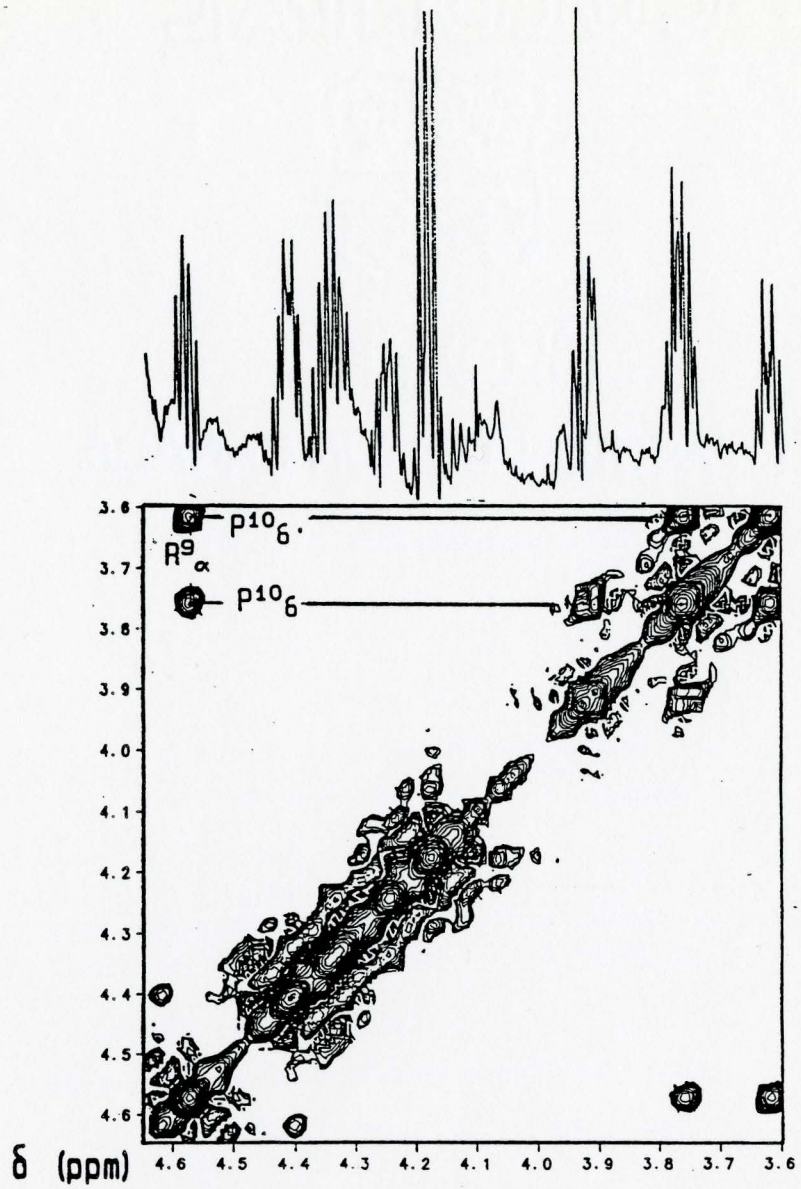

Figure 5.27. The αH-αH region of the NOESY spectrum recorded on 20 mM dynorphin A-(1-13) in CD_3OH with a mixing time of 500 ms. Forty scans were accumulated for each of the 256 FID's containing 1024 data points in F2 over a spectral width of 5200 Hz. A relaxation delay of 1.5 s was employed. The data were zero-filled to 2048 data points in both dimensions. Gaussian window functions were applied to both dimensions before Fourier transformation. The digital resolution was 5.1 Hz/point in both dimensions.

Only positive contour levels are plotted. The $Arg^{9}\alpha$-$Pro^{10}\delta$ and Arg9α-$Pro^{10}\delta$' connectivities are indicated.

The $Arg^{9}\alpha$-$Pro^{10}\delta'$ and $Arg^{9}\alpha$-$Pro^{10}\delta$ connectivities were observed (cf. Figure 5.27), thus further confirming the sequence specific assignments and also indicating a trans Arg^{9}-Pro^{10} peptide bond[1]. The α(i)-NH(i+1) connectivity pattern was reinitiated at the position of the $Pro^{10}\alpha$ resonance and continued via Lys^{11}NH, $Lys^{11}\alpha$, Leu^{12}NH, $Leu^{12}\alpha$, and Lys^{13}NH to the $Lys^{13}\alpha$ resonance. A surprising feature was that the $Lys^{13}\alpha$-NH COSY cross-peak was very weak compared to the others. This was probably due to a broadened amide resonance of the carboxy-terminal residue, a feature which could not be confirmed on this set of spectra because of the superimposition of three amide proton signals (Phe^{4}, Leu^{5}, and Lys^{13}) at the position of interest.

In summary, although the α(i)-NH(i+1) connectivity map did not include the first two residues of the peptide, the whole molecule has been sequence specifically assigned on the basis of the spectra shown in Figures 5.26 and 5.27. The assignments are summarized in Table 5.9.

[1] This is independently indicated by the ^{13}C chemical shifts for the Pro^{10} residue (cf. 5.5).

Table 5.9. ^{1}H NMR assignments of dynorphin A-(1-13) in methanolic solution

	Chemical shift δ (± 0.01 ppm)							
Residue	δ_{NH}[a]	$\delta_{\alpha H}$[a]	$\delta_{\beta H}$	$\delta_{\beta H'}$	other[a]			
Tyr[1]	-	4.10-4.07	3.15	2.99	δ 7.11	ϵ 6.77		
Gly[2]	8.86 - 8.77	3.94	α'3.77					
Gly[3]	8.30 - 8.23	3.91	α'3.76					
Phe[4]	8.17 - 8.13	4.43	3.15	3.08	δ 7.26	ϵ 7.28	ζ 7.21	
Leu[5]	8.17 - 8.13	4.19	1.73	1.55	γ 1.65	δCH_3 0.94	$\delta' CH_3$ 0.89	
Arg[6]	7.88	4.21	1.88	1.80	γ 1.69	δ 3.19	ϵ 7.48-7.43[b]	
Arg[7]	7.94	4.27	1.86	1.79	γ 1.62	δ 3.17	ϵ 7.48-7.44[b]	
Ile[8]	7.76	4.19	1.85	γ 1.48	γ' 1.19	γCH_3 0.87	δCH_3 0.85	
Arg[9]	8.05	4.60	1.88	1.77	γ 1.69	δ 3.19	ϵ 7.51-7.46[b]	
Pro[10]		4.42	2.24	1.91	γ 2.03	γ' 1.96	δ 3.78	δ' 3.64
Lys[11]	8.25 - 8.21	4.35	1.84	1.73	γ 1.50	δ 1.68	ϵ 2.95	
Leu[12]	8.10	4.37	1.63	1.60	γ 1.71	δCH_3 0.95	$\delta' CH_3$ 0.91	
Lys[13]	8.17 - 8.07	4.33	1.91	1.76	γ 1.47	δ 1.67	ϵ 2.92	

a: during the course of this study (approximately two years), some resonances underwent marked downfield shifts. In these cases, the two extreme values are indicated.
b: resonances which were not unambiguously assigned

5.4. Conformational Studies

5.4.1. ROESY or 2-D CAMELSPIN Spectra

As indicated in section 5.3., both the intraresidue ^1H-^1H distance $d_{N\alpha}(i,i)$ and the sequential distance $d_{\alpha N}(i,i+1)$ depend on the conformation of the peptide backbone. While $d_{N\alpha}(i,i)$ depends on ϕ_i, $d_{\alpha N}(i,i+1)$ depends on ψ_i. The relative size of these distances can be deduced from the intensity of the respective nuclear Overhauser effects, as long as the respective rotational correlation times do not differ too much. As described in section 4.2.5.2, the rotating-frame NOE (=ROE) is far less sensitive to τ_c than the laboratory-frame NOE. The ROE is therefore a better indicator of relative distances than the conventional NOE. The ratio of the intensity of the sequential ROE arising from $d_{\alpha N}(i,i+1)$ to that of the intraresidue ROE corresponding to $d_{N\alpha}(i,i)$ differs markedly for different secondary structures (cf. Table 5.10).

Table 5.10. The ratio between the sequential α-NH ROE and the intraresidue NH-α ROE for different secondary structures.

Secondary structure	ϕ_i	$d_{N\alpha}(i,i)^a$ [Å]	ψ_i	$d_{\alpha N}(i,i+1)^b$	$\frac{ROE_{seq.}}{ROE_{intr.}}^c$
α-helix	- 57°	2.7 Å	-47°	3.5 Å	0.2
β-strand					
parallel	-139°	2.85 Å	135°	2.2 Å	4.7
antiparallel	-119°	2.8 Å	113°	2.2 Å	4.3
extended	- 60°	2.7 Å	180°	2.65 Å	1.1

a: values derived from Wüthrich [1986, p. 120]
b: values derived from Wüthrich [1986, p. 121]
c: calculated from: $ROE_{seq.}/ROE_{intr.} = (r_{seq.}^{-6})/(r_{intr.}^{-6})$
with $ROE_{seq.}$ = sequential ROE
$ROE_{intr.}$ = intraresidue ROE
$r_{seq.}$ = sequential distance $d_{\alpha N}(i,i+1)$
$r_{intr.}$ = intraresidue distance $d_{N\alpha}(i,i)$

Three intraresidue ROE's were identified in the NH-α connectivity region of a 2-D CAMELSPIN/ROESY experiment (cf. Fig. 5.28). They were assigned to the residues Arg^7, Ile^8, and Arg^9 and were consistently markedly weaker than the corresponding sequential ROE's (the intraresidue Arg^9 ROE was compared to the sequential $Ile^8\alpha$-Arg^9NH ROE due to the non-existence of a Pro^{10}NH proton). As the intraresidue ROE would be approximately five times stronger than the sequential ROE in the case of a helical conformation (cf. Table 5.10), this was a clear indication for the absence of a helical structure. Thus the ratio of the

intensities of sequential to intraresidue ROE's indicate that the backbone conformation in this central part of the molecule (residues 7 to 9) is a mixture of β-strand and extended structures.

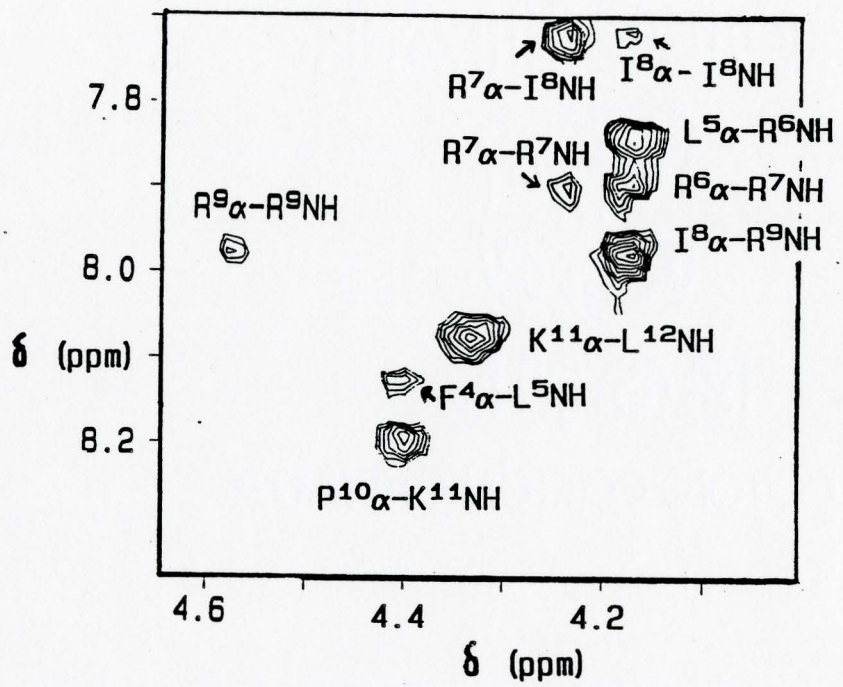

Figure 5.28. 2-D CAMELSPIN/ROESY experiment on 20 mM dynorphin A-(1-13) in CD_3OH. The duration of the spin-lock, i.e. the mixing time employed, was 200 ms. 38 Scans were accumulated for each of the 256 FID's containing 1024 data points in F2 and the data were zero-filled in the F1 dimension only to 1024 data points. The digital resolution was 10.2 Hz/point.

5.4.2. Positive NOE's, Segmental Motion, and Symmetrization Artifacts

In oligopeptides, positive and negative NOEs have been observed simultaneously [Uma et al., 1988]. Local motions dominate dipole-dipole relaxation processes. The observed NOEs are no longer dependent on the overall tumbling of the molecule, but are determined by segmental motion. Negative NOEs are observed in relatively rigid parts of the molecule, and positive NOEs are detected around areas of rapid local motions. This was thought to be the case in the 620 MHz NOESY spectrum of 20 mM dynorphin A-(1-13) in CD_3OH (Figures 5.28 and 5.29).

However, it is well established [Wüthrich, 1986, p. 67] that symmetrization can lead to erroneous peaks, since the crossing of two noise bands in the symmetrization process will result in the presence of two symmetrically located artifactual cross-peaks.

Such noise bands were detected in the unsymmetrized spectra in Fig. 5.29. Analogous 2-D CAMELSPIN/ROESY experiments at mixing times of 500 and 200 ms (cf. section 5.4.1) yielded positive connectivities corresponding to the negative NOESY cross-peaks described above. However, nothing corresponding to the putative positive NOESY connectivities was observed. It was concluded that these cross-peaks did not provide any conformational information as they were experimental artifacts.

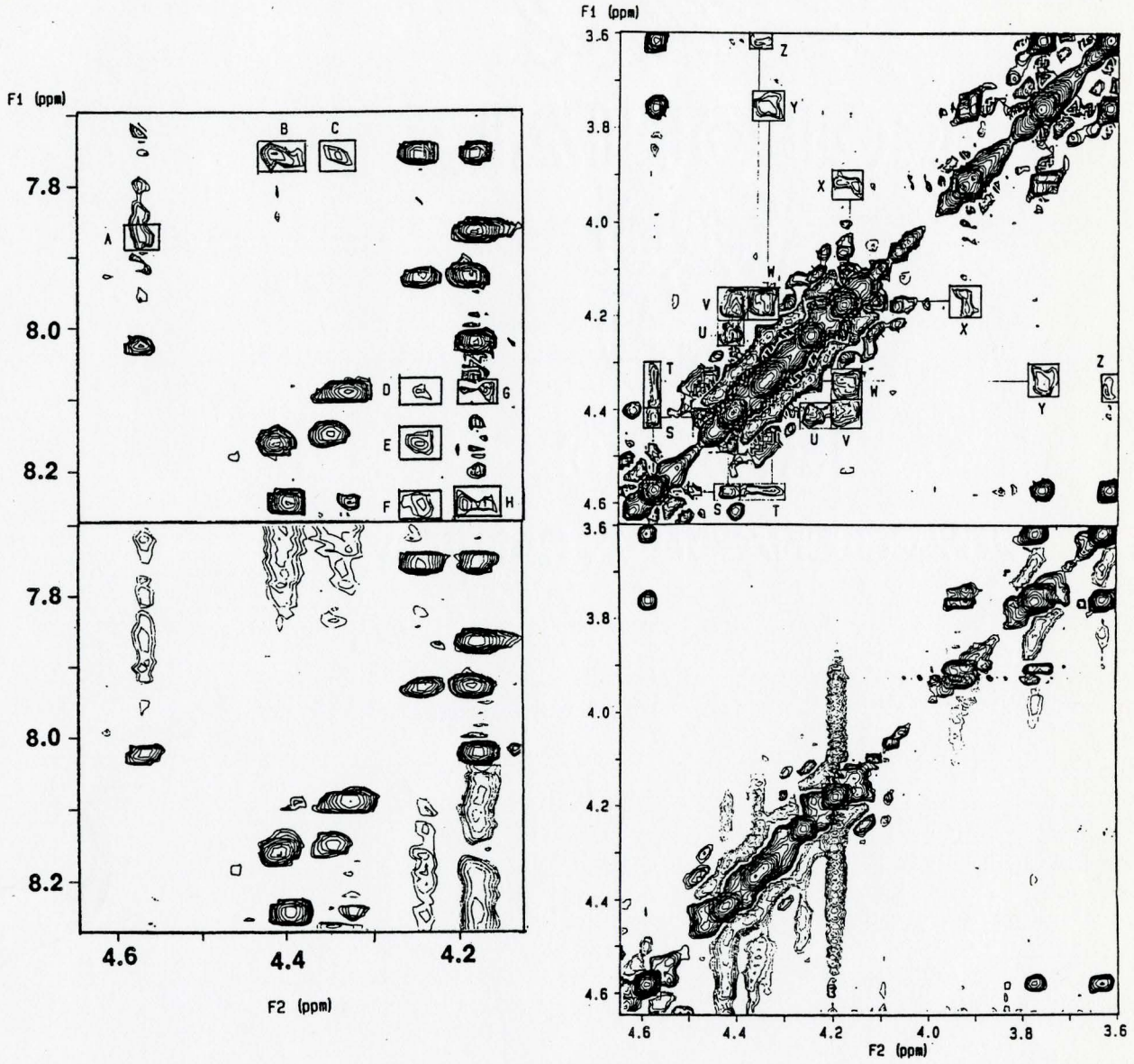

Figure 5.29. Positive and negative cross-peaks in the α-NH (left) and α-α (right) connectivity region of the symmetrized (above) and unsymmetrized (below) 620 MHz NOESY spectrum of 20 mM dynorphin A-(1-13) in CD_3OH. Details of the experiment are described in the caption of Figure 5.27. The putative positive (boxed) NOE's in the symmetrized spectra could not be verified in the unsymmetrized plot-outs. The unsymmetrized spectra were plotted at a slightly lower vertical scale, so that not all of the noise bands leading to the artifactual cross-peaks in the symmetrized spectra are visible.

5.4.3. Vicinal $^3J_{HN\alpha}$ Spin-Spin Coupling Constants

Although a number of different spin-spin coupling constants are related to the various torsional angles associated with peptide conformation (e.g. $^3J_{HC\alpha C\beta H}$ and $^3J_{HC\beta C\alpha 15_N}$ with χ_1[2], $^3J_{HC\alpha C' 15_N}$ and $^2J_{HC\alpha H}$ (of glycine) with ψ, and $^3J_{HNC\alpha 13_{C'}}$, $^3J_{HNC\alpha 13_{C\beta}}$, and $^3J_{HC\alpha N 13_C}$, with ϕ [Bystrov, 1976]), the most experimental data has been accumulated for the vicinal coupling constant $^3J_{HN\alpha}$ and its relationship to the torsional angle ϕ [Bystrov, 1976; Pardi et al., 1984].

For non-glycine residues[3], the dependency of $^3J_{HN\alpha}$ on the dihedral angle $\theta_{HNC\alpha H}$, with $\theta_{HNC\alpha H} = |\phi - 60°|$, is analogous to the formula described by Karplus [1959] for hydrogen atoms on adjacent sp^3 carbons in hydrocarbons and can be expressed as:

$$^3J_{HN\alpha} = A \cdot \cos^2\theta + B \cdot \cos\theta + C \cdot \sin^2\theta,$$

where A, B, C are empirical constants (in Hz [Wüthrich, 1976, p.74]). With $\cos^2\theta + \sin^2\theta = 1$, this simplifies to:

$$^3J_{HN\alpha} = (A-C) \cdot \cos^2\theta + B \cdot \cos\theta + C$$

The constants are "calibrated" by correlation of peptide or polypeptide $^3J_{HN\alpha}$ values measured in solution and ϕ angles derived from other methods (e.g. theoretical approaches, X-ray data). With several authors [Ramachandran, 1971;

---

[2] for a definition of these torsional angles, cf. IUPAC-IUB [1970]

[3] In the case of glycine residues, the angular dependence of the over-all coupling constant $\Sigma^3J_{HN\alpha H2}$ (= $^3J_{HN\alpha}(\theta) + {}^3J_{HN\alpha}(120 \pm \theta)$ is examined [Bystrov, 1976, Bystrov et al., 1973].

Schwyzer, 1971; Bystrov, 1976; Pardi et al., 1984] examining different compounds with various methods, the values for A, B, and C diverge (cf. Figure 5.30).

In addition to this, electronegativity effects of substituents and the rotational states around the ψ ($C\alpha$-C') bond have a slight influence on the value of $^3J_{HN\alpha}$. Ambiguities arise from the fact that up to four different torsional angles can give rise to the same $^3J_{HN\alpha}$ values, so the assignment of a distinct torsional angle on the basis of coupling constant information alone is not straightforward. Wüthrich's group has shown that this problem is alleviated in the case of BPTI, a small globular protein of 58 amino acid residues [Pardi et al., 1984]. The torsional angles ϕ for all amino acid residues except glycine are concentrated in the range of -30° to -180°. This approach can, however, not be transferred directly on to studies of a tridecapeptide.

What can be transferred is the observation that rigid helical structures (ϕ(α-helix) = -57°, ϕ(3_{10}-helix) = -60°) give rise to small $^3J_{HN\alpha}$ values of approximately 4 Hz, whereas antiparallel (ϕ = -139°) and parallel β-sheets (ϕ = -119°) result in large $^3J_{HN\alpha}$ coupling constants of approximately 9 Hz. For instance, small coupling constants have been employed as an indication of α-helical structure in methanolic solutions of the 26 amino acid residue linear peptide δ-hemolysin [Tappin et al., 1988].

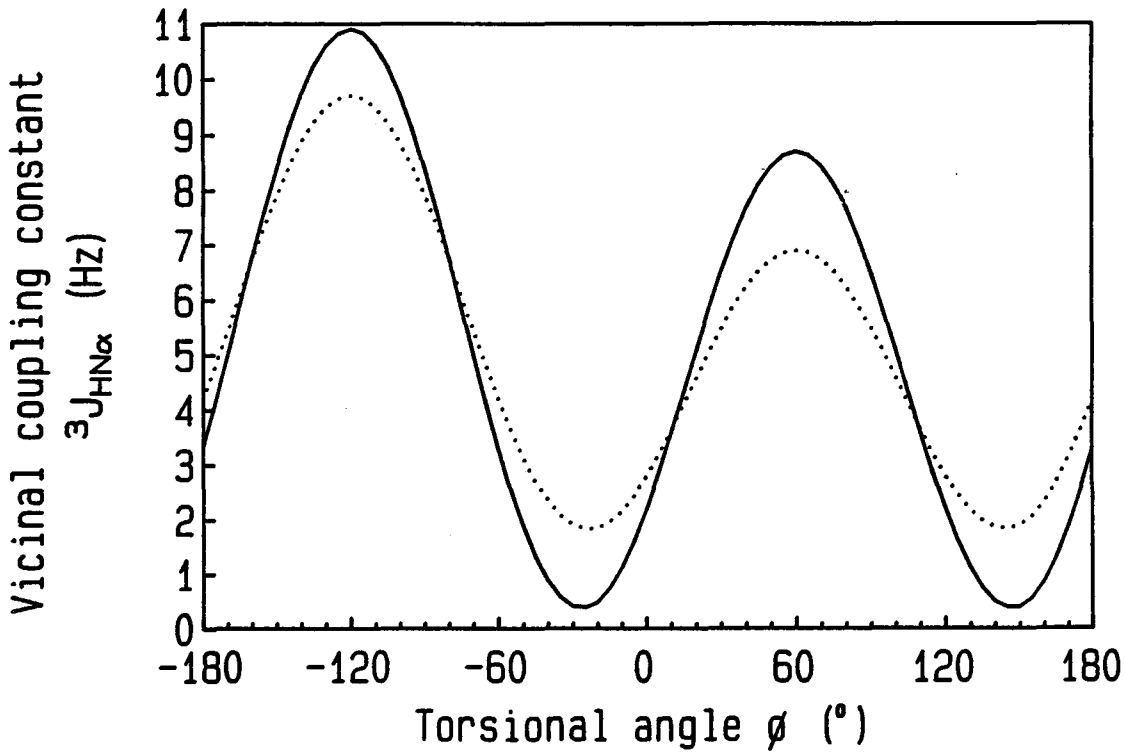

Figure 5.30. Dependence of the $^3J_{HN\alpha}$ spin-spin coupling constants on the torsional angle ϕ, with parameters proposed by Bystrov (-) [1976] and Pardi et al. (••) [1984].

Using the partially protonated solvent (CD_3OH), it was possible to observe the backbone amide protons and determine vicinal ($^3J_{HN\alpha}$) coupling constants. Most of the $^3J_{HN\alpha}$ values were extracted directly from the observed line splitting of the amide protons in the one-dimensional spectrum (cf. Figure 5.2). Those for Gly^2, Gly^3, and Phe^4 were determined from zero-filled DQF phase-sensitive COSY cross-sections (eg. Figure 5.22). The determined values are listed in Table 5.11 along with the corresponding ϕ angles. These are compared to the ϕ angles present in the energy-minimized reference conformations (cf. Chapter 2). The correlation is not good in both cases of reference.

As was emphasized at the beginning of this chapter, very often many energetically nearly equivalent conformations of linear oligopeptides are in rapid equilibrium. The observed NMR parameters correspond to an average taken over numerous rotational states. Consequently, the observed values for $^3J_{HN\alpha}$ may not correspond to a rigid angle θ, but rather to an average over a range of values for θ. This is more and more likely to be the case, the closer the $^3J_{HN\alpha}$ values are to 7.5 Hz [Kessler et al., 1985c, p.441]. Indeed, none of the $^3J_{HN\alpha}$ coupling constants of the non-glycine residues deviated more than 1 Hz from this mean value (Table 5.11).

Pullman and Maigret [1973] have determined such averaged parameters from the conformational energy distribution of the respective "dipeptide" models (H_3C-CO-NH-CH**R**-CO-NH-CH_3) calculated with the quantum mechanical PCILO method [Pullman, 1976]. Ramachandran and coworkers have also calculated averaged $^3J_{HN\alpha}$ values for model dipeptides using potential functions derived from

"hard sphere" conformational theory [Ramachandran and Sasisekharan, 1968]. Effects of the solvent have not been considered in these calculations, but experimentally the solvent dependence of the $^3J_{HN\alpha}$ coupling constants has been shown to be very small (±3%) for a model compound (N-methyl-acetamide) where no change in the conformational state of the N-C bond has to be considered. Thus our experimental data could be compared to the theoretical calculations, which accounted for the slightly larger value for the Ile^8 residue as compared to e.g. the Leu^{12} residue.

Table 5.11. Observed $^3J_{HN\alpha}$ values for dynorphin A-(1-13) in CD_3OH, averaged $^3J_{HN\alpha}$ values calculated for conformationally flexible dipeptide models, ϕ angles for a rigid structure calculated from the experimental $^3J_{HN\alpha}$ values, and the respective ϕ angles in the reference models (correlation is indicated in **bold**).

	δ (ppm)	$^3J_{HN\alpha}$ (Hz)	$^3J_{HN\alpha'}$ (Hz)	— Calculated ^3J — PCILO[a]	Ramach.[b]	Corresponding ϕ angles[c]				ϕ_{hel}	ϕ_{GOR}
Gly^2	8.77	7.5	6.9		6.6	-110°	-80°	+80°	+110°[d]	+ 79°	+ 57°
Gly^3	8.23	6.4	5.9		6.6	-125°	-65°	+65°	+125°[d]	- 50°	+133°
Phe^4	8.13	7.1		8.0		-155°	-85°	+40°	+80°	- 48°	-164°
Leu^5	8.10									- 67°	-160°
Arg^6	7.88	6.6				-160°	-80°	+35°	+85°	- 58°	-154°
Arg^7	7.94	7.0				-165°	-85°	+40°	+80°	- 81°	-155°
Ile^8	7.76	8.1		7.9		-150°	-90°	-	-	- 64°	- 62°
Arg^9	8.07	7.2				-155°	-85°	+40°	+80°	- 54°	-153°
Lys^{11}	8.21	7.6				-150°	-90°	+50°	+70°	- 61°	+ 74°
Leu^{12}	8.10	7.5		7.0		-150°	-90°	+45°	+75°	+ 57°	-155°
Lys^{13}	8.06									- 67°	-153°

a = [Pullman and Maigret, 1973]

b = This value is not the original one calculated by Ramachandran (=Ramach.) and coworkers, but was recalculated by Bystrov [1976] using the averaged values $\langle\cos^2\theta\rangle$, $\langle\cos\theta\rangle$, and $\langle\sin^2\theta\rangle$ of Ramachandran et al. [1971b] and Bystrov's coefficients A,B, and C.

c = calculated by averaging the values yielded by Bystrov's [1976] and Pardi et al.'s [1984] equations. This was possible as the predicted ϕ angles differed only by 1 to 4 degrees. These values were then rounded to the next five degree increment.

d = values calculated from the equation and coefficients proposed by Bystrov et al. [1973] for the over-all coupling constant $^3J_{HN\alpha\alpha'}$

It was therefore concluded that the conformation of the tridecapeptide is not necessarily rigid enough for one conformer to dominate the size of the $^3J_{HN\alpha}$ coupling constants. Therefore the ϕ angles presented in Table 5.11 may have no

physical significance whatsoever. If indeed a methanolic solvent environment mimics the membrane-mediated conformation, then this conformation is apparently not energetically sufficiently preferable to other conformations in this system. On the other hand, the occurrence of the calculated corresponding angles would be consistent with the NMR data, as is shown for the Gly^2 and Arg^7 ϕ angles of the helical reference structure and the Arg^9, Lys^{11} and Leu^{12} ϕ angles of the "GOR" reference model.

5.4.4. $^3J_{\alpha\beta}$ Coupling Constants and Side Chain Rotamer Analysis

Three minimum energy conformations (rotamers) about the C_α-C_β bond exist, where the substituents on the two carbon atoms are staggered. These are denoted a for χ_1 = -60°, b for χ_1 = 180°, and c for χ_1 = 60°, The NMR spectrum is assumed to be an average of the spectra of each of the rotamers, weighted by the relative populations.

Assignment of the two individual β proton resonances is a prerequisite for rotamer analysis. The average coupling constant observed for the two individual β protons is:

$$^3J_{\alpha\beta 1} = f_a \cdot {}^3J_g + f_b \cdot {}^3J_t + f_c \cdot {}^3J_g$$

$$^3J_{\alpha\beta 2} = f_a \cdot {}^3J_t + f_b \cdot {}^3J_g + f_c \cdot {}^3J_g$$

where f_a, f_b, and f_c are the fractional populations of the three rotamers with $f_a + f_b + f_c = 1$. J_g and J_t are the coupling constants for the relationship between the

α proton and each of the β protons, which are in gauche (θ = 60°) or trans (θ = 180°) arrangement to the α proton, respectively. Values for ^3J_t (13.6 Hz) and ^3J_g (2.6 Hz) proposed by Pachler [1964] from the analysis of six independent model systems have been widely used [Bystrov, 1976; Zhou and Gibbons, 1986].

For given values of ^3J_g and ^3J_t, determination of $^3J_{\alpha\beta1}$ and $^3J_{\alpha\beta2}$ yields f_a, f_b, and f_c via:

$$f_a = (^3J_{\alpha\beta2} - {}^3J_g)/(^3J_t - {}^3J_g)$$

$$f_b = (^3J_{\alpha\beta1} - {}^3J_g)/(^3J_t - {}^3J_g)$$

$$f_c = 1 - (f_a + f_b).$$

A problem is the lack of stereospecific assignments for the re (pro-R) and si (pro-S) β methylene protons. The downfield β proton was arbitrarily assigned to β_1, the upfield β proton (β') to β_2. The rotamer populations (Table 5.12 and Figure 5.31) can therefore be reversed for some or all of the residues except Ile[8]. In the case of Ile[8], the second β proton is replaced by the γ methyl group, so that only one rotamer population could be determined.

Table 5.12. Relative populations of the side chain rotamers of dynorphin A-(1-13) in methanolic solution.

Residue	$^3J_{\alpha\beta} \equiv {}^3J_{\alpha\beta 1}$	$^3J_{\alpha\beta'} \equiv {}^3J_{\alpha\beta 2}$	f_a	f_b	f_c
Tyr^1	8.4	8.5	0.54	0.53	-0.06
Phe^4	6.2	8.6	0.55	0.33	0.13
Leu^5	10.1	4.9	0.21	0.68	0.11
Arg^7	5.3	9.1	0.59	0.25	0.16
Ile^8	7.5		a	0.43	a
Arg^9	6.1	8.1	0.50	0.32	0.18
Lys^{11}	5.4	8.9	0.57	0.25	0.17

a: as Ile^8 has only one β proton, only one rotamer population could be determined

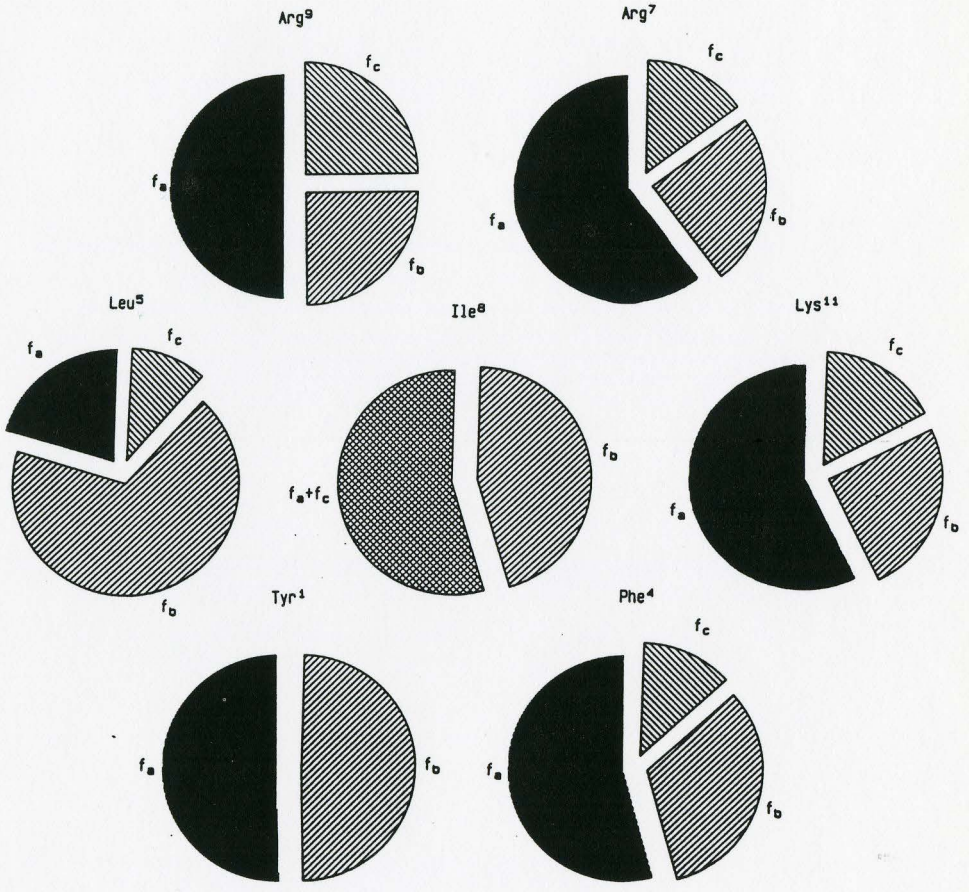

Figure 5.31. Relative populations of some of the side chain rotamers of dynorphin A-(1-13) in methanolic solution

5.4.5. Temperature Dependence of Amide Proton Chemical Shifts

All regular peptide secondary structures involve the formation of hydrogen bonds between backbone amide protons and backbone carbonyl oxygens. Amide protons involved in intramolecular hydrogen bonds or otherwise shielded from the solvent will not only have different chemical shifts from the solvent-exposed amide protons, but also show a decreased temperature sensitivity of their chemical shifts [Kopple et al., 1969a,b; Ohnishi and Urry, 1969].

Temperature dependent studies were performed on the sample containing 20 mM dynorphin-A-(1-13) in CD_3OH. At 30°C, six of the eleven backbone amide protons were resolved, the others being separated into two broadened peaks, so that their chemical shifts were difficult to determine exactly. These overlying peaks were further separated at 11°C, but the upfield glycine amide proton was shifted below one of the doublets, so seven single peaks and two double peaks were resolved. Proceeding to lower temperatures, substantial linebroadening is observed because of loss in rotational mobility (i.e. longer correlation times τ_c) and concomitant reduction of the spin-spin relaxation time (i.e. smaller T_2's). Consequently, the determination of spin-spin coupling constants became increasingly inaccurate and was totally impossible at -30.9°C.

The temperature dependences of 9 of the 11 amide proton resonances are displayed in Figure 5.32. The chemical shifts of the resonances not individually resolved were estimated by assigning the value of the resultant peak maximum to them. The error made does not seem significant. The Gly^3 resonance was shifted below the neighbouring peaks and could not be monitored. Inevitably, additional two-dimensional experiments could have helped to clarify the situation. These were not performed because the experimental time for low temperature experiments was limited.

When the temperature is decreased, the amide proton resonances are shifted progressively downfield. This is ascribed to an increase in the fraction of the amide protons which are accessible to the solvent [Jardetzky and Roberts, 1981, p.166]. Similarly solvent accessible amide protons will show a similar temperature dependence of the chemical shift, $\Delta\delta/\Delta T$.

Apart from two exceptions mentioned below, the chemical shift changes with temperature for all protons were roughly linear. The slopes were determined by linear regression (cf. Table 5.13). The Gly^2 resonance and the Phe^4 resonance displayed a marked decrease in the magnitude of the slope below -10°C, but recalculation of the slopes under omission of the values at the two lowest temperatures did not result in differences greater than the error estimates.

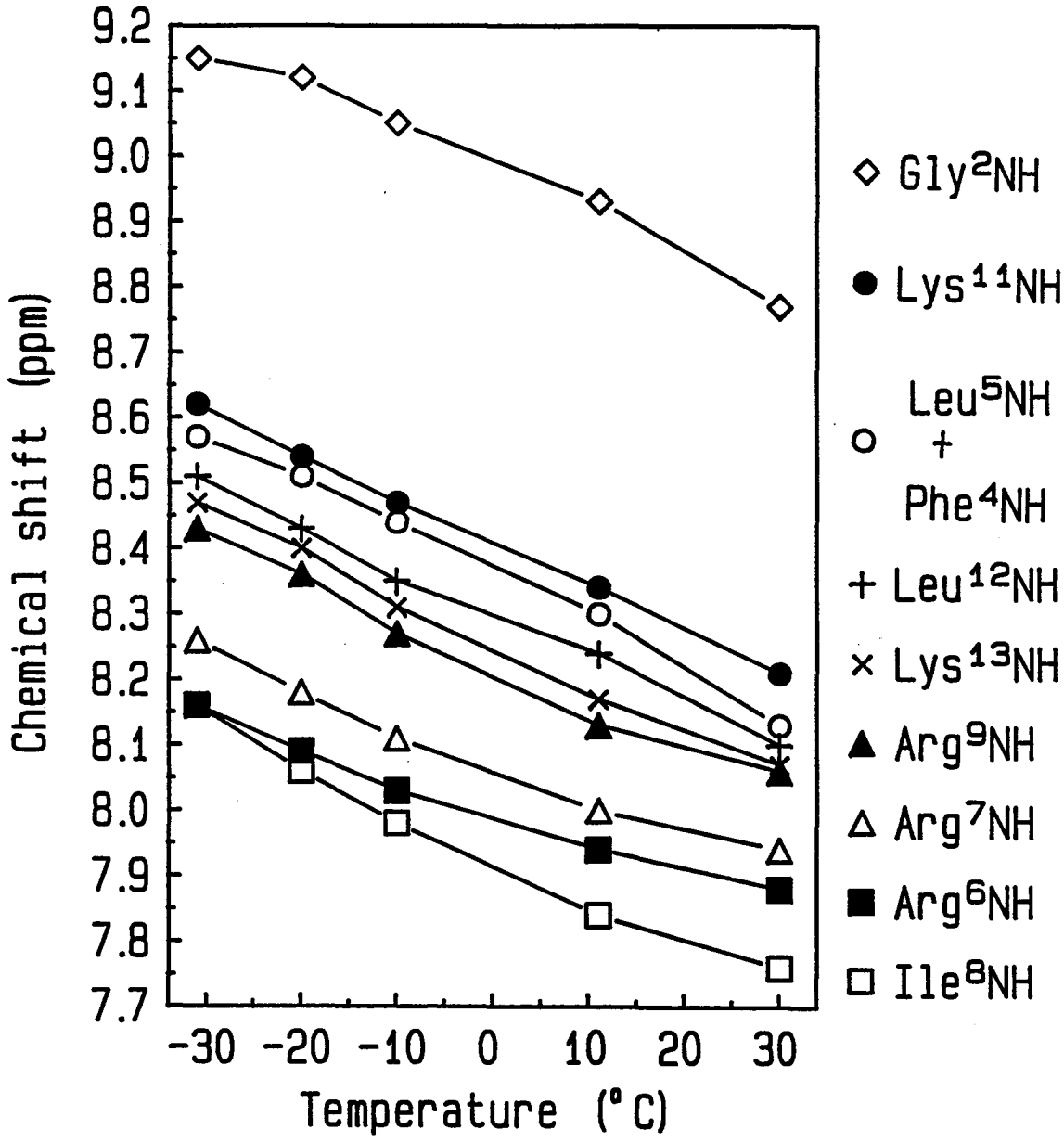

Figure 5.32. Temperature dependence of the amide proton resonances of dynorphin A-(1-13) in methanolic solution.

Table 5.13. Temperature dependence of the amide proton resonances of dynorphin A-(1-13) in methanolic solution.

	******** δ (ppm) **********					δ/ T(ppb/°C)
T (°C)	-31	-20	-10	11	30	(-30 to +30°C)
Gly^{2}	9.15	9.12	9.05	8.93	8.77	-6.3 ± 0.49
Lys^{11}	8.62	8.54	8.47	8.34	8.21	-6.6 ± 0.10
Leu^{5}/Phe^{4}	8.57	8.51	8.44	8.30	8.13	-7.2 ± 0.34
Leu^{12}	8.51	8.43	8.35	8.24	8.10	-6.6 ± 0.25
Lys^{13}	8.47	8.40	8.31	8.17	8.07	-6.7 ± 0.31
Arg^{9}	8.43	8.36	8.27	8.13	8.06	-6.3 ± 0.49
Arg^{7}	8.26	8.18	8.11	8.00	7.94	-5.3 ± 0.47
Arg^{6}	8.16	8.09	8.03	7.94	7.88	-4.6 ± 0.36
Ile^{8}	8.16	8.06	7.98	7.84	7.76	-6.5 ± 0.52

The temperature coefficients ($\Delta\delta/\Delta T$) were comparable to those for solvent accessible protons in dimethyl sulfoxide (-6 ppb/°C) and considerably larger in magnitude than the temperature coefficients for solvent-shielded or hydrogen-bonded amide protons in aqueous solution [Zhou and Gibbons, 1986], where $|\Delta\delta/\Delta T| \leq 3.0$ ppb/°C [Kopple et al., 1969a,b; Ohnishi and Urry, 1969].

Consequently, the temperature dependent studies neither give an indication of significant amide proton involvement in intramolecular hydrogen bonding nor of solvent inaccessibility of the amide protons for steric reasons.

Table 5.14. Temperature Dependence of the Vicinal Coupling Constants $^3J_{HN\alpha}$

	********** ^3J (Hz) **********			
T (°C)	-20	-10	11	30
Lys^{11}		7.2	7.5	7.6
Arg^{9}		6.9	7.2	7.2
Arg^{7}	6.1[a]	6.5	6.6	7.0
Arg^{6}	5.6[a]	5.4	5.6	6.6
Ile^{8}	5.6[a]	6.8	7.9	8.1

a: a considerable error in the determination of these values is possible, as resonance lines are substantially broadened

The vicinal coupling constants $^3J_{HN\alpha}$ decrease with decreasing temperature (Table 5.14). This could be interpreted as a "freezing out" of a conformation associated with smaller coupling constants (e.g. an α-helix), but such a change in the "average" conformation should also be reflected in a nonlinearity of the dependencies of the chemical shifts. In the case of cyclosporin A in $CDCl_3$, this was interpreted by Kessler and collaborators [Loosli et al., 1985] as a destabilization of the conformation by stronger solvation at low temperatures.

Studies on the temperature dependence of the amide proton chemical shifts in a temperature range between -30 °C and +30 °C show no significantly differing solvent proton exchange rate (Fig. 5.32 and Tab. 5.13), thus giving no indication for intramolecular hydrogen bonding. Substantial linebroadening is observed at very low temperatures - it would be advantageous to perform

temperature dependent studies on a sample which could be heated to much higher temperatures (e.g. the peptide in aqueous SDS micelles, aqueous DMPC bilayers, or in DMSO).

5.4.6. Solvent Exchange of Amide Protons

The proton exchange rates of individual backbone NH groups with the solvent indicate whether an amide proton is hydrogen-bonded or not. A slow exchange is indicative of hydrogen-bonding, while rapid exchange suggests a non-involvement in hydrogen bonding. If sequence specific assignments have been made, then the various secondary structure types can be distinguished [Wüthrich, 1986]. All the backbone amide protons are hydrogen-bonded except for those of the first three (in a 3_{10} helix) or four (in an α-helix) residues in a helix and of every second residue in the peripheral strands of β sheets.

Sequence effects on the intrinsic exchange rates of peptide backbone protons are known [Molday, 1972]. Extra evidence can be provided by repeating the exchange studies at higher temperatures. The more slowly exchanging population will disappear [Jardetzky and Roberts, 1981, p.279].

In general, slow NMR timescales are defined by the differences, $\Delta\nu$ of the chemical shifts of interest expressed in Hz [Wüthrich, 1986, p.9]. If the rate of exchange, k, is smaller than $2\pi\Delta\nu$, then the exchange is referred to as slow and separate resonances are observed. In a regime of fast exchange, i.e. when k is

greater than $2\pi\Delta\nu$, the resulting signal will be a weighted average of the original signals. Consequently, fast exchange with the solvent will result in the amide proton signals disappearing beneath the huge solvent resonance. Therefore labile protons are NMR observable only if they exchange with a rate constant smaller than approximately 10^3 min^{-1} [Wüthrich, 1986, p.25].

Measurement of proton exchange between solvent molecules and backbone amide groups can be accomplished by two different approaches.

1. Saturation transfer experiments [Hoffman and Forsén, 1966]

If the longitudinal relaxation time of a labile proton is long compared to its exchange lifetime ($>10^{-3}$ min [Wüthrich, 1986, p.38]), saturation of the solvent resonance (as in the standard experiment for suppression of the solvent signal) causes replacement of the labile protons by saturated solvent spins. This results in the loss of resonance intensity. Comparison with a reference spectrum acquired with a different solvent suppression technique (e.g. selective excitation with the 1-1 hard pulse technique [Clore at al., 1983] reveals which amide protons are exchanged slowly enough to be observed at all, but fast enough to be affected by saturation transfer with concomitant loss in intensity. These protons are regarded as not being involved in hydrogen bonding, while those signals which are unaffected can be attributed to hydrogen-bonded amide protons.

Saturation transfer experiments were not successful in giving information on dissimilar exchange rates of the backbone amide protons with the solvent. Both increasing the decoupler power level (from 2 W to 6.3 mW) and increasing

the irradiation time of the solvent resonance (0.1 s to 2.5 s) did not result in any of the amide signals displaying saturation effects. A comparison between the amide proton region of a spectrum recorded by selective saturation (presaturation) and of one employing selective excitation (1-1 hard pulse) revealed no influence on the intensities of the resonance lines.

As stated above, saturation transfer can be observed if the longitudinal relaxation time of a labile proton is long compared to its exchange lifetime ($>10^{-3}$ min). If the exchange lifetimes are considerably longer ($> 10^{-1}$ min) these signals are unaffected by selective saturation of the solvent signal. If <u>all</u> amide proton resonances behave in the same way, this slower exchange is unlikely to be caused by hydrogen bonding. It is more probable that this slower exchange can be attributed to the lack of acid or base catalysis of the exchange reaction in methanolic solution. Failure to exhibit saturation transfer effects can therefore not be taken as direct evidence for hydrogen bonding of the amide protons.

2. The more slowly exchanging labile protons (e.g. labile protons in the interior of a protein, with exchange lifetimes longer than 10 min) can be observed by dissolving the compound in a perdeuterated protic solvent and recording the spectrum at variable times after sample preparation.

Dynorphin-A-(1-13) was freshly dissolved in perdeuterated methanol (CD_3OD) at two different temperatures and the decrease of the amide signal intensities (or more precisely, of the respective peak areas) as a function of time was observed.

At 30°C (Fig 5.33), all amide proton signals decayed to the noise level in under one hour. The $Ile^{8}NH$ was the slowest to exchange but the determined exchange rate was still a third of the fastest detectable exchange rate (i.e. decay to the noise level in five minutes, which was the first point of measurement). Thus the range of detected exchange rates was insufficient to account for significant differences.

As expected, the exchange lifetimes were considerably longer at -4°C (Fig 5.34). A sufficient number of data points was available for crude estimates of the exchange rates for five amide resonances (Arg^{6}, Arg^{7}, Ile^{8}, Arg^{9}, Lys^{11}). The glycine amide resonances exchanged too fast to be detected in this experimental set-up. This was not unusual and has also been observed by others [Zhou and Gibbons, 1986] in analogous experiments. The other four amide resonances (Phe^{4}, Leu^{5}, Leu^{12}, and Lys^{13}) apparently overlap and can only be measured together (Fig. 5.35, unfilled circles). The appearance and the position of this resultant peak do change, however (Fig. 5.34.), indicating that the four partially overlapping resonances exchange with different rates.

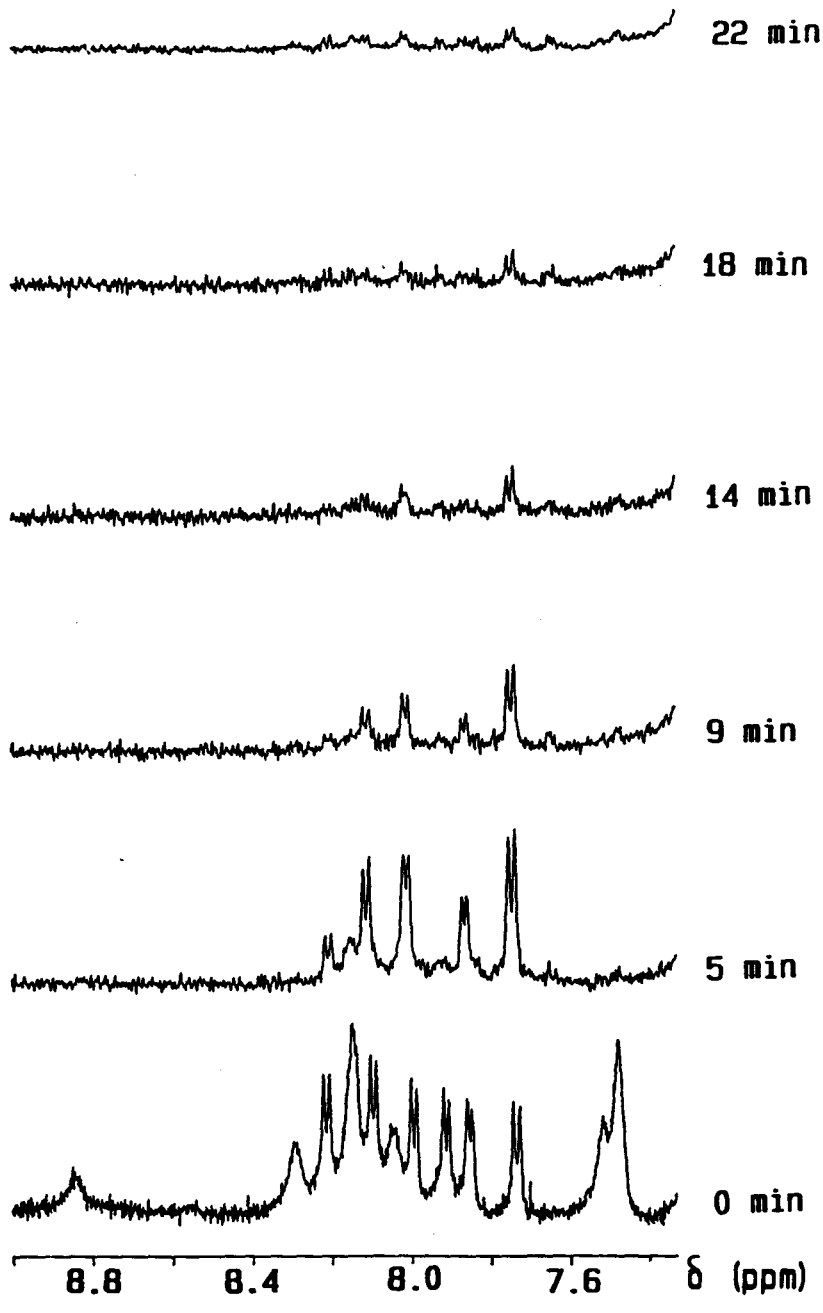

Figure 5.33. Amide H,D-exchange experiment at 30°C. The spectra were acquired at the times after dynorphin A-(1-13) was dissolved in CD_3OD indicated on the right. The individual spectra are only approximately scaled. Numerical analysis was performed by scaling the peak heights to the respective Tyr^1_ϵ resonance at 6.77 ppm.

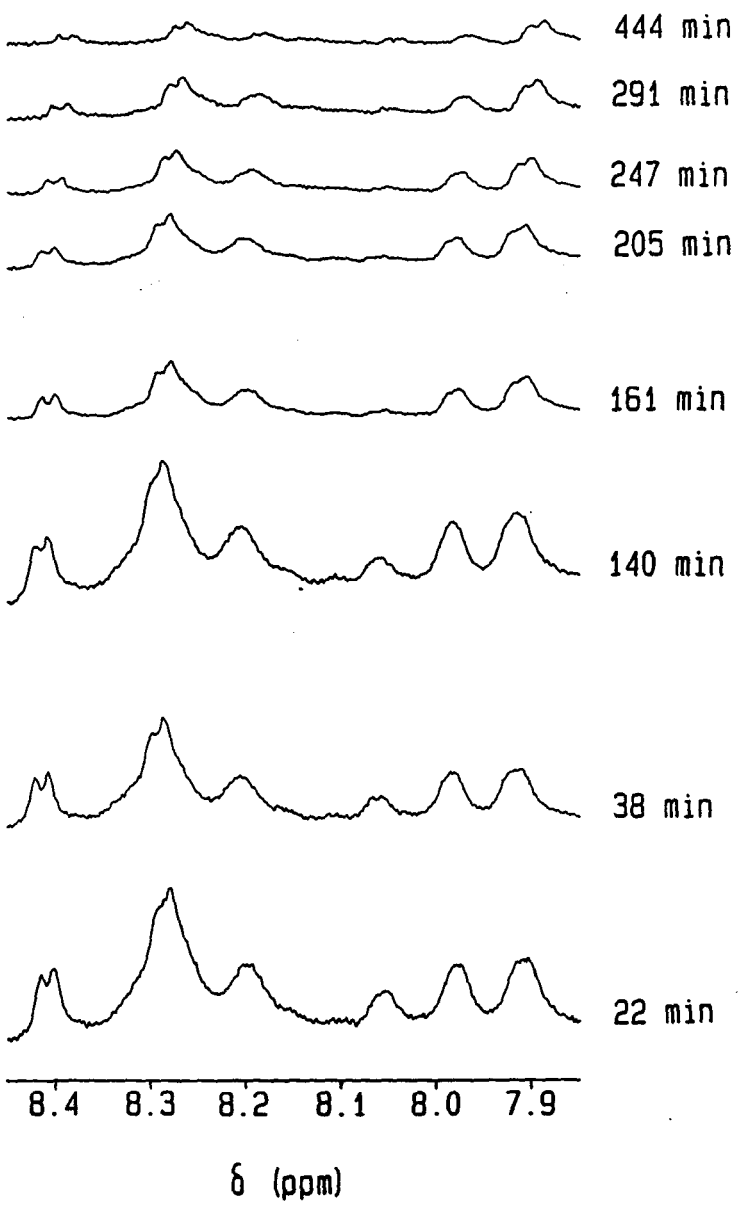

Figure 5.34. Amide H,D-exchange experiment at -4°C. The spectra were acquired at the times after dynorphin A-(1-13) was dissolved in CD_3OD indicated on the right. The individual spectra were scaled to the respective $Tyr^1{}_\epsilon$ resonance at 6.72 ppm. It took ca. 10 min to record the individual spectra and the time noted is for the middle of the acquisition (i.e. ca. 5 min after commencing with the acquisition).

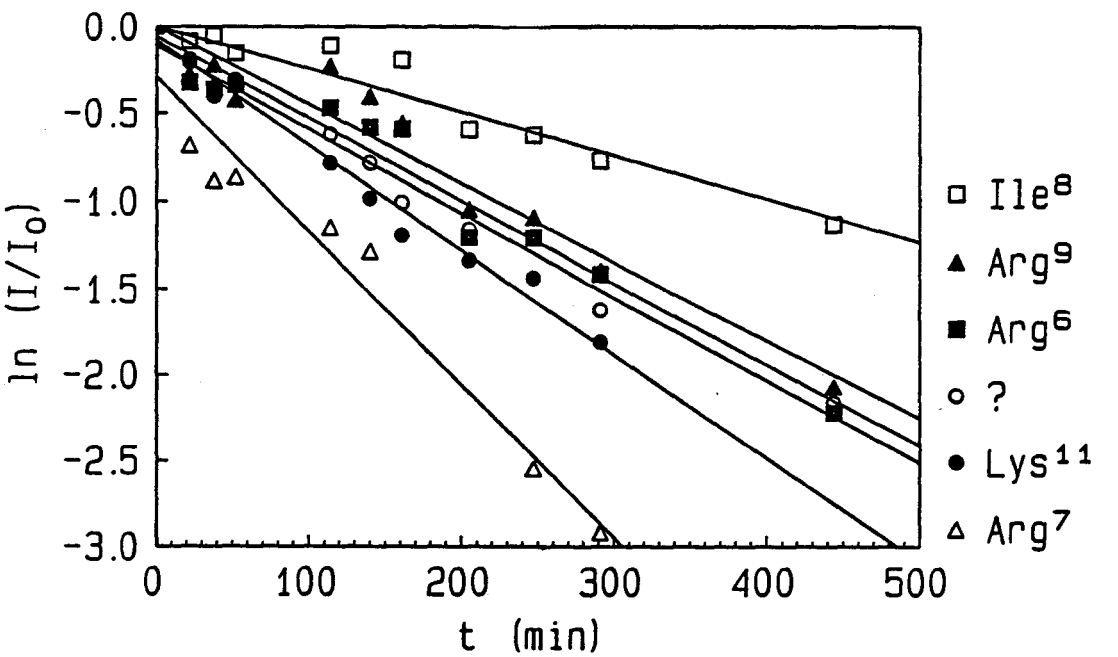

Figure 5.35. Amide H,D-exchange experiment at -4°C. Logarithmic plot of the scaled integrals of the amide proton resonances at the time points of measurement t. The regression lines do not all pass through the origin. The reason for this is the imprecision involved in determining I_0 (no spectrum in CD_3OH was recorded at -4°C prior to the exchange experiment). The I_0 values were only estimated from the spectrum at 30°C. It is stressed at this point that this imprecision only affects the offset from the x-axis but not the slope of the lines, and therefore not the determination of k'.

The apparent first order exchange rate constants[4] were determined from the slopes (= -k') in Fig 5.35 and are listed in Table 5.15. The values are not claimed to be very accurate, but it was obvious that they do not differ significantly enough (i.e. by an order of magnitude) to account for differential inaccessibility of the respective amide protons due to hydrogen bonding.

Table 5.15. Amide H,D exchange experiment at -4°C. Apparent first order exchange rate constants calculated from the slopes in Figure 5.35.

	k' [10^{-3}·min^{-1}]
?(= Phe^4 + Leu^5 + Leu^{12} + Lys^{13})	4.8
Arg^6	4.7
Arg^7	8.9
Ile^8	2.5
Arg^9	4.5
Lys^{11}	6.0

[4] Apparent first-order exchange: $I = I_0 \cdot e^{-k't}$
or: $\ln(I/I_0) = -k't$
with I = integrated intensity
I_0 = integrated intensity at t = 0

5.5. Natural Abundance 125 MHz ^{13}C NMR Studies

In the broadband-decoupled ^{13}C NMR spectrum of dynorphin A-(1-13) in methanol (Figure 5.36, upper trace), only 10 of the 13 carbonyl resonances and 35 of the aliphatic carbons were resolved. Therefore, no complete assignment of the ^{13}C spectrum of the tridecapeptide could be achieved. The assignments in Table 5.16 are based on the results of the J-modulated ^{13}C spin-sort experiment (Figure 5.36, lower trace), connectivities to protons in the heteronuclear COSY experiment (Figure 5.37) and on reference values of peptides and proteins in aqueous solution [Howarth and Lilley, 1978]. Disappointingly, hardly any methylene ^{13}C nuclei displayed connectivities to their directly bonded protons above the noise level in the heteronuclear COSY experiment (Figure 5.37). This is assumed to be due to short transverse relaxation times of the methylene carbons.

The ^{13}C chemical shift values of the $Pro^{10}{}_{\alpha}$ and $_{\beta}$ resonances, which were unequivocally identified by their heteronuclear shift correlation connectivities, are indicative of a <u>trans</u> peptide bond[5] [Howarth and Lilley, 1978, p.6]. The broad resonance at approximately 163 ppm was assigned to the Tyr^{1} ζ carbon, implying an intermediate exchange rate [Wüthrich, 1986, p.10].

---

[5] This is independently indicated by the observation of $^{1}H,^{1}H$ NOEs between the $Pro^{10}{}_{\delta}$ and the $Arg^{9}{}_{\alpha}$ protons (cf. Figure 5.27).

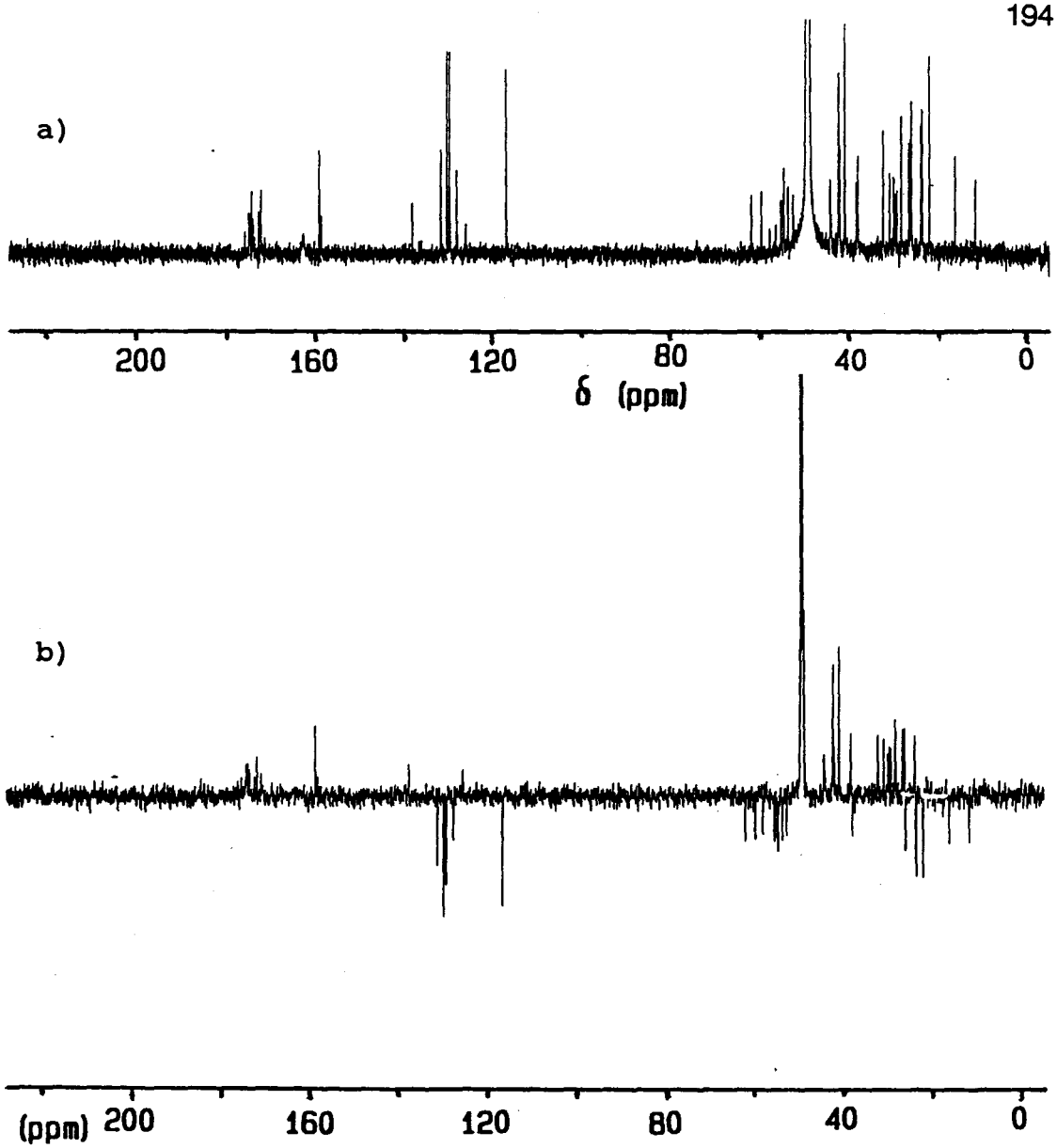

Figure 5.36. ^{13}C broadband decoupled spectra of dynorphin A-(1-13) in CD_3OH.
a) routine one-dimensional spectrum. The peptide concentration was 5.5 mM, 46584 scans were accumulated in 32K data points (0.577 s acquisition time). 2 Hz line broadening was employed for the exponential multiplication of the FID's. The digital resolution was 1.8 Hz/point.
b) ^{13}C spin-sort experiment. The peptide concentration was 20 mM. 3500 scans were accumulated in 16K data points (0.279 s acquisition time). Sensitivity enhancement was achieved with 5 Hz line broadening. The digital resolution was 3.6 Hz/point. CH_3 and CH signals are inverted, CH_2 and quarternary carbons give rise to positive signals.

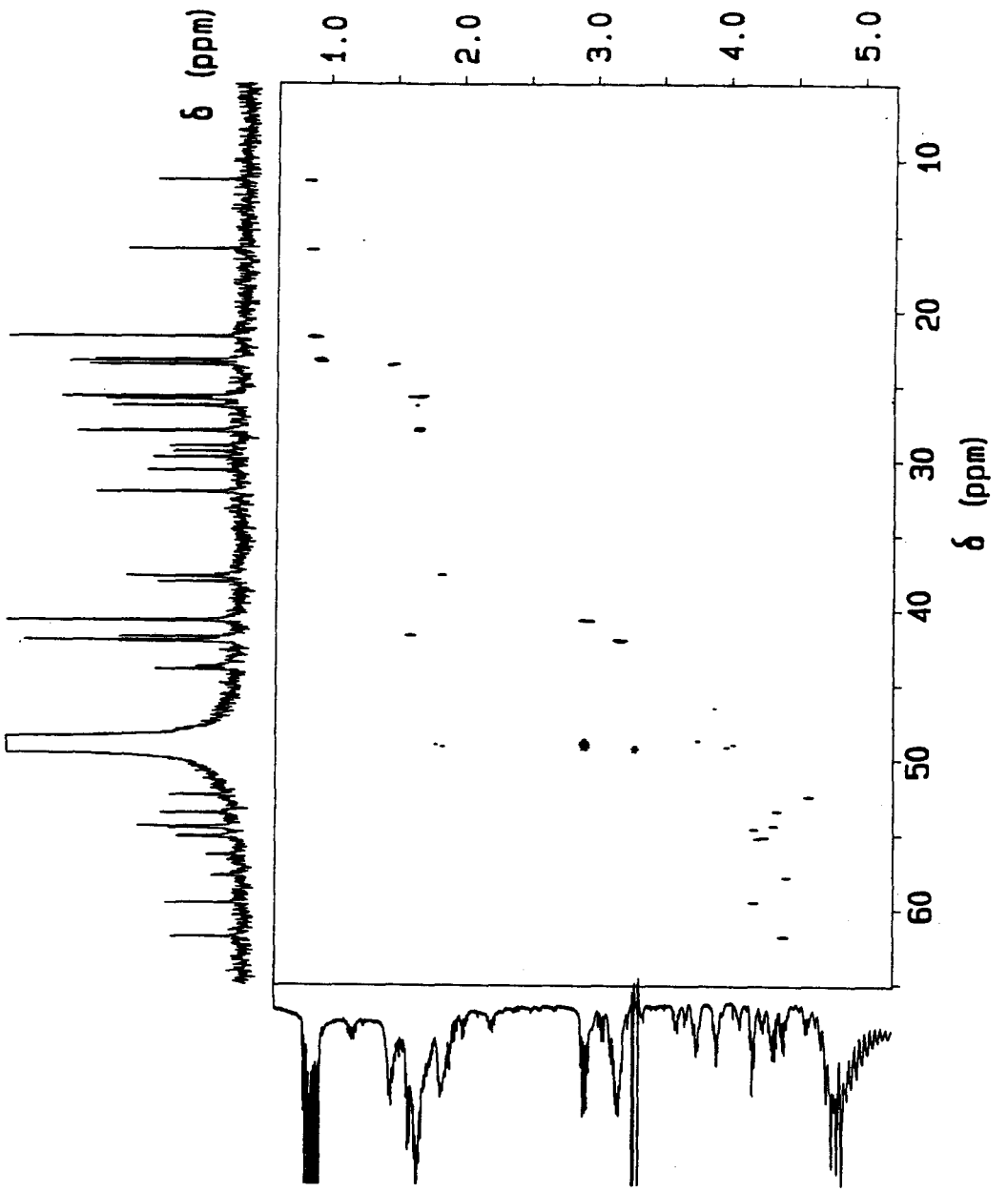

Figure 5.37. $^{1}H,^{13}C$ heteronuclear COSY spectrum of 20 mM dynorphin A-(1-13) in CD_3OH. The spectra in F2 were acquired over the aliphatic carbon spectral range of 7575 Hz in 4K data points. The 128 FID's in the F1 dimension were obtained over a spectral width of 1157 Hz. See the respective section in Chapter 4 for further details. Exponential multiplication was applied in the t_2 dimension (4.0 Hz line broadening) and unshifted sine bell in the t_1 dimension. Zero filling to 512 data points in only t_1 resulted in a digital resolution of 4.5 Hz/point in F1 and 3.7 Hz/point in F2. With the exception of the Pro^{10} β and the $Gly^{2,3}$ methylene groups, no CH_2 ^{1}H-^{13}C connectivities could be observed.

In order to characterize the conformational dynamics of the tridecapeptide in methanolic solution, measurements of spin-lattice (T_1) and spin-spin (T_2) relaxation time constants as well as quantifications of heteronuclear NOE's were attempted.

The relaxation of all protonated non-methyl ^{13}C nuclei is usually dominated by dipolar interaction with the directly-bonded proton(s) (for a review, see Wright et al. [1979]). On the basis of different models of intramolecular motion [Woessner, 1962; Deslauriers et al., 1977], specific expressions can be derived for T_1's, T_2's and NOE's as a function of the respective correlation times [Doddrell et al., 1972]. Through the construction of relaxation phase diagrams [King et al., 1978], these models can be shown to be in agreement or disagreement with experimentally determined parameters. However, all three parameters must be measured in order to check for internal consistency [Jardetzky, 1979].

The only class of ^{13}C nuclei, for which T_2 values could be reliably determined, were the aromatic resonances (Figure 5.40 and Table 5.16). The measured enhancements in the full-NOE versus NOE-suppressed spectra ranged from -30% to +528%, the latter limit being more than twice the maximum theoretical NOE [Doddrell et al., 1972]. Obviously more sophisticated techniques [Kövér and Batta, 1987] must be applied.

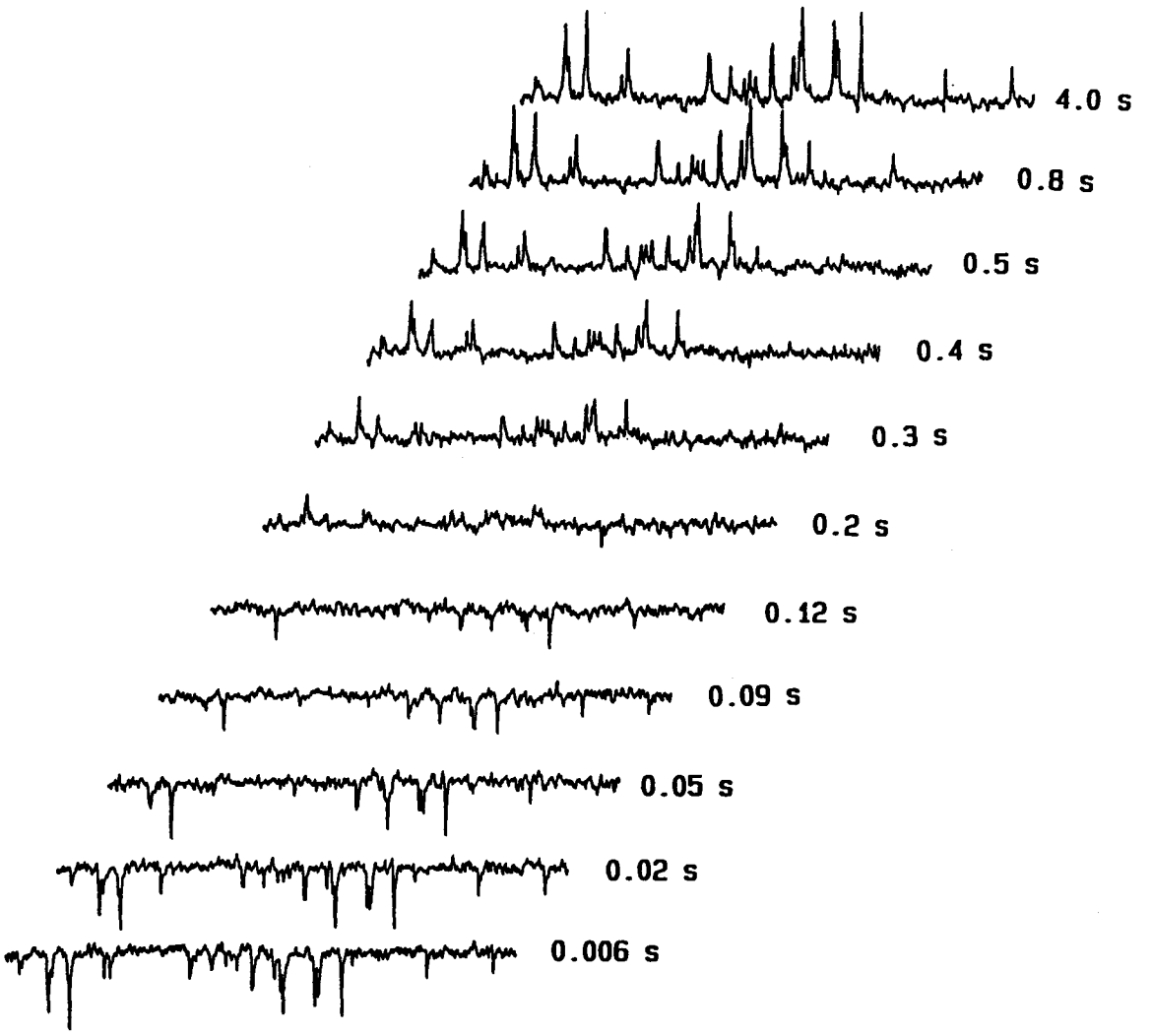

Figure 5.38. ^{13}C NMR inversion recovery experiment. The region shown is upfield from the solvent resonance (45 to 10 ppm). The individual spectra were recorded with the delay times τ indicated on the right.

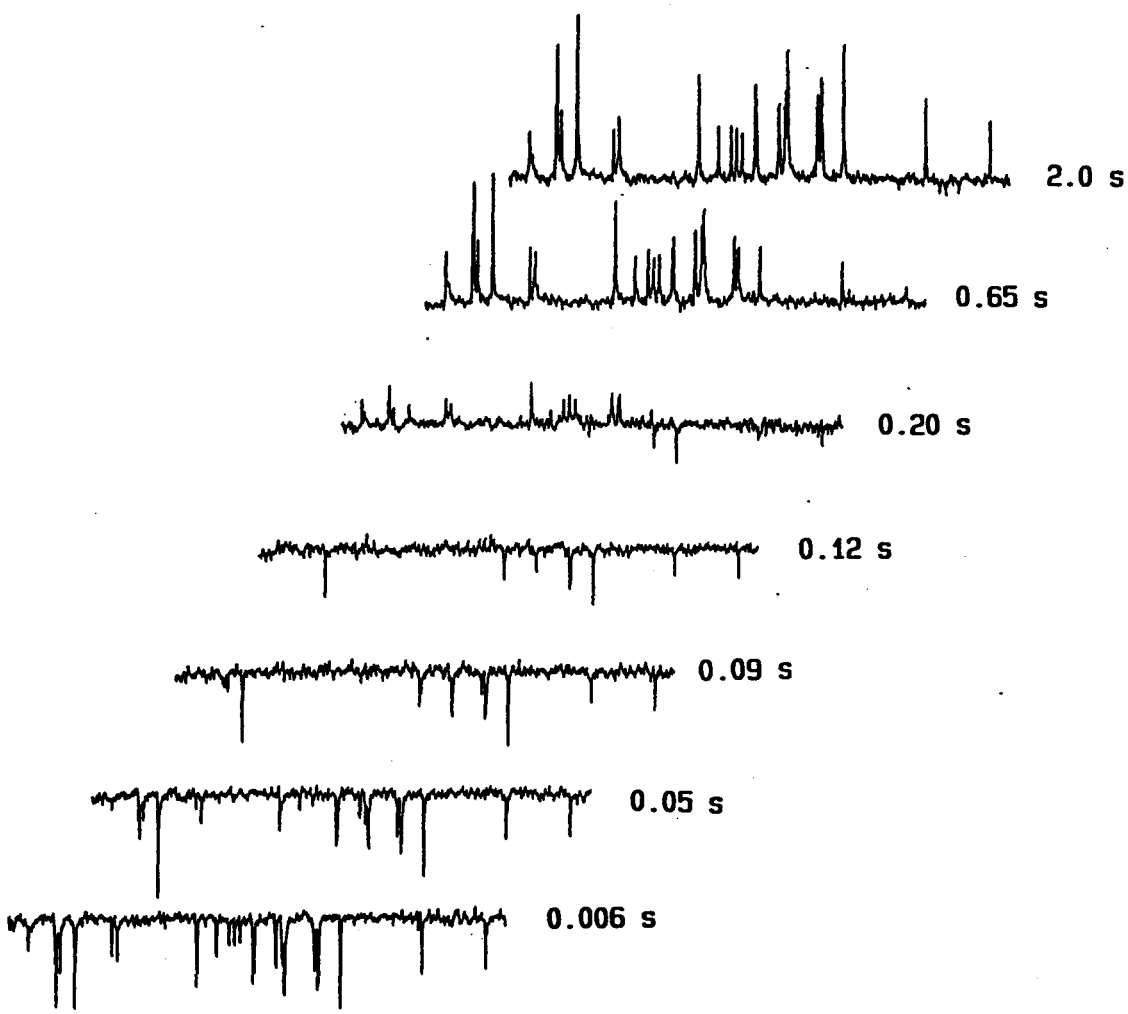

Figure 5.39. ^{13}C NMR inversion recovery spectra recorded with a fewer number of delay times, but more scans per FID. The region shown is upfield from the solvent resonance (45 to 10 ppm). The individual spectra were recorded with the delay times τ indicated on the right.

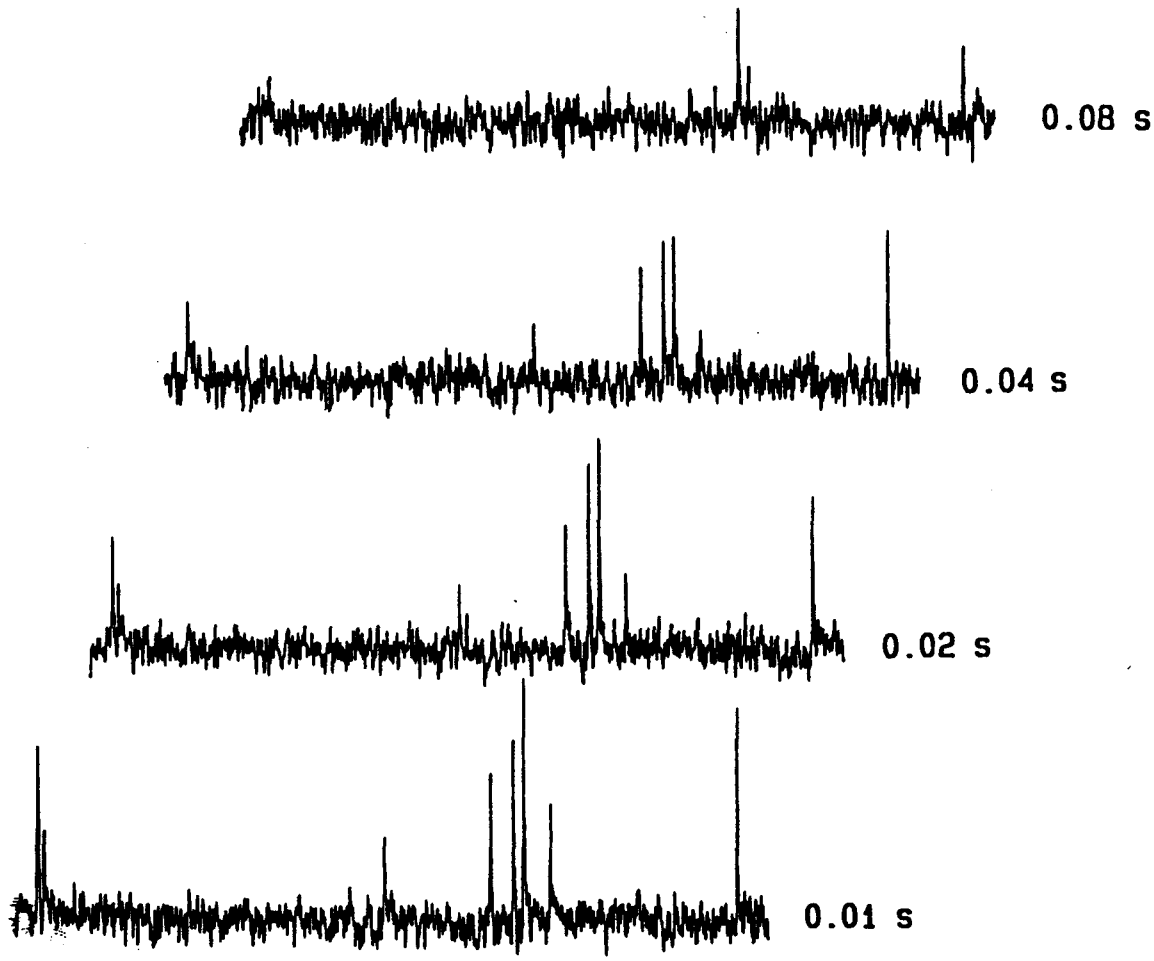

Figure 5.40. ^{13}C NMR CPMG spin-echo experiment. Spectra were recorded with only four different delay times as indicated on the right. 2600 scans were accumulated per FID. See Chapter 4 for experimental details. The region shown is from 160 to 115 ppm and contains the aromatic resonances and the Arg guanidino carbons.

Table 5.16. ^{13}C NMR data of dynorphin A-(1-13) in methanolic solution[a].

δ (ppm)[b]	Spin-sort result[c]	Assignment[d,e,f]	Directly Bonded Proton[g]	T_1 (s)	±(%)[h]	conf. limits[i] (%)	N•T_1 (s)	T_2 (s)	±(%)[h]
163.5-162.5		$Tyr^1\zeta$							
158.7		$Arg^{6/7/9}\zeta^d$						0.033	9.1
158.7		$Arg^{6/7/9}\zeta^d$						0.033	9.1
158.3		$Arg^{6/7/9}\zeta^d$						0.044	1.1
138.0	+	$Phe^4\zeta$						0.076	5.9
131.6	-	$Tyr^1\delta$		0.30	±11%	+26 -20	0.30	0.042	6.1
130.2	-	$Phe^4\delta$		0.45	±1	+28 -21	0.45		
129.6	-	$Phe^4\epsilon$		0.43	±4	+36 -26	0.43	0.067	6.4
128.0	-	$Phe^4\gamma$		0.28	±21	+83 -43	0.28		
126.0	+	$Tyr^1\gamma$							
116.9	-	$Tyr^1\epsilon$		0.34	±6	+28 -21	0.34	0.112	10.4
61.9	- trans	$Pro^{10}\alpha$	4.41	0.19	±26	+64 -45	0.17		
59.6	-	$Ile^8\alpha$	4.19	0.24	±20	+95 -59	0.10		
57.7	-	$Phe^4\alpha$	4.43	0.25	±28				
56.3	-	$Tyr^1\alpha$	4.09						
55.2	-	$Arg^6\alpha$	4.21	0.19	±26				
55.2	-	$Arg^7\alpha$	4.26	0.19	±26				
54.7	-	$Leu^5\alpha$	4.19	0.17	±29				
54.4	-	$Lys^{13}\alpha^f$	4.33	0.15		+233 -86	0.15		
54.4	-	$Lys^{11}\alpha^f$	4.33	0.15		+233 -86	0.15		
53.5	-	$Leu^{12}\alpha$	4.36	0.16	±31	+96 -49			
52.4	-	$Arg^9\alpha$	4.59	0.15	±20				
44.0	+	$Gly^{2/3}\alpha^d$		0.16	±35				
43.2		$Gly^{2/3}\alpha^d$							

a: Carbonyl ^{13}C nuclei were not assigned and therefore omitted
b: ppm values are quoted at an accuracy of ±0.1 ppm
c: refers to the result of the J-modulated ^{13}C spin-echo experiment:
"+" denotes a positive intensity in Figure 5.36b and is indicative of a secondary or quarternary carbon,
"-" represents a negative intensity and is indicative of a tertiary or primary carbon.
d,e,f: ambiguous assignments are denoted with d, e, or f.
g: The chemical shift in ppm is given as determined from the heteronuclear shift correlation experiment. The values may deviate slightly from those listed in Table 5.9.
h: percentages are the standard deviations of the rate constants $R_1 = 1/T_1$ and $R_2 = 1/T_2$, respectively.
i: Confidence limits calculated with a computer algorithm kindly provided by Dr. A.D. Bain, a "more realistic" error estimation [A.D. Bain, personal communication].

Table 5.16 cont. ^{13}C NMR data of dynorphin A-(1-13) in methanolic solution[a]. See previous page for annotations.

δ (ppm)[b]	Spin-sort result[c]	Assignment[d,e,f]	Directly Bonded Proton[g]	T_1 (s)	±(%)[h]	conf. limits[i] (%)	N•T_1 (s)	T_2 (s)	±(%)[h]
42.1	+	$Arg^{6/7/9e}$		0.22	±10				
42.0	+	$Arg^{6/7/9e}$		0.18	±8	+33 -25	0.18	0.036	6.3
42.0	+	$Arg^{6/7/9e}$		0.18	±8	+33 -25	0.18	0.036	6.3
41.8	+			0.25	±20	+139 -56			
40.7				0.16	±18	+46 -35			
40.5				0.39	±18	+39 -27			
38.1				0.08	±28	+338 -81			
37.7				0.28	±21	+48 -31			
32.2				0.24	±20	+329 -25			
30.7		$Pro^{10}\beta CH_2$	2.25/1.92	0.29	±20	+411 -83	0.58		
29.8				0.17	±17				
29.4				0.16	±45				
29.0				0.14	±18				
28.0		$Lys^{11\&13}\delta CH_2$[f]	1.67	0.32	±4	+38 -25			
26.4				0.19	±8	+43 -32			
26.0				0.21		+36 -25			
25.9	-			0.29	±20	+32 -24			
23.7	+	$Lys^{11/13}\gamma$[f]		1.46	0.28	±15	+32 -24		
23.7	+	$Lys^{11/13}\gamma$[f]		0.26	±20	+32 -24			
23.5	-	$Leu^{12}\delta CH_3$		0.44	±3	+37 -26			
23.4	-	$Leu^{5}\delta CH_3$	0.93	0.40	±4	+33 -24			
21.8	-	$Leu^{12}\delta CH_3$		0.63	±4	+20 -17			
21.8	-	$Leu^{5}\delta CH_3$	0.88	0.63	±4	+20 -17			
16.0	-	Ile^{8} CH_3	0.86	0.55	±4				
11.5	-	$Ile^{8}\delta CH_3$	0.84	0.74	±4				

Of the most interest for information on backbone mobility were the data concerning the $^{13}C_{\alpha}$ nuclei. The only parameters to be determined with reasonable reliability for these nuclei were the T_1 values (cf. Table 5.16), ranging from 150 to 250 msec. These values are in line with those obtained for both linear and cyclic peptides of similar size [Deslauriers and Smith, 1976; Deslauriers et al., 1977].

In summary, limitations on sample availability, spectrometer time, and ^{13}C abundance have imposed severe restrictions on the signal-to-noise ratio of the spectra and the accuracy of the desired data, but a quantitative assessment of the backbone rigidity based on T_1, T_2, and NOE data does seem feasible, if the ^{13}C abundance is increased by isotopic labelling.

6. DYNORPHIN A-(1-13) IN WATER-BASED ENVIRONMENTS

6.1. Dynorphin A-(1-13) in Aqueous Solution

A ^1H NMR study of 10 mM dynorphin A-(1-13) in D_2O, has been conducted by Zhou and Gibbons [1986]. The assignments of the non-labile protons (cf. Table 6.1) are not sequence-specific and have been achieved with the aid of 2-D spin-echo correlated (SECSY) spectra [Nagayama et al., 1980; Wider et al., 1984] and a 2-D J-resolved experiment [Aue et al., 1976b]. The only labile protons assigned are the two backbone amide protons of Gly^2 and Gly^3. No DQF phase-sensitive COSY, RELAY, or NOESY experiments were performed. The virtues of the latter three experiments and their important roles in the assignment strategy have been discussed in detail in the preceding chapters.

The one-dimensional 620 MHz spectrum of dynorphin A-(1-13) in D_2O is shown in Figure 6.1. Although we did not attempt rigorous, sequence-specific assignments for this sample, we did record a COSY (in the absolute value mode) and a phase-sensitive NOESY spectrum (with a mixing time of 500 ms).

Table 6.1. Assignments of the ^1H NMR spectrum of dynorphin A-(1-13) in D_2O [Zhou and Gibbons, 1986].

Amino acid	δ_{NH}	$\delta_{\alpha H}$	$\delta_{\beta H}$	Chemical shift in ppm $\delta_{\beta H'}$	other			
Tyr^1		4.25	3.15	3.15	δ 7.17	ϵ 6.88		
Gly^2	8.57	3.92	α'3.90					
Gly^3	7.93	3.88	α'3.85					
Phe^4		4.60	3.11	3.02	δ 7.24	ϵ 7.36	ζ 7.31	
Leu^{5b}		4.35	1.66	1.62	γ 1.65	δ 0.94		δ' 0.88
Arg^{6a}		4.30	1.85	1.80	γ 1.72	δ 3.22		
Arg^{7a}		4.29	1.80	1.74	γ 1.63	δ 3.22		
Ile^8		4.16	1.83	γ 1.46	γ'1.9?	γCH_3 0.88		δ 0.84
Arg^{9a}		4.27	1.76	1.73	γ 1.60	δ 3.16		
Pro^{10}		4.40	2.30	1.88	γ 2.01	δ 3.83	δ,3.65	
Lys^{11}		4.18	1.75	1.72	γ 1.40	δ 1.70	ϵ 3.01	
Leu^{12b}*		4.33	1.56	1.52	γ 1.52	δ 0.90	δ'0.85	
Lys^{13}		4.62	1.73	1.67	γ 1.40	δ 1.70	ϵ 3.02	

^{a,b} = spin systems which were not unambiguously assigned

? The value in original table for Ile^8 ' was 1.92 ppm, but this was corrected to 1.19 on account of the illustration provided (cf. Table 1 and Figure 5 in [Zhou and Gibbons, 1986]).

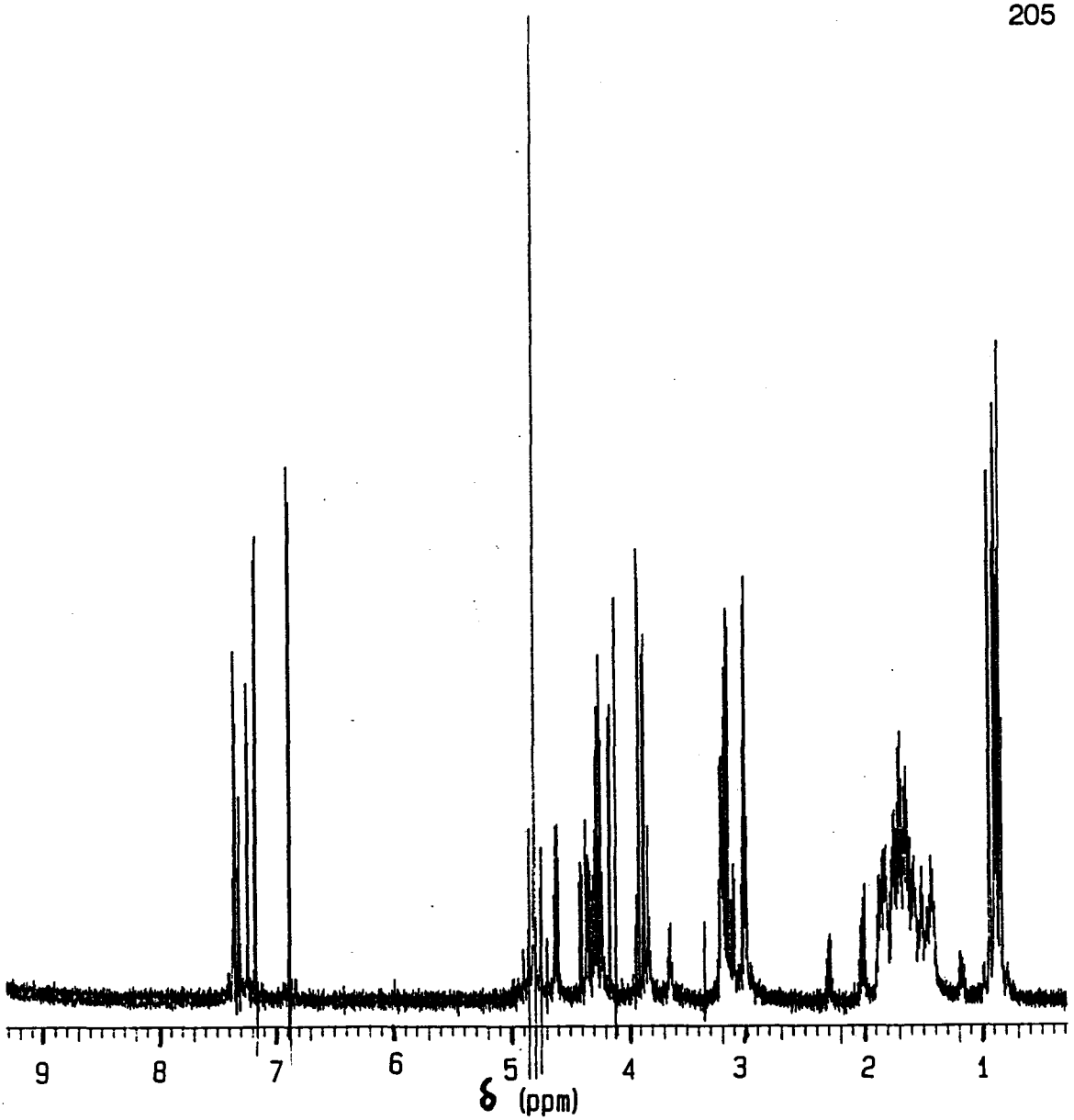

Figure 6.1. The 620 MHz one-dimensional spectrum of 12.5 mM dynorphin A-(1-13) in D_2O. 577 scans were accumulated over a spectral width of 5600 Hz in 30016 data points (2.68 s acquisition time). The solvent resonance was suppressed by presaturation during a 1.5 s delay prior to acquisition. The free induction decay was processed using Lorentz-Gauss transformation with **G** = $e^{t/0.11}.e^{-t^2/0.36^2}$ for resolution enhancement and was zero-filled to 64K before Fourier transformation. The digital resolution was 0.17 Hz/point.

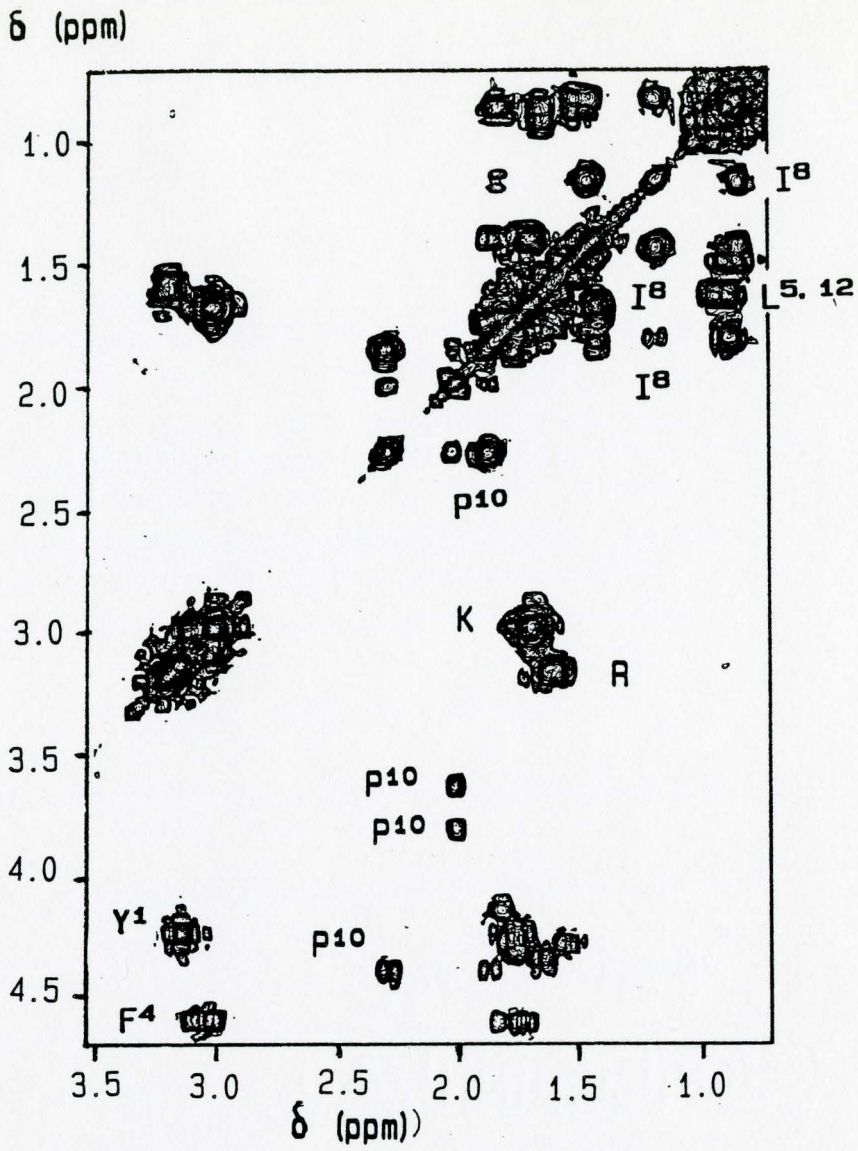

Figure 6.2. An upfield expansion of the 620 MHz COSY spectrum of 12.5 mM dynorphin A-(1-13) in D_2O. The Tyr^1 and Phe^4 α-β, Leu^5, Ile^8, and Leu^{12} γ-δCH_3 and Pro^{10} connectivities are indicated. The region from 1.9 ppm to 1.4 ppm in both dimensions was too crowded to be labelled completely. The relaxation delay (which was also the period for presaturation of the solvent) was 1 s. 16 Scans were accumulated for each of the 256 FID's containing 1024 data points in F2 over a spectral width of 5600 Hz (0.091 s acquisition time). Zero-filling to 2048 data points was applied in both dimensions. Strong window functions ($f(t) = e^{t/0.006} \cdot e^{-t^2/0.023^2}$) were applied to both dimensions before Fourier transformation. The digital resolution was 5.5 Hz/point in both dimensions.

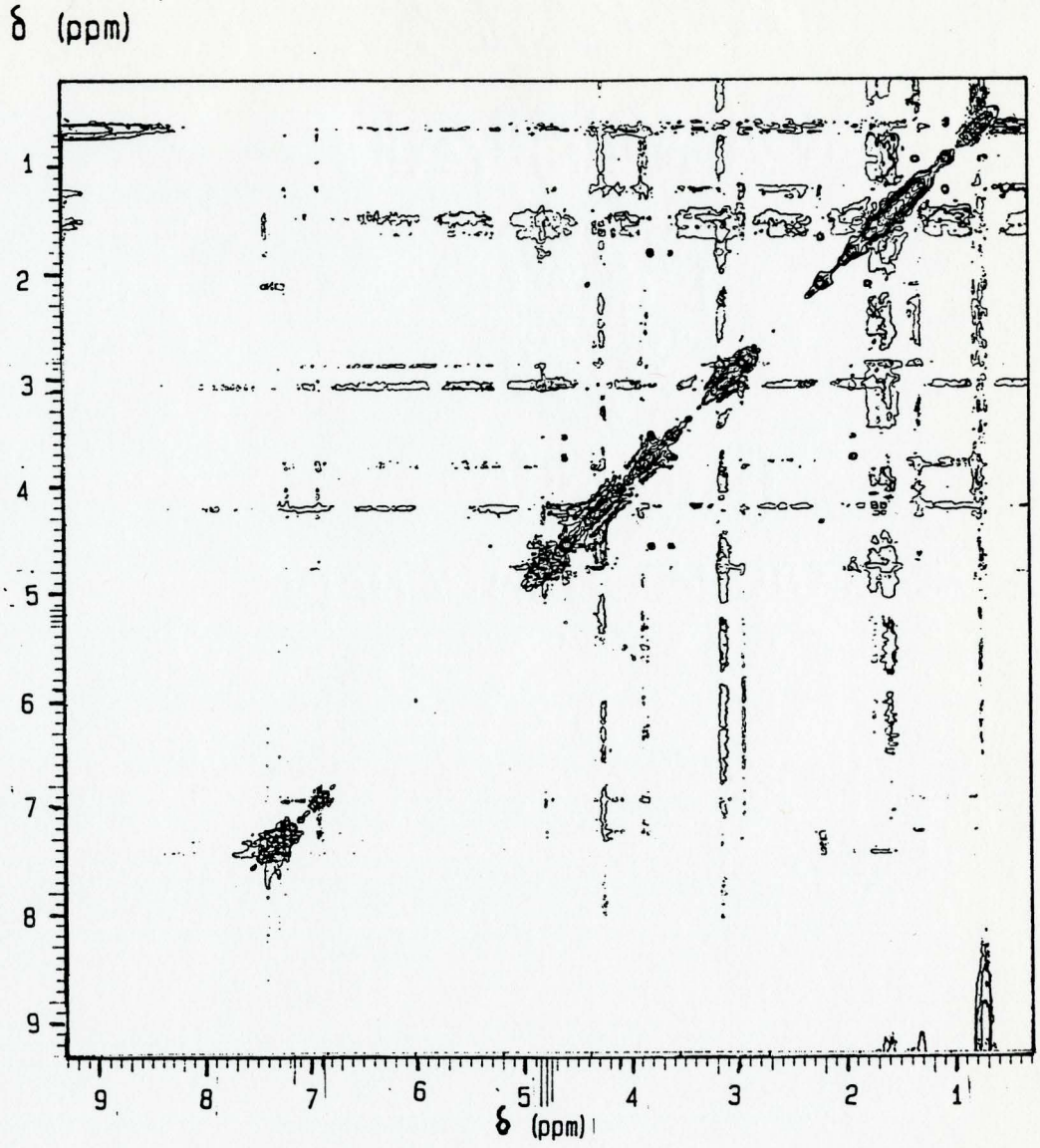

Figure 6.3. A 620 MHz pure absorption phase NOESY spectrum of 12.5 mM dynorphin A-(1-13) in D_2O over the full spectral width of 5400 Hz in both dimensions. 56 Scans were accumulated for each of the 256 FID's containing 1024 data points (0.095 s acquisition time). The relaxation delay (which was also the period for presaturation of the solvent) was 1 s. Zero-filling to 2048 data points was applied in both dimensions. Strong window functions ($f(t) = e^{-t/3.183} \cdot e^{-t^2/0.046^2}$) were applied to both dimensions before Fourier transformation. The digital resolution was 5.3 Hz/point in both dimensions.

Generally, the analysis of the COSY spectrum (Figure 6.2) was in line with the assignments of Zhou and Gibbons. As expected, the NOESY spectrum (Figure 6.3) displayed very few connectivities. In those cases where spatial proximity did not result in a cross-peak, it was inferred that the respective correlation times were in the order of the reciprocal of the Larmor frequency of the protons ($\omega \cdot \tau_c \approx 1$). Some of the few NOESY cross-peaks are shown in expansions of Figure 6.3. The Ile^{8} - ' and the Pro^{10} β-β' connectivities are indicated in Figure 6.4. The $Arg^{9}\alpha$-$Pro^{10}\delta$ and $Arg^{9}\alpha$-$Pro^{10}\delta$' connectivities featured in Figure 6.5 indicate that, at least in the case of our sample, the α proton resonance at lowest field was <u>not</u> $Lys^{13}\alpha$ (as attributed by Zhou and Gibbons [1986]), but $Arg^{9}\alpha$. Due to severe overlap in the β proton region, assignment of the α proton resonances should be regarded as tentative without confirmation from RELAY spectra. For the same reason, not all of the amide proton resonances of dynorphin A-(1-13) in H_2O at pH 2.95 (cf. Figure 6.6.) have been unambiguously assigned. A DQF phase-sensitive COSY experiment should yield an α-β connectivity region with improved resolution (cf. Figure 5.12) and thus assist in the complete assignment of the spectrum.

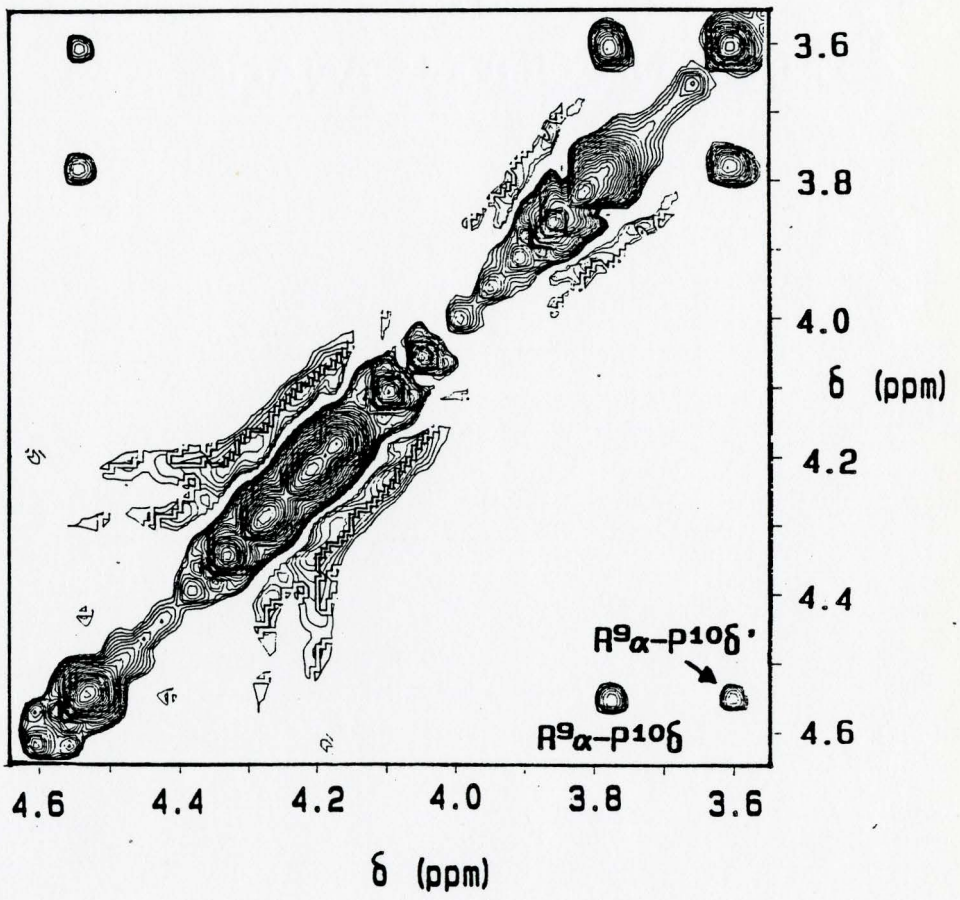

Figure 6.4. An expansion of the 620 MHz pure absorption phase NOESY spectrum of 12.5 mM dynorphin A-(1-13) in D_2O (Figure 6.3) No α-α connectivities can be detected. The only two observed are the Arg^{9}_{α}-Pro^{10}_{δ} and Arg^{9}_{α}-Pro^{10}_{δ}' connectivities.

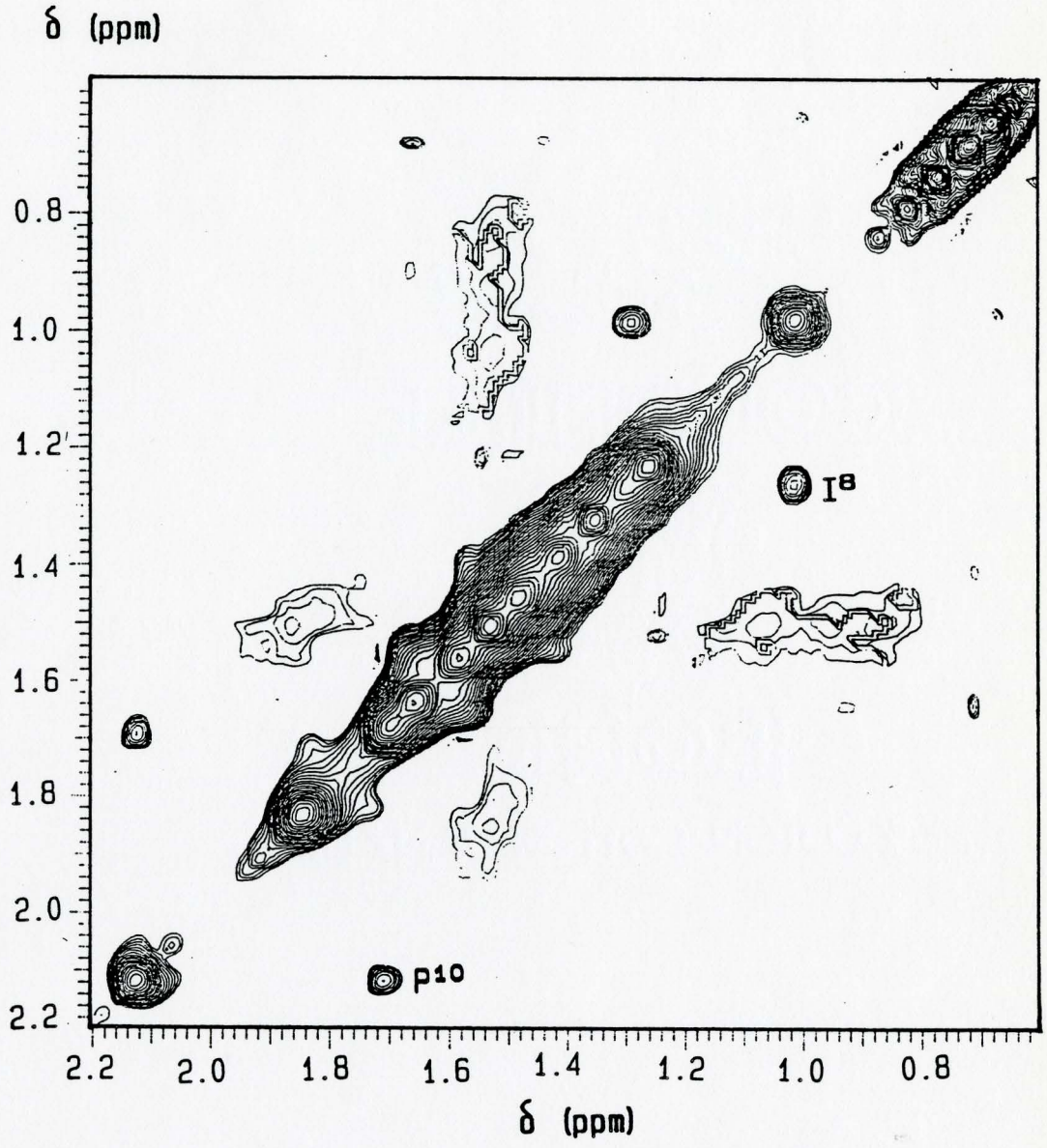

Figure 6.5. An upfield expansion of the 620 MHz pure absorption phase NOESY spectrum of 12.5 mM dynorphin A-(1-13) in D_2O (Figure 6.3). The only two connectivities observed are the Pro^{10} β-β' and Ile^{8} γ-γ' connectivities.

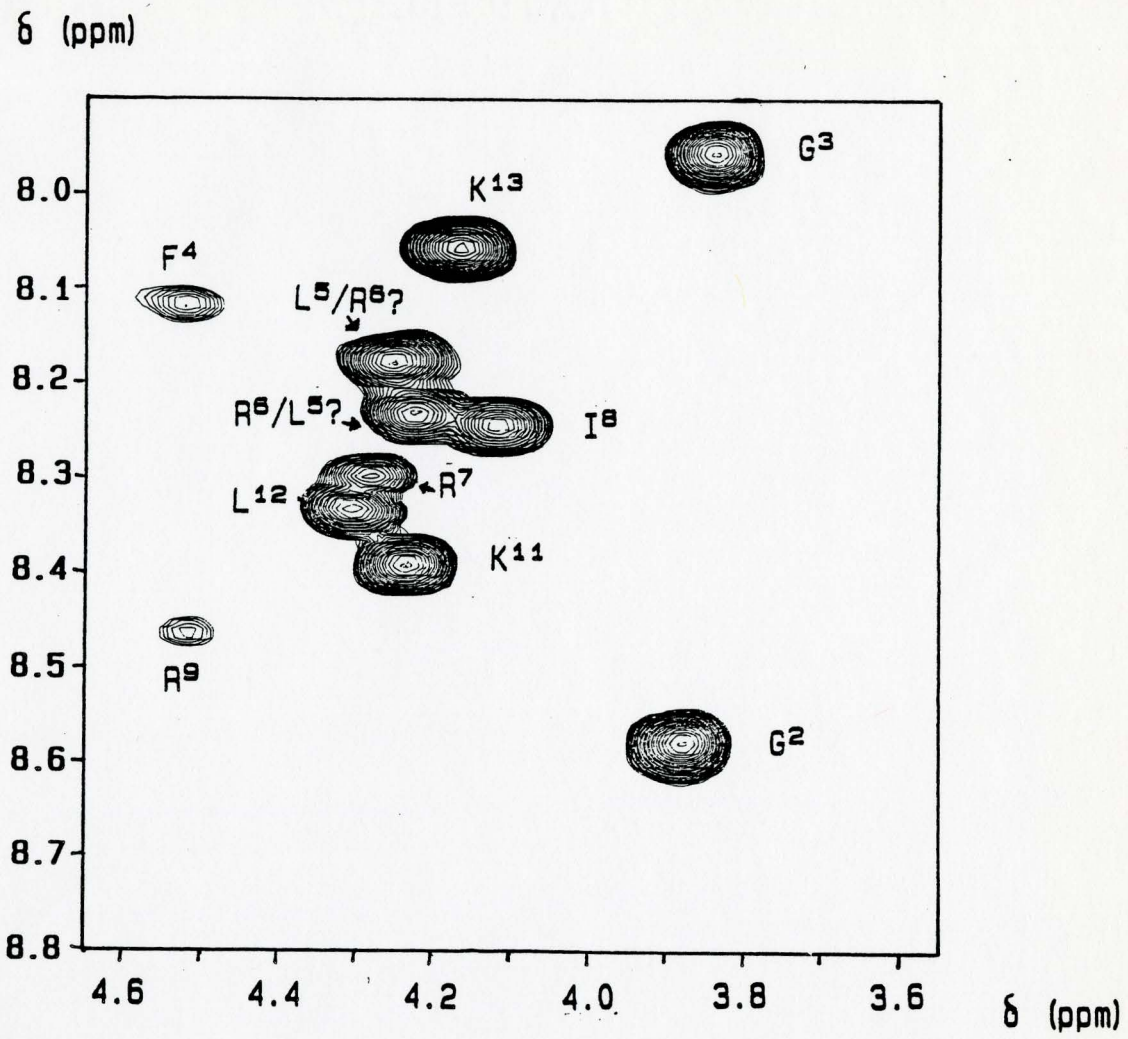

Figure 6.6. The α-NH "fingerprint" region of the COSY spectrum of 14 mM dynorphin in H_2O/D_2O (9:1, v/v) at pH 2.95. The relaxation and solvent presaturation delay was 1.5 s. 32 Scans were accumulated for each of the 256 FID's containing 1024 data points in F2 over a spectral width of 5400 Hz. Zero-filling to 2048 data points and pseudo sine-bell window functions were applied to both dimensions before Fourier transformation, resulting in a digital resolution of 5.3 Hz/point.

All 11 α-NH connectivities are resolved, but they could not all be unequivocally assigned because of ambiguities in the α-β region of the spectrum.

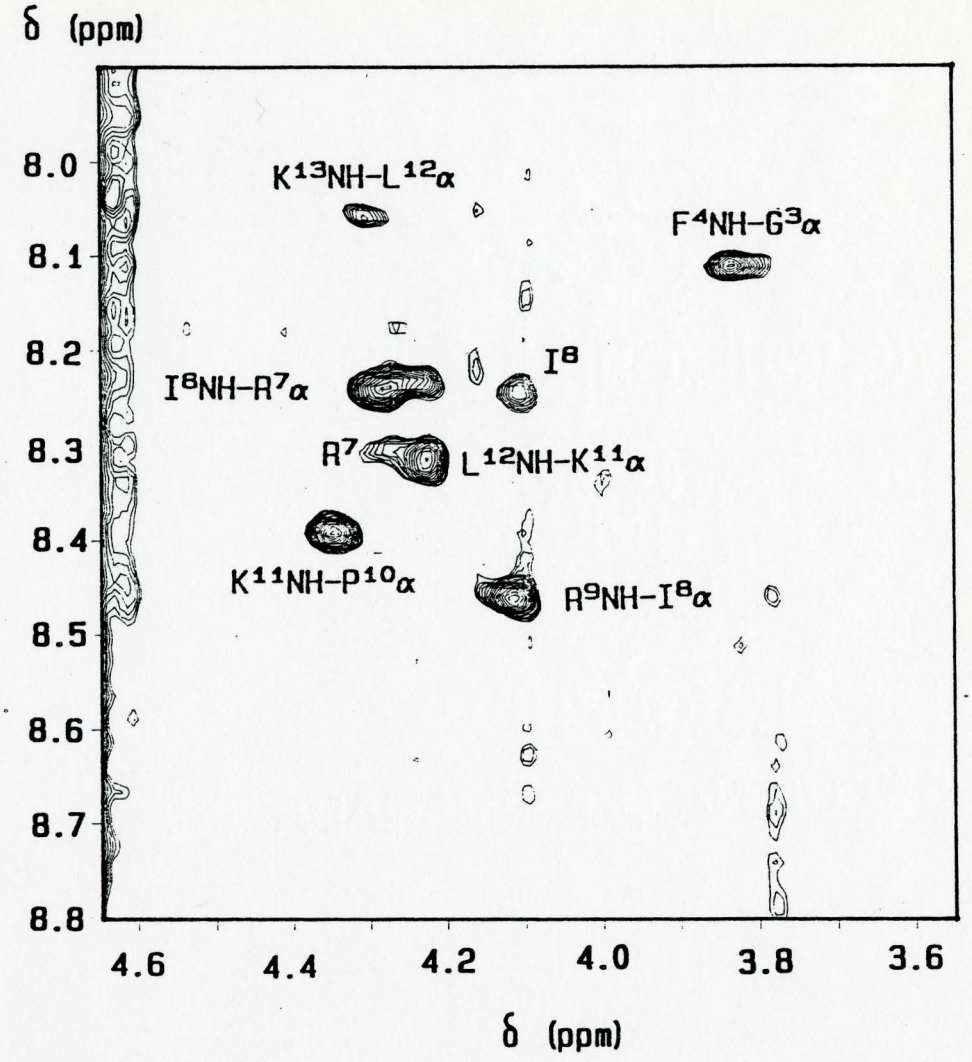

Figure 6.7. The α-NH "fingerprint" region of the NOESY spectrum recorded with a mixing time of 500 ms on 14 mM dynorphin in H_2O/D_2O (9:1, v/v) at pH 2.95. The relaxation and solvent presaturation delay was 1.5 s. 48 Scans were accumulated for each of the 256 FID's containing 1024 data points in F2 over a spectral width of 5400 Hz. Zero-filling to 2048 data points and pseudo sine-bell window functions were applied to both dimensions before Fourier transformation, resulting in a digital resolution of 5.3 Hz/point.

Not all α-NH connectivities are well resolved, impeding sequence specific assignments.

6.2. Water-Methanol Titration Experiments

Studies on the solvent composition dependence of peptide NMR spectra were originally introduced [Pitner and Urry, 1972; Kumar and Urry, 1973] as a method for determining whether amide protons are "exposed to" or "shielded from" the solvent either sterically or through the formation of intramolecular hydrogen bonds. This interpretation is, however, only straightforward if no change in the backbone conformation of the peptide is incurred [Higashijima et al., 1979].

The backbone amide proton regions of the spectra of dynorphin A-(1-13) in water-methanol solvent mixtures are shown in Figures 6.8 and 6.9. The respective mole fractions of methanol are indicated on the right. The samples for the spectra in Figure 6.8 were obtained by adding d_4-methanol in 0.5 mL increments to 0.5 mL of a 6.2 mM solution of dynorphin A-(1-13) in H_2O, pH 2.8 (cf. Chapter 5), those in Figure 6.9 by adding 140 mM d_6-acetic acid in H_2O in 0.1 mL increments to 28 mM dynorphin A-(1-13) in CD_3OD.

The assumption was made that the ^1H NMR spectrum was independent of the peptide concentration in the range of interest (i.e. from approximately 3 to 30 mM). Although no rigorous study on the concentration dependence of the spectrum was performed, this presumption seems reasonable, as there were no

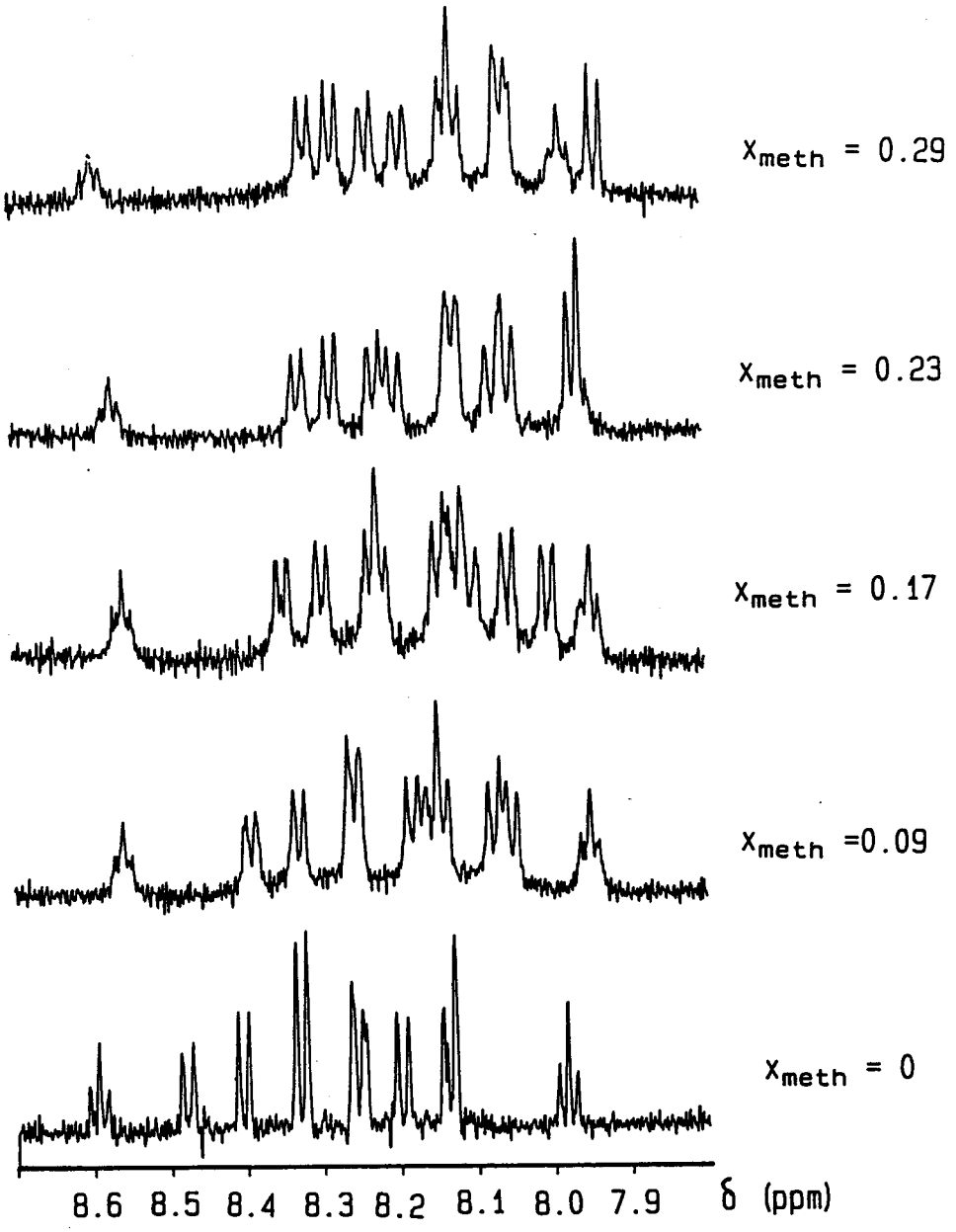

Figure 6.8. The backbone amide proton regions of the 500 MHz spectra of dynorphin A-(1-13) in mixtures of water and methanol at the indicated mole fractions of CD_3OD. At least 128 scans were accumulated over a spectral width of 4200 Hz in 16384 data points (1.95 s acquisition time). The free induction decays were processed using Gaussian multiplication for resolution enhancement and were zero-filled to 32K before Fourier transformation. The digital resolution was 0.26 Hz/point.

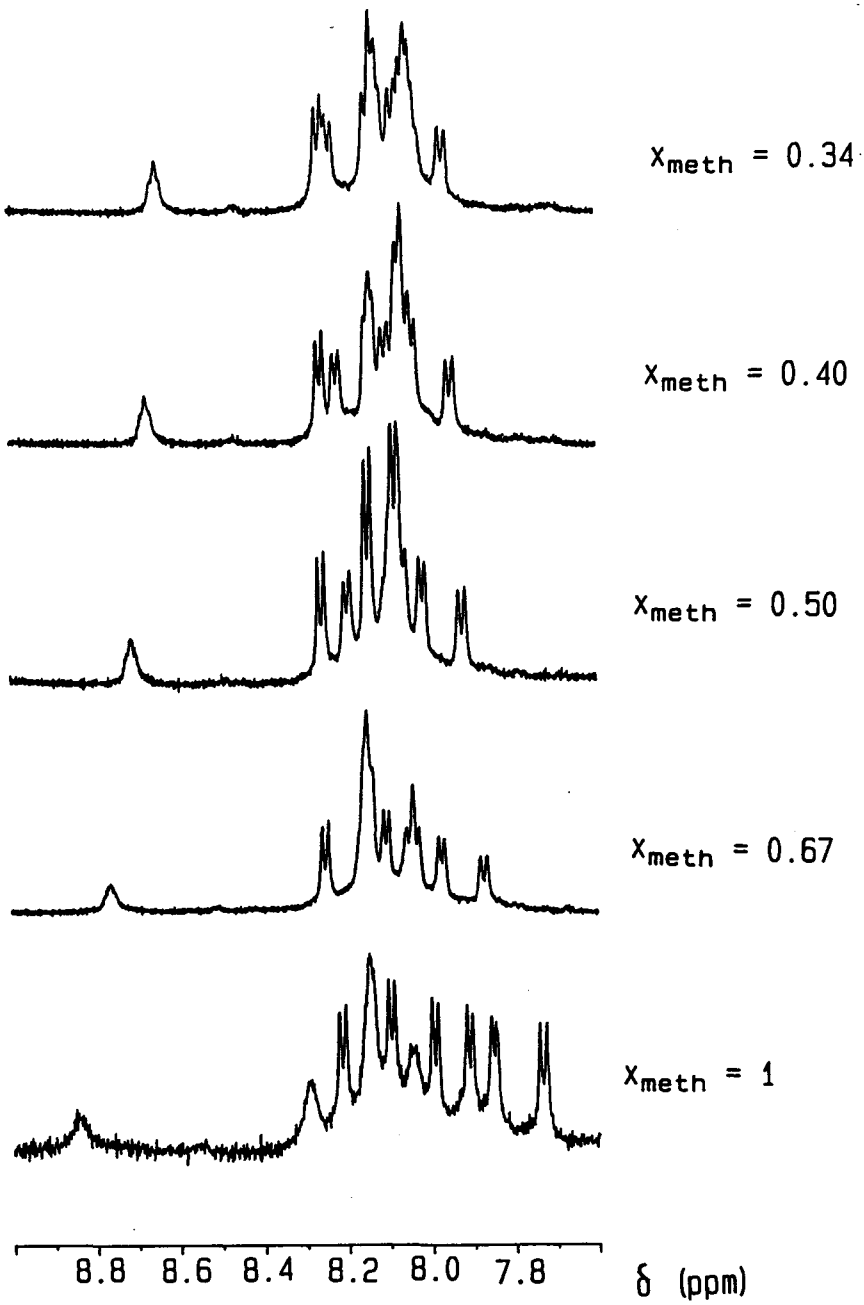

Figure 6.9. The backbone amide proton regions of the 500 MHz spectra of dynorphin A-(1-13) in mixtures of water and methanol at the indicated mole fractions of CD_3OD. At least 128 scans were accumulated over a spectral width of 5000 Hz in 16384 data points (1.64 s acquisition time). The free induction decays were processed using Gaussian multiplication for resolution enhancement and were zero-filled to 32K before Fourier transformation. The digital resolution was 0.31 Hz/point.

significant differences in the CD spectra of methanolic (CD_3OH) solutions of 5.5 and 20 mM dynorphin A-(1-13). Therefore all changes in the spectra were assumed to result from the differences in solvent composition.

Taking into account that the spread (in cm/ppm) in Figure 6.8 was nearly double that of Figure 6.9, the top traces in both figures (which are at similar solvent compositions) did not seem to differ profoundly, although the peptide concentration in Figure 6.9 was four times as strong as was the case in Figure 6.8. Consequently, even though the experiments were performed on two different samples, it seemed justifiable to incorporate both experiments into one diagram (Figure 6.9).

Although COSY spectra were recorded at three different mole fractions of methanol (x_{meth} = 0, 0.34, 1, cf. Figure 6.8), not all amide proton resonances could be identified unequivocally in all spectra. Consequently, not all of the amide proton resonances could be followed through all stages of the titration experiments. Those resonances which could be assigned unambiguously are indicated in Figure 6.11.

With respect to the chemical shifts in water (x_{meth} = 0), all resonances initially experienced an upfield shift upon addition of methanol. This was expected as addition of the less polar solvent (methanol) causes less deshielding of the

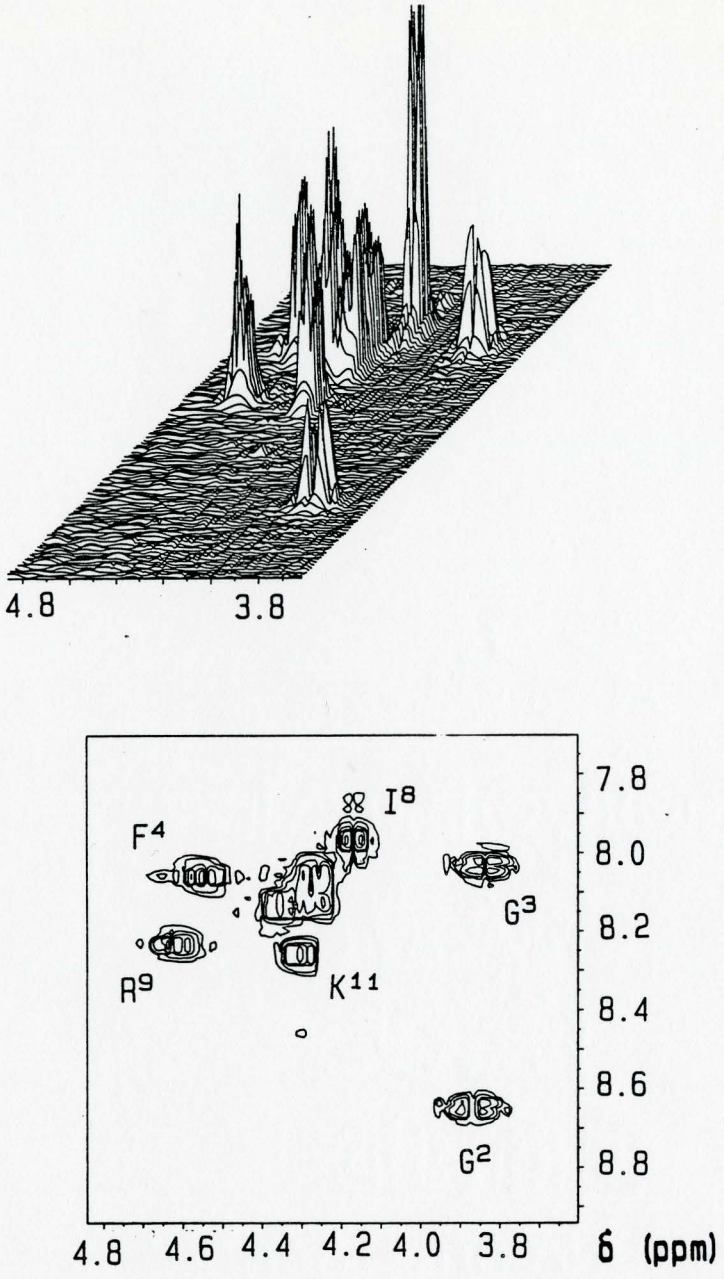

Figure 6.10. Stacked and contour plots of the NH-α "fingerprint" region of the 500 MHz COSY spectrum of dynorphin A-(1-13) in a mixture of water and methanol at a mole fraction of x_{meth} = 0.34. The exact position of the Gly^3NH resonance can be extracted, which was not possible from the one-dimensional spectrum, because of considerable overlap in that region.

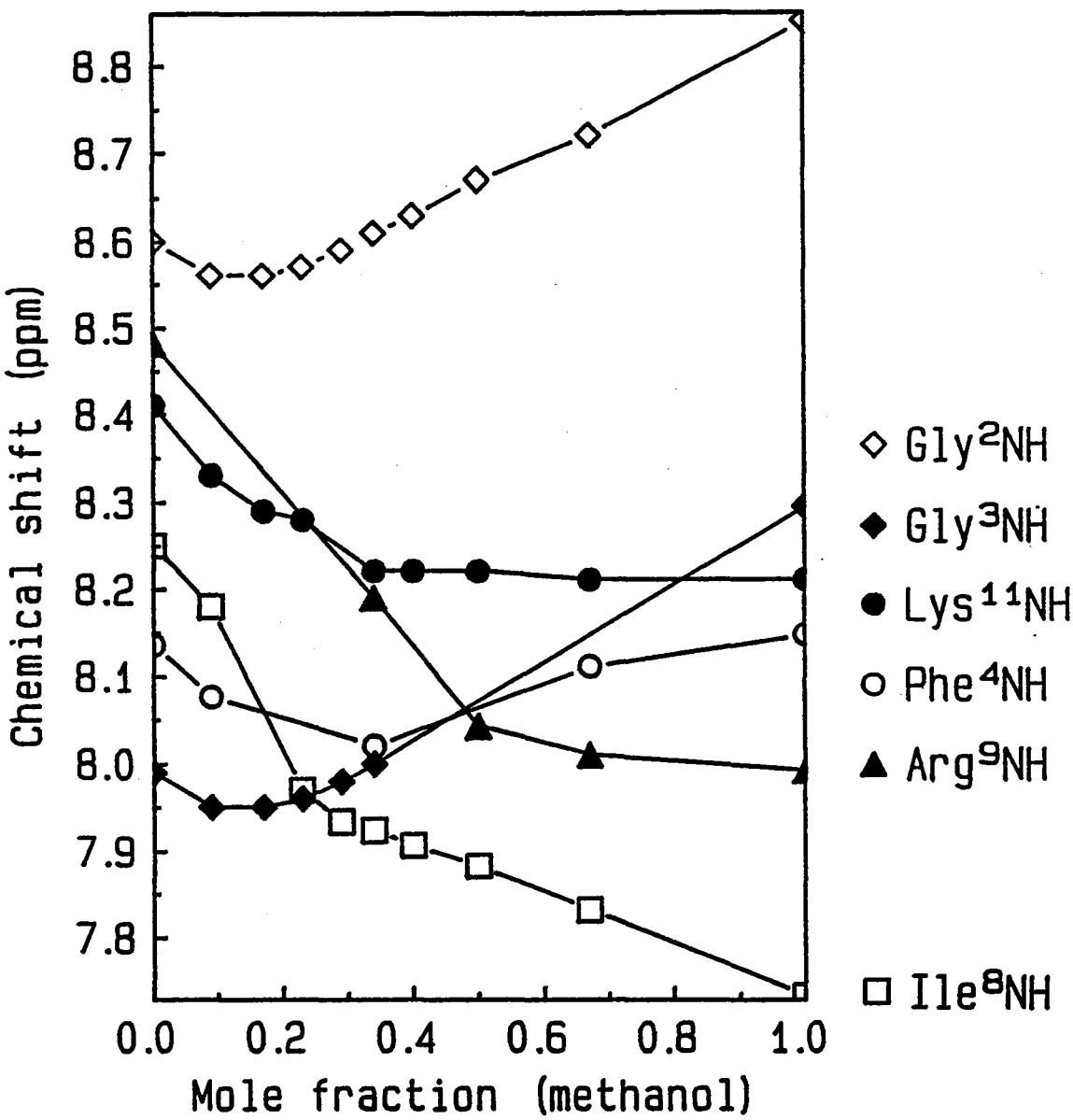

Figure 6.11. The chemical shifts of the backbone amide protons of dynorphin A-(1-13) in mixtures of water and methanol at different mole fractions of CD_3OD. Not all resonances could be monitored over the whole titration range.

protons, inducing upfield shifts. The magnitude of this effect was very different for the individual amide resonances, most noticeable was the large shift to higher field incurred by the $Arg^{9}NH$ resonance. Further addition of methanol resulted in progressive upfield shifts.

The solvent composition dependences were, however, not monotonous for $Gly^{2}NH$, $Gly^{3}NH$, and $Phe^{4}NH$. If a conformational change is induced, changes in hydrogen bonding will be reflected in alterations of the electron densities of amide groups [Schwyzer and Ludescher, 1969; Llinas and Klein, 1975] and manifest themselves in a downfield shift upon hydrogen bond formation. This provides a good explanation for the eventual increase in the chemical shifts of $Gly^{2}NH$, $Gly^{3}NH$, and $Phe^{4}NH$ at higher mole fractions of methanol (Figure 6.8).

It is interesting to note that these eventual downfield shifts could be observed only for the three amide protons nearest to the amino terminus. This could be an indication of major conformational rearrangement in the N-terminal region of the peptide upon a change of the solvent environment from water to methanol. However, such conclusions should be viewed with caution as the data set is incomplete. Another indication for a change in conformational was given by significant solvent dependences of the α protons (Figure 6.12). Particularly striking was the effect on $Phe^{4}{}_{\alpha}$ as is indicated. A slight downfield shift of the

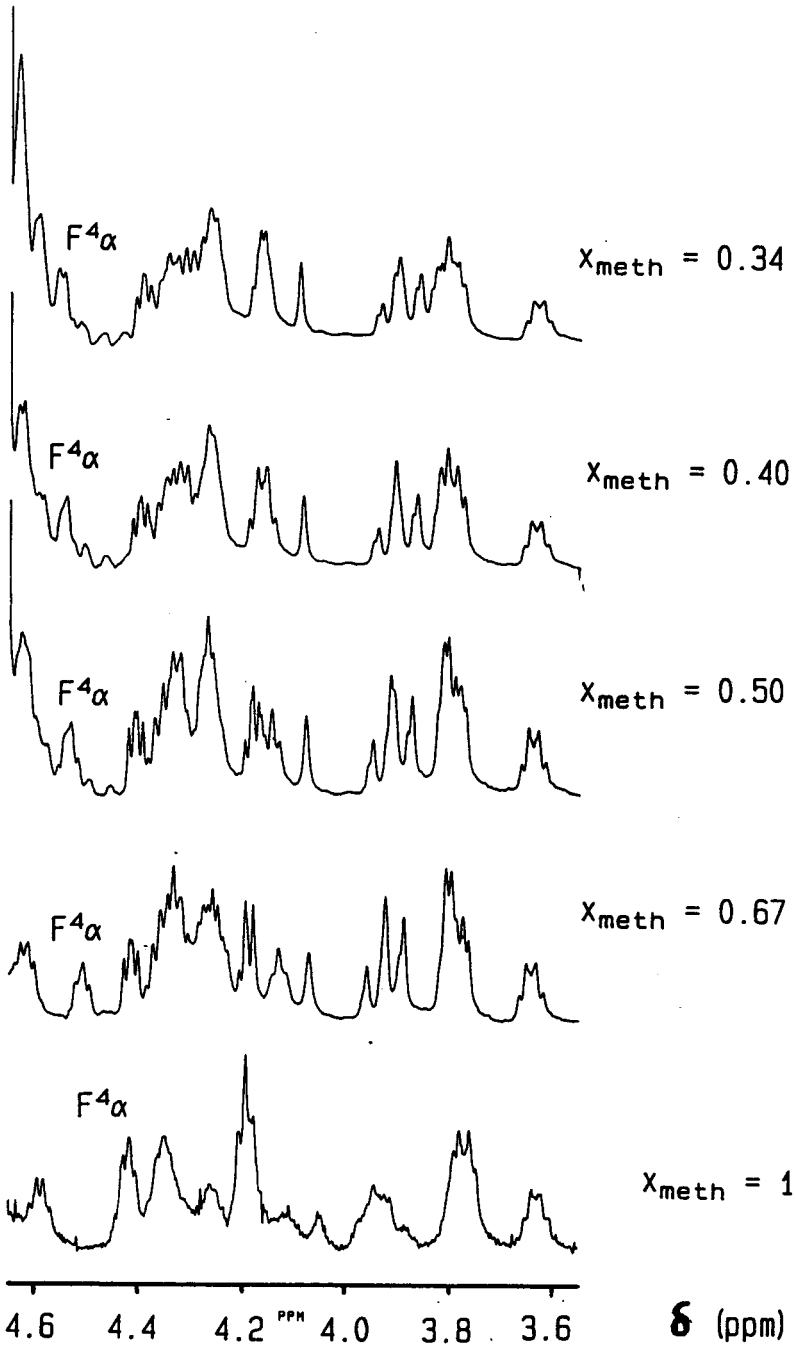

Figure 6.12. The α proton region of the spectrum of dynorphin A-(1-13) in mixtures of water and methanol at the indicated mole fractions of CD_3OD as featured in Figure 6.9. The digital resolution was 0.31 Hz/point. The particularly striking solvent dependence of Phe^4_α is indicated.

$Leu^5\delta CH_3$ resonances could be due to a minor change in the ring current effect arising from the Phe^4 ring, but this change was minute compared to the ring current effects observed in folded proteins [McDonald and Phillips, 1967].

In summary, interpretation of the data was not sufficiently unambiguous to allow the delineation of conformational features. Certainly, a more rigorous analysis of the spectra is required, encompassing the need for additional experiments (e.g. RELAY, DQF phase-sensitive COSY) at all different solvent compositions.

6.3. Dynorphin A-(1-13) in Aqueous Phospholipid Bilayers

The ^{1}H NMR spectrum of a suspension of 32 mM (non-deuterated) dimyristoyl-phosphatidylglycerol (DMPG) vesicles is shown in the top half of Figure 6.13. The resonance lines in the spectrum of the pure aqueous lipid suspension were quite sharp indicating a high mobility and good solvation of the vesicles. The sample itself was clear and became slightly turbid when it was added to the lyophilized tridecapeptide. The peptide was apparently tightly bound to the lipid and evidently induced aggregation (or even fusion[1]) of the vesicles, as could also be deduced from the appearance of the spectrum in the bottom half of Figure 6.13. Binding of the peptide has been reported to be due to both hydrophobic and electrostatic interactions [Gysin and Schwyzer, 1983], although the much stronger binding of the polycationic peptide to anionic DMPG compared to peptide binding to zwitterionic DMPC vesicles (see below) must be explained by electrostatic interactions alone. Both the stronger electrostatic attraction between lipid and peptide and the weaker competing lipid-lipid interaction as a result of electrostatic repulsion contribute to the increased strength of binding. In Figure 6.13., observation of, for instance, the aromatic proton resonances of the peptide (at approximately 7 ppm) was not thwarted by superimposition with any phospholipid signals but by substantial linebroadening

[1] The mediation of membrane fusion by amphiphilic peptides and polycations is discussed in a recent review [Stegmann et al., 1989].

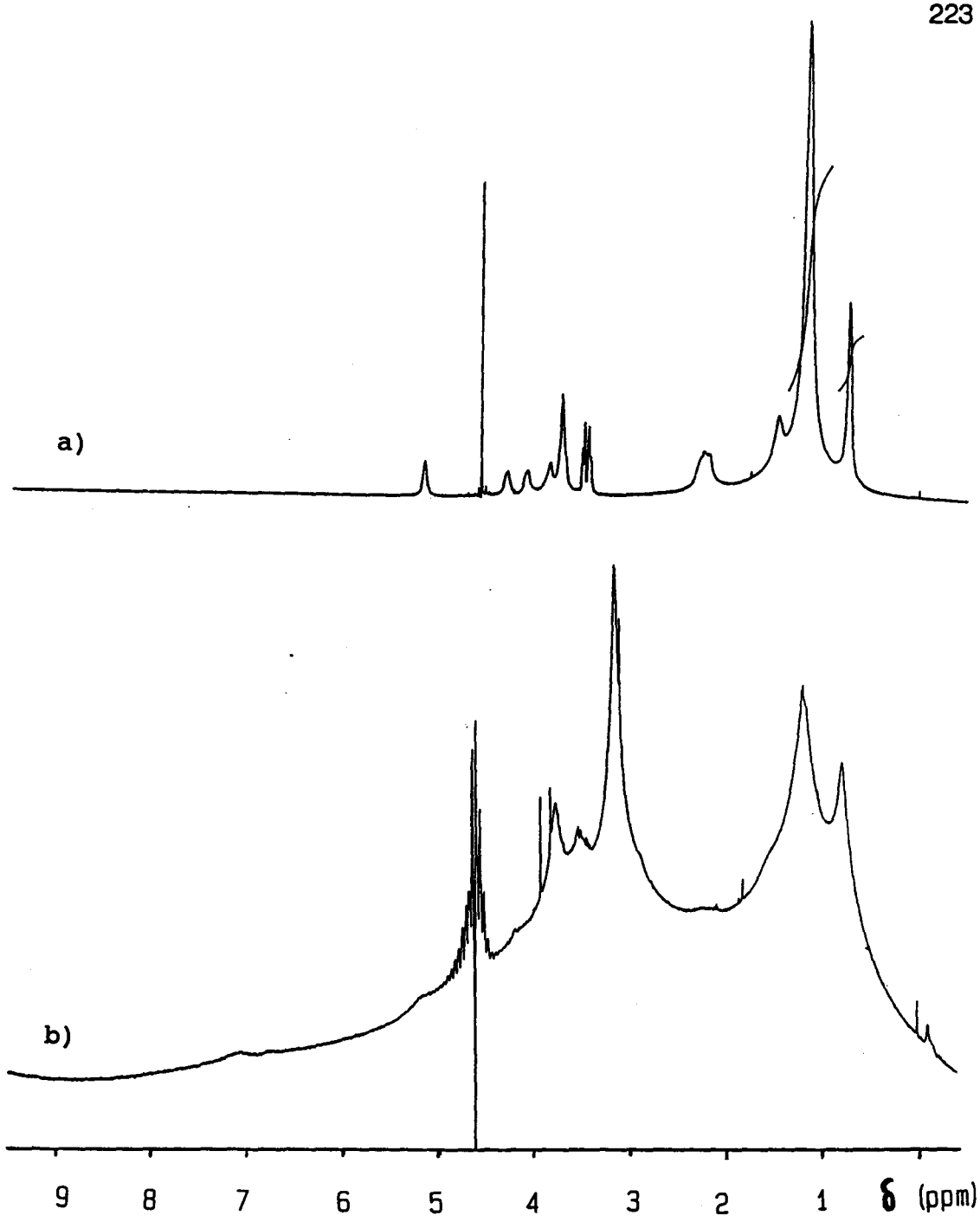

Figure 6.13. 500 MHz ^{1}H NMR spectra of, a), an suspension of DMPG vesicles in D_2O and, b), dynorphin A-(1-13) in an aqueous suspension of DMPG vesicles.

due to the low mobility of the molecular aggregates. Thus, although this system provided the best sample for CD studies (cf. Chapter 4) it was not a practical sample for NMR analysis.

NMR analyses of membrane-bound peptides are nevertheless possible at high resolution if a system can be found with fast chemical exchange between membrane-bound and free peptide molecules [Wakamatsu et al., 1986b]. Such experimental conditions were apparently satisfied for dynorphin A-(1-13) in the presence of d_{54}-dimyristoyl-phosphatidylcholine (d_{54}-DMPC) vesicles. The deuterated phospholipid displayed a gel-to-liquid crystalline phase transition temperature of 20°C as was measured by differential scanning calorimetry [Lancaster and Epand, unpublished observations]. This means that at an NMR probe temperature of 30°C (in the case of the 500 MHz measurements) or 23°C (in the case of the 620 MHz measurements), the lipid is definitely in the liquid crystalline state, which is a better approximation of a biological membrane than the gel state lipid. Additionally the rate of exchange of a peptide agonist (e.g. glucagon [Epand, 1978]) with sonicated DMPC bilayers is dramatically elevated above the phase transition temperature of the model membrane lipid. A high exchange rate is vital for the observation of the effects described below. The free form in solution dominated the NMR spectrum (Figure 6.14). The line broadening due to chemical exchange is only slight compared with the spectrum of the tridecapeptide in D_2O (also featured in Figure 6.14). Such a system is amenable to transferred nuclear Overhauser effect studies [Clore and Gronenborn, 1982] as has been demonstrated for membrane-bound peptides in the case of, e.g.,

the tetradecapeptide mastoparan-X [Wakamatsu et al., 1983] and the tridecapeptide α-mating factor [Wakamatsu et al., 1986a].

With a few exceptions (cf. Figures 6.3-6.5), the NOE's of the free molecule were negligible. NOE's of the membrane-bound peptide molecule will be transferred back to the free peptide if the exchange rate is fast compared to the cross-relaxation rate. This is demonstrated in Figure 6.15. Irradiation of the methyl signal at highest field (0.86 ppm) in a one-dimensional 500 MHz NOE difference experiment[2] gave rise to negative NOE's. Of particular interest in this experiment were the NOEs in the aromatic region. Negative NOEs were observed for all Phe^4 ring protons but no effect was seen in the case of the Tyr^1 ring protons. Extending the irradiation time to 500 ms (data not shown) and 1 s (Figure 6.16, bottom trace) led to an increase in the intensity of the observed effects and to a reduction of the appearance of artifacts, but did not seem to result in any change of the observed NOE patterns. Irradiation of the methyl resonance at lowest field (0.95 ppm) failed to reveal any NOE's in the region of interest (Figure 6.16, top trace). These results demonstrated that the observed effects were not due to spin diffusion [Hull and Sykes, 1975; Kalk and Berend-

[2] The selectivity of the irradiation is estimated at ± 20 Hz (± 0.04 ppm)

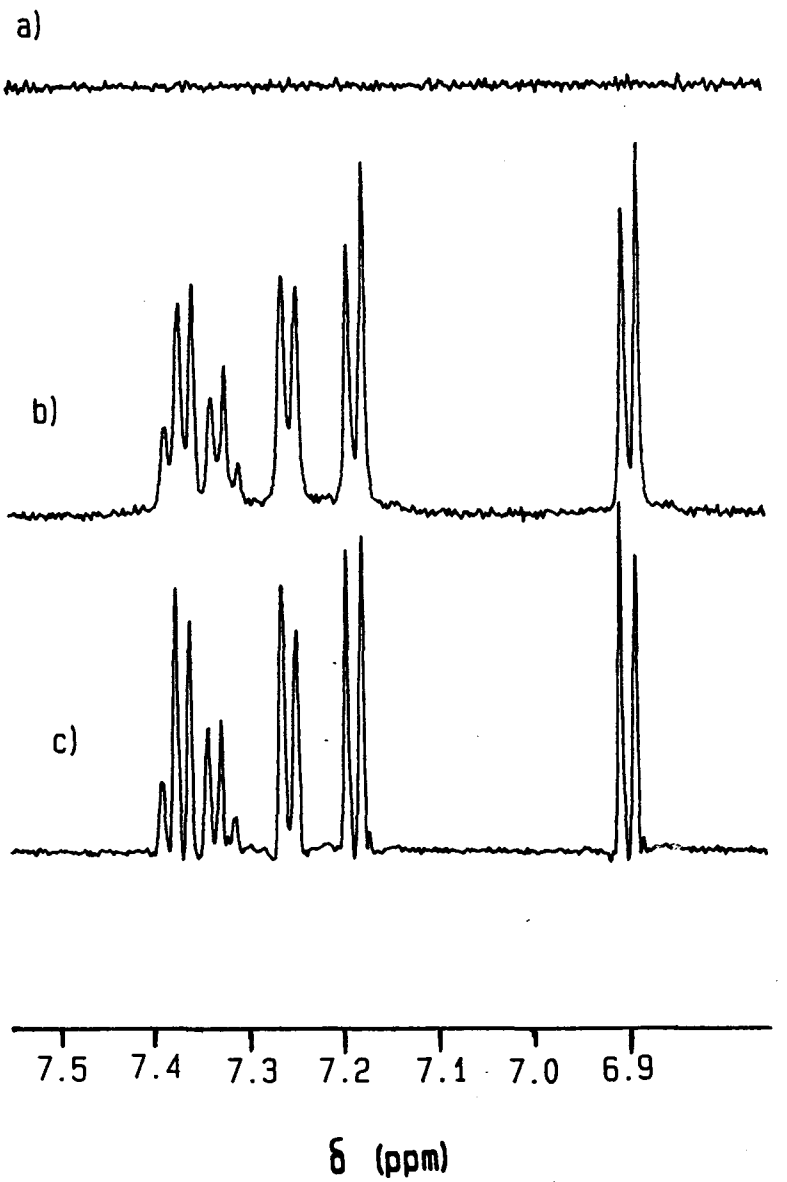

Figure 6.14. 500 MHz ^{1}H NMR spectra of, a), d_{54}-DMPC vesicles in D_2O, b), dynorphin A-(1-13) in an aqueous suspension of d_{54}-DMPC vesicles, and, c), dynorphin A-(1-13) in D_2O. All FIDs were zero-filled to 64K data points and processed with the same resolution enhancement function. The digital resolution was 0.15 Hz/point. The lines in trace b) are only slightly broader than those in trace c).

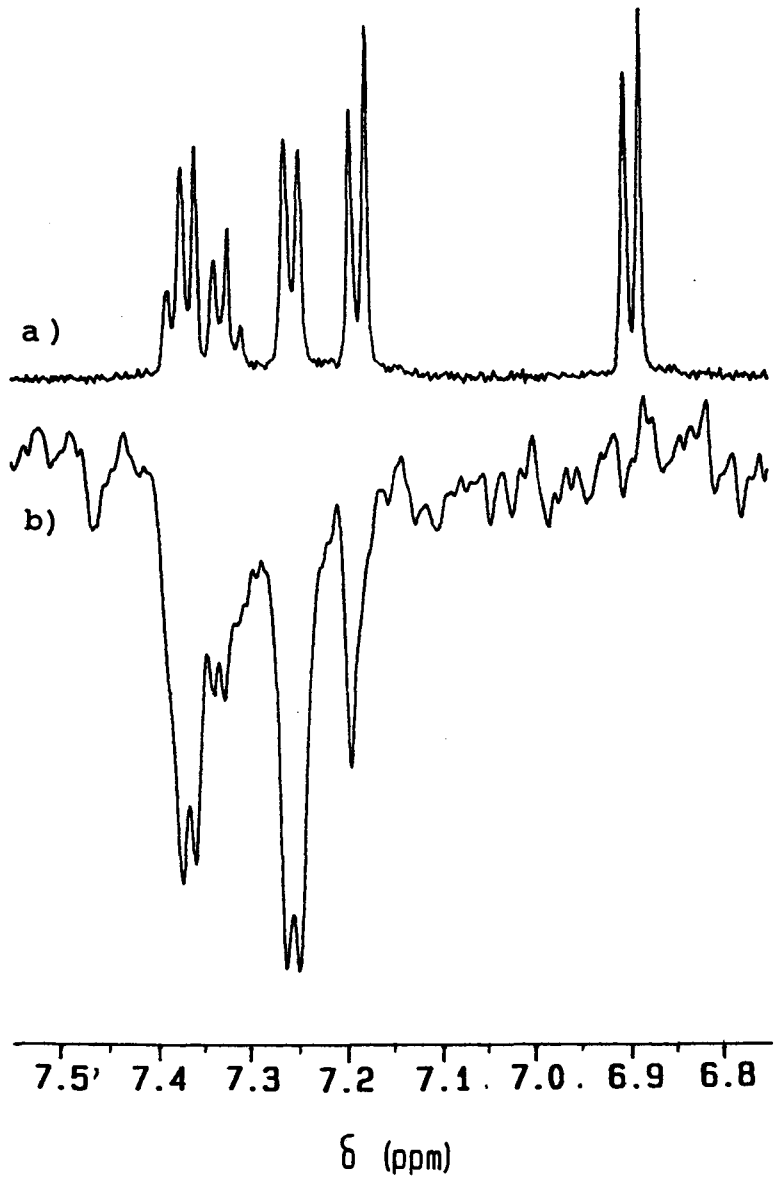

Figure 6.15. A 500 MHz ^{1}H NMR regular one-dimensional spectrum (a, from Fig 6.14b) and a one-dimensional transient NOE difference spectrum (b) of 8 mM dynorphin A-(1-13) in an aqueous suspension of 32 mM d_{54}-DMPC vesicles. The on-resonance frequency corresponded to 0.86 ppm, the off-resonance frequency to 9.89 ppm. 768 scans were accumulated for both the on- and off-resonance FIDs. The irradiation time was 350 ms.

sen, 1976]. Irradiation of the methyl resonance at highest field (0.86 ppm) in the same 500 MHz one-dimensional experiment on an aqueous solution of the peptide did not lead to the observation of NOEs (data not shown, but this can also be deduced from the corresponding 620 MHz NOESY spectrum (Figure 6.3)), indicating that the effects are transferred NOEs.

The two-dimensional 620 MHz transferred NOE spectrum is shown in Figure 6.17. There were evidently more cross-peaks present than in the corresponding NOESY spectrum in D_2O (Figure 6.3). On the other hand, there were only very few cross-peaks present, for instance, in the α-α connectivity region (Figure 6.18) suggesting that the mixing time employed (500 ms) was not long enough to allow significant spin diffusion to occur.

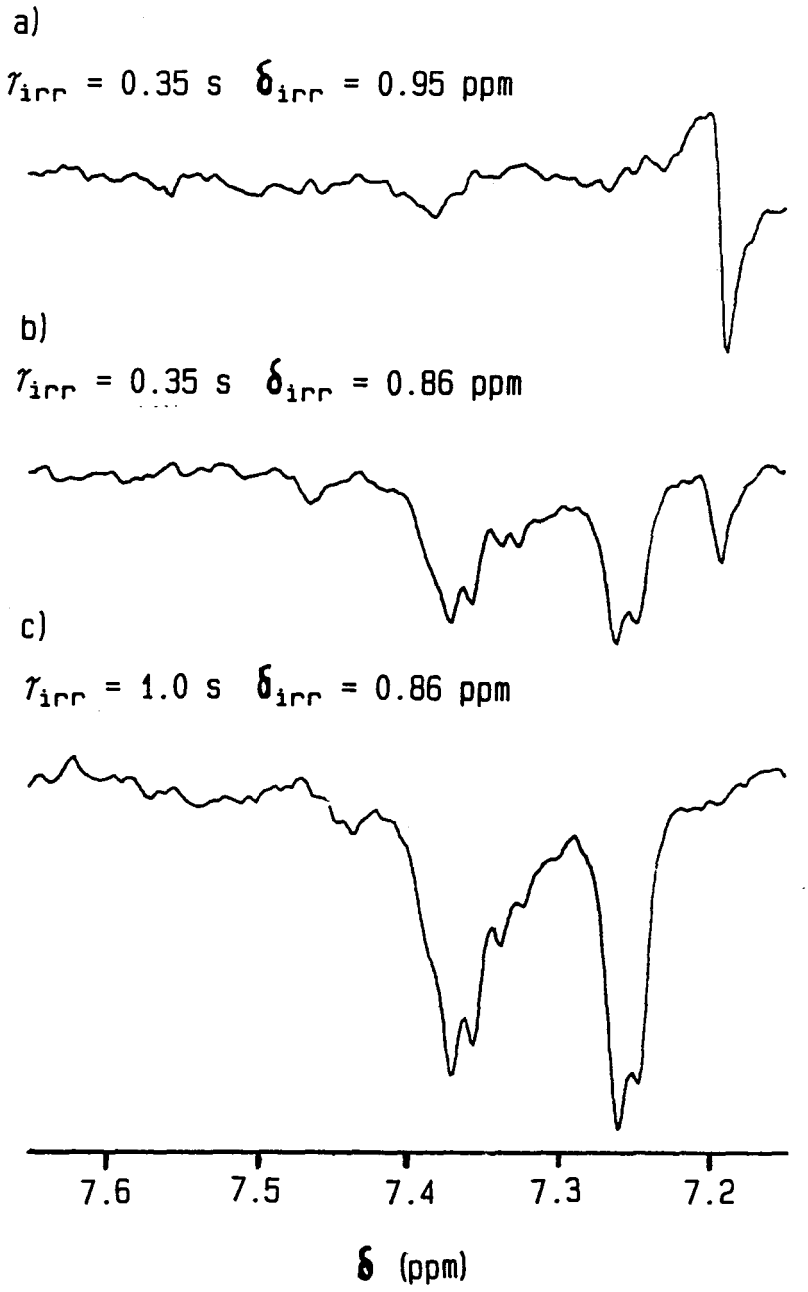

Figure 6.16. 500 MHz ^{1}H NMR transient NOE difference spectra of 8 mM dynorphin A-(1-13) in an aqueous suspension of 32 mM d_{54}-DMPC vesicles. The off-resonance frequency corresponded to 9.89 ppm. 768 (a and b) or 256 (c) scans were accumulated for both the on- and off-resonance FIDs. The chemical shifts corresponding to the on-resonance frequencies and the irradiation times are indicated.

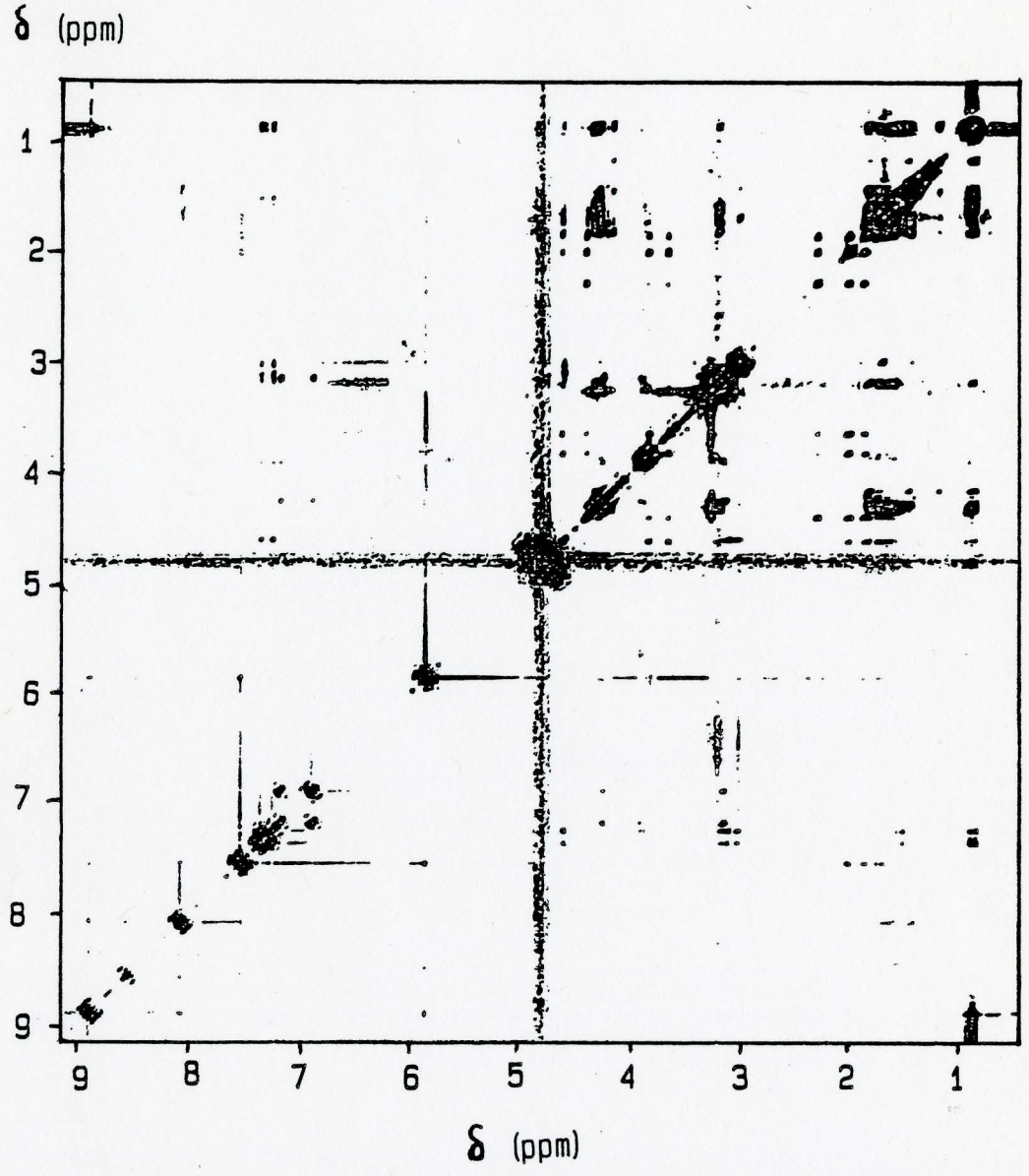

Figure 6.17. A 620 MHz pure absorption phase NOESY spectrum of 12.5 mM dynorphin A-(1-13) in an aqueous suspension of 50 mM d_{54}-DMPC vesicles over the full spectral width of 5400 Hz in both dimensions. The acquisition and processing of the spectrum was identical to the one featured in Figure 6.3 with the exception that 72 scans were accumulated for each of the 256 FID's (instead of 56).

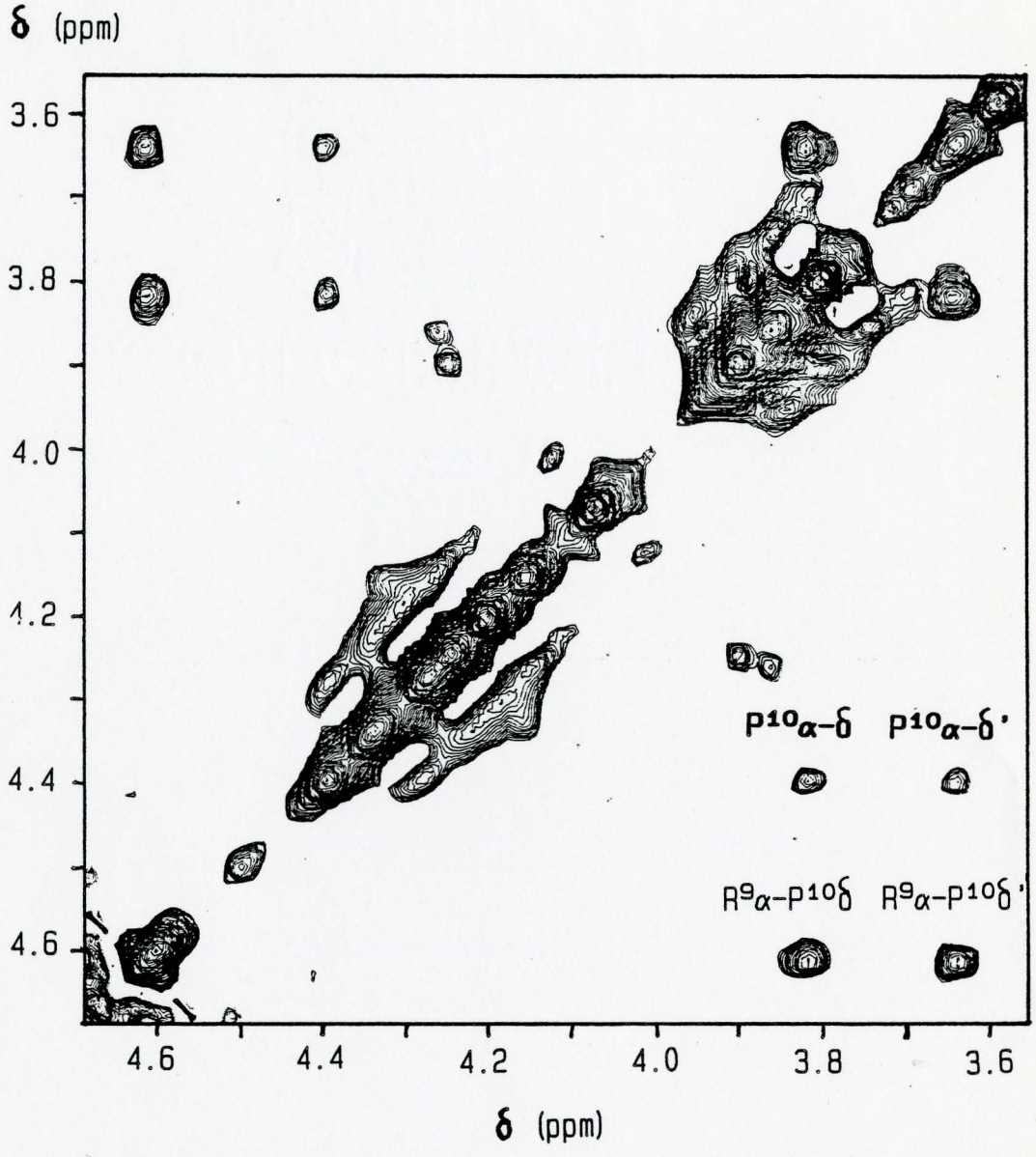

Figure 6.18. An expansion of the 620 MHz pure absorption phase NOESY spectrum of 12.5 mM dynorphin A-(1-13) in a suspension of 50 mM d_{54}-DMPC vesicles in D_2O (Figure 6.17) Most of the cross-peaks are associated with the Pro^{10} spin system.

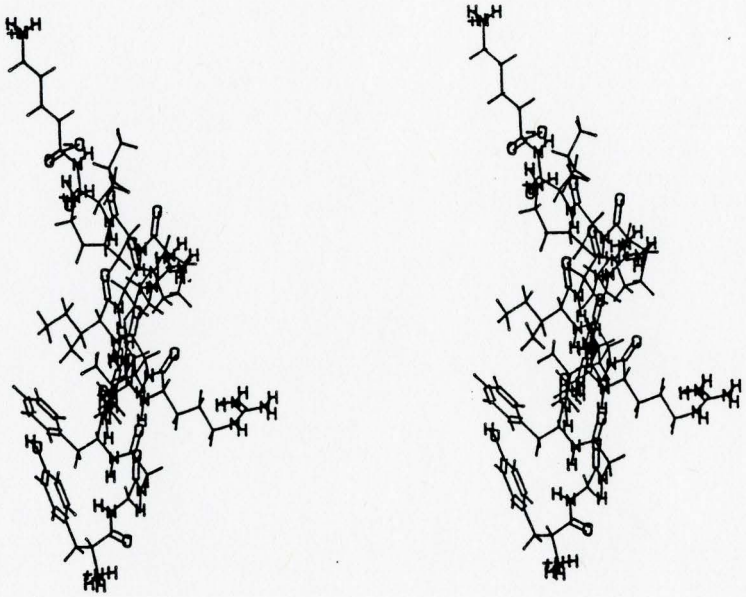

Figure 6.19. A stereoview of the minimized α-helical conformation of dynorphin A-(1-13).

Although not all of the cross-peaks have been assigned (cf. also section 6.1), some important conclusions regarding the membrane-bound conformation could be derived. Possible conformations were subjected to energy minimization (cf. Chapter 2) and proximity relationships were derived from these optimized structures. This distance information was then compared with the NOESY data. The assumption was made that, at the employed mixing time of 500 ms, ^1H, ^1H distances shorter than approximately 5 Å [Braun et al., 1981; Wüthrich et al.,

Table 6.2. Selected interresidue distances of the energy minimized α-helical conformation of dynorphin A-(1-13) and their correlation to 2-D transferred NOE data

Considered protons[a]	Internuclear distance [Å]	NOE expected?[b]	NOE observed?[b]
Tyr^1_δ Phe^4_β	3.4	yes	no
Tyr^1_ϵ Phe^4_β	3.1	yes	no
Tyr^1_ϵ Phe^4_δ	3.6	yes	no
Tyr^1_ϵ Leu^5_β	3.8	yes	no
Tyr^1_ϵ $Leu^5_\delta CH_3$	4.4	yes	no
Tyr^1_β Phe^4_δ	7.1	no	yes
Tyr^1_β Phe^4_ϵ	8.9	no	yes
Phe^4_δ $Ile^8_\gamma CH_3$	3.8	yes	no
Phe^4_δ $Ile^8_\delta CH_3$	3.9	yes	?
Phe^4_ϵ Ile^8 CH_3	3.4	yes	no
Phe^4_ϵ $Ile^8_\delta CH_3$	2.6	yes	?

a : Due to lack of stereospecific assignments (in the case of the β protons and $Leu_\delta CH_3$ groups) and rapid aromatic ring flipping (in the case of $Tyr_{\delta,\epsilon}$ and $Phe_{\delta,\epsilon}$ protons) on the one hand, and the sharp decline of the NOE with increasing distance, only the shortest distance is quoted.
b : "yes" when $r < 5$ Å, "no" when otherwise.

1984] were represented by cross-peaks in the NOESY spectra. In the postulated nonapeptide α-helical conformation (cf. Chapter 1), side-chain protons three or four residues apart could well be sufficiently close to give rise to NOESY cross-peaks. Analysis of the distances of interest the energy-minimized helical structure (Figure 6.19) indicated that a number of such protons would be expected give rise to the respective NOESY connectivities (cf. Table 6.2).

Also included in Table 6.2 are two pairs of protons which were too distant in the minimized α-helical structure to account for NOESY cross-peaks but for which (albeit weak) connectivities were detected in the NOESY experiment (Figure 6.20).

None of the cross-peaks shown in Figure 6.20 were observed in the corresponding experiment on the peptide in D_2O (the expansion is not shown, but this is also evident from Figure 6.3). Consequently, all peaks are assumed to originate from NOEs transferred from the membrane-bound peptide to the free peptide in solution. The presence of the connectivities listed in Table 6.2 between the aromatic Phe^4 protons and the $Ile^8\delta$ methyl protons could not be ruled out because of the overlap of the $Ile^8\delta CH_3$ with the $Leu^5\delta'CH_3$ resonance. Apart from this ambiguity, none of the cross-peaks expected from Table 6.2 could be observed in Figure 6.20.

Thus, the two-dimensional transferred NOE experiment strongly indicated that the membrane-mediated conformation of the tridecapeptide is <u>not</u> a regular α-helical structure. However, the presence of Phe^4 - Leu^5 and the $Phe^4\epsilon,\delta$ - $Tyr^1\beta$ cross-peaks (Figure 6.21) suggested that at least this part of the molecule is

not in an extended conformation. The structure predicted with the Garnier-Robson method cannot account for any of the interresidue cross-peaks observed in Figure 6.20. Further analysis of the data after full assignment of the spectrum and additional data (i.e. the same experiment in H_2O, approximately pH 3, for the inclusion of NH-NOEs) are required for a more detailed picture. Experiments were performed on such samples at 500 MHz (cf. Figure 6.22) and 620 MHz, but the NOESY experiment was not yet successful due to pure solvent suppression of the H_2O resonance. Therefore no additional information could be obtained.

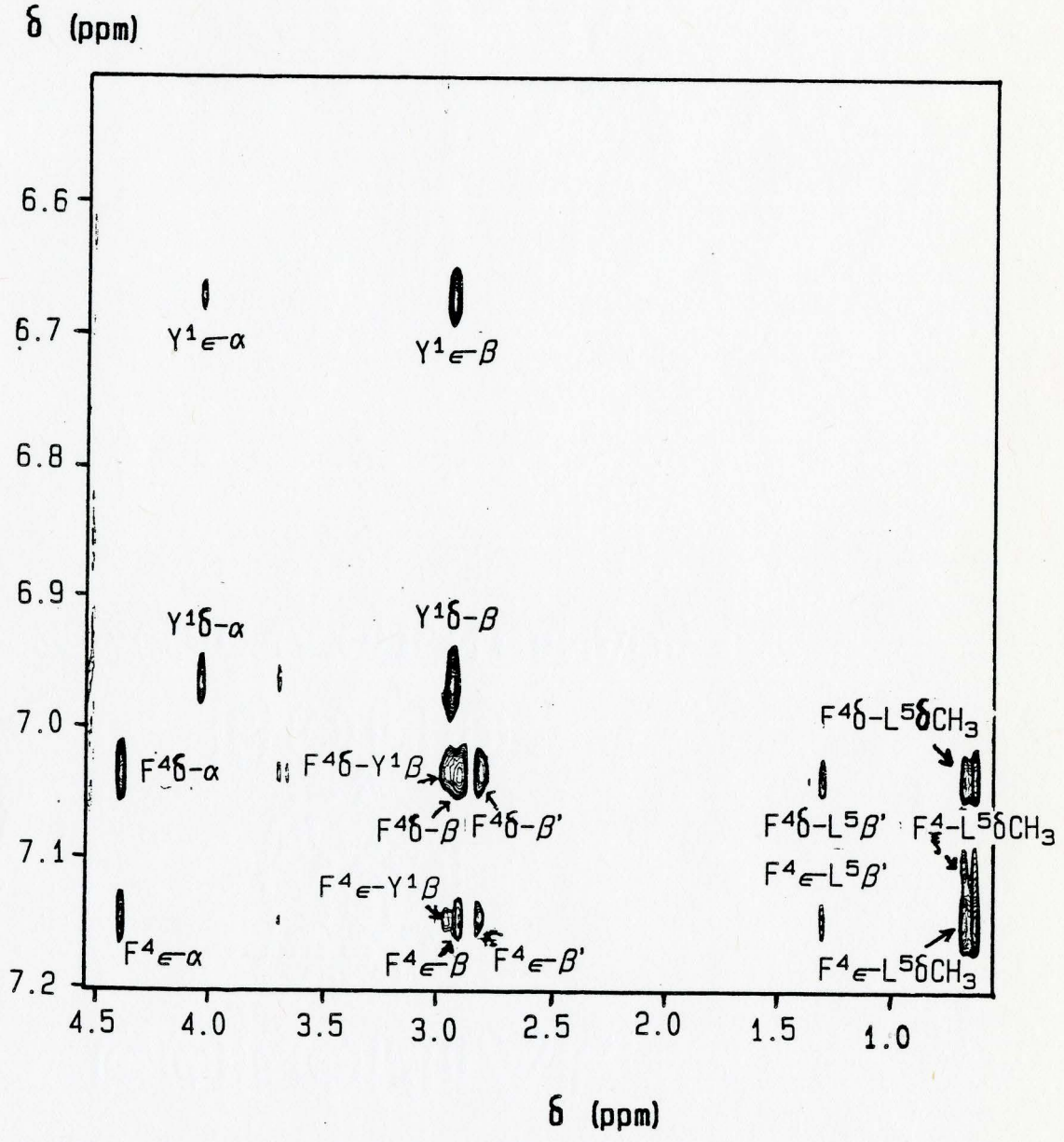

Figure 6.20. An expansion of the 620 MHz pure absorption phase NOESY spectrum of 12.5 mM dynorphin A-(1-13) in a suspension of 50 mM d_{54}-DMPC vesicles in D_2O (Figure 6.17). Intra- and interresidue connectivities from aromatic to aliphatic protons.

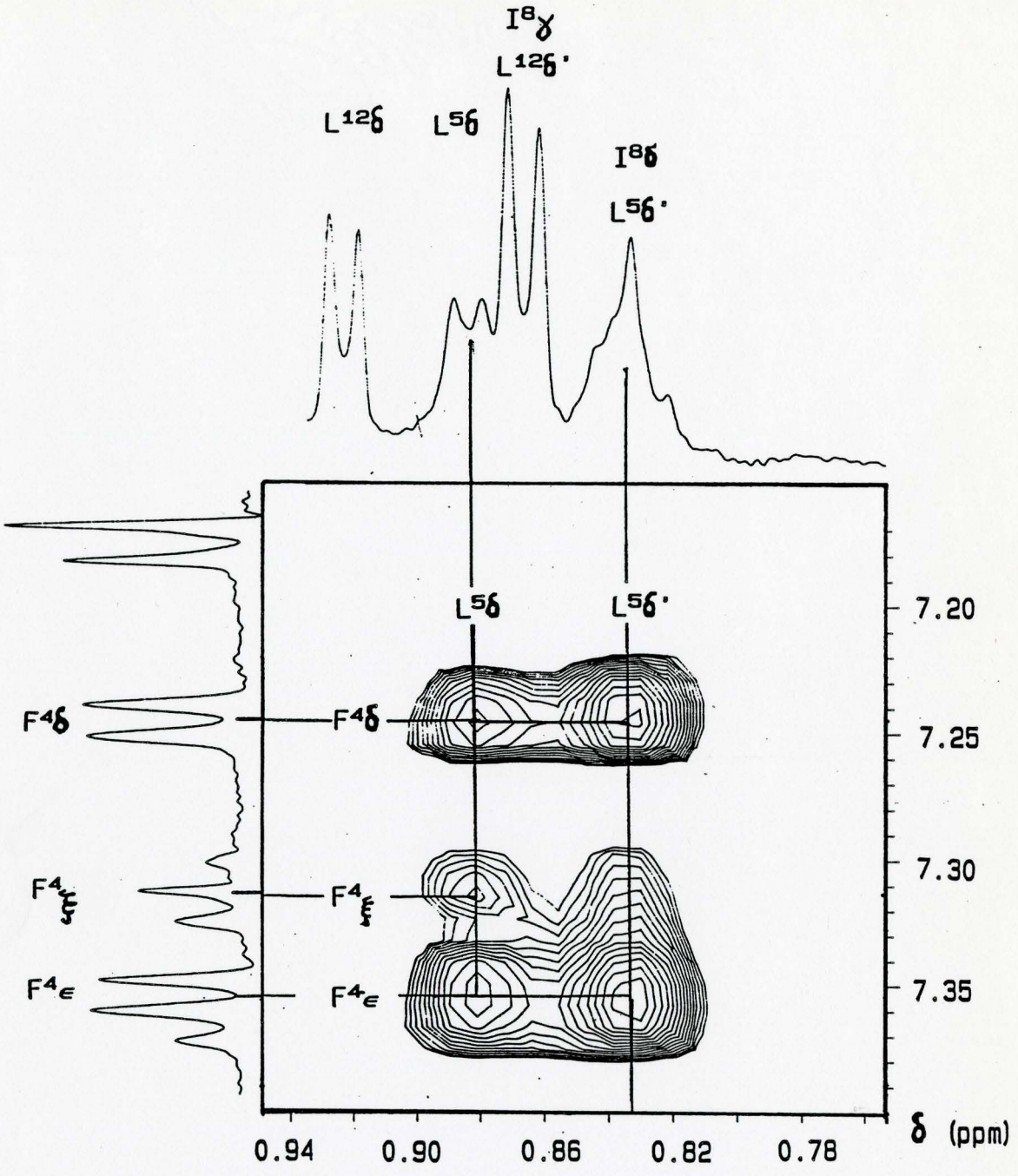

Figure 6.21. An expansion of the 620 MHz pure absorption phase NOESY spectrum of 12.5 mM dynorphin A-(1-13) in a suspension of 50 mM d_{54}-DMPC vesicles in D_2O (Figure 6.20). Interresidue connectivities from aromatic to aliphatic protons.

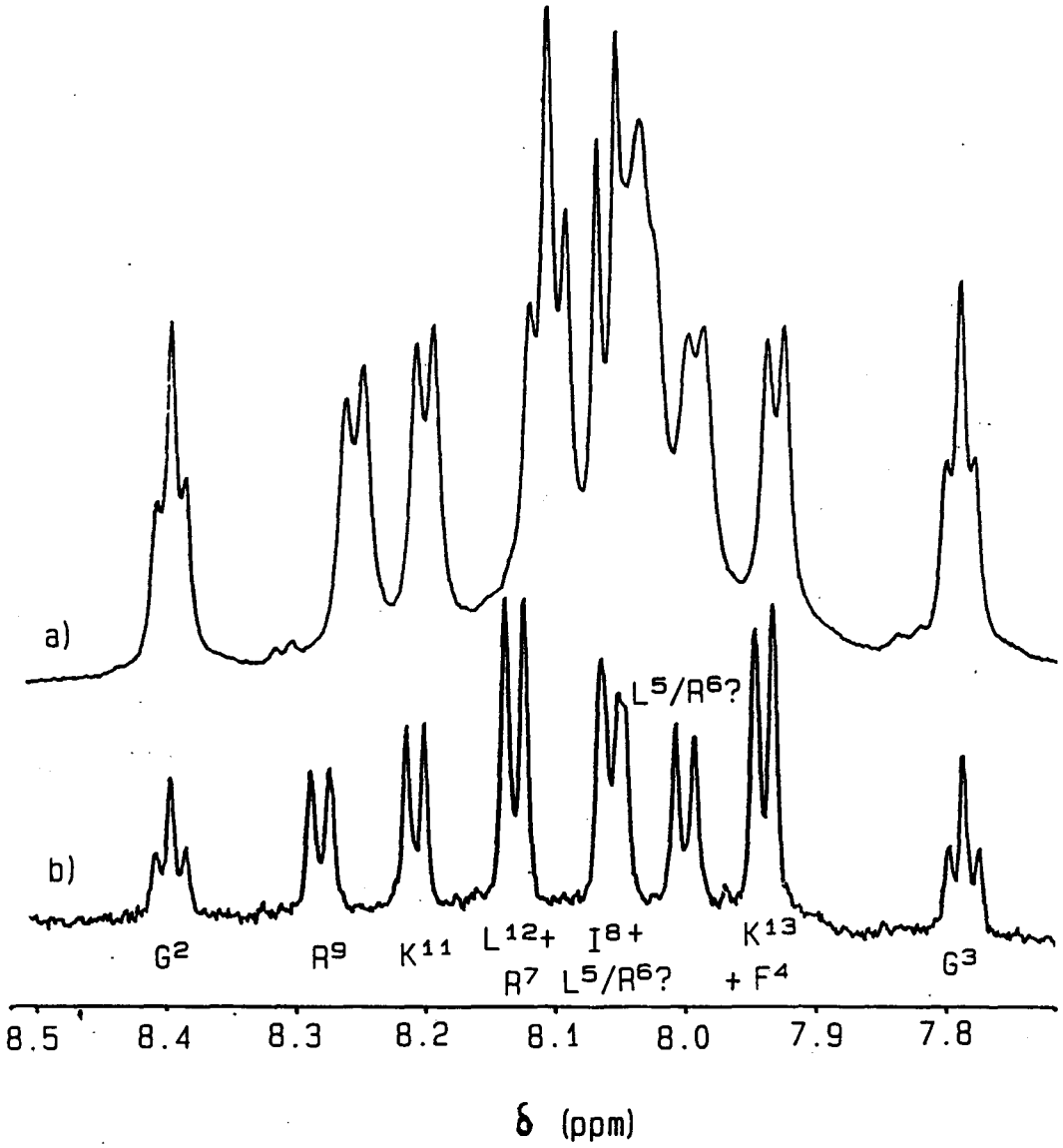

Figure 6.22. The backbone amide proton region of the 500 MHz ^{1}H NMR spectrum of 8 mM dynorphin A-(1-13) in a) a suspension of 32 mM d_{54}-DMPC vesicles in "H_2O", adjusted to pH 2.8; b) in "H_2O", adjusted to pH 2.8 (cf. Table 4.1); The assignments in spectrum b) are derived from a corresponding COSY experiment and comparison with the analogous 620 MHz COSY experiment (cf. Fig 6.6). They are therefore only tentative. Comparison of the 620 MHz spectrum, which was recorded at pH 2.95, with the 500 MHz spectrum (pH 2.8) show that the Lys^{13}NH was especially susceptible to pH-changes. This figure demonstrates that unequivocal assignments regarding the 5 central amides in spectrum a) may be difficult to obtain.

6.4. Dynorphin A-(1-13) in the Presence of Detergent Micelles

An expansion of the 1-D ^{1}H NMR spectrum of 5.6 mM dynorphin A-(1-13) in the presence of SDS detergent micelles is shown in Figure 6.23. The signals in the 1-D ^{1}H-NMR spectrum are considerably broadened compared to the samples in methanolic solution. $^3J_{HN\alpha}$ coupling constants could not be determined. 1-D NOE difference spectra were not successful. No additional experiments were performed on this sample.

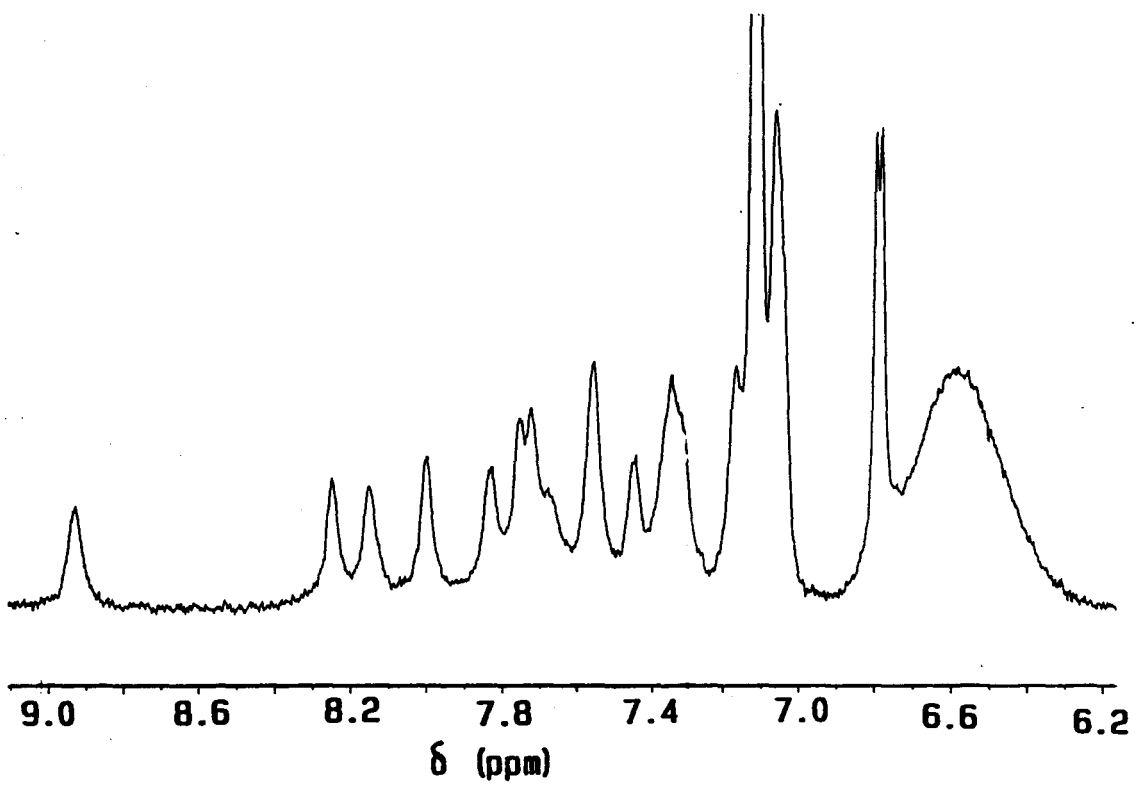

Figure 6.23. ^{1}H NMR spectrum of 5.6 mM dynorphin A-(1-13) in the presence of SDS detergent micelles

7. FROM SPECTRA TO STRUCTURE

7.1. From NMR Spectra to Spatial Structure

There are numerous approaches used to determine the 3-D structure from experimental NMR data [Clore and Gronenborn, 1989]. Most of these strategies employ various combinations of energy minimization and molecular dynamics. A summary of proteins and peptides whose three-dimensional structures have been determined by NMR has recently been published [ibid].

7.2. Methods for Molecular Modelling

Molecular mechanics and molecular dynamics simulations were performed on a personal IRIS computer (Silicon Graphics, Inc.) with the BIOGRAF software package (BioDesign, Inc.), Version 2.09.

7.2.1. Molecular Mechanics

We employed the DREIDING force field [Mayo et al., 1989], in which the force field parameters are estimated using general rules based only on the

element and its hybridization. Although the AMBER force field would seem superior as it was specifically designed as a force field for proteins (and nucleic acids), the BIOGRAF implementation of AMBER allows only non-carbon-bonded hydrogens. Carbon-bonded hydrogens are only implicitly included as CH, CH_2, and CH_3 spheres ("united atom field"). This is not advantageous for introducing ^1H-^1H distance restraints.

A more efficient combination of minimization algorithms than the one used in section 2.1.4 was employed. The starting structure was initially minimized using a steepest descent algorithm [Mackay et al., 1989, p. 323f.; Press et al., 1986, p. 302f.]. The steepest descent method converges rapidly when the first derivatives of the energy are large, i.e. when the energy is far from the minimum, but converges slowly once the atomic energy derivatives become smaller, i.e., when the energy is close to a minimum [Burkert and Allinger, 1982, p. 66]. The minimization was continued with a conjugate gradient algorithm [Fletcher and Reeves, 1964; Mackay et al., 1989, p. 325f., Press et al., 1986, 301-307].

A pre-molecular dynamics minimization was judged to have converged when the root-mean-square value of the atomic energy derivatives (gradient RMS) was at least below 0.1 kcal/Å·mol (unless otherwise stated). Although this represented a much more crude convergence criterion than the 0.04 kJ/Å·mol (approx. 0.01 kcal/Å·mol) employed in section 2.1.4, it was sufficient to ensure that the molecule was adequately relaxed before beginning the molecular dynamics run. This usually required 50 iterations with the steepest descent algorithm and about 700 conjugate gradient iterations.

The convergence criterion for post-molecular dynamics minimizations was a gradient RMS of under 0.03 kcal/Å·mol.

7.2.2. Molecular Dynamics

Molecular dynamics [Karplus and McCammon, 1983] can be used to compute the dynamics of the peptide system [Hagler, 1985]. These include structural fluctuations and conformational transitions as well as time-averaged structural[1] and energetic properties [ibid]. While energy minimization is achieved by computing the forces on the atoms and changing their positions to minimize the interaction energies, molecular dynamics are realized by moving the atoms in response to these forces. Newton's third law of motion, $F = m \cdot a$, is set up for each atom in the system and integrated forward in time. The velocity and position of each atom is updated after each time step (in our case $t = 10^{-15}$ s) to a new velocity using a standard Verlet [1967] algorithm.

However, it is not possible to run simulations long enough to ensure that all of conformational space is sampled [Bensen et al., 1990]. Therefore, dynamic simulated annealing [Clore and Gronenborn, 1989], involving high temperature dynamics is used to increase the sampling of conformational space by enhancing

---

[1] For instance, the time averaged value $\langle {}^3J_{HN\alpha} \rangle$ of the respective vicinal coupling constants can be obtained by monitoring the torsional angle ϕ along the dynamic trajectory of the peptide system [Hagler, 1985]. Molecular dynamics can also be used to detect conformational heterogeneity and obtain crude estimates to the relative populations of the conformations involved [Kessler et al., 1988b].

the likelihood of transitions between (local) minima. The molecular dynamics parameters employed are given in section 7.4.

7.3. Summary of Interresidue NOE's Observed in Chapter 6

The 7 interresidue NOE's detected in Chapter 6 (cf. Figure 7.1) and used for the construction of a model are very few compared to the average of 10 NOE's per residue identified for the best NMR structures of proteins [Wagner, 1990] and to the 99 interresidue NOE's obtained for the eleven-residue cyclic peptide cyclosporin A in $CDCl_3$ [Kessler et al., 1990].

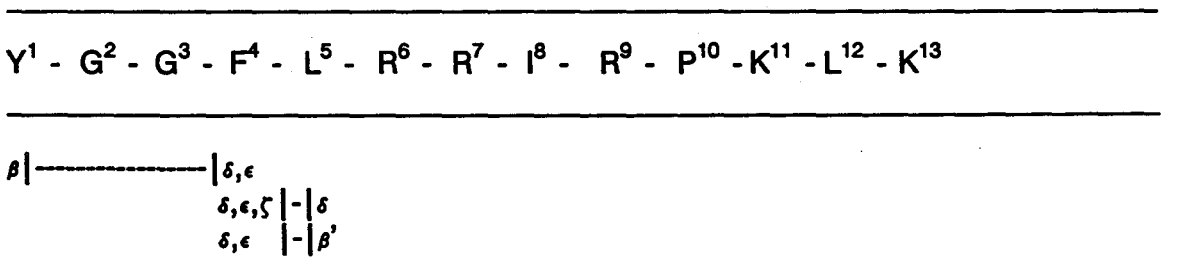

Figure 7.1. Sequence of dynorphin A-(1-13) with a survey of interresidue NOE's.

7.4. Building a Model

As the NOE-derived restraints only applied to the N-terminal end of the molecule, the conformation of the C-terminal half of the molecule was modelled without experimental input data. In this sense, the aim of the model building was two-fold. One was to translate the observed distance relationships in the N-terminal part of the peptide into a molecular structure. The second was to perform a conformational search of the rest of the peptide in order to obtain a set of conformations which could be distinguished by NMR-observable properties. We employed an approach analogous to that pursued by Hagler and coworkers for a conformational search of ANF [Mackay et al., 1989].

7.4.1. Generating a Starting Geometry

A starting geometry was generated by building the sequence into an extended conformation using standard amino acid bond lengths, angles and side chain dihedrals. A solvent was not included as we were interested in the membrane-bound form. Without a specific membrane model, we had several options. One was to complement the charges on the Arg and Lys side chains by introducing fixed negative charges spaced at 8 Å distances, as this is the distance between phosphate groups in phospholipid monolayers [Ovchinokov and Ivanov, 1975]. This work is still in progress.

In view of knowing only the relative distances, but not the relative positions of such negative charges, the other alternative was to restrain only the distances between successive charges, but not to fix their positions. This was the option which received top priority.

7.4.2. Conformational Energy Searches

The NOE-derived interresidue distance restraints[2] (cf. Figure 7.1) were introduced (cf. Table 7.1) with force constants set to 1000 kcal/(mol·Å^2) and the respective connecting backbone and side chain torsional angles were varied in numerous conformational energy searches.

In general two, three, or four torsional angles were varied simultaneously. Initially, full 360° rotations were searched in 40° intervals followed by finer searches (2.5° intervals) at indicated potential energy surface minima. A starting structure which satisfied all restraints with 3.5 ± 1 Å was then subjected to energy minimization (50 iterations steepest descent, 329 iterations conjugate gradient, restraining the distances listed in Table 7.1 at their current values) until the pre-molecular dynamics convergence criterion (gradient RMS < 0.1 kcal/(Å·mol)) was met.

---

[2] Additional restraints were introduced to avoid the formation of cis peptide bonds (12 torsional restraints with force constants at 20 kcal/mol) and D-amino acid residues (11 inversion restraints with force constants at 40 kcal/(mol·radian^2)) and to keep the $Tyr^1NH_3^+$ and $Lys^{13}COO^-$ from interacting with other negative and positive charges, respectively (4 distance restraints with force constants at 50 kcal/(mol·Å^2). These and the NOE-derived interresidue distance restraints were kept throughout the whole process of model building.

Table 7.1. Introduced NOE-derived interresidue distance restraints.

Hydrogen atoms	Restrained distance for conformational energy search (target values)	Restrained distance for mechanics and dynamics (current values)
$Tyr^1{}_\beta$-$Phe^4{}_\delta$	3.5 Å	3.99 Å
$Tyr^1{}_\beta$-$Phe^4{}_\epsilon$	3.5 Å	2.98 Å
$Leu^5{}_\beta$-$Phe^4{}_\delta$	3.5 Å	4.06 Å
$Leu^5{}_\beta$-$Phe^4{}_\epsilon$	3.5 Å	3.94 Å
$Leu^5{}_\delta CH_3$-$Phe^4{}_\delta$	3.5 Å	3.29 Å
$Leu^5{}_\delta CH_3$-$Phe^4{}_\epsilon$	3.5 Å	2.54 Å
$Leu^5{}_\delta CH_3$-Phe^4	3.5 Å	4.27 Å

7.4.3. High Temperature Dynamics

This structure was then subjected to the molecular dynamics runs indicated in Table 7.2. Temperature changes were performed by heating or cooling by 20 K/0.1 ps. 20 Picoseconds were allowed for equilibration at the respective temperatures. All runs were quenched, i.e. subjected to 10 steps of conjugate gradient energy minimization in 0.1 ps intervals. The time step employed was 0.001 ps. The trajectory was updated every 0.1 ps except for the 100 ps runs at 900 K, where the update frequency was 1 ps. The first run was performed for equilibration of the system, and the second run for conformational analysis.

Table 7.2. Summary of the parameters for the various molecular dynamics runs performed.

Run #	Temperature [K] Initial	Final	Duration [ps]
1	0	300	1.5
2	300	300	20
3	300	600	1.5
4	600	600	20
5	600	900	1.5
6	900	900	100
7	900	900	100
8	900	300	3
9	300	300	20
10	300	300	20

With a time step of 10^{-15} s, 100 000 conformations were sampled during one 100 ps run, but only every 1000th of these conformations was written to the trajectory file, reducing the number of structures to be analyzed to 100. In order to classify the similarity between the 100 different conformers of the second run, the RMS deviations from the atom positions of each conformer were computed for all the other conformers [cf. Mackay et al., 1989, p. 350]. Conformers with an RMS deviation of less than 2 Å were judged to be similar, and all RMS deviations below this threshold value were plotted in a 100 x 100 matrix (cf. Fig 7.2).

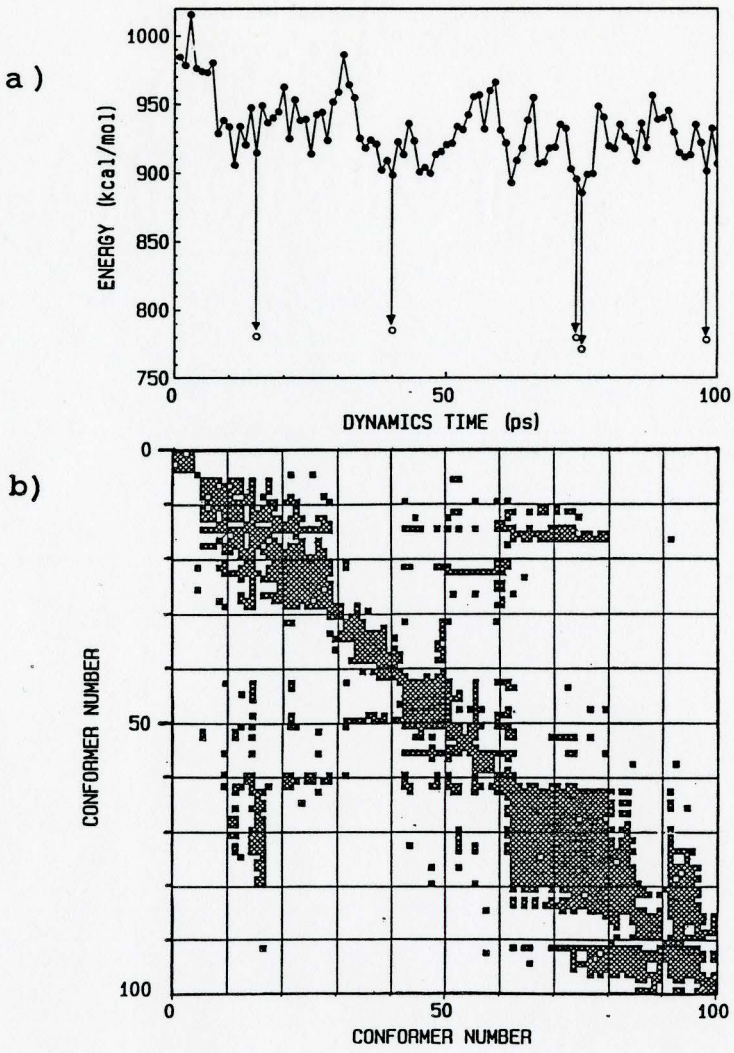

Figure 7.2. Minimized energies and RMS deviations of the conformers of the second 100 ps molecular dynamics run at 900 K.
a) The filled circles represent the minimized energies for each of the 100 minimized structures (10 iterations conjugate gradient, RMS gradient ≈ 3 - 4 kcal/(Å·mol)). The open circles show the lowest energy found by annealing representative (cf. b) structures at 300 K for 20 ps and minimizing the lowest energy conformer of that run to an RMS gradient of under 0.03 kcal/(Å·mol), cf. Table 7.3.
b) A matrix of RMS deviations between the atoms of dynorphin A-(1-13) for 100 minimized conformers with each other. RMS deviations below are plotted. The conformer number corresponds to the time in ps at which it was extracted.

7.4.4. Annealing and Energy Minimization

Representative structures were found at 15, 40, 74, 75, and 98 ps, respectively. These conformers were extracted from the trajectory and subjected to cooling from 900 K to 300 K in 3 ps and annealing at 300 K for 20 ps, as indicated in Table 7.2, followed by energy minimization to an RMS gradient of under 0.03 (cf. Fig. 7.2 and Tab. 7.3). As high temperature dynamics resulted in considerable strain on bonds and angles [Mackay et al., 1989], the annealing process was important. It removed 80 to 105 kcal/mol during cooling and

Table 7.3. Representative conformers extracted from the second 100 ps molecular dynamics run at 900 K and their further processing.

Conformer	A	B	C	D	E
extracted at time [ps]	15	40	74	75	98
Energy [kcal/mol]	914.7	898.3	895.2	885.3	901.2
20 ps run 300 K conformer extracted at time [ps]	13.1	17.0	20.0	18.5	18.8
Energy [kcal/mol]	809.1	808.8	814.3	800.1	808.5
Energy minimization # iterations	2806	601	1236	3137	1052
Energy [kcal/mol]	780.6	785.1	779.5	771.0	777.9

equilibration. The relative ordering of the representative conformers with respect to their energy changed during the annealing process (cf. Table 7.3). After energy minimization, conformers A and E were found to be visually similar, as were conformers C and D. Therefore only conformers B, D, and E were compared in Figure 7.3. The only striking difference was the position of the Tyr^1 ring, although some of the backbone torsional angles were markedly different[3]. The remaining analysis concentrated on conformer D as this was the energetically most favourable structure.

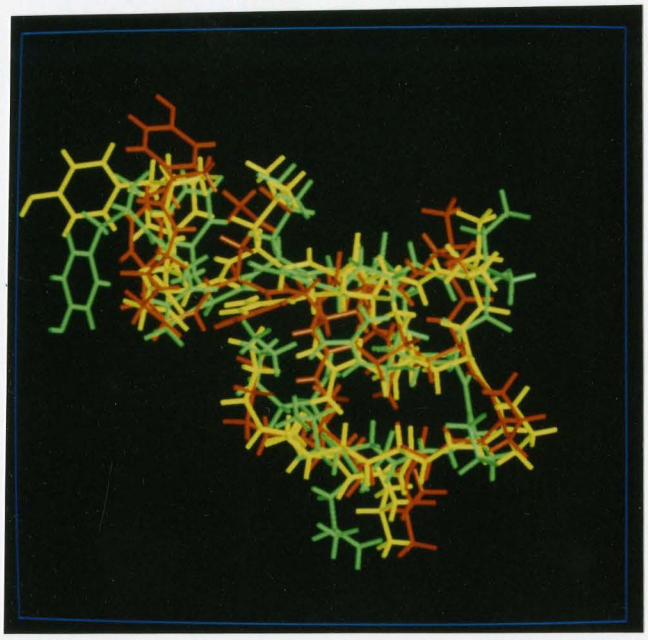

Figure 7.3. Conformers B (green), D (red) and E (yellow) after annealing and energy minimization. The only striking difference between the conformers is the position of the tyrosine ring.

[3] This correlates well with the observation that more than one backbone conformation may be tolerated at opioid receptors [Schiller, 1984].

7.4.5. Final Molecular Dynamics Run without NOE-Derived Distance Restraints

A final 20 ps molecular dynamics run at 300 K (run #10 in Table 7.2) was performed on the final structure of run #9 after inactivating all seven NOE-derived distance restraints. All other restraints remained active. The results are shown in Fig. 7.4. Although the formally restrained protons show a distinct tendency to move apart, they are within the threshold of 5 Å for the observation of NOE's in at least one of the two lowest energy conformers of run (cf. Table 7.4). This information adds feasibility to the proposed conformation of the N-terminal part of the molecule. However, it would not necessarily be required for the respective protons to remain within NOE-observable distances from each other since forces not included in the simulation, but encountered upon binding to phospholipid, may lead to stabilizing the observed spatial proximity.

Table 7.4. Shortest distances in the two conformers of minimum energy during the final 20 ps run at 300 K after inactivating the NOE-derived distance restraints.

Conformer extracted at time [ps]	14.4	16.3
Energy [kcal/mol]	793.4	793.8
Shortest distance [Å]		
Tyr^{1}_{β}-Phe^{4}_{δ}	4.6	5.3
Tyr^{1}_{β}-Phe^{4}_{ϵ}	3.5	4.5
Leu^{5}_{β}-Phe^{4}_{δ}	4.0	4.3
Leu^{5}_{β}-Phe^{4}_{ϵ}	3.9	4.3
Leu^{5}_{δ}-Phe^{4}_{δ}	4.8	4.5
Leu^{5}_{δ}-Phe^{4}_{ϵ}	4.6	3.5
Leu^{5}_{δ}-Phe^{4}	5.1	4.5

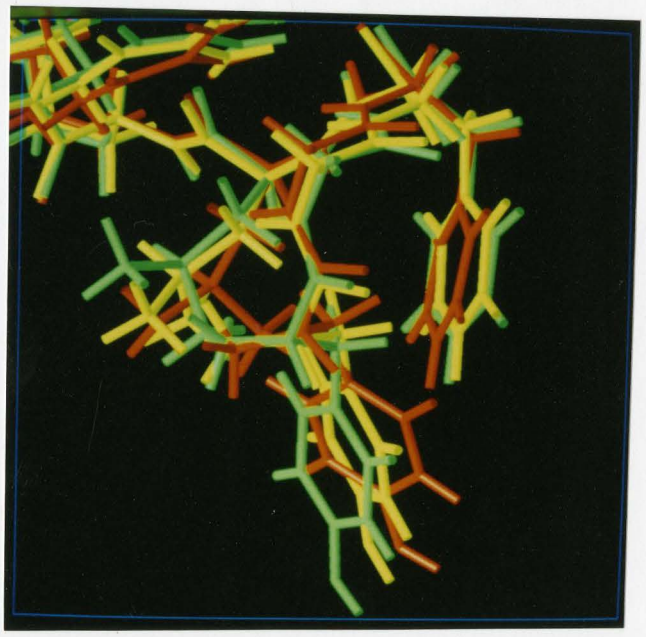

Figure 7.4. Selected structures of the final 20 ps molecular dynamics run at 300 K. The final structure from run#9 (cf. Table 7.2) was extracted, and the NOE-derived restraints removed. Red: The starting structure obtained after energy minimization for 50 conjugate gradient iterations (RMS gradient = 1.3). Yellow: The conformer at 14.4 ps. Green: The conformer at 16.3 ps.

7.5. The Model and its Correlation to Experimental Data

7.5.1. The Model

A space-filling model of conformer D (cf. section 7.4.4) is shown in Figure 7.5. This model of the membrane-mediated conformation of dynorphin A-(1-13) is tentative for several reasons. Firstly, only very little experimental data could be used as constraints for the construction of the model (cf. section 7.3). Secondly, the possibility of incorrect folding of the peptide backbone is an inherent limitation to molecular dynamics [Nilges et al., 1988]. Other reasons are discussed below.

This tentative model displays a high degree of amphiphilicity with the side chains of Tyr^{1}, Phe^{4}, Leu^{5}, and Ile^{8} constituting the hydrophobic side of the molecule and those of Arg^{6}, Arg^{7}, Arg^{9}, Lys^{11}, and Lys^{13} making up the hydrophilic region. The only exception is Leu^{12}, which is not incorporated into the hydrophobic part, but, on the other hand, does not interfere with the hydrophilic residues. The negative charges, originally spaced out with the positively charged side chains in an extended manner, were also affected by the folding of the molecule, but are still spaced out at 8 Å distance. They are situated in the plane formed by the hydrophilic residues.

Although the backbone is folded, there is no tight turn at Pro^{10} as is predicted by the GOR method (cf. Chapter 2)[4]. Instead, the folding is initiated at Ile^{8}, with a second kink at Pro^{10}. Therefore the backbone from residues 11 to 13 is too distant from the backbone from residues 5 to 7 to give rise to stabilizing intramolecular hydrogen bonds (cf. Fig. 7.6). The conformation is apparently mainly stabilized by the matrix of negative charges.

[4] Preliminary molecular dynamics experiments employing the approach of Mackay et al. [1989] by setting all amino acids to be in their neutral states (in order to stop electrostatic interactions between the side chains from dominating the search) also demonstrate the folding of the extended backbone at Pro^{10} and the formation of a tight turn.

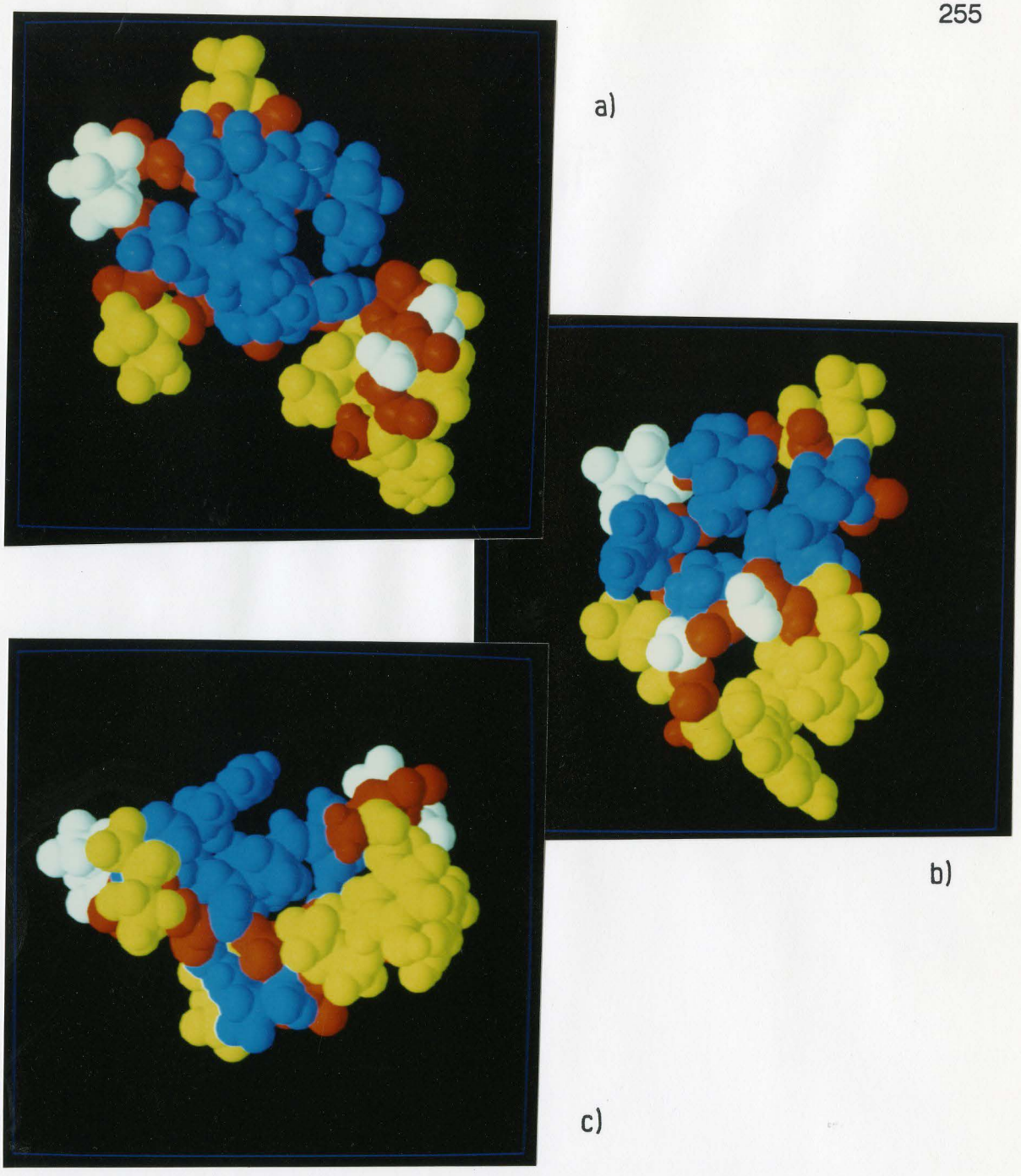

Figure 7.5. Tentative model of the membrane-mediated conformation of dynorphin A-(1-13) in a space-filling representation. The colour-coding is as follows: red = peptide backbone; yellow = hydrophobic residues (Tyr, Phe, Leu, Ile); blue = hydrophilic residues (Arg, Lys); white = ambivalent residues (Gly, Pro). The relative views are: a) xy-projection; b) yz-projection viewed from the right of a); c) xz-projection viewed from the bottom of a).

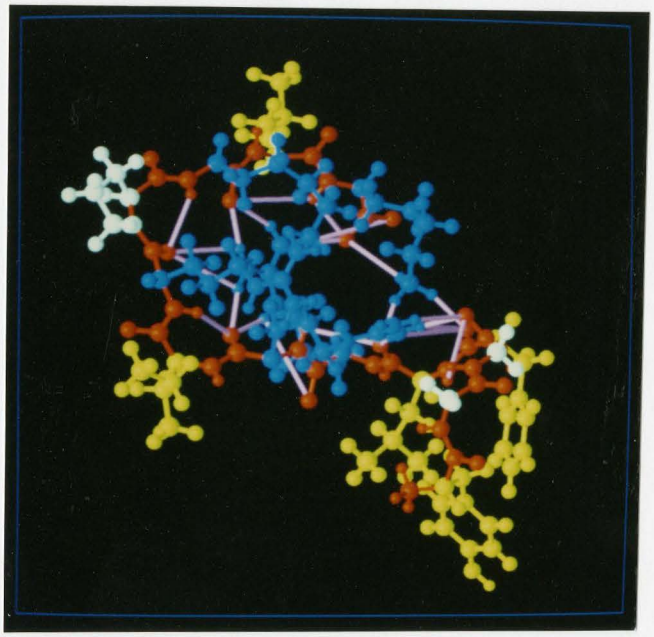

Figure 7.6. Tentative model of the membrane-mediated conformation of dynorphin A-(1-13) in a ball-and-stick representation. The intramolecular hydrogen bonds are coloured in purple. All other colours are as in Fig. 7.5.

7.5.2. Correlation of the Model to Experimental Data

7.5.2.1. Correlation to Transferred NOE Data

As the restrained distances listed in Table 7.1. for the construction of the model were derived from the transferred NOE data, the model correlates well with the results from these experiments.

7.5.2.2. Correlation to Methanol Data

Torsional angles ϕ and α-NH distances of the model were extracted and the respective $^3J_{HN\alpha}$ coupling constants and sequential-to-intraresidue ROE ratios were calculated as described in Chapter 5. The results were compared to the experimentally observed data (cf. Table 7.5). Correlation is obtained only for the Gly^2, Phe^4 $^3J_{HN\alpha}$ and for the Arg^7 sequential-to-intraresidue ROE intensity ratio. The coupling constants calculated for Arg^7 and Leu^{12} are higher than those experimentally observed. The lower experimental values can be explained by motional averaging.

The most striking discrepancies are observed for the Ile^8 residue. The $Ile^8\alpha$-Arg^9NH distance is too large and the calculated $^3J_{HN\alpha}$ coupling constant is too small to correlate with the methanol data. This is due to the initiation of backbone folding at the Ile^8 residue.

Table 7.5. Torsional angles ϕ and α-NH distances in the tentative model and their correlation to experimentally observed data for dynorphin A-(1-13) in methanolic solution (Chapter 5).

Residue	ϕ_{Model} [°]	Calculated $^3J_{HN\alpha}$ [Hz] Pardi et al.[a]	Bystrov[a]	Observed $^3J_{HN\alpha}$ [Hz]	Correlation?[b]
Gly^2	78		14.3[c]	14.4[c]	+
Gly^3	175		6.7[c]	12.3[c]	-
Phe^4	-83	7.1	7.3	7.1	+
Arg^6	-67	5.1	4.5	7.0	-
Arg^7	-99	8.8	9.6	7.0	-
Ile^8	-76	6.2	6.1	8.1	-
Arg^9	-74	6.0	5.8	7.2	-
Lys^{11}	-77	6.3	6.2	7.6	-
Leu^{12}	-116	9.7	10.9	7.5	-

Residue	$d_{N\alpha}(i,i)$ [Å]	$d_{\alpha N}(i,i+1)$ [Å]	$ROE_{seq.}/ROE_{intr.}$[d] Calculated	Observed	Correlation?[b]
Arg^7	2.78	2.37	2.6	≈ 2	+
Ile^8	2.68	3.64	0.16	≈ 4.5	-
Arg^9	2.63	3.64	0.16	≈ 3	-

a = calculated by Bystrov's [1976] and Pardi et al.'s [1984] equations, respectively (cf. Fig. 5.30).
b = "+" = correlation, "-" = no correlation.
c = over-all coupling constant $\Sigma^3J_{HN\alpha}$ [Bystrov et al., 1973].
d = calculated from: $ROE_{seq.}/ROE_{intr.} = (r_{seq.}^{-6})/(r_{intr.}^{-6})$, cf. section 5.4.1.
e = In the case of Arg^9, the intraresidue ROE is compared to the preceding sequential ROE $Ile^8\alpha$-Arg^9NH due to the lack of a Pro^{10}NH proton.

The folded structure is apparently mainly stabilized by the corresponding negative charges (vide supra). In methanolic solution, counterions will be very dilute and not restrained to distances of approximately 8 Å. Therefore it is not

surprising the conformation of dynorphin A-(1-13) in methanol does not correlate with the tentatively proposed membrane-mediated structure. It is plausible that the accuracy of the determination of secondary structure by CD (Chapter 3) is not sufficient to detect such a difference in conformation, especially if the main discrepancy involves a single residue and is between an extended and a turn-like conformation.

7.5.2.3. Correlation to Other Data

The discovery of the high potency of the synthesized cyclic dynorphin analogue [$Cys^{5,11}$]-dynorphin A-(1-11)-amide [Kawasaki et al., 1990] indicates that the folding of the backbone between residues Arg^{6} and Pro^{10} in our tentative model may well have a biological significance. Other findings are discussed in section 8.2.

7.5.3. Characteristics for Experimental Verification

The presented model must be verified by additional experiments. Of particular interest are experiments which include observation of the backbone amide protons. The most obvious choice would be to try to improve the transferred-NOESY studies on the peptide in d_{54}-DMPC/H_2O, pH 3. A prerequisite is, however, that a sufficient signal-to-noise ratio and adequate solvent sup-

pression can be achieved. The advantage of this model is that it spells out exact criteria for which can either be verified or refuted by future experiments. The distances listed in Table 7.6 should give rise to observable NOESY connectivities between the respective protons.

Table 7.6. Characteristics for experimental verification. Internuclear distances leading to characteristic NOE connectivities.

Protons involved	Distance [Å]
Tyr^{1}_{β}-$Gly^{2}NH$	2.60
$Gly^{2}NH$-$Gly^{3}NH$	2.93
$Gly^{3}NH$-Gly^{3}_{α}	2.68
$Phe^{4}NH$-Phe^{4}_{α}	2.65
$Leu^{5}NH$-Leu^{5}_{α}	2.67
Leu^{5}_{α}-$Arg^{6}NH$	2.45
$Arg^{6}NH$-Arg^{6}_{α}	2.64
Arg^{9}_{β}-$Lys^{11}NH$	3.06

8. SUMMARY

8.1. Summary of the Results

Hydrophobic moment, helix probability and four-state secondary structure prediction profiles indicated that dynorphin A-(1-13) is unlikely to adopt an α-helical conformation on the basis of amphiphilicity, in the presence of anionic and zwitterionic lipids, and on the basis of statistical occurrences in globular proteins, respectively. This was confirmed by CD spectra of dynorphin A-(1-13) in dispersions of DMPG bilayers. CD spectra also indicated that the aqueous-membraneous interphase can be mimicked by methanol.

The results of the NMR studies are summarized in Figure 8.1. The resonances of all of the non-labile backbone amide protons in the ^{1}H NMR spectrum of dynorphin A-(1-13)-tridecapeptide in methanolic solution were unambiguously assigned (cf. Table 5.9). $^3J_{HN\alpha}$ coupling constants were not indicative of rigid ϕ angles corresponding to an α-helical or a β-strand conformation, but seemed to represent averages over numerous rotational states of the backbone. The values were, however, consistent with those derived for the Gly^2 and Arg^7 ϕ angles of the reference α-helix and the Arg^9, Lys^{11}, and Leu^{12} ϕ angles of the "GOR" reference model. The observation of sequential α-NH

	Y^1	G^2	G^3	F^4	L^5	R^6	R^7	I^8	R^9	P^{10}	K^{11}	L^{12}	K^{13}
a)													
$^3J_{HN\alpha}$ (Hz)	-	7.5 6.9	6.4 5.9	7.1	n.d.[e]	6.6	7.0	8.1	7.2	-	7.6	7.5	nd
7.5±1 Hz[c]				▲		▲	▲	▲	▲		▲	▲	
≥ 7 Hz[d]				■			■	■	■		■	■	
χ_1 Rotamer Populations													
all < 70 %	▲	-	-	▲	▲	n.d.	▲	▲	▲	-	▲	n.d.	nd
NH Exchange k' (10^{-3} min^{-1})													
= 2.5 to 9	-	n.d.	n.d.	n.d.	n.d.	■	■	■	■	-	■	n.d.	nd
Temperature Dependence $\Delta\delta_{NH}/\Delta T$ =													
-6±2 ppb/°C	-	■		■	■	■	■	■	■	-	■	■	■
ROE													
1. α(i)-NH(i+1)				■	■	■	■	■		■	■		
2. NH(i)-α(i)							■	■	■				
1 > 2							■	■	■[f]				
NOE													
α(i)-NH(i+1)			■	■	■	■	■	■		■	■	■	
NH(i)-α(i)						■	■	■		■			

	β												
b)	|	----------	|	δ,ϵ								
Interresidue				δ,ϵ,ζ	|	-	|	δ				
NOE's				δ,ϵ	|	-	|	β'				

Figure 8.1. Sequence of dynorphin A-(1-13) with a survey of the most important results: a) in methanol (Chapter 5): $^3J_{HN\alpha}$ coupling constants, rotamer populations, NH exchange rates, temperature coefficients, intraresidue and sequential NOE's and ROE's; ▲ = consistent with motional averaging, ■ = consistent with an extended structure; b) in aqueous DMPC bilayers (Chapter 6): transferred interresidue NOE's. NOTES: c) criterium for conformational heterogeneity (cf. section 4.1.4 and Table 5.11); d) criterium for extended/β-strand conformation (cf. Fig. 5.30); e) n.d. = not determined; f) cf. p. 166.

ROE's stronger than the corresponding intraresidue NH-α ROE's for Arg^7, Ile^8, and Arg^9 indicated a β-strand or extended conformation for this part of the molecule. Temperature dependences and deuterium exchange rates of the backbone amide protons demonstrated that the amide protons were all solvent accessible.

χ_1 side chain rotamer analysis revealed no single preferred conformation of the side chains. The experimental NOE observations showed a poor correlation to the two energy-minimized reference models constituting an extended conformation with two reverse turns at Gly^2 and Pro^{10}, and an α-helix, respectively. No interresidue NOE's (apart from the sequential α-NH (i, i+1) NOE's) were observed. In summary, there was some indication of an extended or β-structure from Arg^7 to Arg^9, but most of the criteria listed in section 4.1.4 for the dominance of a single conformation were not met.

The transferred nuclear Overhauser effect studies on dynorphin A-(1-13) in an aqueous dispersion of DMPC bilayers revealed a more compact structure in the N-terminal part of the molecule with a total of 7 interresidue NOE's observed between the Tyr^1, Phe^4, and Leu^5 side chains. More information will be likely to be obtained by changing from deuterated to protonated solvent as then interresidue NOE's will include the backbone amide protons.

On the basis of the interresidue NOE's observed for the phospholipid-bound peptide, a model was constructed using annealed high temperature restrained molecular dynamics and spatially restricted corresponding negative

charges for the simulation of an anionic phospholipid surface. This model displayed a high degree of amphiphilicity but did not correlate well with the results of the structural analysis of the methanol sample, especially for the Ile^{8} residue. This was attributed to the lack of spatially restricted negative charges in methanolic solution. The feasibility of the proposed structure of the N-terminal segment was demonstrated by a molecular dynamics run in which none of the NOE-derived constraints were active. A list of characteristic distances which have to be confirmed by future experiments has been compiled.

8.2. Relationship to Other Results

A β-structure in the central part of the molecule as indicated by the ROESY/2-D CAMELSPIN experiments on the peptide in methanol would correlate well with the hydrophobic moment profile. Indeed, such a β-structure has been proposed for residues Arg^{7} to Asp^{15} in the case of dynorphin A-(1-17) by Taylor and Kaiser [1986] and experimentally demonstrated for a model dynorphin peptide [Vaughn and Taylor, 1989]. However, we have no evidence for a β-structure beyond Arg^{9}. On the contrary, Taylor [1990] has shown that a peptide model devoid of Pro^{10} has a more pronounced β-strand forming capacity but is less potent in biological assays, thus indicating that only a limited region of β-structure is beneficial for biological effectiveness. The existence of a reverse turn at Pro^{10}, as predicted by the GOR method, can not be proven with our

spectroscopic data. This is not surprising since the identification of turns is less reliable than the identification of other structures both by CD [Chang et al., 1986, p.13] and NMR spectroscopy [Wüthrich, 1986, p. 166]. However, in a review on FT-IR, Surewicz and Mantsch [1988] have pointed out that amide I bands around 1665 cm^{-1} are regarded as being highly characteristic of turns. The IR spectrum of dynorphin A-(1-13) on a POPC membrane surface [Erne et al., 1985] displays an amide I band at 1665 cm^{-1}. Originally the authors took this as evidence for the formation of a short helix consisting of six to nine amino acid residues. Surewicz and Mantsch [1988], however, state that an α-helical segment would exhibit an amide I band between approximately 1650 and 1658 cm^{-1}. Therefore, the aforementioned IR-ATR spectrum could be interpreted as an indication for the occurrence of turns, most probably at Gly^2 and Pro^{10}, but perhaps also at Ile^8, as is proposed by our tentative model.

Finally, one must be aware of the fact that the membrane-bound conformation may be different from the conformation the peptide adopts when intercalating into the membrane. Through FT-IR and CD studies, Briggs et al. [1986] have shown that signal peptides undergo a transition from "random coil" to β-structures at the membrane surface, but subsequently an α-helical conformation when inserting into the membrane. As Schiller [1984] has pointed out in the case of the enkephalins, the absolute receptor-bound conformation of the peptide can only be determined by direct studies of the peptide-receptor complex once isolated and purified opioid receptors are available. A recent report

[Simon et al., 1990] on the 19600-fold purification of a κ-opioid receptor subtype by dynorphin affinity chromatography is encouraging.

8.3. Suggestions for Future Experiments

Although some progress has been made, a much more complete set of conformational NMR data must be accrued before a reliable model can be constructed. Some modifications to the sample systems used in this thesis are discussed below.

8.3.1. Improvements Concerning the Methanol System

It is desirable to restrain the flexibility of the molecule by making the medium more viscous. This could be done without any significant changes to the spectrum by adding small amounts of ethylene glycol to the methanolic solution [A.A. Bothner-By, personal communication, Bothner-By and Johner, 1978]. However, this should not be overdone as a too viscous solvent will give rise to short T_2's, i.e. fast spin-spin relaxation. These will in turn result in linebroadening in the NMR spectrum and cause complications in experiments using pulse sequences with longer delay times.

8.3.2. Improvements Concerning the Phospholipid System

In addition to performing more studies on the DMPC/"H_2O" system, a further modification of the sample could be achieved by the synthesis of specifically spin-labelled phospholipids. These compounds could be employed to observe the electron-spin mediated quenching of the transferred NOEs [Wakamatsu et al., 1987], which would yield more information on the orientation of the tridecapeptide binding to the phospholipid bilayer.

8.3.3. Other Potentially Useful Systems

Crown Ethers [Pedersen, 1988]

A more structured solvent medium, which is basically hydrophobic but is still capable of solvating molecules with positive charges, is represented by 18-crown-6-ether in $CDCl_3$. This system is amenable to NMR analysis, as has been shown for enkephalin amides [Temussi et al., 1987]. However, the presence of many positive charges on the peptide might inhibit the use of these bulky compounds on sterical grounds.

8.3.4. Other Techniques

Resolution-enhanced infrared spectroscopic evidence shows that an atrial natiuretic peptide forms β-structures in the presence of lipid [Surewicz et al., 1987]. Such resolution-enhanced IR spectroscopic studies on dynorphin A-(1-13) binding to dimyristoyl phosphatidylglycerol should be able to prove the presence of β-strand or β-turn structures. However, IR does not possess the molecular "resolution" NMR displays, so assigning structural features to certain parts of the molecule is not possible on the basis of this technique alone.

8.3.5. Improvements Concerning Heteronuclear Experiments

Information on Backbone Dynamics by Isotopic Labelling

Labelling of the peptide with ^{13}C or ^{15}N isotopes opens new dimensions of accessible conformational data. Heteronuclear coupling constants [Bystrov, 1976] might be useful for conformational studies on more rigid samples, whereas ^{13}C or ^{15}N NOE's, T_1's, and T_2's can be employed for the analysis of backbone dynamics (cf. section 5.5 and [Clore et al., 1990]). Also, such labelled peptides in the presence of hydrated phospholipids could be amenable to solid state NMR studies [Opella and Gierasch, 1985].

9. REFERENCES

9.1. Literature

Abragam, A. (1961). *The Principles of Nuclear Magnetism.* Clarendon Press, Oxford, UK.

Aceto, M. D., Dewey, W. L., Chang, J. K., Lee, N. M. (1982). Dynorphin-(1-13): Effects in non-tolerant and morphine-dependent rhesus monkeys. *Eur. J. Pharmacol.* **83**: 139-142.

Aitkens, P. W. (1986). *Physical Chemistry.* Third Edition. Oxford University Press, Oxford, UK.

Alberts, B., Bray, D., Lewis, J., Raff, M., Roberts, K., Watson, J. D. (1989). *Molecular Biology of the Cell.* Second edition, Garland Publishing, New York, USA.

Archer, S. (1986). The search for nonaddicting strong analgesics: hopes and frustrations. *NIDA Res. Monogr. Ser.* **69**: 364-376.

Argos, P., MohanaRao, J. K. (1986). Prediction of Protein Structure. *Methods in Enzymol.* **130**: 185-207.

Aristoteles (350 B.C.) as quoted by Benedetti and Premuda [1990]

Aue, W. P., Bartholdi, E., Ernst, R. R. (1976a). Two-dimensional spectroscopy. Application to nuclear magnetic resonance. *J. Chem. Phys.* **64**: 2229-2246.

Aue, W. P., Karhan, J., Ernst, R. R. (1976b). Homonuclear broad band decoupling and two-dimensional J-resolved NMR spectroscopy. *J. Chem. Phys.* **64**: 4226-4227.

Bain, A. D. (1988). The superspin formulism for pulse NMR. *Prog. NMR Spectrosc.* **20**: 295-315.

Barnard, E. A., Demoliou-Mason, C. (1983). Molecular properties of opioid receptors. *Br. Med. Bull.* **39**: 37-45.

Baumann, R., Wider, G., Ernst, R. R., Wüthrich, K. (1981). Improvement of 2D NOE and 2D correlated spectra by symmetrization. *J. Magn. Reson.* **44**: 402-406.

Bax, A. (1983). Broadband decoupling in heteronuclear shift correlation NMR spectroscopy. *J. Magn. Reson.* **53**: 517-520.

Bax, A. (1989). Two-dimensional NMR and protein structure. *Annu. Rev. Biochem.* **58**: 223-256.

Bax, A. and Davis, D. G. (1985). Practical aspects of two-dimensional transverse NOE spectroscopy. *J. Magn. Reson.* **63**: 207-213.

Bax, A., Drobny, G. (1985). Optimization of two-dimensional homonuclear relayed coherence transfer NMR spectroscopy. *J. Magn. Reson.* **61**: 306-320.

Bax, A., Freeman, R. (1981). Investigation of complex networks of spin-spin coupling by two-dimensional NMR. *J. Magn. Reson.* **44**: 542-561.

Bax, A., Lerner, L. (1986). Two-dimensional nuclear magnetic resonance spectroscopy. *Science* **232**: 960-967.

Bean, J. W., Erne, D., Sargent, D. F., Schwyzer, R. (1988). Binding of dynorphin-A-(1-13) and some N-terminal fragments to neutral lipid bilayer membranes. In: Marshall [1988]: 328-329.

Bell, R. A., Saunders, J. K. (1970). Correlation of the intramolecular nuclear Overhauser effect with internuclear distance. *Can. J. Chem.* **48**: 1114-1122.

Bendetti, C., Premuda, L. (1990). The history of opium and its derivatives. In: Benedetti et al. [1990]: 1-35.

Bendetti, C., Chapman, C. R., Giron, G. (1990). *Opioid Analgesia: Recent Advances in Systematic Administration.* Advances in Pain Research and Therapy, Volume **14**, Raven Press, New York, USA.

Benn, R., Günther, H. (1983). Modern pulse methods in high-resolution NMR spectroscopy. *Angew. Chem. Int. Ed. Engl.* **22**: 350-380.

Bensen, D. D., Iijima, H., Marshall, G. R. (1990). Structures from NMR distance constraints. *Biochem. Pharmacol.* **40**: 173-175.

Bergland, S. S., DeLander, G. E., Murray, T. F., Lovett, J. A. (1989). Synthesis and opioid activity of 2-substituted analogues of the opioid peptide dynorphin A-(1-13) amide. *Eleventh American Peptide Symposium* (The Salk Institute and U. of California, San Diego, La Jolla, California, July 9-14, 1989) *Abstracts*: P-247.

Bergmann, E. D., Pullman, B. (1973). *Conformation of Biological Molecules and Polymers.* Proceedings of an international symposium held in Jerusalem, 3-9 April, 1972. The Israel Academy of Sciences and Humanities, Jerusalem, Israel.

Berger, A., Linderstrøm-Lang, K. (1957). Deuterium exchange of poly-DL-alanine in aqueous solution. *Arch. Biochem. Biophys.* **69**: 106-118.

Beychok, S. (1967). Circular dichroism of poly-α-amino acids and proteins. In: Fasman [1967], Chapter 7: 293-337.

Billeter, M., Braun, W., Wüthrich, K. (1982). Sequential resonance assignments in protein ^{1}H nuclear magnetic resonance spectra. Computation of sterically allowed proton-proton distances and statistical analysis of proton-proton distances in single crystal protein conformations. *J. Mol. Biol.* **155**: 321-346.

Bloch, F. (1954). Recent developments in nuclear induction (Paper presented at the Symposium on Nuclear Magnetism during the 1953 Winter meeting of the American Physical Society, Stanford University). *Phys. Rev.* **93**: 944.

Blumenstein, M. (1985). Nuclear magnetic resonance of peptide macromolecule interactions. In: Hruby [1985a], Chapter **7**: 355-403.

Blundell, T., Wood, S. (1982). The conformation, flexibility, and dynamics of polypeptide hormones. *Annu. Rev. Biochem.* **51**: 123-154.

Bodenhausen, G., Freeman, R., Turner, D. L. (1976a). Two-dimensional J spectroscopy: proton-coupled carbon-13 NMR. *J. Chem. Phys.* **65**: 839-840.

Bodenhausen, G., Freeman, R., Niedermeyer, R., Turner, D. L. (1976b). High resolution NMR in inhomogeneous magnetic fields. *J. Magn. Reson.* **24**: 291-294.

Bodenhausen, G., Freeman, R., Niedermeyer, R., Turner, D. L. (1977). Double Fourier transformation in high-resolution NMR. *J. Magn. Reson.* **26**: 133-164.

Bodenhausen, G., Kogler, H., Ernst, R. R. (1984). Selection of coherence-transfer pathways in NMR pulse experiments. *J. Magn. Reson.* **58**: 370-388.

Bothner-By, A. A. (1965). Geminal and vicinal proton-proton coupling constants in organic compounds. *Adv. Magn. Reson.* **1**: 195-316.

Bothner-By, A. A. (1979). Nuclear Overhauser effects on protons, and their use in the investigation of the structures of biomolecules. In: Shulman [1979], Chapter **4**: 177-219.

Bothner-By, A. A., Dadok, J. (1979). High resolution NMR spectroscopy at higher magnetic fields. In: Opella and Lu [1979], Chapter **12**: 169-202.

Bothner-By, A. A., Johner, P. E. (1978). Specificity of interproton nuclear Overhauser effects in gramicidin-S dissolved in deuterated ethylene glycol. *Biophys. J.* **24**: 779-790.

Bothner-By, A. A., Noggle, J. H. (1979). Time development of nuclear Overhauser effects in multispin systems. *J. Am. Chem.* Soc. **101**: 5152-5155.

Bothner-By, A. A., Stephens, R. L., Lee, J., Warren, C. D., Jeanloz, R. W. (1984). Structure determination of a tetrasaccharide: Transient nuclear Overhauser effects in the rotating frame. *J. Am. Chem. Soc.* **106**: 811-813.

Botticelli, L. J., Cox, B. M., Goldstein, A. (1981). Immunoreactive dynorphin in mammalian spinal cord and dorsal root ganglia. *Proc. Natl. Acad. Sci. USA* **78**: 7783-7786.

Bracewell, R. N. (1990). Numerical transforms. *Science* **248**: 697-704.

Bradbury, A. F., Smyth, D. G., Snell, C. R., Birdsall, N. J. M., Hulme, E. C. (1976). C fragment of lipotropin has a high affinity for brain opiate receptors. *Nature (London)* **260**: 793-795.

Braun, W., Bösch, C., Brown, L. R., Gô, N., Wüthrich, K. (1981). Combined use of proton-proton Overhauser enhancements and a distance geometry algorithm for determination of polypeptide conformations. Application to micelle-bound glucagon. *Biochim. Biophys. Acta* **667**: 377-396.

Braun, W., Wider, G., Lee, K. H., Wüthrich, K. (1983). Conformation of glucagon in a lipid-water interphase by ^{1}H nuclear magnetic resonance. *J. Mol. Biol.* **169**: 921-948.

Briggs, M. S., Cornell, D. G., Dluhy, R. A., Gierasch, L. M. (1986). Conformation of signal peptides induced by lipids suggest initial steps in protein export. *Science* **233**: 206-208.

Bundi, A., Wüthrich, K. (1979). ^{1}H-NMR parameters of the common amino acid residues measured in aqueous solutions of the linear tetrapeptides H-Gly-Gly-**X**-L-Ala-OH. *Biopolymers* **18**: 285-297.

Burkert, U., Allinger, N. L. (1982). *Molecular Mechanics.* ACS Monograph 177, American Chemical Society, Washington, D.C., USA.

Bystrov, V. F., Ivanov, V. T., Portnova, S. L., Balashova, T. A., Ovchinnikov, Y. A. (1973). Refinement of the angular dependence of the peptide vicinal NH-C_αH coupling constant. *Tetrahedron* **29**: 873-877.

Bystrov, V. F. (1976). Spin-spin coupling and the conformational states of peptide systems. *Prog. NMR Spectrosc.* **10**: 41-81.

Campbell, I. D., Dobson, C. M., Williams, R. J. P., Wright, P. E. (1975). Pulse methods for the simplification of protein NMR spectra. *FEBS Lett.* **57**: 96-99.

Carr, H. Y., Purcell, E. M. (1954). Effects of diffusion on free precession in nuclear magnetic resonance experiments. *Phys. Rev.* **94**: 630-639.

Cármenes, R. S., Freije, J. P., Molina, M. M., Martín, J. M. (1989). Predict7, a program for protein structure prediction. *Biochem. Biophys. Res. Commun.* **159**: 687-693.

Cassim, J. Y., Yang, J. T. (1969). A computerized calibration of the circular dichrometer. *Biochemistry* **8**: 1947-1951.

Chang, C. T., Wu, C.-S. C., Yang, J. T. (1978). Circular dichroic analysis of protein conformation: Inclusion of the β-turns. *Anal Biochem.* **91**: 13-31.

Chang, K. J., Cuatrecasas, P. (1979). Multiple opiate receptors. Enkephalins and morphine bind to receptors of different specificity. *J. Biol. Chem.* **254**: 2610-2618.

Chapman, D., Fluck, D. J., Penkett, S. A., Shipley, G. G. (1968). Physical studies of phospholipids. X. The effect of sonication on aqueous dispersions of egg yolk lecithin. *Biochim. Biophys. Acta* **163**: 255-261.

Chavkin, C., Goldstein, A. (1981a). Demonstration of a specific dynorphin receptor in guinea pig ileum myenteric plexus. *Nature (London)* **291**: 591-593.

Chavkin, C., Goldstein, A. (1981b). Specific receptor for the opioid peptide dynorphin: Structure-activity relationships. *Proc. Natl. Acad. Sci. USA* **78**: 6543-6547.

Chavkin, C., James, I. F. (1982). Dynorphin is a specific endogenous ligand of the opioid receptor. *Science* **215**: 413-415.

Chen, Y. H., Yang, J. T., Chau, K. H. (1974). Determination of the helix and β-form of proteins in aqueous solution by circular dichroism. *Biochemistry* **13**: 3350-3359.

Chen, G. C., Yang, J. T. (1977). Two-point calibration of circular dichrometer with d-10-camphorsulfonic acid. *Anal. Lett.* **10**: 1195-1207.

Childers, S. R., Creese, I., Snowman, A. M., Snyder, S. H. (1979). Opiate receptor binding affected differentially by opiates and opioid peptides. *Eur. J. Pharmacol.* **55**: 11-18.

Chou, P. Y., Fasman, G. D. (1978a). Empirical predictions of protein conformation. *Ann. Rev. Biochem.* **47**: 251-276.

Chou, P. Y., Fasman, G. D. (1978b). Prediction of the secondary structure of proteins from their amino acid sequence. *Adv. Enzymol.* **47**: 45-148.

Civelli, O., Douglass, J., Herbert, E. (1984). Pro-opiomelanocortin: A polyprotein at the interface of the endocrine and nervous systems In: Udenfriend and Meienhofer [1984], Chapter **3**: 69-94.

Clore, G. M., Gronenborn, A. M. (1982). Theory and applications of the transferred nuclear Overhauser effect to the study of the conformations of small ligands bound to proteins. *J. Magn. Reson.* **48**: 402-417.

Clore, G. M., Gronenborn, A. M. (1989). Determination of three-dimensional structures of proteins and nucleic acids in solution by nuclear magnetic resonance spectroscopy. *C.R.C. Crit. Rev. Biochem. Mol. Biol.* **24**: 479-564.

Clore, G. M., Kimber, B. J., Gronenborn, A. M. (1983). The 1-1 hard pulse: A simple and effective method of water resonance suppression in FT ^{1}H NMR. *J. Magn. Reson.* **54**: 170-173.

Clore, G. M., Brünger, A. T., Karplus, M., Gronenborn, A. M. (1986a). Application of molecular dynamics with interproton distance restraints to three-dimensional protein structure determination. A model study of crambin. *J. Mol. Biol.* **191**: 523-551.

Clore, G. M., Martin, S. R., Gronenborn, A. M. (1986b). Solution structure of human growth hormone releasing factor (hGHRF). Combined use of circular dichroism and nuclear magnetic resonance spectroscopy. *J. Mol. Biol.***191**: 553-561.

Clore, G. M., Driscoll, P. C., Wingfield, P. T., Gronenborn, A. M. (1990). Analysis of backbone dynamics of interleukin-1β using two-dimensional inverse detected heteronuclear ^{15}N-^{1}H NMR spectroscopy. *Biochemistry* **29**: 7387-7401.

Codd, E. E., Aloyo, V. J., Walker, R. F. (1990). A non-opioid pattern characterizes inhibition of growth hormone releasing peptide binding by dynorphin-related peptides. *Neuropeptides* **15**: 133-137.

Corbett, A. D., Paterson, S. J., McKnight, A. T., Magnan, J., Kosterlitz, H. W. (1982). Dynorphin$_{1-8}$ and dynorphin$_{1-9}$ are ligands for the kappa-subtype of the opiate receptor. *Nature (London)* **299**: 79-81.

Crippen, G. M. (1981). *Distance Geometry and Conformational Calculations.* Research Studies Press, Chichester, UK, Chemometrics research studies series; v. 1.

Deber, C. M., Torchia, D. A., Blout, E. R. (1971). Cyclic peptides. I. Cyclo (tri-L-prolyl) and derivatives. Synthesis and molecular conformation from nuclear magnetic resonance. *J. Am. Chem. Soc.* **93**: 4893-4897.

DeGrado, W. F. (1988). Design of peptides and proteins. *Adv. Protein Chem.* **39**: 51-124.

DeMarco, A., Llinás, M., Wüthrich, K. (1978). Analysis of the ^{1}H-NMR spectra of ferrichrome peptides. I. The non-amide protons. *Biopolymers* **17**: 617-636.

DeMarco, A., Llinás, M., Wüthrich, K. (1978). Analysis of the ^{1}H-NMR spectra of ferrichrome peptides. II. The amide resonances. *Biopolymers* **17**: 637-650.

Derome, A. E. (1987). *Modern NMR Techniques for Chemistry Research.* Pergamon Press, Oxford, GB, Organic Chemistry series; v. 6.

Deslauriers, R., Smith, I. C. P. (1976). Conformation and structure of peptides. In: Levy, G.C. [1976], Chapter **1**: 1-80.

Doddrell, D., Glushko, V., Allerhand, A. (1972). Theory of nuclear Overhauser enhancement and ^{13}C-^{1}H dipolar relaxation in proton-decoupled carbon-13 NMR spectra of macromolecules. *J. Chem. Phys.* **56**: 3683-3689.

Doi, M., Tanaka, M., Ikuma, K., Nabae, M., Kitamura, K., Inoue, M., Ishida, T. (1988). Conformational characteristics of receptor-selective opioid peptides. ^{1}H NMR and CD spectroscopic studies of δ-kephalin and [Val^{4}]morphiceptin. *Biochem. J.* **251**: 581-588.

Drobny, G., Pines, A., Sinton, S., Weitekamp, D. P., Wemmer, D. (1979). Fourier transform multiple quantum nuclear magnetic resonance. *Faraday Symp. Chem. Soc.* **13**: 49-55.

Duysens, L. N. M. (1956). The flattening of the absorption spectrum of suspensions, as compared to that of solutions. *Biochim. Biophys. Acta* **19**: 1-12.

Dyson, H. J., Cross, K. J., Houghton, R. A., Wilson, I. A., Wright, P. E., Lerner, R. A. (1985). The immunodominant site of a synthetic immunogen has a

conformational preference in water for a type-II reverse turn. *Nature (London)* **318**: 480-483.

Dyson, H. J., Rance, M., Houghten, R. A., Lerner, R. A., Wright, P. E. (1988a). Folding of immunogenic peptide fragments of proteins in water solution. I. Sequence requirements for the formation of a reverse turn. *J. Mol. Biol.* **201**: 161-200.

Dyson, H. J., Rance, M., Houghten, R. A., Wright, P. E., Lerner, R. A. (1988b). Folding of immunogenic peptide fragments of proteins in water solution. II. The nascent helix. *J. Mol. Biol.* **201**: 201-217.

Eggenberger, U., Bodenhausen, G. (1990). Moderne NMR-Pulsexperimente: eine graphische Beschreibung der Entwicklung von Spinsystemen. *Angew. Chem.* **102**: 392-402.

Eich, G., Bodenhausen, G., Ernst, R. R. (1982). Exploring nuclear spin systems by relayed magnetization transfer. *J. Am. Chem. Soc.* **104**: 3731-3732.

Eisenberg, D., Weiss, R. M., Terwilliger, T. C. (1982a). The helical hydrophobic moment: a measure of the amphiphilicity of a helix. *Nature (London)* **299**: 371-374.

Eisenberg, D., Weiss, R. M., Terwilliger, T. C., Wilcox, W. (1982b). Hydrophobic moments and protein structure. *Faraday Symp. Chem. Soc.* **17**: 109-120.

Eisenberg, D., Weiss, R. M., Terwilliger, T. C. (1984). The hydrophobic moment detects periodicity in protein hydrophobicity. *Proc. Natl. Acad.Sci. USA* **81**: 140-144.

Eisenberg, D., Wesson, M., Wilcox, W. (1989). Hydrophobic moments as tools for analyzing protein sequences and structures. In: Fasman [1989], Chapter **16**: 635-646.

Emmett, J. C., ed. (1990). *Comprehensive Medicinal Chemistry: The Rational Design, Mechanistic Study & Therapeutic Application of Chemical Compounds. Volume 3: Membranes & Receptors.* Pergamon Press, Oxford, UK.

Epand, R. M. (1978). Studies on the effect of the lipid phase transition on the interaction of glucagon with dimyristoyl glycerophosphocholine. *Biochim. Biophys. Acta* **514**: 185-197.

Epand, R. M. (1983a). Relationships among several different non-homologous polypeptide hormones. *Molec. Cell. Biochem.* **57**: 41-47.

Epand, R. M. (1983b). The amphipathic helix: its possible role in the interaction

of glucagon and other peptide hormones with membrane receptor sites. *Trends Biochem. Sci.* **8**: 205-207.

Epand, R. M., Epand, R. F. (1991). Lipid-peptide interactions. In: Yeagle [1991], in press.

Epand, R. M., Jones, A. J. S., Schreier, S. (1977). Interaction of glucagon with dimyristoyl glycerophosphocholine. *Biochim. Biophys. Acta* **491**: 296-304.

Epand, R. M., Epand, R. F., Orlowski, R. C., Seyler, J. K., Colescott, R. L. (1986). Conformational flexibility and biological activity of salmon calcitonin. *Biochemistry* **25**: 1964-1968.

Epand, R. M., Gawish, A., Iqbal, M., Gupta, K. B., Chen, C. H., Segrest, J. P., Anantharamaiah, G. M. (1987). Studies of synthetic peptide analogs of the amphipathic helix. *J. Biol. Chem.* **262**: 9389-9396.

Erne, D., Sargent, D. F., Schwyzer, R. (1985). Preferred conformation, orientation and accumulation of dynorphin A-(1-13)-tridecapeptide on the surface of neutral lipid membranes. *Biochemistry* **24**: 4261-4263.

Ernst, R. R. (1966). Sensitivity enhancement in magnetic resonance. *Adv. Magn. Reson.* **2**: 1-135.

Ernst, R. R., Anderson, W. A. (1966). Application of Fourier transform spectroscopy to magnetic resonance. *Rev. Sci. Instrum.* **37**: 93-102.

Ernst, R. R., Bodenhausen, G., Wokaun, A. (1987). *Principles of Nuclear Magnetic Resonance in One and Two Dimensions.* Clarendon Press, Oxford, UK.

Fasman, G. D., ed. (1967). *Poly-α-Amino Acids. Protein Models for Conformational Studies.* Volume 1. Marcel Dekker Inc., New York, USA.

Fasman, G. D., ed. (1976). *Handbook of Biochemistry and Molecular Biology.* Third edition. Physical and chemical data. Volume II. CRC Press, Cleveland, Ohio, USA.

Fasman, G. D., ed. (1989). *Prediction of Protein Structure and the Principles of Protein Conformation.* Plenum Press, New York, USA.

Fischli, W., Goldstein, A., Hunkapiller, M., Hood, L. E. (1982). Isolation and amino acid sequence analysis of a 4,000-dalton dynorphin from porcine pituitary. *Proc. Natl Acad. Sci. USA* **79**: 5435-5437.

Fletcher, R., Reeves, C. M. (1964). Function minimization by conjugate gradients. *Comp. J.* **7**: 149-154.

Forsén, S., Hoffman, R. A. (1963a). A new method for the study of moderately rapid chemical exchange rates employing nuclear magnetic double resonance. *Acta Chem. Scand.* **17**: 1787-1788.

Forsén, S., Hoffman, R. A. (1963b). Study of moderately rapid chemical exchange reactions by means of nuclear magnetic double resonance. *J. Chem. Phys.* **39**: 2892-2901.

Forsén, S., Hoffman, R. A. (1964). Exchange rates by nuclear magnetic multiple resonance. III. Exchange reactions in systems with several nonequivalent sites. *J. Chem. Phys.* **40**: 1189-1196.

Freeman, R., Hill, H. D. W. (1975). Determination of spin-spin relaxation times in high resolution NMR. In: Jackman and Cotton [1975], Chapter **5**: 131-162.

Freeman, R. (1988). *A Handbook of Nuclear Magnetic Resonance.* Longman Scientific & Technical, Harlow, Essex, England.

Fukushima, D., Kaiser, E. T., Kézdy, F. J., Kroon, D. J., Kupferberg, J. P., Yokoyama, S. (1980). Rational design of synthetic models for lipoproteins. *Ann. N. Y. Acad. Sci.* **348**: 365-373.

Gairin, J. E., Gouarderes, C., Mazarguil, H., Alvinerie, P., Cros, J. (1984). [D-Pro^{10}]dynorphin-(1-11) is a highly potent and selective ligand for kappa opioid receptors. *Eur. J. Pharmacol.* **106**: 457-458.

Gairin, J. E., Jomary, C., Pradayrol, L., Cros, J., Meunier, J.-C. (1986). ^{125}I-DPDYN, Monoiodo[D-Pro^{10}]dynorphin-(1-11) a highly radioactive and selective probe for the study of kappa opioid receptors. *Biochem. Biophys. Res. Commun.* **134**: 1142-1150.

Garbow, J. R., Weitekamp, D. P. and Pines, A. (1982). Bilinear Rotation Decoupling of Homonuclear Scalar Interactions. *Chem. Phys. Lett.* **93**: 504-509.

Garnier, J., Osguthorpe, D. J., Robson, B. (1978). Analysis of the accuracy and implications of simple methods for predicting the secondary structure of globular proteins. *J. Mol. Biol.* **120**: 97-120.

Garnier, J., Robson, B. (1989). The GOR method for predicting secondary structure in proteins. In: Fasman [1989], Chapter **10**: 417-465.

Gates, M. (1966). Analgesic Drugs. *Sci. Am.* **215(5)**: 131-136.

Geraci, G., Parkhurst, L. J. (1981). Circular dichroism spectra of hemoglobins. *Methods in Enzymol.* **76**: 262-275.

Goldstein, H. (1980). *Classical Mechanics.* Second edition. Addison-Wesley Publishing, Reading, MA, USA.

Goldstein, A. (1984). Biology and chemistry of the dynorphin peptides. In: Udenfriend and Meienhofer [1984], Chapter **4**: 95-145.

Goldstein, A., James, I. F. (1984). Multiple opioid receptors. Criteria for identification and classification. *Trends Pharmacol. Sci.* **5**: 503-505.

Goldstein, A., Tachibana, S., Lowney, L. I., Hunkapiller, M., Hood, L. (1979). Dynorphin-(1-13), an extraordinarily potent opioid peptide. *Proc. Natl. Acad. Sci. USA* **76**: 6666-6670.

Goldstein, A., Fischli, W., Lowney, L. I., Hunkapiller, M., Hood, L. (1981). Porcine pituitary dynorphin: Complete amino acid sequence of the biologically active heptadecapeptide. *Proc. Natl. Acad. Sci. USA* **78**: 7219-7223.

Gottschlich, R. (1990). On the contribution of medicinal chemistry to a better understanding of opiate-mediated analgesia. *Kontakte (Darmstadt)* **1990(1)**: 3-12.

Gráf, L., Cseh, G., Barát, E., Rónai, A. Z., Székely, J. I., Kenessey, A., Bajusz, S. (1977). Structure-function relationships in lipotropins. *Annals N.Y. Acad. Sci.* **297**: 63-83.

Gratzer, W. B. (1967). Ultraviolet Absorption Spectra of Polypeptides. In: Fasman [1967], Chapter 5: 177-238.

Gysin, B., Schwyzer, R. (1983). Head group and structure specific interactions of enkephalins and dynorphin with liposomes: investigation by hydrophobic photolabelling. *Arch. Biochem. Biophys.* **225**: 467-474.

Hagler, A. T. (1985). Theoretical simulation of conformation, energetics, and dynamics of peptides. In: Hruby [1985a], Chapter **5**: 213-299.

Hahn, E. L. (1950). Spin Echoes. *Phys. Rev.* **80**: 580-594.

Hallenga, K., Hull, W. E. (1982). Connectivities between amide and alpha protons in peptides and proteins in aqueous solution by a combination of selective population transfer and the Redfield pulse sequence. *J. Magn. Reson.* **47**: 174-179.

Hamed, M. M., Robinson, R. M., Mattice, W. L. (1983). Behaviour of amphipathic helices on analysis via matrix methods, with application to glucagon, secretin, and vasoactive intestinal peptide. *Biopolymers* **22**: 1003-1021.

Hansen, P. E. (1981). Carbon-hydrogen spin-spin coupling constants. *Prog. NMR Spectrosc.* **14**: 175-296.

Hansen, P.E., Morgan, B. A. (1984). Structure-activity relationships in enkephalin peptides. In: Udenfriend and Meienhofer [1984], Chapter **8**: 269-321.

Harris, R. K. (1986). *Nuclear Magnetic Resonance Spectroscopy: A Physicochemical View.* Longman Scientific and Technical, Essex, UK.

Higashijima, T., Kobayashi, J., Nagai, U., Miyazawa, T. (1979). Nuclear magnetic resonance study on Met-enkephalin and Met-enkephalinamide. Molecular association and conformation. *Eur. J. Biochem.* **97**: 43-57.

Höllt, V. (1986). Opioid peptide processing and receptor selectivity. *Ann. Rev. Pharmacol. Toxicol.* **26**: 59-77.

Hoffman, R. A., Forsén, S. (1966). High resolution nuclear magnetic double and multiple resonance. *Prog. NMR Spectrosc.* **1**: 15-204.

Holzwarth, G. and Doty, P. (1965). The ultraviolet circular dichroism of polypeptides. *J. Am. Chem. Soc.* **87**: 218-228.

Hope, M. J., Bally, M. B., Webb, G., Cullis, P. R. (1985). Production of large unilamellar vesicles by a rapid extrusion procedure. Characterization of size distribution, trapped volume and ability to maintain a membrane potential. *Biochim. Biophys. Acta* **812**: 55-65.

Hoppe, W., Lohmann, W., Markl, H., Ziegler, H., eds. (1982). *Biophysik.* Second edition, Springer Verlag, Berlin and Heidelberg, FRG.

Hore, P. J. (1983). Solvent suppression in Fourier transform nuclear magnetic resonance. *J. Magn. Res.* **55**: 283-300.

Horwitz, J. (1976). Modern design of circular dichroism spectrophotometers. In: Fasman [1976]: 201-202.

Hoult, D. J., Richards, R. E. (1975). Critical factors in the design of sensitive high resolution nuclear magnetic resonance spectrometers. *Proc. Roy. Soc. London A* **344**: 311-340.

Howarth, O. W., Lilley, D. M. J. (1978). Carbon-13-NMR of Peptides and Proteins. *Prog. NMR Spectrosc.* **12**: 1-40.

Hruby, V. J., Mosberg, H. I., Sawyer, T. K., Knittel, J. J., Rockway, T. W., Ormberg, J., Darman, P., Chan, W. Y., Hadley, M. E. (1983). Conformational and dynamic considerations in the design of peptide hormone analogs. *Biopolymers* **22**: 517-530.

Hruby, V. J., ed. (1985a). *The Peptides - Analysis, Synthesis, Biology. Volume 7: Conformation in Biology and Drug Design.* Treatise editors: Udenfriend, S., Meienhofer, J., Academic Press, Orlando, Fla., USA.

Hruby, V. J. (1985b). A perspective on the application of physical methods to peptide conformational-biological activity studies. In: Hruby [1985a], Chapter **1**: 1-14.

Hruby, V. J. (1990). Design of drugs acting at peptidergic receptors. In: Emmett [1990], Chapter **13.1**: 797-804.

Hughes, J., Smith, T. W., Kosterlitz, H. W., Fothergill, L. A., Morgan, B. A., Morris, H. R. (1975). Identification of two related pentapeptides from the brain with potent opiate agonist activity. *Nature (London)* **258**: 577-579.

Hughes, J., Kosterlitz, H. W. (1983). Introduction. *Br. Med. Bull.* **39**: 1-3.

Hughes, D. W., Bell, R. A., Neilson, T., Bain, A. D. (1985). Assignment of the deoxyribofuranoside protons in DNA oligomers by the application of relayed coherence transfer two-dimensional nuclear magnetic resonance spectroscopy. *Can. J. Chem.* **63**: 3133-3139.

Hull, W. E., Sykes, B. D. (1975). Dipolar nuclear spin relaxation of ^{19}F in multispin systems. Application to ^{19}F labelled proteins. *J. Chem. Phys.* **63**: 867-880.

IUPAC-IUB Commission on Biochemical Nomenclature (1970). Abbreviations and Symbols for the Description of the Conformation of Polypeptide Chains. Tentative Rules (1969). *Biochemistry* **9**: 3471-3479.

IUPAC-IUB Joint Commission on Biochemical Nomenclature (JCBN) (1984). Nomenclature and symbolism for amino acids and peptides. Recommendations 1983. *Eur. J. Biochem.* **138**: 9-37.

Jackman, L. M. and Cotton, F. A. (1975). *Dynamic Nuclear Magnetic Resonance Spectroscopy.* Academic Press, New York, USA.

James, I. F. (1986). Opioid receptors for the dynorphin peptides. *NIDA Res. Monogr. Ser.* **70**: 192-208.

Jardetzky, O. (1979). NMR relaxation studies of protein dynamics. In: Opella and Lu [1979], Chapter **11**: 141-167.

Jardetzky, O. (1980). On the nature of molecular conformations inferred from high resolution NMR. *Biochim. Biophys. Acta* **621**: 227-232.

Jardetzky, O., Roberts, G. C. K. (1981). NMR in molecular biology. Academic Press. New York, USA.

Jeener, J. (1971). unpublished lecture. *Ampère International Summer School*, Basko Polje, Yugoslavia.

Jeener, J., Meier, B. H., Bachmann, P., Ernst, R. R. (1979). Investigation of exchange processes by two-dimensional NMR spectroscopy. *J. Chem. Phys.* **71**: 4546-4553.

Jhamandas, K., Sutak, M., Lemaire, S. (1986). Comparative spinal analgesic action of dynorphin A-(1-8), dynorphin A-(1-13) and a æ-receptor agonist U-50,488. *Can. J. Physiol. Pharmacol.* **64**: 263-268.

Johnston, P. D., Redfield, A. G. (1977). An NMR study of the exchange rates for protons involved in the secondary and tertiary structure of yeast $tRNA^{Phe}$. *Nucleic Acids Res.* **4**: 3599-3615.

Jones, C. R., Gibbons, W. A., Garsky, V. (1976). Proton magnetic resonance studies of conformation and flexibility of enkephalin peptides. *Nature (London)* **262**: 779-782.

Kabsch, W., Sander, C. (1983). How good are predictions of protein secondary structure? *FEBS Lett.* **155**: 179-182.

Kahn, P. C. (1979). The interpretation of near-ultraviolet circular dichroism. *Methods in Enzymol.* **61**: 339-378.

Kaiser, E. T., Kézdy, F. J. (1983). Secondary structures of proteins and peptides in amphiphilic environments (a review). *Proc. Natl. Acad Sci. USA* **80**: 1137-1143.

Kaiser, E. T. (1989a). Synthetic approaches to biologically active peptides and proteins including enzymes. *Acc. Chem. Res.* **22**: 47-54.

Kaiser, E. T. (1989b). Guide for studies on structure and function employing synthetic polypeptides. In: Fasman [1989], Chapter **20**: 761-775.

Kaiser, E. T., Kézdy, F. J. (1984). Amphiphilic secondary structure: Design of peptide hormones. *Science* **223**: 249-255.

Kaiser, E. T., Kézdy, F. J. (1987). Peptides with affinity for membranes. *Ann. Rev. Biophys. Biophys. Chem.* **16**: 561-581.

Kakidani, H., Furutani, Y., Takahashi, H., Noda, M., Morimoto, Y., Hirose, T., Asai, M., Inayama, S., Nakanishi, S., Numa, S. (1982). Cloning and sequence analysis of cDNA for porcine β-neo-endorphin/dynorphin precursor. *Nature (London)* **298**: 245-249.

Kalk, A., Berendsen, H. J. C. (1976). Proton magnetic relaxation and spin diffusion in proteins. *J. Magn. Reson.* **24**: 343-366.

Karplus, M. (1959). Contact electron-spin coupling of nuclear magnetic moments. *J. Chem. Phys.* **30**: 11-15.

Karplus, M., McCammon, J. A. (1983). Dynamics of proteins: Elements and function. *Annu. Rev. Biochem.* **52**: 263-300.

Kasha, M. (1963). Energy transfer mechanisms and the molecular exciton model for molecular aggregates. *Radiat. Res.* **20**: 55-71.

Kauzmann, W. (1959). Some factors in the interpretation of protein denaturation. *Adv. Protein Chem.* **14**: 1-63.

Kawasaki, A. M., Knapp, R. J., Kramer, T. H., Wire, W. S., Vasquez, O. S., Yamamura, H. I., Burks, T. F., Hruby, V. J. (1990). Design and synthesis of highly potent and selective cyclic dynorphin A analogues. *J. Med. Chem.* **33**: 1874-1879.

Kay, L. E., Clore, G. M., Bax, A., Gronenborn, A. M. (1990). Four-dimensional heteronuclear triple-resonance NMR spectroscopy of interleukin-1β in solution. *Science* **249**: 411-414.

Keeler, J., Neuhaus, D. (1985). Comparison and evaluation of methods for two-dimensional NMR spectra with absorption-mode lineshapes. *J. Magn. Reson.* **63**: 454-472.

Kessler, H. (1982). Conformation and biological activity of cyclic peptides. *Angew. Chem. Int. Ed. Engl.* **21**: 512-523.

Kessler, H., Bermel, W. (1986). Conformational analysis of peptides by two-dimensional NMR spectroscopy. In: Takeuchi and Marchand [1986], Chapter **6**: 179-205.

Kessler, H., Oschkinat, H. (1985). Simplification of spectra for the determination of coupling constants from homonuclear correlated 2D NMR spectra. *Angew. Chem. Int. Ed. Engl.* **24**: 690-692.

Kessler, H., Loosli, H.-R., Oschkinat, H. (1985a) Assignment of the ^{1}H, ^{13}C, and ^{15}N-NMR spectra of cyclosporin A in $CDCl_3$ and C_6D_6 by a combination of homo- and heteronuclear two-dimensional techniques. *Helv. Chim. Acta* **68**: 661-681.

Kessler, H., Müller, A., Oschkinat, H. (1985b). Differences and sums of traces within COSY spectra (DISCO) for the extraction of coupling constants: "Decoupling" after the measurement. *Magn. Reson. Chem.* **23**: 844-852.

Kessler, H., Bermel, W., Müller, A., Pook, K.-H. (1985c). Modern nuclear magnetic resonance spectroscopy of peptides. In: Hruby [1985a], Chapter **9**: 437-473.

Kessler, H., Gehrke, M., Griesinger, C. (1988a). Two-dimensional NMR spectroscopy: Background and overview of the experiments. *Angew. Chem. Int. Ed. Engl.* **27**: 490-536.

Kessler, H., Griesinger, C., Lautz, J., Müller, A., van Gunsteren, W. F., Berendsen, H. J. C. (1988b). Conformational dynamics detected by nuclear magnetic resonance NOE values and J coupling constants. *J. Am. Chem. Soc.* **110**: 3393-3396.

Kessler, H., Gehrke, M., Lautz, J., Köck, M., Seebach, D., Thaler, A. (1990). Complexation and medium effects on the conformation of cyclosporin A studied by NMR spectroscopy and molecular dynamics calculations. *Biochem. Pharmacol.* **40**: 169-173.

Khazan, N., Young, G. A., Calligaro, D. (1983). Self-administration of dynorphin-(1-13) and D-ala^2-dynorphin-(1-11) (kappa-opioid agonists) in morphine (mu-opioid agonist)-dependent rats. *Life Sci.* **33(Suppl. 1)**: 559-562.

Kimura, S., Sasaki-Yagi, Y., Imanishi, Y. (1990). Receptor selectivity of enkephalin analogs carrying artificial address peptides. *Int. J. Peptide Protein Res.* **35**: 550-556.

König, H. (1980). Pharmaceutical chemistry today - changes, problems and opportunities. *Angew. Chem. Int. Ed. Engl.* **19**: 749-761.

Kövér, K. E., Batta, G. (1987). Theoretical and practical aspects of one- and two-dimensional heteronuclear Overhauser experiments and selective ^{13}C T_1-determinations of heteronuclear distances. *Prog. NMR Spectrosc.* **19**: 223-266.

Kojro, E., Gwizdala, E., Grzonka, Z. (1987). The study of circular dichroism of some enkephalins, β-casomorphins and dynorphins. *Pol. J. Chem.* **61**: 415-424.

Kopple, K. D., Ohnishi, M., Go, A. (1969a). Conformation of cyclic peptides. III. Cyclopentaglycyltyrosyl and related compounds. *J. Am. Chem. Soc.* **91**: 4264-4272.

Kopple, K. D., Ohnishi, M., Go, A. (1969b). Conformations of cyclic peptides. IV. Nuclear magnetic resonance studies of cyclo-pentaglycyl-L-leucyl and cyclo-diglycyl-L-histidyldiglycyl-L-tyrosyl. *Biochemistry.* **8**: 4087-4095.

Kosterlitz, H. W. (1987). Biosynthesis of morphine in the animal kingdom. *Nature* **330**: 606.

Kumar, N. G., Urry, D. W. (1973). Conformational analysis of the polypeptide antibiotic telomycin by nuclear magnetic resonance. *Biochemistry* **12**: 4392-4399.

Kumar, A., Wagner, G., Ernst, R. R., Wüthrich, K. (1981). Buildup rates of the nuclear Overhauser effect measured by two-dimensional proton magnetic resonance spectroscopy: Implications for studies of protein conformation. *J. Am. Chem. Soc.* **103**: 3654-3658.

Lautz, J., Kessler, H., Blaney, J. M., Scheek, R. M., van Gunsteren, W. F. (1989). Calculating three-dimensional molecular structure from atom-atom distance information: cyclosporin A. *Int. J. Peptide Protein Res.* **33**: 281-288.

Lemaire, S., Bérubé, A., Derome, G., Lemaire, I., Magnan, J., Regoli, D., St-Pierre, S. (1978). Synthesis and biological activity of β-endorphin and analogues. Additional evidence for multiple opiate receptors. *J. Med. Chem.* **21**: 1232-1235.

Lemaire, S., Chouinard, L., Denis, D., Panico, M., Morris, H. R. (1982). Mass spectrometric identification of various molecular forms of dynorphin in bovine adrenal medulla. *Biochem. Biophys. Res. Commun.* **108**: 51-58.

Lemaire, S., Valette, A., Chouinard, L., Dupuis, N., Day, R., Porthe, G., Cros, J. (1983). (Identification of dynorphin in the placenta). *Neuropeptides* **3**: 181-191.

Levitt, M. H. (1986). Composite pulses. *Prog. NMR Spectrosc.* **18**: 61-122.

Levitt, M. H., Freeman, R. (1981). Composite pulse decoupling. *J. Magn. Reson.* **43**: 502-507.

Levy, G. C., ed. (1976). *Topics in Carbon-13 NMR Spectroscopy.* Volume **2**, John Wiley and Sons, New York, USA.

Levy, G. C., ed. (1979). *Topics in Carbon-13 NMR Spectroscopy.* Volume **3**, John Wiley and Sons, New York, USA.

Lewis, P. N., Momany, F. A., Scheraga, H. A. (1973). Energy parameters in polypeptides. VI. Conformational energy analysis of the N-acetyl N'-methyl amides of the twenty naturally occurring amino acids. *Isr. J. Chem.* **11**: 121-152.

Li, C. H., Chung, D. (1976). Isolation and structure of an untriakontapeptide with opiate activity from camel pituitary glands. *Proc. Natl. Acad. Sci. USA* **73**: 1145-1148.

Li, C. H., Yamashiro, D., Tseng, L.-F., Chang, W.-C., Ferrara, P. (1980). β-Endorphin omission analogs: Dissociation of immunoreactivity from other biological activities. *Proc. Natl. Acad. Sci. USA* **77**: 3211-3214.

Lilley, D. M. J., Howarth, O. W. (1977). Empirical Investigation of the spin-echo determination of short T_2 values in proton-decoupled ^{13}C NMR. Applications to the study of protein mobility. *J. Magn. Reson.* **27**: 335-338.

Lin, N., Burgus, R., Guillemin, R. (1976). Isolation, primary structure, and synthesis of α-endorphin and γ-endorphin, two peptides of hypothalamic-hypophysial origin with morphinomimetic activity. *Proc. Natl. Acad. Sci. USA* **73**: 3942-3946.

Llinás, M., Klein, M. P. (1975). Charge relay at the peptide bond. A proton magnetic resonance study of solvation effects on the amide electron density distribution. *J. Am. Chem. Soc.* **97**: 4731-4737.

Loh, H. H., Smith, A. P. (1990). Molecular characterization of opioid receptors. *Ann. Rev. Pharmacol. Toxicol.* **30**: 123-147.

Loosli, H. R., Kessler, H., Oschkinat, H., Weber, H. P., Petcher, T. J., Widmer, A. (1985). The conformation of cyclosporin A in the crystal and in solution. *Helv. Chim. Acta* **68**: 682-704.

Lord, J. A. H., Waterfield, A. A., Hughes, J., Kosterlitz, H. W. (1977). Endogenous opioid peptides: multiple agonists and receptors. *Nature (London)* **267**: 495-499.

McDonald, C. C., Phillips, W. D. (1967). Manifestations of the tertiary structures of proteins in high-frequency nuclear magnetic resonance. *J. Am. Chem. Soc.* **89**: 6332-6341.

McDonald, C. C., Phillips, W. D. (1969). Perturbation of the PMR spectrum of lysozyme by Co^{2+}. *Biochem. Biophys. Res. Commun.* **35**: 43-51.

Macura, S., Ernst, R. R. (1980). Elucidation of cross relaxation in liquids by two-dimensional NMR spectroscopy. *Mol. Phys.* **41**: 95-117.

Macura, S., Huang, Y., Suter, D., Ernst, R. R. (1981). Two-Dimensional Chemical Exchange and Cross-Relaxation Spectroscopy of Coupled Nuclear Spins. *J. Magn. Reson.* **43**: 259-281.

Mackay, D. H. J., Cross, A. J., Hagler, A. T. (1989). The role of energy minimization in simulation strategies of biomolecular systems. In: Fasman [1989], Chapter **7**: 317-358.

Mammi, S., Mammi, N. J., Peggion, E. (1988). Conformational studies of human des-Trp^{1},Nle^{12}-minigastrin in water-trifluoroethanol mixtures by ^{1}H NMR and circular dichroism. *Biochemistry* **27**: 1374-1379.

Manavalan, P., Momany, F. (1981a). Conformational energy calculations on enkephalins and enkephalin analogs. Classification of conformations to different configurational types. *Int. J. Peptide Protein Res.* **18**: 256-275.

Manavalan, P., Momany, F. (1981b). Conformational energy studies on N-methylated analogs of thyrotropin releasing hormone, enkephalin, and luteinizing hormone-releasing hormone. *Biopolymers* **19**: 1943-1973.

Maneckjee, R., Zukin, R. S., Archer, S., Michael, J., Osei-Gyimah, P. (1985). Purification and characterization of the μ opiate receptor from rat brain using affinity chromatography. *Proc. Natl. Acad. Sci. USA* **82**: 594-598.

Mansour, A., Khachaturian, H., Lewis, M. E., Akil, H., Watson, S. J. (1988). Anatomy of CNS opioid receptors. *Trends Neurosci.* **11**: 308-314.

Marion, D., Wüthrich, K. (1983). Application of phase sensitive two-dimensional correlated spectroscopy (COSY) for measurements of ^{1}H-^{1}H spin-spin coupling constants in proteins. *Biochem. Biophys. Res. Commun.* **113**: 967-974.

Maroun, R., Mattice, W. L. (1981). Solution conformations of the pituitary opioid peptide dynorphin-(1-13). *Biochem. Biophys. Res. Commun.* **103**: 442-446.

Marshall, G. R., ed. (1988). *Peptides: Chemistry and Biology.* Proceedings of the Tenth American Peptide Symposium 1987, Escom Science, Leiden NL.

Martin, W. R., Eades, C. G. Thompson, J. A. Huppler, R. E., Gilbert, P. E. (1976). The effect of morphine- and nalorphine-like drugs in the non-dependent and morphine-dependent chronic spinal dog. *J. Pharmacol. Exp. Ther.* **197**: 517-532.

Mattice, W. L. (1989). The β-sheet to coil transition. *Annu. Rev. Biophys. Biophys. Chem.* **18**: 93-111.

Mattice, W. L., Robinson, R. M. (1981a). Conformational properties of central nervous system myelin basic protein, β-endorphin, and β-lipotropin in water and in the presence of anionic lipids. *Biopolymers* **20**: 1421-1434.

Mattice, W. L., Robinson, R. M. (1981b). Conformational changes expected in endogenous opioid peptides upon their interaction with acidic lipids. *Biophys. Res. Commun.* **101**: 1311-1317.

Maudsley, A. A., Muller, L., Ernst, R. R. (1977). Cross-correlation of spin-decoupled NMR spectra by heteronuclear two-dimensional spectroscopy. *J. Magn. Reson.* **28**: 463-469.

Mayer, L. D., Hope, M. J., Cullis, P. R. (1986). Vesicles of variable sizes produced by a rapid extrusion procedure. *Biochim. Biophys. Acta* **858**: 161-168.

McLawhon, R. W., Ellory, J. C., Dawson, G. (1983). Molecular size of opiate (enkephalin) receptors in neuroblastoma-glioma hybrid cells as determined by radiation inactivation analysis. *J. Biol. Chem.* **258**: 2102-2105.

Mehlkopf, A. F., Korbee, D., Tiggelman, T. A., Freeman, R. (1984). Sources of t_1 noise in two-dimensional NMR. *J. Magn. Res.* **58**: 315-323.

Meiboom, S., Gill, D. (1958). Modified spin-echo method for measuring nuclear relaxation times. *Rev. Sci. Instrum.* **29**: 688-691.

Merrifield, R. B. (1963). Solid phase peptide synthesis. I. The synthesis of a tetrapeptide. *J. Am. Chem. Soc.* **85**: 2149-2154.

Metzler, W. J., Hare, D. R., Pardi, A. (1989). Limited sampling of conformational space by the distance geometry algorithm: Implications for structures generated from NMR data. *Biochemistry* **28**: 7045-7052.

Michne, W. F., Albertson, N. F. (1972). Analgetic 1-oxidized-2,6-methano-3-benzazocines. *J. Med. Chem.* **15**: 1278-1281.

Millan, M. J. (1986). Multiple opioid systems and pain. *Pain* **27**: 303-347.

Millan, M. J. (1990). -Opioid receptors and analgesia. *Trends Pharmacol. Sci.* **11**: 70-76.

Miyazawa, T., Higashijima, T. (1981). NMR analyses of conformations of linear peptides in solution. *Biopolymers* **20**: 1949-1958.

Molday, R. S., Englander, S. W. and Kallen, K. G. (1972). Primary structure effects on peptide group hydrogen exchange. *Biochemistry* **11**: 150-158.

Morgenstern, C. (1972). *Galgenlieder, Der Ginganz und Horatius Travestitus.* Sämtliche Dichtungen I. Band 6. Zbinden Verlag, Basel, CH.

Morley, J. S. (1983). Chemistry of opioid peptides. *Br. Med. Bull.* **39**: 5-10.

Morris, G. A., Freeman, R. (1979). Enhancement of nuclear magnetic resonance signals by polarization transfer. *J. Amer. Chem. Soc.* **101**: 760-762.

Nagayama, K., Anil Kumar, Wüthrich, K., Ernst, R. R. (1980). Experimental techniques of two-dimensional correlated spectroscopy. *J. Magn. Reson.* **40**: 321-334.

Nakanishi, S., Inoue, A., Kita, T., Nakamura, M., Chang, A. C. Y., Cohen, S. N., Numa, S. (1979). Nucleotide sequence of cloned cDNA for bovine corticotropin-β-lipotropin precursor. *Nature (London)* **278**: 423-427.

Neuberger, A., van Deenen, L. L. M., eds. (1985). *Modern Physical Methods in Biochemistry, Part A.*, Elsevier Publishers B.V., NL,

Neuhaus, D., Williamson, M. P. (1989). *The Nuclear Overhauser Effect in Structural and Conformational Analysis.* VCH Publishers, New York, USA.

Nilges, M., Clore, G. M., Gronenborn, A. M. (1988). Determination of three-dimensional structures of proteins from interproton distance data by hybrid distance-geometry-dynamical simulated annealing calculations. *FEBS Lett.* **229**: 317-324.

Noda, M., Furutani, Y., Takahashi, H., Toyosato, M., Hirose, T., Inayama, S., Nakanishi, S., Numa, S. (1982). Cloning and sequence analysis of cDNA for bovine adrenal preproenkephalin. *Nature (London)* **295**: 202-206.

Noggle, J. H., Schirmer, R. E. (1971). *The Nuclear Overhauser Effect.* Academic Press, New York, USA, and London, UK.

Numa, S. (1984). Opioid peptide precursors and their genes. In: Udenfriend and Meienhofer [1984], Chapter **1**: 1-23.

Ohnishi, M., Urry, D. W. (1969). Temperature dependence of the amide proton chemical shifts: The secondary structures of gramicidin S and valinomycin. *Biochem. Biophys. Res. Commun.* **36**: 194-202.

Olson, G. A., Olson, R. D., Kastin, A. J. (1987). Endogenous opiates: 1986. *Peptides* **8**: 1135-1164.

Opella, S. J., Lu, P., eds. (1979). *NMR and Biochemistry.* A symposium honoring Mildred Cohn. Marcel Dekker, New York, USA.

Opella, S. J., Gierasch, L. M. (1985). Solid-state nuclear magnetic resonance of peptides. In: Hruby [1985a], Chapter **8**: 405-436.

Oschkinat, H., Freeman, R. (1984). Fine structure in two-dimensional NMR correlation spectroscopy. *J. Magn. Reson.* **60**: 164-169.

Oschkinat, H., Griesinger, C., Kraulis, P. J., Sørensen, O. W., Ernst, R. R., Gronenborn, A. M., Clore, G. M. (1988). Three-dimensional NMR spectroscopy of a protein in solution. *Nature (London)* **332**: 374-376.

Osterman, D. G., Kaiser, E. T. (1985). Design and characterization of peptides with amphiphilic β-strand structures. *J. Cell. Biochem.* **29**: 57-72.

Ovchinnikov, Y. A., Ivanov, V. T., Bystrov, V. F., Miroshnikov, A. I., Shepel, E. N., Abdullaev, N. D., Efremov, E. S., Senjavina, L. B. (1970). The conformation of gramicidin S and its N,N'-diacetyl derivative in solutions. *Biochem. Biophys. Res. Commun.* **39**: 217-225.

Ovchinnikov, Y. A., Ivanov, V. T. (1975). Conformational states and biological activity of cyclic peptides. *Tetrahedron* **31**: 2177-2209.

Overhauser, A. W. (1953). Polarization of nuclei in metals. *Phys. Rev.* **92**: 411-415.

Pachler, K. G. R. (1964). Nuclear magnetic resonance study of some α-amino acids-II. Rotational isomerism. *Spectrochim. Acta* **20**: 581-587.

Pardi, A., Billeter, M., Wüthrich, K. (1984). Calibration of the angular dependence of the amide proton-C^{α} proton coupling constants, $^{3}J_{HN\alpha}$, in a globular protein. Use of $^{3}J_{HN\alpha}$ for identification of helical secondary structure. *J. Mol. Biol.* **180**: 741-751.

Pardi, A., Galdes, A., Florance, J., Maniconte, D. (1989). Solution structures of α-conotoxin G1 determined by two-dimensional NMR spectroscopy. *Biochemistry* **28**: 5494-5501.

Paterson, S. J., Robson., L. E., Kosterlitz, H. W. (1984). Opioid receptors. In: Udenfriend and Meienhofer [1984], Chapter **5**: 147-189.

Paul, H.-H., Penka, V., Lohmann, W. (1982). Kernresonanz-spektroskopie. In: Hoppe, W. et al. [1982], Section 3.4.: 196-214.

Pedersen, C. J. (1988). The discovery of crown ethers. *Science* **241**: 536-540.

Perutz, M. F., Kendrew, J. C., Watson, H. C. (1965). Structure and function of haemoglobin. II. Some relations between polypeptide chain configuration and amino acid sequence. *J. Mol. Biol.* **13**: 669-678.

Piantini, U., Sørensen, O. W., Ernst, R. R. (1982). Multiple quantum filters for elucidating NMR coupling networks. *J. Amer. Chem. Soc.* **104**: 6800-6801.

Pitner, T. P., Urry, D. W. (1972). Proton magnetic resonance studies in trifluoroethanol. Solvent mixtures as a means of delineating peptide protons. *J. Amer. Chem. Soc.* **94**: 1399-1400.

Polak, E. and Ribiere, G.: Note sur la convergence de méthodes de directions conjugueés. *Revue Française Informat. Recherche Operationelle* **16(R-1)**: 35-43.

Pople, J. A., Schneider, W. G., Bernstein, H. J. (1959). *High Resolution NMR.* McGraw-Hill, New York, USA.

Porthoghese, P. S. (1965). A new concept on the mode of interaction of narcotic analgesics with receptors. *J. Med. Chem.* **8**: 609-616.

Press, W. H., Flannery, B. P., Teukolsky, S., A., Vetterling, W. T. (1986). *Numerical Recipes. The Art of Scientific Computing.* Cambridge University Press, Cambridge, UK.

Przybytek, J. T. (1982). *High Purity Solvent Guide.* Burdick & Jackson Laboratories Inc., Second Edition, Muskegon, Michigan, USA.

Pullman, B. (1976). *Quantum Mechanics of Molecular Conformations.* John Wiley & Sons, London, UK.

Pullman, B., Maigret, B. (1973). The "dipeptide" model - its significance and limitations. In: Bergmann and Pullman [1973], pp. 13-35.

Quadrofoglio, F., Urry, D. W. (1968). Ultraviolet rotary properties of polypeptides in solution. II. Poly-L-serine. *J. Am. Chem. Soc.* **90**: 2760-2765.

Rabenstein, D. L., Nakashima, T. T. (1979). Spin-echo Fourier transform nuclear magnetic resonance spectroscopy. *Anal. Chem.* **51**: 1465A-1474A.

Ramachandran, G. N. (1973). Accuracy of potential functions in the analysis of biopolymer conformation. In: Bergmann and Pullman [1973]: 1-11.

Ramachandran, G. N., Chandrasekaran, R. (1971). Conformational energy map of a dipeptide unit in relation to infrared and nuclear magnetic resonance data. *Biopolymers* **10**: 935-939.

Ramachandran, G. N., Sasisekharan, V. (1968). Conformation of polypeptides and proteins. *Adv. Prot. Chem.* **23**: 283-437.

Ramachandran, G. N., Chandrasekaran, R., Kopple, K. D. (1971). Variation of the NH-$C^{\alpha}H$ coupling constant with dihedral angle in the NMR spectra of peptides. *Biopolymers* **10**: 2113-2131.

Rance, M., Sørensen, O. W., Bodenhausen, G., Wagner, G., Ernst, R. R., Wüthrich, K. (1983). Improved spectral resolution in COSY ^{1}H NMR spectra of proteins via double quantum filtering. *Biochem. Biophys. Res. Commun.* **117**: 479-485.

Rapaka, R. S. (1986). Research topics in the medicinal chemistry and molecular pharmacology of opioid peptides-present and future. *Life Sci.* **39**: 1825-1843.

Rapaka, R. S., Renugopalakrishnan, V., Collette, T. W., Dobbs, J. C., Carreira, L. A., Bhatnagar, R. S. (1987a). Conformational features of dynorphin A-(1-13). *Int. J. Peptide Protein Res.* **30**: 284-287.

Rapaka, R. S., Renugopalakrishnan, V., Huang, S.-G., Dobbs, J. C., Carreira, A. (1987b). Secondary structure of dynorphin in solution: Lipid involvement. *Tenth American Peptide Symposium* (Wash. U., St. Louis, Missouri, May 23-28, 1987) *Abstracts*: P-205.

Rees, D. C., Hunter, J. C. (1990). Opioid receptors. In: Emmett [1990], Chapter **13.2**: 805-846.

Renugopalakrishnan, V., Rapaka, R. S., Huang, S.-G., Moore, S., Hutson, T. B. (1988). Dynorphin A-(1-13) peptide NH groups are solvent exposed: FT-IR and 500 MHz ^{1}H NMR spectroscopic evidence. *Biochem. Biophys. Res. Commun.* **151**: 1220-1225.

Richardson, J. S. (1981). The anatomy and taxonomy of protein structure. *Adv. Protein Chem.* **34**: 167-339.

Roberts, J. K. M., Jardetzky, O. (1985). Nuclear magnetic resonance spectroscopy in biochemistry. In: Neuberger and van Deenen [1985], Chapter **1**: 1-67.

Rooman, M. J., Wodak, S. J. (1988). Identification of predictive sequence motifs limited by protein structure data base size. *Nature* **335**: 45-49.

Roques, B. P., Garbay-Jaureguiberry, Oberlin, R., Anteunis, M., Lala, A. K. (1976). Conformation of Met^5-enkephalin determined by high field PMR spectroscopy. *Nature (London)* **262**: 778-779.

Rose, G. D., Gierasch, L. M., Smith, J. A. (1985). Turns in peptides and proteins. *Adv. Protein Chem.* **37**: 1-109.

Rutar, V. (1984). Suppression of homonuclear J couplings in ^{1}H-^{13}C chemical shift correlation maps. *J. Magn. Reson.* **58**: 306-310.

Sander, H. W., Kream, R. M., Gintzler, A. R. (1989). Spinal dynorphin involvement in the analgesia of pregnancy: effects of intrathecal dynorphin antisera. Eur. J. Pharmacol. **159**: 205-209.

Sanders, J. K. M. and Hunter, B. K. (1987). *Modern NMR Spectroscopy. A Guide for Chemists.* Oxford University Press, Oxford, UK.

Sargent, D. F., Schwyzer, R. (1986). Membrane lipid phase as catalyst for peptide-receptor interactions. *Proc. Natl. Acad. Sci. USA* **83**: 5774-5778.

Sargent, D. F., Bean, J. W., Kosterlitz, H. W., Schwyzer, R. (1988). Cation dependence of opioid receptor binding supports theory on membrane-mediated receptor selectivity. *Biochemistry* **27**: 4974-4977.

Schaefer, J. (1973). Distributions of correlation times and the carbon-13 nuclear magnetic resonance spectra of polymers. *Macromolecules* **6**: 882-888.

Schiffer, M., Edmundson, A. B. (1967). Use of helical wheels to represent the structures of proteins and to identify segments with helical potential. *Biophys. J.* **7**: 121-135.

Schiller, P. W. (1983). Fluorescence study on the solution conformation of dynorphin in comparison to enkephalin. *Int. J. Peptide Protein Res.* **21**: 307-312.

Schiller, P. W. (1984). Conformational analysis of enkephalin and conformation-activity relationships. In: Udenfriend and Meienhofer [1984], Chapter **7**: 219-268.

Schiller, P. W. (1985). Application of fluorescence techniques in studies of peptide conformations and interactions. In: Hruby [1985a], Chapter **3**: 115-164.

Schiller, P.W., Nguyen, T. M.-D., Lemieux, C. (1988). Synthesis and opioid activity profiles of cyclic dynorphin analogs. *Tetrahedron* **44**: 733-743.

Schimmel, P. R. and Flory, P. J. (1968). Conformational energies and configurational statistics of copolypeptides containing L-proline. *J. Mol. Biol.* **34**: 105-120.

Schwyzer, R. (1971). Private communication cited by Weinkem and Jorgensen [1971].

Schwyzer, R. (1977). ACTH: A short introductory review. *Ann. N.Y. Acad. Sci.* **297**: 3-26.

Schwyzer, R. (1986a). Estimated conformation, orientation, and accumulation of dynorphin A-(1-13)-tridecapeptide on the surface of neutral lipid membranes. *Biochemistry* **25**: 4281-4286.

Schwyzer, R. (1986b). Molecular mechanism of opioid receptor selection. *Biochemistry* **25**: 6335-6342.

Schwyzer, R. (1988). Estimated membrane structure and receptor subtype selection of an opioid alkaloid-peptide hybrid. *Int. J. Peptide Protein Res.* **32**: 476-483.

Schwyzer, R., Ludescher, U. (1969). Untersuchungen über die Konformation des cyclischen Hexapeptids cyclo-Glycyl-L-prolyl-glycyl-glycyl-L-prolyl-glycyl. *Helv. Chim. Acta* **52**: 2033-2040.

Schwyzer, R., Grathwohl, C., Meraldi, J.P., Tun-Kyi, A., Vogel, R., Wüthrich, K. (1972). The solution conformation of cyclo-glycyl-L-prolyl-glycyl-glycyl-L-prolyl-glycyl. *Helv. Chim. Acta* **55**: 2545-2549.

Segrest, J. P., Jackson, R. L., Morrisett, J. D., Gotto, A. M. (1974). A molecular theory of lipid protein interactions in the plasma lipoproteins. *FEBS Lett.* **38**: 247-253.

Sertürner, F. W. (1805-1806). Darstellung der reinen Mohnsäure (Opiumsäure). *J. Pharmacol.* **14**: 47, 93, 193, cited by Benedetti and Premuda [1990].

Shulman, R. G., ed. (1979). *Biological Applications of Magnetic Resonance.* Academic Press, New York, USA.

Simon, J., Benhye, S., Hepp, J., Varga, E., Medzihradszky, K., Borsodi, A., Wollemann, M. (1990). Method for isolation of kappa-opioid binding sites by dynorphin affinity chromatography. *J. Neurosci. Res.* **25**: 549-555.

Simonds, W. F., Burke, T. R., Rice, K. C., Jacobson, A. E., Klee, W. A. (1985). Purification of the opiate receptor of NG108-15 neuroblastoma-glioma hybrid cells. *Proc. Natl. Acad. Sci. USA* **82**: 4974-4978.

Smith, A. P., Lee, N. M. (1988). Pharmacology of dynorphin. *Ann. Rev. Pharmacol. Toxicol.* **28**: 123-140.

Snell, C. R. (1984). A classification of peptide ligands based on their predicted receptor conformation. *Biochim. Biophys. Acta* **787**: 53-60.

Sober, H. A., ed. (1970). *CRC Handbook of Biochemistry.* Selected data for molecular biology. 2nd edition. The Chemical Rubber Co., Cleveland, Ohio, USA.

Soloman, I. (1955). Relaxation processes in a system of two spins. *Phys. Rev.* **99**: 559-565.

States, D. J. Haberkorn, R. A., Ruben, D. J. (1982). A two-dimensional nuclear Overhauser experiment with pure absorption phase in four quadrants. *J. Magn. Reson.* **48**: 286-292.

Stegmann, T., Doms, R. W., Helenius, A. (1989). Protein-mediated membrane fusion. *Annu. Rev. Biophys. Biophys. Chem.* **18**: 187-211.

Stern, A., Gibbons, W. A., Craig, L. C. (1968). A conformational analysis of gramicidin S-A by nuclear magnetic resonance. *Proc. Natl. Acad. Sci. USA* **61**: 734-741.

Sternlicht, H., Wilson, D. (1967). Magnetic resonance studies of macromolecules. I. Aromatic-methyl interactions and helical structure effects in lysozyme. *Biochemistry* **6**: 2881-2892.

Stevens, C. W., Yaksh, T. L. (1986). Dynorphin A and related peptides administered intrathecally in the rat: a search for putative æ opiate receptor activity. *J. Pharmacol. Exp. Ther.* **238**: 833-838.

Still, C. (1989). *MacroModel Version 2.5 Documentation.* Columbia University, New York, USA.

Stimson, E. R., Meinwald, Y. C., Scheraga, H. A. (1979). Solution conformation of enkephalin. A nuclear magnetic resonance study of ^{13}C-enriched carbonyl carbons in [Leu^5]-enkephalin. *Biochemistry* **18**: 1661-1671.

Surewicz, W. K., Mantsch, H. H. (1988). New insight into protein secondary structure from resolution-enhanced infrared spectra. *Biochim. Biophys. Acta* **952**: 115-130.

Surewicz, W. K., Mantsch, H. H. (1989). The conformation of dynorphin A-(1-13) in aqueous solution as studied by Fourier transform infrared spectroscopy. *J. Mol. Struct.* **214**: 143-147.

Surewicz, W. K., Mantsch, H. H., Stahl, G. L., Epand, R. M. (1987). Infrared spectroscopic evidence of conformational transitions of an atrial natiuretic peptide. *Proc. Natl. Acad. Sci USA* **86**: 7028-7030.

Sykes, B. D., Scott M. D. (1972). Nuclear magnetic resonance studies of the dynamic aspects of molecular structure and interactions in biological systems. *Ann. Rev. Biophys. Bioenerg.* **1**: 27-50.

Tachabina, S., Araki, K., Ohya, S., Yoshida, S. (1982). Isolation and structure of dynorphin, an opioid peptide, from porcine duodenum. *Nature (London)* **295**: 339-340.

Tainter, M. L. (1948). Pain. *Ann. N. Y. Acad. Sci.* **51**: 3-11.

Takeuchi, Y., Marchand, A. P., eds. (1986). *Applications of NMR Spectroscopy to Problems in Stereochemistry and Conformational Analysis.* VCH, Deerfield Beach, Fla., USA.

Tappin, M. J., Pastore, A., Norton, R. S., Freer, J. H., Campbell, I. D. (1988). High resolution ^{1}H NMR study of the solution structure of δ-hemolysin. *Biochemistry.* **27**: 1643-1647.

Taylor, J. W. (1989). Conformation induction in amphiphilic peptide hormones bound to model interfaces. *Eleventh American Peptide Symposium* (The Salk Institute and University of California, San Diego, La Jolla, California, July 9-14, 1989) Abstracts: P-145.

Taylor, J. W. (1990). Peptide models of dynorphin A-(1-17) incorporating minimally homologous substitutes for the potential amphiphilic β-strand in residues 7-15. *Biochemistry* **29**: 5346-5373.

Taylor, J. W., Kaiser, E. T. (1986). The structural characterization of β-endorphin and related peptide hormones and neurotransmitters. *Pharmacol. Rev.* **38**: 291-319.

Taylor, J. W., Kaiser, E. T. (1989). Opioid receptor selectivity of peptide models of β-endorphin. *Int. J. Peptide Protein Res.* **34**: 75-80.

Temussi, P. A., Tancredi, T., Pastore, A., Castiglione-Morelli, M. A. (1987). Experimental attempt to simulate receptor site environment. A 500-MHz ^{1}H nuclear magnetic resonance study of enkephalin amides. *Biochemistry* **26**: 7856-7863.

Temussi, P. A., Picone, D., Castiglione-Morelli, M. A., Motta, A., Tancredi, T. (1989). Bioactive conformation of linear peptides in solution: An elusive goal?. *Biopolymers* **28**: 91-107.

Tulunay, F. C., Jen, M.-F., Loh, H. H. (1982). Possible physiological control of morphine analgesia in mice. *Eur. J. Pharmacol.* **83**: 317-319.

Turcotte, A., Lalonde, J. M., St.-Pierre, S., Lemaire, S. (1984). Dynorphin 1-13. I. Structure-function relationships of Ala-containing analogs. *Int. J. Peptide Protein Res.* **23**: 361-367.

Udenfriend, S., Kilpatrick, D. L. (1984). Proenkephalin and the products of its processing: chemistry and biology. In: Udenfriend and Meienhofer [1984], Chapter **2**: 25-68.

Udenfriend, S., Meienhofer, J., eds. (1984). *The Peptides - Analysis, Synthesis, Biology. Volume 6: Opioid Peptides: Biology, Chemistry, and Genetics.* Academic Press, Orlando, Fla., USA.

Uma, K., Balaram, H., Raghothama, S., Balaram, P. (1988). Simultaneous observation of positive and negative nuclear Overhauser effects in oligopeptides due to segmental motion. *Biochem. Biophys. Res. Commun.* **151**: 153-157.

Urry, D. W. (1985). Absorption, circular dichroism and optical rotary dispersion of polypeptides, proteins, prosthetic groups and biomembranes. In: Neuberger and van Deenen [1985], Chapter **4**: 275-346.

Urry, D. W., Masotti, L., Krivacic, J. R. (1971). Circular dichroism of biological membranes. I. Mitochondria and red blood cell ghosts. *Biochim. Biophys. Acta* **241**: 600-612.

Urry, D. W., Long, M. M., Ohnishi, T., Jacobs, M. (1974). Circular dichroism and absorption of the polytetrapeptide of elastin: A polymer model for the β-turn. *Biochem. Biophys. Res. Commun.* **61**: 1427-1433.

Vaughn, J. B., Taylor, J. W. (1989). Proton NMR and CD solution conformation determination and opioid receptor binding studies of a dynorphin A-(1-17) model peptide. *Biochim. Biophys. Acta* **999**: 135-146.

Verlet, L. (1967). Computer "experiments" on classical fluids. I. Thermodynamical properties of Lennard-Jones molecules. *Phys. Rev.* **159**: 98-103.

Vold, R. L., Waugh, J. S., Klein, M. P., Phelps, D. E. (1968). Measurement of spin relaxation in complex systems. *J. Chem. Phys.* **48**: 3831-3832.

Vold, R. L., Vold, R. R., Simon, H. E. (1973). Errors in measurements of transverse relaxation rates. *J. Magn. Reson.* **11**: 283-298.

Wagner, G., Wüthrich, K. (1982). Sequential resonance assignments in protein ^{1}H nuclear magnetic resonance spectra. Basic pancreatic trypsin inhibitor. *J. Mol. Biol.* **155**: 347-366.

Wagner, G. (1983). Two-dimensional relayed coherence transfer spectroscopy of a protein. *J. Magn. Reson.* **55**: 151-156.

Wagner, G. (1990). NMR investigations of protein structure. *Prog. NMR Spectrosc.* **22**: 101-139.

Wakamatsu, K., Higashijima, T., Fujino, M., Nakajima, T., Miyazawa, T. (1983). Transferred NOE analyses of conformations of peptides as bound to membrane bilayer of phospholipid; mastoparan-X. *FEBS Lett.* **162**: 123-126.

Wakamatsu, K., Okada, A., Suzuki, M., Higashijima, T., Masui, Y., Sakakibara, S., Miyazawa, T. (1986a). Nuclear-magnetic-resonance studies on the conformation of membrane-bound α-mating factor. Transferred nuclear Overhauser effect analysis. *Eur. J. Biochem.* **154**: 607-615.

Wakamatsu, K., Okada, A., Higashijima, T., Miyazawa, T. (1986b). NMR analysis of the conformations of membrane-bound peptides. *Eur. J. Biochem.* **25**: S193-S200.

Wakamatsu, K., Okada, A., Miyazawa, T. , Masui, Y., Sakakibara, S., Higashijima, T. (1987). Conformations of yeast α-mating factor and analog peptides as bound to phospholipid bilayer. Correlation of the membrane-bound conformation with physiological activity. *Eur. J. Biochem.* **163**: 331-338.

Wallace, B. A., Teeters, C. L. (1987). Differential absorption flattening effects are significant in the circular dichroism spectra of large membrane fragments. *Biochemistry* **26**: 65-70.

Weast, R.C., ed. (1985). *CRC Handbook of Chemistry and Physics.* A Ready-Reference Book of Chemical and Physical Data. CRC Press, 66th Edition, Boca Raton, FLA, USA.

Weber, E., Evans, C. J., Barchas, J. D. (1982). Predominance of the amino-terminal octapeptide fragment of dynorphin in rat brain regions. *Nature (London)* **299**: 77-79.

Wehrli, F. W., Wirthlin, T. (1976). *Interpretation of Carbon-13 NMR Spectra.* Heyden, London, UK.

Weiner, S. J., Kollman, P. A., Case, D. A., Singh, U. C., Ghio, C., Alagona, G., Profeta, S., Weiner, P. (1984). A new force field for molecular mechanical simulation of nucleic acids and proteins. *J. Am. Chem. Soc.* **106**: 765-784.

Weiner, S. J., Kollman, P. A., Nguyen, D. T., Case, D. A. (1986). An all atom force field for simulations of proteins and nucleic acids. *J. Comp. Chem.* **7**: 230-252.

Weinkem R. J., Jorgensen, S. C. (1971). Angiotensin II analogs. IX. Conformational studies of angiotensin II by proton magnetic resonance. *J. Am. Chem. Soc.* **93**: 7038-7044.

Weitz, C. J., Faull, K. F., Goldstein, A. (1987). Synthesis of the skeleton of morphine molecule by mammalian liver. *Nature* **330**: 674-677.

Wen, H. L., Ho, W. K. K. (1984). Suppression of withdrawal symptoms by dynorphin in heroin addicts. *Eur. J. Pharmacol.* **82**: 183-186.

Wider, G., Macura, S., Kumar, A., Ernst, R. R., Wüthrich, K. (1984). Homonuclear two-dimensional ^{1}H NMR of proteins. Experimental procedures. *J. Magn. Reson.* **56**: 207-234.

Wilde, J. A., Bolton, P. H. (1984). Suppression of homonuclear couplings in heteronuclear two-dimensional spectroscopy. *J. Magn. Reson.* **59**: 343-346.

Woody, R. W. (1985). Circular dichroism of peptides. In: Hruby [1985a], Chapter **2**: 15-114.

Wright, D. A., Axelson, D.E., Levy, G. C. (1979). Physical chemical applications of ^{13}C spin relaxation measurements. In: Levy [1979], Chapter **2**: 103-170.

Wu, C.-S. C., Yang, J. T. (1981). Sequence dependent conformations of short polypeptides in a hydrophobic environment. *Mol. Cell. Biochem.* **40**: 109-122.

Wu, C.-S. C., Hachimori, A., Yang, J. T. (1982). Lipid-induced conformation of some peptide hormones and bioactive oligopeptides: Predominance of helix over β form. *Biochemistry* **21**: 4556-4562.

Wüthrich, K. (1976). *NMR in Biological Research: Peptides and Proteins.* North Holland, Amsterdam, NL, and Oxford, UK.

Wüthrich, K. (1986). *NMR of Proteins and Nucleic Acids.* Wiley-Interscience, New York, USA.

Wüthrich, K. (1989a). Protein structure determination in solution by nuclear magnetic resonance spectroscopy. *Science* **243**: 45-50.

Wüthrich, K. (1989b). The development of nuclear magnetic resonance spectroscopy as a technique for protein structure determination. *Acc. Chem Res.* **22**: 36-44.

Wüthrich, K., Wider, G., Wagner, G., Braun, W. (1982). Sequential resonance assignments as a basis for determination of spatial protein structures by high resolution proton nuclear magnetic resonance. *J. Mol. Biol.* **155**: 311-319.

Wüthrich, K, Billeter, M., Braun, W. (1983). Pseudo-structures for the 20 common amino acids for use in studies of protein conformations by measurements of intramolecular proton-proton distance constraints with nuclear magnetic resonance. *J. Mol. Biol.* **169**: 949-961.

Yang, C.-C., Taylor, J. W. (1989). The design, synthesis and biological studies of synthetic peptide models of dynorphin A-(1-17). *Eleventh American Peptide Symposium* (The Salk Institute and U. of California, San Diego, La Jolla, California, July 9-14, 1989) *Abstracts*: P-246.

Yang, J. T., Bewley, T. A., Chen, G. C., Li, C. H. (1977). Conformation of β-endorphin and β-lipotropin: Formation of helical structure in methanol and sodium dodecyl sulfate solutions. *Proc. Natl. Acad. Sci. USA* **74**: 3235-3238.

Yang, J.T., Wu, C.-S. C., Martinez, H.M. (1986). Calculation of protein conformation from circular dichroism. *Methods in Enzymol.* **130**: 208-269.

Yeagle, P. L., ed. (1991). *The Structure of Biological Membranes.* The Telford Press, Caldwell, NJ, USA, in press.

Zhou, N., Gibbons, W.A. (1986). A ^{1}H nuclear magnetic resonance study of the opioid peptide dynorphin-(1-13) in aqueous solution. *J. Chem. Soc. Perkin Trans. II* **1986**: 637-644.

Zimm, B. H., Bragg, J. K. (1959). Theory of the phase transition between helix and random coil in polypeptide chains. *J. Chem. Phys.* **31**: 526-535.

Zimmermann, S. S. (1985). Theoretical methods in the analysis of peptide conformation. In: Hruby [1985a], Chapter **4**: 165-212.

Zipser, B., Ruff, M. R., O'Neill, J. B., Smith, C. C., Higgins, W. J., Pert, C. B. (1988). The opiate receptor: a single 110 kDa recognition molecule appears to be conserved in Tetrahymena, leech, and rat. *Brain Res.* **463**: 296-304.

Zukin, R. S., Zukin, S. R. (1981). Demonstration of [^{3}H]cyclazocine binding to multiple opiate receptor sites. *Mol. Pharmacol.* **20**: 246-254.

9.2. Computer Software

BIOGRAF Molecular Simulation Software (1989), Version 2.09, BioDesign, Inc., Pasadena, California, USA.

MacroModel Molecular Modelling System (1987), Version 2.5, Columbia University, Department of Chemistry, New York, USA.

T_1 estimation program. Version 880325.1 (1988), A. D. Bain, McMaster University, Department of Chemistry, Hamilton, Ontario, Canada.